To the Graduate Council:

I am submitting herewith a dissertation written by Sanjiv R. Malkan entitled **"Process-Structure-Property Relationships in Different Molecular Weight Polypropylene Melt Blown Webs."** I have examined the final copy of this dissertation for form and content and recommend that it be accepted in partial fulfillment of the requirements for the degree of Doctor of Philosophy, with a major in Human Ecology.

Larry C. Wadsworth, Major Professor

We have read this dissertation
and recommend its acceptance:

Accepted for the Council:

Vice Provost
and Dean of The Graduate School

PROCESS-STRUCTURE-PROPERTY RELATIONSHIPS IN DIFFERENT MOLECULAR WEIGHT POLYPROPYLENE MELT BLOWN WEBS

A Dissertation

Presented for the

Doctor of Philosophy

Degree

The University of Tennessee, Knoxville

Sanjiv R. Malkan

May 1990

Copyright © Sanjiv R. Malkan , 1990
All rights reserved

TO MY PARENTS

आ नो भद्राः क्रतवो यंतु विश्वतो

Ā no bhadrāḥ kratavo yantu viśvataḥ

Let noble thoughts come to us from every side

Rigveda 1-89-i

ACKNOWLEDGEMENTS

In undertaking a research project of this magnitude, a researcher must draw upon the expertise of many people. I have done this and I wish to express my sincere gratitude to them for their assistance.

This study is specifically indebted to my advisor, Dr. Larry Wadsworth. His interest and enthusiasm in the project served as a catalyst and stimulant in enabling me to successfully complete this reserarch project.

I would like to thank Dr. Bogue, Dr. Bresee, Dr. Duckett, and Dr. Milligan for serving on dissertation committe and for their helpful suggestions.

Special thanks is extended to Mr. Richard Meade and Mr. Larry Spires for their technical support during melt blowing trial runs, Mrs. Barbara Webber for her help in typing tables, and Mr. Rajen Patel for his advice and assistance.

I am grateful to the Exxon Chemical Company for their financial and technical support to this research project.

Finally, I would like to thank my parents and brothers for their continuous support and encouragement throughout the course of this research.

ABSTRACT

A fundamental study was undertaken to assess the **process-structure-property** relationships as a function of the molecular weight of polypropylene resins, polymer throughput rate, air flow rate, melt blowing die orifice diameter, and extrusion and attenuation air temperatures. The properties studied were: stress-strain behavior of webs and single fibers; failure modes; bending rigidity; bursting strength; average fiber diameter; fiber distribution; air permeability; web density; shear behavior of webs; birefringence of single fibers; crystallinity of resins and webs; x-ray diffraction of webs; and gel permeation chromatography of resins and webs.

The **35**, **300**, **600**, and **1000 melt flow rate (MFR)** resin were melt blown at three throughput rates using two air flow rates and two different orifice diameter die. Generally, all of the resins processed well under the different processing conditions required in this study; however, the optimization of the web properties was more difficult at the higher polymer throughput conditions. The webs produced at the lowest throughput rate of **160 g/min** were thicker and loftier than the webs produced at **320** and **480 g/min** (**0.4**, **0.8**, and **1.2 g/min/orifice**, respectively). The higher throughput webs had a harsher hand and were thin.

Among the process variables studied, polymer throughput rate had the most notable effects on the physical and morphological properties of melt blown webs. It was hypothesized that the **fiber-to-fiber thermal bonding** was a dominant factor in controlling the physical properties of melt blown webs; and, the final fiber diameter was dependent on the **die swell** and the change in **polymer-to-air ratio for a given air flow rate**. The increase in air flow

rate at a given throughput rate appeared to have minimal effect on final diameter.

The average fiber diameter, breaking stress, initial modulus, air permeability, shear stiffness, and web density increased as the polymer throughput rate increased. The breaking strain and bursting strength decreased as the polymer throughput rate increased, indicating a more brittle behavior of the fabric at high throughput rates. The tensile properties and bursting strength decreased with increased MFR. The observed failure modes were different for different processing conditions.

There were minimal differences in molecular weight, percent crystallinity, and x-ray peak intensities between low and high throughput webs. However, the differences in molecular weight, percent crystallinity, and x-ray peak intensities between resin and web was noticeable, especially in low MFR resin webs. The web crystallinity increased with increased MFR; and, the web molecular weight decreased with increased MFR.

The DSC thermograms and x-ray diffractograms of higher throughput webs (especially in 35 and 300 MFR webs) indicated the presence of **two crystalline species**.

TABLE OF CONTENTS

Chapter		Page
1.	**INTRODUCTION**	**1**
	Background	1
	Objectives	2
	Present Study	3
2.	**REVIEW OF LITERATURE**	**4**
	Nonwoven Technology	4
	Classification of Nonwoven fabrics	7
	Melt Blowing Process	9
	Historical Perspective	9
	Process Definition	12
	Process Description	13
	Process Variables	22
	Status of Nonwoven Research	26
	Melt Blowing	27
	Mechanical Properties of Nonwovens	38
	Failure Modes of Nonwovens	42
	Polypropylene	45
	Polypropylene Crystalline Forms	46
3.	**EXPERIMENTAL DESIGN**	**49**
	Materials	49
	Web Preparation	49
4.	**EXPERIMENTAL PROCEDURES**	**58**
	Physical Property Measurements	58

Microscopical Analysis of Fibers 68
Differential Scanning Calorimetry 70
Wide Angle X-Ray Diffraction 71
Gel Permeation Chromatography 73
Melt Flow Rate 73

5. **RESULTS AND DISCUSSION 75**

Process Conditions 75
Effects of Process Variables on Melt Blown Fibers 85
Fiber diameter 85
Fiber attenuation 90
Fiber characteristics 91
Fiber diameter distribution 94
Fiber birefringence 94
Effects of Process Variables on Molecular Weight 99
Effects of Process Variables on Physical Properties 104
Tensile Properties 104
Failure Modes 120
Bursting Strength 125
Flexural Rigidity 128
Shear Stiffness 131
Air Permeability and Web Density 133
Web Uniformity 139
Effects of Process Variables on Morphological Properties 143
Differential scanning calorimetry 143
Wide angle x-ray diffraction 148

6. **CONCLUSIONS AND RECOMMENDATIONS 154**

LIST OF REFERENCES 157

APPENDICES 167

A. Determination of air flow rate 168

B. Procedure for normalizing load-extension data 177
C. Procedure for averaging load-extension curves 181
D. Tables 185
E. Figures 213
F. Crystallization kinetics study of polypropylene resins 257

VITA 268

LIST OF TABLES

Table		Page
3.1	Characteristics of polymers	50
3.2	Melt blown processing conditions for webs processed at 75% air flow rate using standard orifice die	54
3.3	Melt blown processing conditions for webs processed at 90% air flow rate using standard orifice die.	55
3.4	Melt blown processing conditions for webs processed at 75% air flow rate using small orifice die	56
5.1	Probable causes and solutions for "shot" Source: Anonymous : Melt Blowing Nonwoven Web Technology, Exxon Chemical Company, 1982.	77
5.2	Probable causes and solutions for "rope and fly" Source: Anonymous : Melt Blowing Nonwoven Web Technology, Exxon Chemical Company, 1982.	78
5.3	Birefringence of melt blown fibers	98
5.4	Shear properties of melt blown webs	132
5.5	Basis weight of webs processed at 75% air flow rate using standard orifice die	140
5.6	Basis weight of webs processed at 90% air flow rate using standard orifice die	141
5.7	Basis weight of webs processed at 75% air flow rate using small orifice die	142

A.1 Flow coefficients 175
Source: Anonymous : Flow Measurement, American Society of Mechanical Engineers, Power Test Coce, PTC 19.5;4-1959.

D.1 Average fiber diameter of webs processed at 75% air flow rate using standard orifice die 186

D.2 Average fiber diameter of webs processed at 90% air flow rate using standard orifice die 187

D.3 Average fiber diameter of webs processed at 75% air flow rate using small orifice die 188

D.4 Intrinsic viscosity, molecular weight, and polydispersity index of resins and webs processed at 75% air flow rate using standard orifice die 189

D.5 Intrinsic viscosity, molecular weight, and polydispersity index of resins and webs processed at 90% air flow rate using standard orifice die 190

D.6 Intrinsic viscosity, molecular weight, and polydispersity index of resins and webs processed at 75% air flow rate using small orifice die 191

D.7 Measured melt flow rate of resins and webs processed at 75% air flow rate using standard orifice die 192

D.8 Measured melt flow rate of resins and webs processed at 90% air flow rate using standard orifice die 193

D.9 Measured melt flow rate of resins and webs processed at 75% air flow rate using small orifice die 194

D.10 Tensile properties of webs and single fibers processed at 75% air flow rate using standard orifice die 195

D.11 Tensile properties of webs and single fibers processed at 90% air flow rate using standard orifice die 196

D.12 Tensile properties of webs and single fibers processed at 75% air flow rate using small orifice die..... 197

D.13 Breaking stress of webs and single fibers processed at 75% air flow rate using standard orifice die 198

D.14 Breaking stress of webs and single fibers processed at 90% air flow rate using standard orifice die 199

D.15 Breaking stress of webs and single fibers processed at 75% air flow rate using small orifice die..... 200

D.16 Flexural rigidity and bursting strength of webs processed at 75% air flow rate using standard orifice die 201

D.17 Flexural rigidity and bursting strength of webs processed at 90% air flow rate using standard orifice die 202

D.18 Flexural rigidity and bursting strength of webs processed at 75% air flow rate using small orifice die..... 203

D.19 Air permeability of webs processed at 75% air flow rate using standard orifice die..... 204

D.20 Air permeability of webs processed at 90% air flow rate using standard orifice die..... 205

D.21 Air permeability of webs processed at 75% air flow rate using small orifice die 206

D.22 Basis weight, web thickness, and web density of webs processed at 75% air flow rate using standard orifice die 207

D.23 Basis weight, web thickness, and web density of webs processed at 90% air flow rate using standard orifice die 208

D.24 Basis weight, web thickness, and web density of webs processed at 75% air flow rate using small orifice die 209

D.25 Crystallinity of resins and webs processed at 75% air flow rate using standard orifice die 210

D.26 Crystallinity of resins and webs processed at 90% air flow rate using standard orifice die 211

D.27 Crystallinity of resins and webs processed at 75% air flow rate using small orifice die 212

F.1 Avarami Index, Rate Constant, Crystallization Half-time ($t_{1/2}$), and Equilibrium Melting Point (T_m°) for various PP Resins 266

LIST OF FIGURES

Figure		Page
2.1	Flow diagram of the nonwovens industry complex	5
2.2	Flow diagram of classification of nonwoven fabric formation techniques Source: Nutter, W. : Textile Month, No.5, 1970, pp. 94-100	8
2.3	Schematic of melt blowing process	14
2.4	Schematic of a screw extruder Source: Rodriguez, F. : Principles of Polymer Engineering, McGraw Hill, New York, 1982, pp. 330 - 331.	15
2.5	Schematic of a metering pump	17
2.6	Schematic of die nosepieces	19
2.7	Schematic showing primary and secondary air flow and web formation	21
2.8	Melt blown process variables	23
3.1	Flow diagram of experimental design	52
4.1	Schematic showing specimen cutting procedure for basis weight determination	59
4.2	Schematic showing specimen cutting procedure for tensile testing	60

4.3	Schematic showing collection of low-basis weight melt blown web	62
4.4	Schematic showing single fiber mounting procedure	63
4.5	Optical photomicrograph of a single fiber	64
4.6	Schematic of a typical shear curve	66
4.7	Schematic showing fiber diameter measurement	69
4.8	Schematic of an x-ray diffractometer	72
4.9	Schematic of an x-ray flat plate camera set-up	74
5.1	Photomicrograph showing "shot."	79
5.2	Photograph showing "fly."	81
5.3	Photograph showing "rope."	82
5.4	Perceived process condition window for 35, 300, 600, and 1000 MFR polypropylene resins	83
5.5.	Effect of MFR and process variables on average fiber diameter	86
5.6	Photomicrographs of 1000 MFR webs processed at 75% air flow rate using standard orifice die	87
5.7	Photomicrograph showing variation in fiber diameter along a single fiber	92
5.8	Photomicrograph showing thermal branching	93

5.9 Fiber diameter distribution of melt blown webs processed at 75% air flow rate using standard orifice die 95

5.10 Fiber diameter distribution of melt blown webs processed at 90% air flow rate using standard orifice die 96

5.11 Fiber diameter distribution of melt blown webs processed at 75% air flow rate using small orifice die..... 97

5.12 Effect of MFR and process variables on weight average molecular weight of the webs..... 100

5.13 GPC chromatograms of 300 MFR resin and webs processed at 75% air flow rate using standard orifice die..... 101

5.14 Effect of MFR and process variables on melt flow rate of the webs..... 103

5.15 Effect of MFR and process variables on MD breaking stress..... 105

5.16 Effect of MFR and process variables on CD breaking stress..... 106

5.17 Photomicrograph showing fiber-to-fiber thermal bonding..... 108

5.18 Effect of MFR and process variables on MD breaking strain..... 110

5.19 Effect of MFR and process variables on CD breaking strain..... 111

5.20 Effect of MFR and process variables on MD initial modulus 113

5.21 Effect of MFR and process variables on CD initial modulus 114

5.22 Average MD and CD stress-strain curves of 35 MFR webs processed at 75% air flow rate using standard orifice die 116

5.23 Effect of MFR and process variables on single fiber breaking stress 117

5.24 Effect of MFR and process variables on single fiber breaking strain 118

5.25 Photograph showing melt blown web failure modes 121

5.26 Photomicrograph showing fiber pull-out zone 122

5.27 Photomicrograph showing brittle failure zone 123

5.28 Photomicrograph showing fiber fracture 124

5.29 Photograph showing positions of specimen break 126

5.30 Effect of MFR and process variables on bursting strength 127

5.31 Effect of MFR and process variables on MD flexural rigidity 129

5.32 Effect of MFR and process variables on CD flexural rigidity 130

5.33 Effect of MFR and process variables on web air permeability 134

5.34 Photomicrographs showing "openness" of the webs as a function of polymer throughput rate 135

5.35 Effect of MFR and process variables on web density 137

5.36 Web air permeability versus web density 138

5.37 Effect of MFR and process variables on web crystallinity 144

5.38 DSC thermograms of 35 MFR resin and webs processed at 75% air flow rate using standard orifice die 146

5.39 X-ray diffractograms of various crystalline forms of polypropylene 149
Source: Turner, J. A. et al. : Die Makromol. Chem., Volume 75, 1964, pp. 134 - 158.

5.40 X-ray diffractograms of 300 MFR webs processed at 75% air flow rate using standard orifice die 150

5.41 X-ray diffraction patterns of 300 and 1000 MR webs (160 and 320 g/min) processed at 75% air flow rate using standard orifice die 152

A.1 Schematic of air delivery system 173

B.1 Schematic of a typical load-extension curve 179

C.1 Schematic of a typical load-extension curve with selected load levels 183

E.1 Photomicrographs of 35 MFR webs processed at 75% air flow rate using standard orifice die 214

E.2 Photomicrographs of 300 MFR webs processed at 75% air flow rate using standard orifice die 215

E.3 Photomicrographs of 600 MFR webs processed at 75% air flow rate using standard orifice die 216

E.4 Photomicrographs of 35 MFR webs processed at 90% air flow rate using standard orifice die 217

E.5 Photomicrographs of 300 MFR webs processed at 90% air flow rate using standard orifice die 218

E.6 Photomicrographs of 600 MFR webs processed at 90% air flow rate using standard orifice die 219

E.7 Photomicrographs of 300 MFR webs processed at 75% air flow rate using small orifice die 220

E.8 Photomicrographs of 100 MFR webs processed at 75% air flow rate using small orifice die 221

E.9 GPC chromatograms of 35 MFR resin and webs processed at 75% air flow rate using standard orifice die 222

E.10 GPC chromatograms of 600 MFR resin and webs processed at 75% air flow rate using standard orifice die 223

E.11 GPC chromatograms of 1000 MFR resin and webs processed at 75% air flow rate using standard orifice die 224

E.12 GPC chromatograms of 35 MFR resin and webs processed at 90% air flow rate using standard orifice die 225

E.13 GPC chromatograms of 300 MFR resin and webs processed at 90% air flow rate using standard orifice die 226

E.14 GPC chromatograms of 600 MFR resin and webs processed at 90% air flow rate using standard orifice die 227

E.15 GPC chromatograms of 300 MFR resin and webs processed at 75% air flow rate using small orifice die 228

E.16 GPC chromatograms of 1000 MFR resin and webs processed at 75% air flow rate using small orifice die 229

E.17 Average MD and CD stress-strain curves of 300 MFR webs processed at 75% air flow rate using standard orifice die 230

E.18 Average MD and CD stress-strain curves of 600 MFR webs processed at 75% air flow rate using standard orifice die 231

E.19 Average MD and CD stress-strain curves of 1000 MFR webs processed at 75% air flow rate using standard orifice die 232

E.20 Average MD and CD stress-strain curves of 35 MFR webs processed at 90% air flow rate using standard orifice die 233

E.21 Average MD and CD stress-strain curves of 300 MFR webs processed at 90% air flow rate using standard orifice die 234

E.22 Average MD and CD stress-strain curves of 600 MFR webs processed at 90% air flow rate using standard orifice die 235

E.23 Average MD and CD stress-strain curves of 300 MFR webs processed at 75% air flow rate using small orifice die 236

E.24 Average MD and CD stress-strain curves of 1000 MFR webs processed at 75% air flow rate using small orifice die 237

E.25 Shear curves of 300 MFR webs processed at 75% air flow rate using standard orifice die 238

E.26 Shear curves of 300 MFR webs processed at 90% air flow rate using standard orifice die 239

E.27 Shear curves of 300 MFR webs processed at 75% air flow rate using small orifice die 240

E.28 DSC thermograms of 300 MFR resin and webs processed at 75% air flow rate using standard orifice die 241

E.29 DSC thermograms of 600 MFR resin and webs processed at 75% air flow rate using standard orifice die 242

E.30 DSC thermograms of 1000 MFR resin and webs processed at 75% air flow rate using standard orifice die 243

E.31 DSC thermograms of 35 MFR resin and webs processed at 90% air flow rate using standard orifice die 244

E.32 DSC thermograms of 300 MFR resin and webs processed at 90% air flow rate using standard orifice die 245

E.33 DSC thermograms of 600 MFR resin and webs processed at 90% air flow rate using standard orifice die 246

E.34 DSC thermograms of 300 MFR resin and webs processed at 75% air flow rate using small orifice die 247

E.35 DSC thermograms of 1000 MFR resin and webs processed at 75% air flow rate using small orifice die 248

E.36 X-ray diffractograms of 35 MFR webs processed at 75% air flow rate using standard orifice die 249

E.37 X-ray diffractograms of 600 MFR webs processed at 75% air flow rate using standard orifice die 250

E.38 X-ray diffractograms of 1000 MFR webs processed at 75% air flow rate using standard orifice die 251

E.39 X-ray diffractograms of 35 MFR webs processed at 90% air flow rate using standard orifice die 252

E.40 X-ray diffractograms of 300 MFR webs processed at 90% air flow rate using standard orifice die 253

E.41 X-ray diffractograms of 600 MFR webs processed at 90% air flow rate using standard orifice die 254

E.42 X-ray diffractograms of 300 MFR webs processed at 75% air flow rate using small orifice die 255

E.43 X-ray diffractograms of 1000 MFR webs processed at 75% air flow rate using small orifice die 256

F.1 Computer program for calculating relative crystallinity 260

F.2 Relative crystallinity versus time at different crystallization temperatures (T_c) 262

F.3 Relative crystallinity versus time for different polymers at agiven crystallization temperature (T_c) 263

F.4 Relative crystallinity versus temperature for different polymers 264

F.5 Relative crystallinity versus temperature at different cooling rates 265

CHAPTER 1
INTRODUCTION

Background

Nonwoven fabric technology is the most modern branch of the textile industry [1], and in recent years, has been the subject of much interest. Today, nonwoven fabrics play key roles in hundreds of everyday products, from luxury automobiles to the familiar teabag [2].

In the past thirty years, the nonwoven industry has observed a phenomenal growth mainly because of a close alliance among nonwoven producers, fiber producers, binder producers, and machinery manufacturers. There are many nonwoven manufacturing processess and products that have been developed and commercialized in the past thirty years to address a variety of end-use markets. As an example, in the early 1950's, melt blown nonwoven fabric technology was developed to make microfiber filters to collect radioactive particles from the upper atmosphere. Since then many researchers have perfected melt blown technology in order to make an increasingly varied range of melt blown products. Although, the research work on this technology was started in the early 1950's, and an extensive number of processing and products patents were developed, there has been a dramatic resurgence of research and developmental work in the past few years.

In recent years, the increased acceptance of melt blown fabrics in many end-use products has sparked an interest in the melt blowing process from both a commercial and a scientific point of view. Therefore, melt blown technology is

still considered to be in a strong growth stage and has very good market potential.

Melt blown fabric properties are highly dependent on the process conditions. A wide variety of fabrics can be engineered by manipulating the process conditions. Therefore, it is essential to study the interrelationships among various melt blown processing conditiions, such as resin melt flow rate, polymer and air throughput rate, process temperatures, die orifice size, and others. Moreover, the rapid development in high melt flow rate resins, combined with industry's push for high production rate, also warrants a more complete understanding of these interrelationships. It is this aspect of research into melt blown fabric that this dissertation explores. This research project is also an outcome of a continuous effort to gain knowledge on the fundamentals of the melt blowing process by the researchers at the University of Tennessee, Knoxville and Exxon Chemical Company.

Objectives

The main focus of this research has been to develop a more complete fundamental understanding of why the properties of melt blown fabrics change in the observed manner with various resin and process variables.

The main objective were:

- To assess the effects of polymer melt flow rate (proportional to molecular weight), polymer and air throughput rates, and die orifice diameter on melt blown fabric properties and fiber diameter.
- To establish optimum processing temperatures with respect to melt flow rate, polymer throughput rate and air flow rate.

- To generate a reliable data base by testing a greater number of samples; thereby, minimizing the possibility of incorrect conclusions being drawn from a limited set of data.

Present Study

The study of process-structure-property relationships in melt blowning is the topic of the research presented in this dissertation. Four different melt flow rate (MFR) polypropylene resins were melt blown as a function of three polymer throughput rates, two air flow rates, and two die orifice diameters.

Melt blown web properties were evaluated in terms of stress-strain behavior of webs, single fiber stress-strain properties, bending rigidity, bursting strength, failure modes, air permeability, web density, web uniformity, shear stiffness, fiber diameter and diameter distribution, web crystallinity, wide angle x-ray diffraction (WAXD) patterns, gel permeation chromatography (GPC), web melt flow rate and fiber birefringence. This characterization work should better clarify relationships among processing conditions, mechanical properties, and structure at both macroscopic and microscopic levels.

The scope of this research is broad because it encompasses many aspects of the melt blowing process. The results obtained from this study are expected to bring forth several factors that will have an important bearing on the fundamental understanding of the melt blowing process.

CHAPTER 2
REVIEW OF LITERATURE

Nonwoven Technology

Nonwoven fabric technology embodies both quite old and the very new processing techniques and materials [3]. The term "nonwoven fabrics" has been defined in many ways. In fact, the definition of nonwoven fabrics has been an area of considerable debate and discussion. Apparently, all the definitions proposed so far state in some detail what nonwovens are not, rather than what they are. The American Standard for Testing Materials (ASTM) [4] has defined the term "nonwoven fabrics" as:

> **A structure produced by bonding or the interlocking of fibers, or both, accomplished by mechanical, chemical, thermal, or solvent means and the combination thereof. The term does not include paper or fabrics that are woven, knitted, tufted, or those made by wool or other felting processes.**

The versatile and complex nature of the nonwovens industry is depicted in Figure 2.1 [5]. Nonwoven fabric is essentially an assemblage of fibers held together by mechanical or chemical means, resulting in a mechanically stable, self-supporting, and generally flexible, web-like structure. The most significant feature of nonwoven fabrics, and the one that contributes most to their economic appeal [2], is that the fabrics are usually made directly from raw materials in a continuous production line, thus partially or completely eliminating conventional

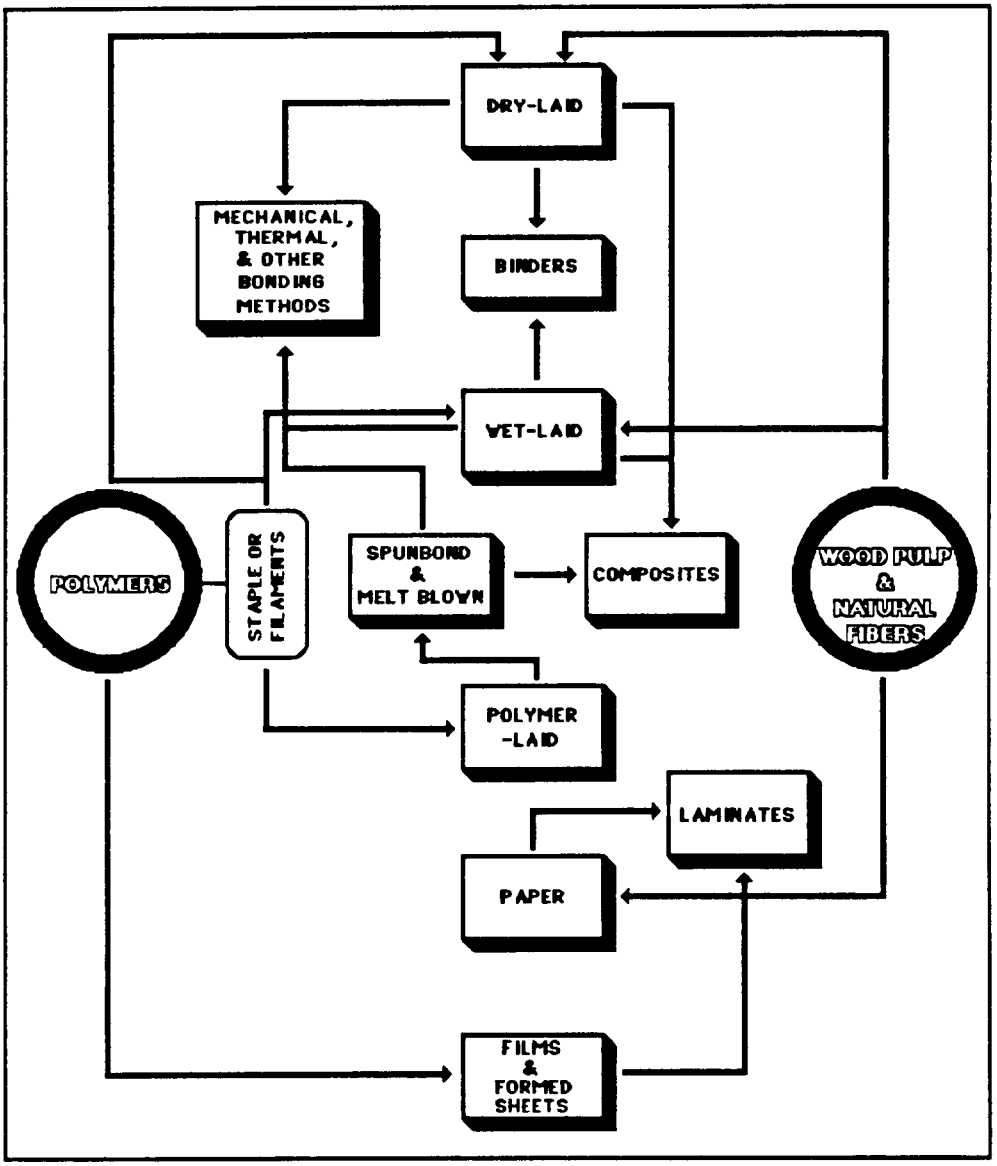

Figure 2.1. Flow diagram of the nonwovens industry complex.

textile operations, such as carding, roving, spinning, weaving or knitting. The simplicity of fabric formation, coupled with high productivity, allows nonwovens to compete favorably with wovens and knits on a performance per cost basis in many industrial applications (as in packaging materials, for example). However, in fashion outer-wear apparel fabric applications, where good drape properties, flexibility, and strength are required, nonwovens have yet to gain a significant technological advancement. On the other hand, nonwoven fabrics and composites have gained the major share of healthcare products such as surgical face masks, operating room drapes and gowns, instrument steralization wraps, surgical towels, and personal hygiene products. Nonwovens are also used extensively for gaseous and liquid filtration applications. Nevertheless, there has been a continuous effort through innovative manufacturing processes to develop newer nonwoven products that emulate the drape and flexibility of woven or knitted structures.

Nonwoven fabrics are quite distinct and versatile in their properties and structures compared to the conventional woven and knitted fabrics. Woven and knitted fabrics manifest their properties from the arrangement of fibers in the yarn and the arrangement of yarns in the fabrics [6]. Likewise, the properties of nonwoven fabrics are largely dependent on fiber properties, fabric structural geometry, and particularly the type of fiber-to-fiber bonding. Moreover, nonwoven fabric properties can be "tailor-made" through the use of the various web manufacturing and bonding processes, the selective use of raw materials--fibers and bonding means, and various finishing processes.

Nonwoven fabric technology is the most exciting segment of the textile industry and will be one of the most important in the years ahead as nonwoven

fabrics penetrate many more areas now occupied predominantly by conventional textiles [7].

Classification of Nonwoven Fabrics

Nonwoven fabrics can be classified in many ways, but the most accepted classification scheme is based on web formation techniques. There are many nonwoven web formation techniques, and as depicted in Figure 2.2, they can be divided into the following three generic catergories [8] : 1) Dry laid; 2) Wet laid; and, 3) Polymer laid.

Dry laid. In the dry laid process, first a natural or man-made staple fibrous web is prepared by using one of the following techniques: a) parallel laid carded webs produced by layering carded webs; b) cross lapping of carded webs; c) composite webs produced by combining parallel carded and cross lapped carded webs; and, d) random oriented fibrous webs produced by air-laying or mechanical fiber randomizing processes. The web is then processed to achieve fiber-to-fiber bonding by chemical, mechanical, solvent, or thermal means to produce a nonwoven fabric with sufficient dimensional stability. Typical end-uses for dry laid nonwoven fabrics are interlinings for garments, fabrics for carpet backing, diaper coverstock, apparel and upholstery backings, filter media, wipes, and personal hygiene fabrics.

Wet laid. In the wet laid process, natural or man-made fibers are first mixed with chemicals and water to obtain a uniform dispersion called a "slurry." The "slurry" is then deposited on a moving wire screen where the excess water

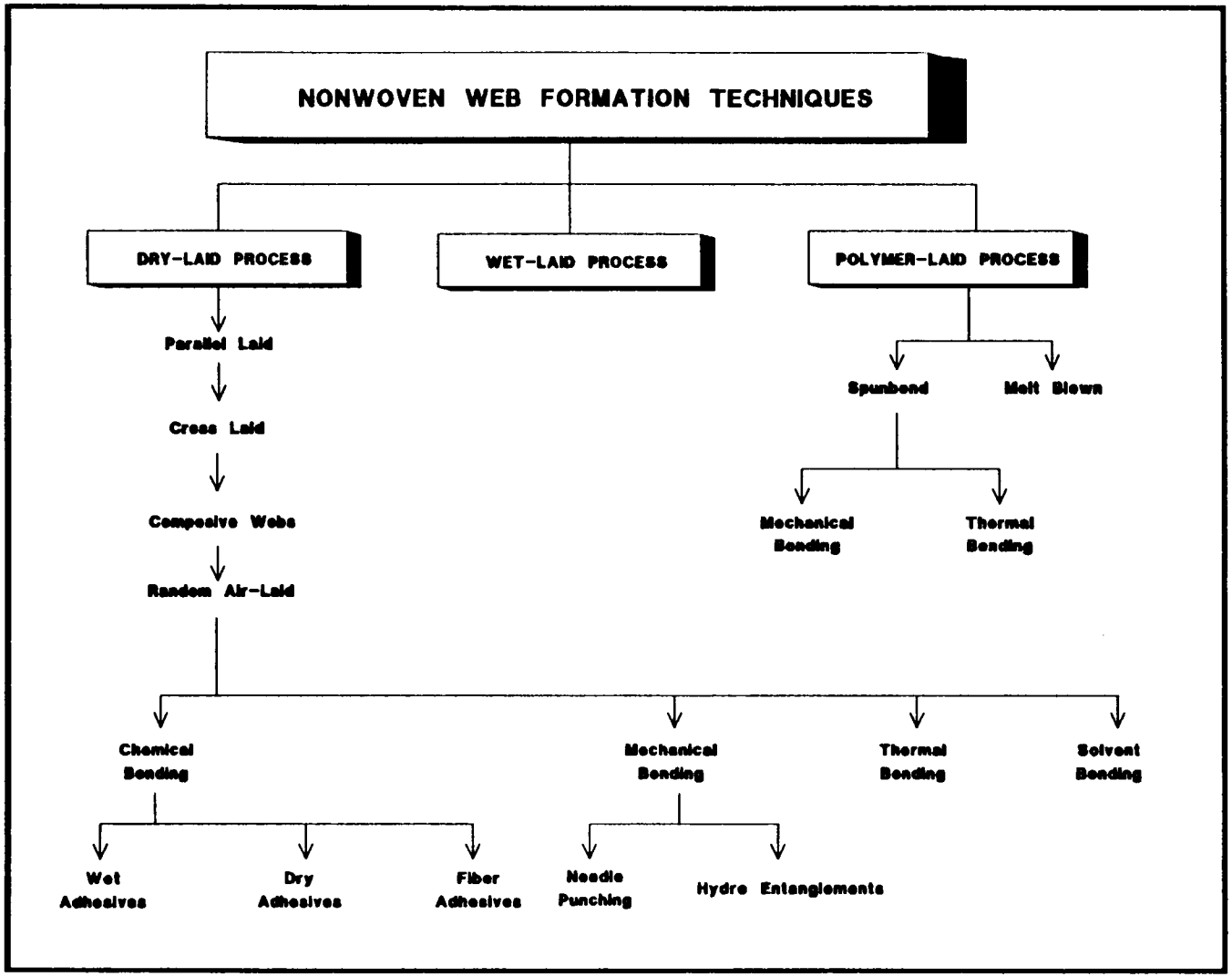

Figure 2.2. Flow diagram of classification of nonwoven fabric formation techniques.

Source: Nutter, W. : Textile Month, No.5, 1970, pp. 94-100.

is drained off, leaving the fibers randomly laid in a uniform web, which is then bonded and finished as required. Typical end-uses for wet laid nonwoven fabrics are tea bags, towels, wipes, surgical gowns and drapes, and others.

Polymer laid. In polymer laid process, first a molten polymer is extruded through a spinneret to form filaments or fibers. These filaments or fibers are then laid down on a moving conveyor belt to form a continuous web. This web is then bonded mechanically or thermally to make a polymer-laid nonwoven fabric. Typical end-uses for ploymer laid nonwoven fabrics are carpet underlay, packaging material, durable papers, geotextile fabrics, diaper and personal hygiene top sheeting, apparel and upholstery backing fabrics, and surgical drapes and gowns.

Melt Blowing Process

Historical Perspective

The microfibers (also referred as superfine or melt blown fibers) are fibrous materials less than about 10 microns in diameter. Such fibers are found in nature in the form of spider silk and pineapple leaf fiber [9]. Man-made microfibers are produced using a variety of materials and production techniques. The submicron glass fibers in "glass wool" are a prime example. There are basically two production techniques: **spray spinning** and **melt blowing.** These two techniques differ somewhat in details, but both involve the introduction of dissolved or molten polymers into high velocity streams of air or gas which rapidly convert the liquid into microfibers.

The first deliberate attempt to develop a useful commercial process for making organic textile like microfibers was made by **Carlton Francis**, an independent inventor, in 1939. **Francis** visualized that a spray gun which could produce fibers might be used for a wide variety of applications, including the combining of adhesive or potentially adhesive sprayed fibers with other textile fibers to form microfibrous nonwoven fabrics [10]. In the early 1950's, the **American Viscose Corporation** acquired the rights to Francis's work on sprayed fiber technology and retained **Arthur D. Little, Inc.** to research and develop the spray fiber field. No major commercial products were developed, and the company eventually discontinued the research work.

During this period of time, Dow Chemical Company also had a Research and Development program to develop microfiber products using polystyrene [11]. Dow Chemical Company did not foresee any success, so decided to abandon the project. Soon afterwards, the Army Chemical Warfare Laboratories continued Dow's work in order to produce microfibers to collect radioactive particles from the United States and Russian nuclear weapons testing. At the same time, **Van A. Wente** at the United States Naval Research Laboratory, the DuPont Company, and the Chemstrand Company (now Monsanto Textile Company) also started an investigation on producing micro organic fibers. During their investigation it was found that it was possible to construct a nonwoven fabric of very fine fibers for a possible use as filter media for fine aerosols [12]. This investigation eventually led the DuPont Company to market its first commercial organic mircrofiber known as **"Textryls"**, but the product was later withdrawn from the market because of an insufficient demand [9].

In the late 1960's, the **Esso Research and Engineering Company** (now **Exxon Chemical Company**) recognized the strength and potential of microfiber technology for commercial applications. The Exxon Chemical Company started developing a low-cost method of producing blown microfibers from polypropylene. After the extensive research and development based on Wente's original work on microfiber technology [13], Exxon researchers patented the blown microfiber process (usually called as melt blown process). Later, Exxon decided to license the melt blown technology to others and concentrate primarily on producing resins to supply this novel process [14].

Based on prototype demonstration of the melt blown process, Exxon negotiated several licenses with the U.S. companies. A number of companies obtained the licenses and moved quickly into commercial production. Because of the rapid commercialization of melt blown technology, Exxon needed a source of melt blown equipment. Exxon first licensed **Beloit Corporation** of Michigan, USA to manufacture complete melt blown equipment [14] and that arrangement continued for a few years. Presently, the Accurate Products Company of New Jersey, USA; Reifenhauser GmBH & Corporation of West Germany; GL&M laboratory of Gainsville, Georgia, USA; and Kasson Nozzle of Japan are licensed to manufacture melt blown production lines.

Besides Exxon's patented melt blowing process, there are other companies who have their own proprietory blown microfiber production processes, such as 3M company of USA, Biax-Fiberfilm Corporation of USA, and Freudenberg Nonwovens of West Germany. However, most of the melt blown production lines in operation today in the nonwoven industry are licensed through Exxon Chemical Company. Since the early 1970's, Exxon has become industry leader and has been continuously developing and

improving the melt blowing process and more recently, in conjunction with Tonen Petrochemical Company of Japan and The University of Tennessee.

Process Definition

In recent years, there has been considerable interest in the melt blowing process from both commercial and scientific points of view. The melt blowing process falls under the general classification of polymer laid nonwoven fabrics. The melt blowing process is defined as follows [15]:

> **It is a process in which usually a thermoplastic, fiber forming polymer is extruded through a linear die containing several hundred small orifices. Convergent streams of hot air (exiting from the top and bottom sides of the die nosepiece) rapidly attenuate the extruded polymer streams to form extremely fine diameter fibers (1-5 μm). The attenuated fibers subsequently get blown by high velocity air onto a collector screen--thus forming a fine fibered self-bonded nonwoven melt blown web.**

The fibers in the melt blown web are held together by a combination of entanglement and cohesive sticking. Because the fibers are drawn to their final diameters while still in the semi-molten state, there is no downstream method of drawing the fibers before they are deposited onto the collector, and hence the webs exhibit low to moderate strength. Examples of melt blown products in either the pure or the composite form are oil spill sorbents, wipes, surgical gowns, surgical face masks, liquid and air filtration fabrics, lithium battery separators, clothing insulation, and feminine hygiene products [13].

Process Description

The schematic of the melt blowing process is shown in Figure 2.3. A typical melt blowing process consists of the following elements: **extruder**, **metering pump**, **die assembly**, **web formation**, and **winding**.

Extruder. The polymer pellets or granules are fed into the extruder hopper. A gravity feed supplies pellets to the screw, which rotates within the heated barrel. The pellets are conveyed forward along hot walls of the barrel between the flights of the screw [16], as shown in Figure 2.4. As the polymer moves along the barrel, it melts due to the heat and friction of viscous flow and the mechanical action between the screw and barrel. The screw is divided into feed, transition, and metering zones. The feed zone preheats the polymer pellets in a deep screw channel and conveys them to the transition zone. The transition zone has a decreasing depth channel in order to compress and homogenize the melting plastic. The melted polymer is discharged to the metering zone, which serves to generate maximum pressure for pumping the molten polymer. The pressure of molten polymer is highest at this point and is controlled by the breaker plate with a screen pack placed near the screw discharge, as shown in Figure 2.4. The screen pack and breaker plate also filter out dirt and unfused polymer lumps [17]. The pressurized molten polymer is then conveyed to the metering pump.

Metering Pump. The metering pump is a positive displacement constant volume device for uniform melt delivery to the die assembly. It ensures the consistent flow of clean polymer mix under process variations in viscosity,

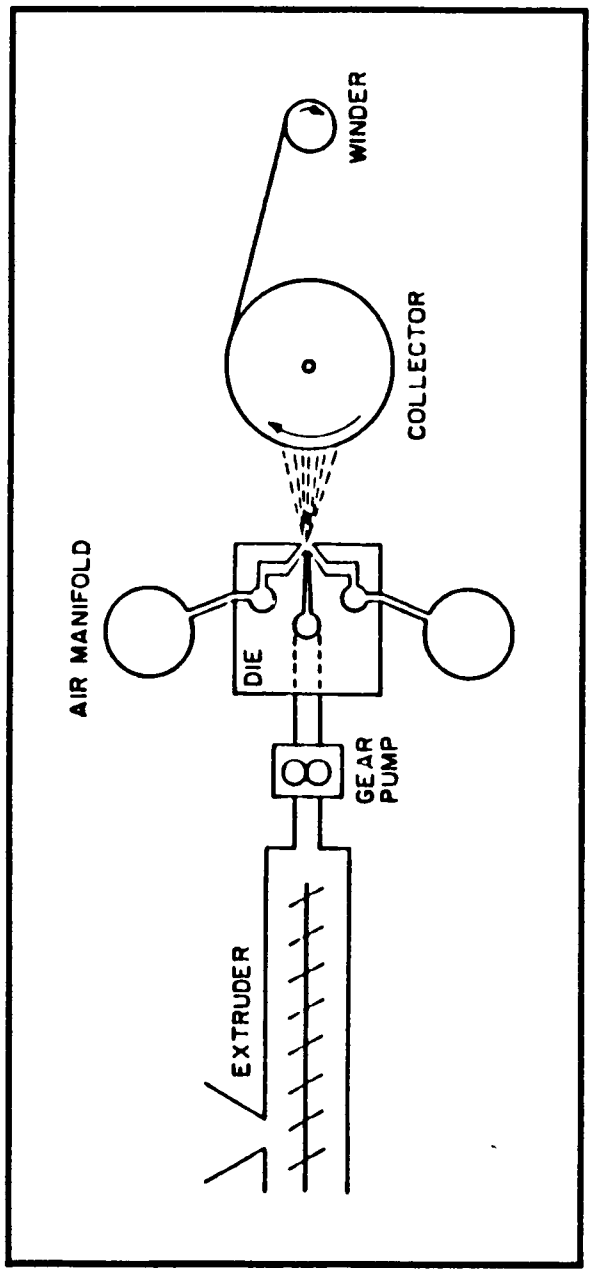

Figure 2.3. Schematic of melt blowing process.

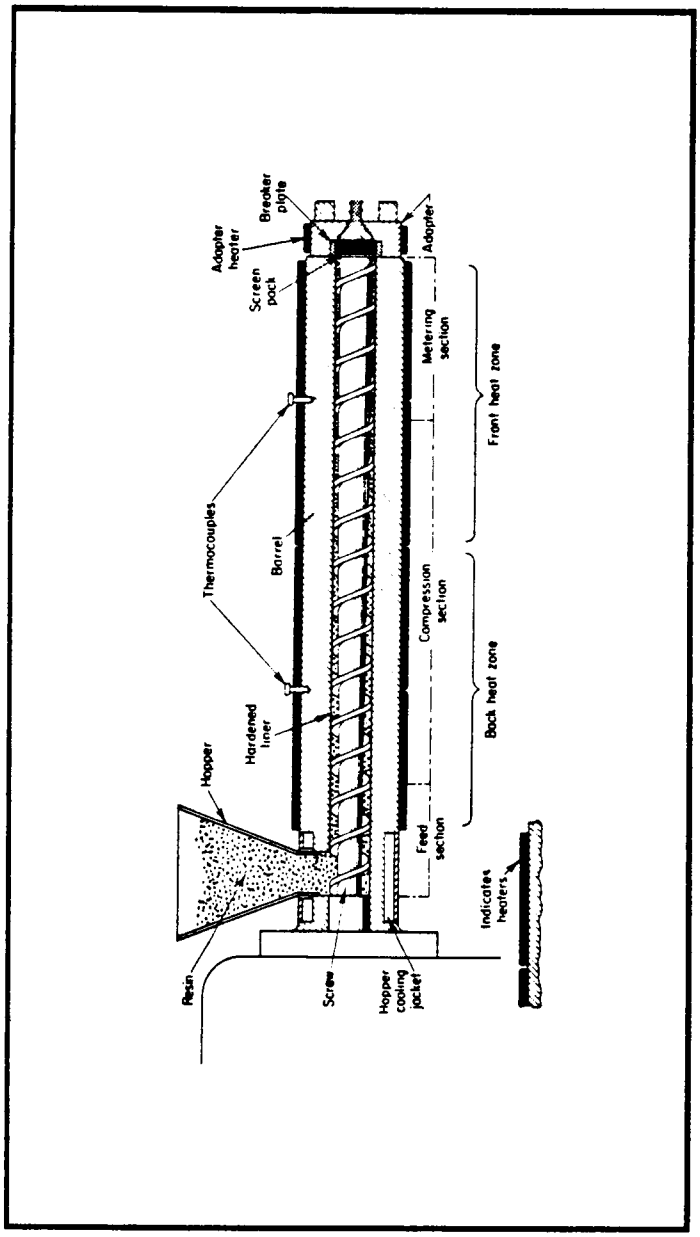

Figure 2.4. Schematic of a screw extruder.
Source: Rodriguez, F. : Principles of Polymer Engineering, McGraw Hill, New York, 1982, pp. 330-331.

pressure, and temperature. The metering pump also provides polymer metering and the required process pressure. The metering pump typically has two intermeshing, counter-rotating, teethed gears. The positive displacement is accomplished by filling each gear tooth with polymer on the suction side of the pump and carrying the polymer around to the pump discharge, as shown in Figure 2.5. The molten polymer from the gear pump goes to the feed distribution system to provide uniform flow to the die nosepiece in the die assembly (or fiber forming assembly).

Die Assembly. The die assembly is the most important element of the melt blown process. The die assembly has three distinct components: **polymer feed distribution**, **die nosepiece**, and **air manifolds**.

Polymer Feed Distribution. The feed distribution in a melt blowing die is more critical than in a film or sheeting die for two reasons. First, the melt blowing die usually has no mechanical adjustments to compensate for variations in polymer flow across the die width. Second, the process is often operated in a temperature range where thermal breakdown of polymers proceeds rapidly. The feed distribution is usually designed in such a way that the polymer distribution is less dependent on the shear sensitivity of the polymer. This feature allows the melt blowing of widely different polymeric materials with one distribution system. The feed distribution balances both the flow and the residence time across the width of the die. There are basically two types of feed distribution that have been employed in the melt blowing die: **T-type** (tappered and untappered) and **coathanger-type**. An in-depth mathematical and design description of feed distribution types is given by Matsura [18-22]. Presently, the coathanger-type feed distribution is widely used

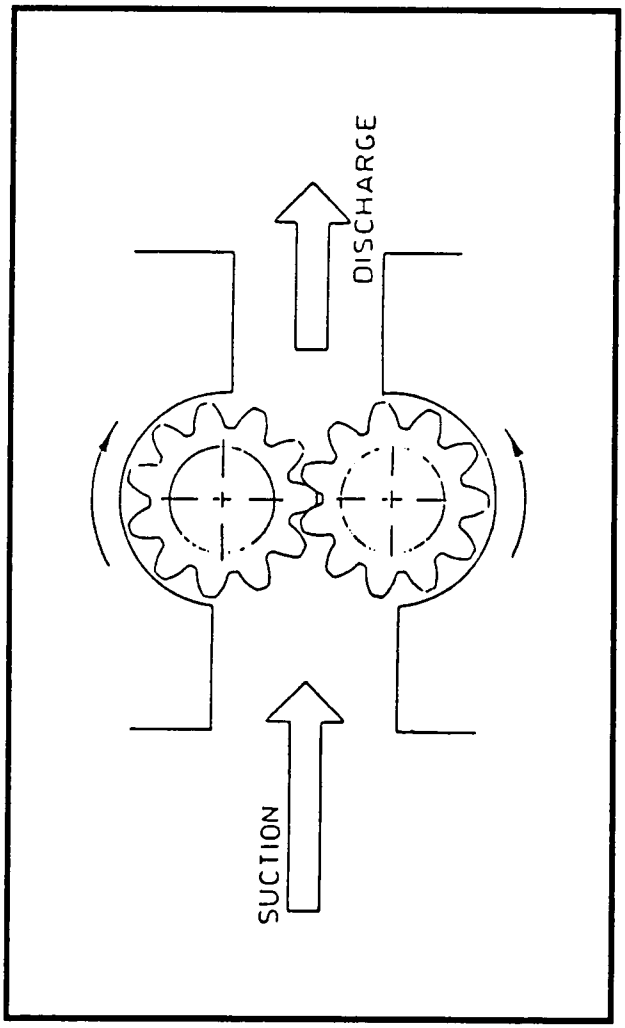

Figure 2.5. Schematic of a metering pump.

because it gives both even polymer flow and even residence time across the full width of the die.

Die Nosepiece. From the feed distribution channel the polymer melt goes directly to the die nosepiece. The die nosepiece is one of the components of the die assembly. The web uniformity hinges largely on the design and fabrication of the nosepiece. Therefore, the die nosepiece in melt blowing process requires very close tolerances, which has made their fabrication very costly. The die nosepiece is a wide and hollow, tapered piece of metal having several hundred orifices or holes across the width. The polymer melt is extruded from these holes to form filament strands which are subsequently attenuated by hot air, forming fine fibers. In a melt blowing die nosepiece, smaller orifices are usually employed than are generally used in either fiber spinning or sunbonding processes. A typical die nosepiece has approximately 0.4 mm diameter orifices spaced at 1 to 4 per milimeters (20 to 40 per linear inch).

There are two types of die nosepiece used: **capillary type** and **drilled hole type**. In the capillary type, the individual orifices are actually slots that are milled into a flat surface and then matched with identical slots milled into a mating surface. The two halves are then matched and carefully aligned to form a row of openings or holes [23], as shown in Figure 2.6. By using the capillary type, the problems associated with precise drilling of very small holes are avoided. And also, the capillary tubes can be precisely aligned so that the holes follow a straight line accurately. In the drilled hole type, very small holes are drilled by mecahnical drilling or electric discharge machining (EDM) in a single block of metal, as shown in Figure 2.6. The drilled hole type die nosepiece is widely used.

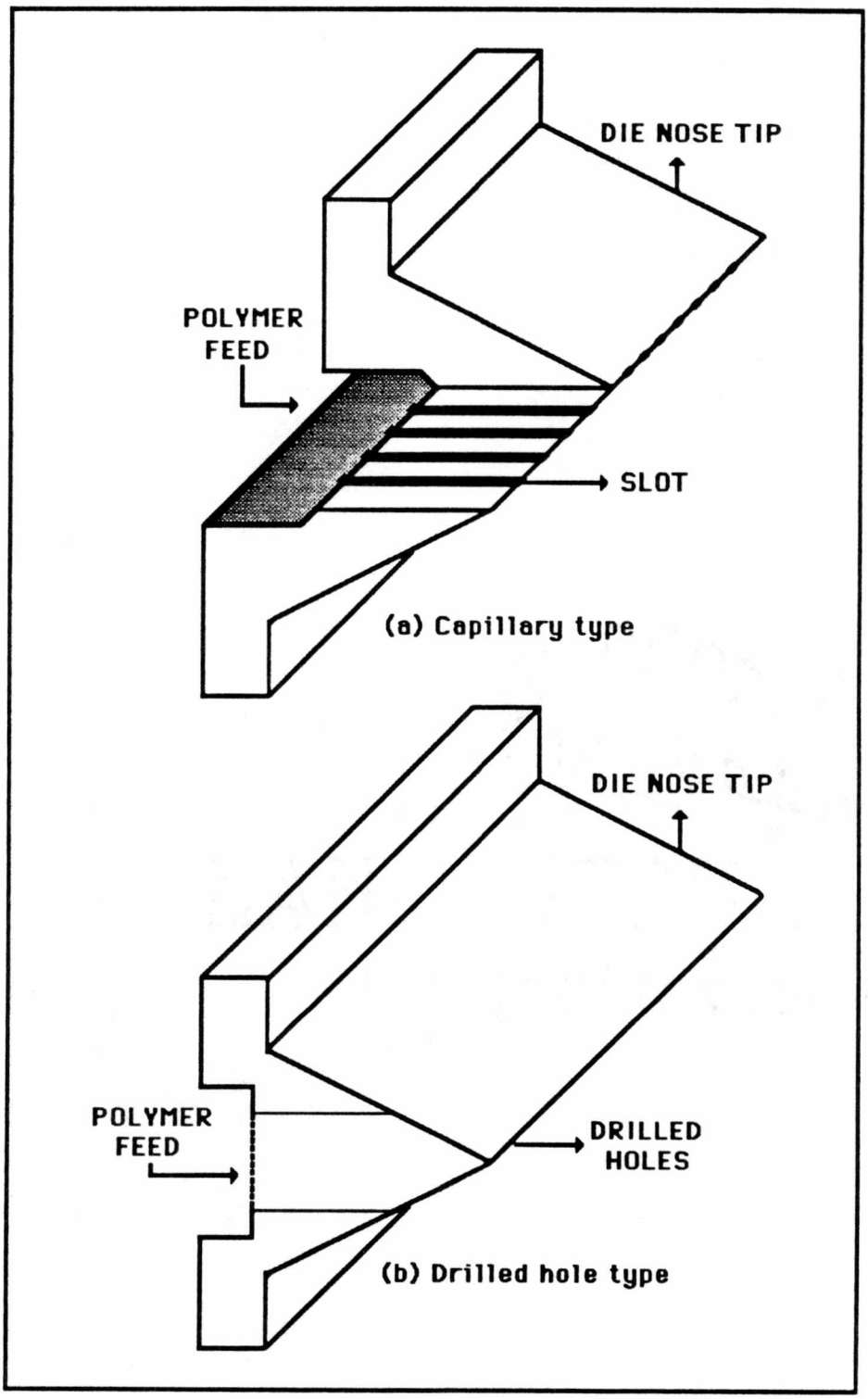

Figure 2.6. Schematic of die nosepieces.

During processing, the whole die assembly is heated sectionwise using external heaters or cartridge to attain desired processing temperatures. It is important to monitor the die temperatures closely in order to produce uniform, defect-free webs. The typical die temperatures range from 215 °C to 340 °C.

Air Manifolds. The air manifolds supply the high velocity hot air (also called as **primary air**) through the slots to the top and bottom sides of the die nosepiece, as shown in Figure 2.7. The high velocity air is generated using an air compressor. The compressed air from the compressor is passed through a heat exchange unit such as an electrically or gas heated furnace to heat the air to desired processing temperatures. The heated air is conveyed to the top and bottom air manifolds and eventually exits from the top and bottom sides of the die through narrow air gaps, as shown in Figure 2.7. Typical air temperatures range from 230 °C to 360 °C at velocities of 0.5 to 0.8 the speed of sound.

Web Formation. As soon as the molten polymer is extruded from the die holes, high velocity hot air streams (exiting from the top and bottom sides of the die nosepiece) attenuate the polymer streams to form the microfibers. As the hot air stream containing the microfibers progresses toward the collector screen, it draws a large amount of surrounding air (also called as secondary air) that cools and solidifies the fibers, as shown in Figure 2.7. The solidified fibers subsequently get laid randomly onto the collecting screen, forming a self-bonded nonwoven web. The fibers are generally laid randomly (and also highly entangled) because of the turbulence in the air stream, but there is a small bias in the machine direction due to some directionality imparted by the moving collector. The collector speed and the collector distance from the die nosepiece can be varied to produce a variety of melt blown webs. Usually, a

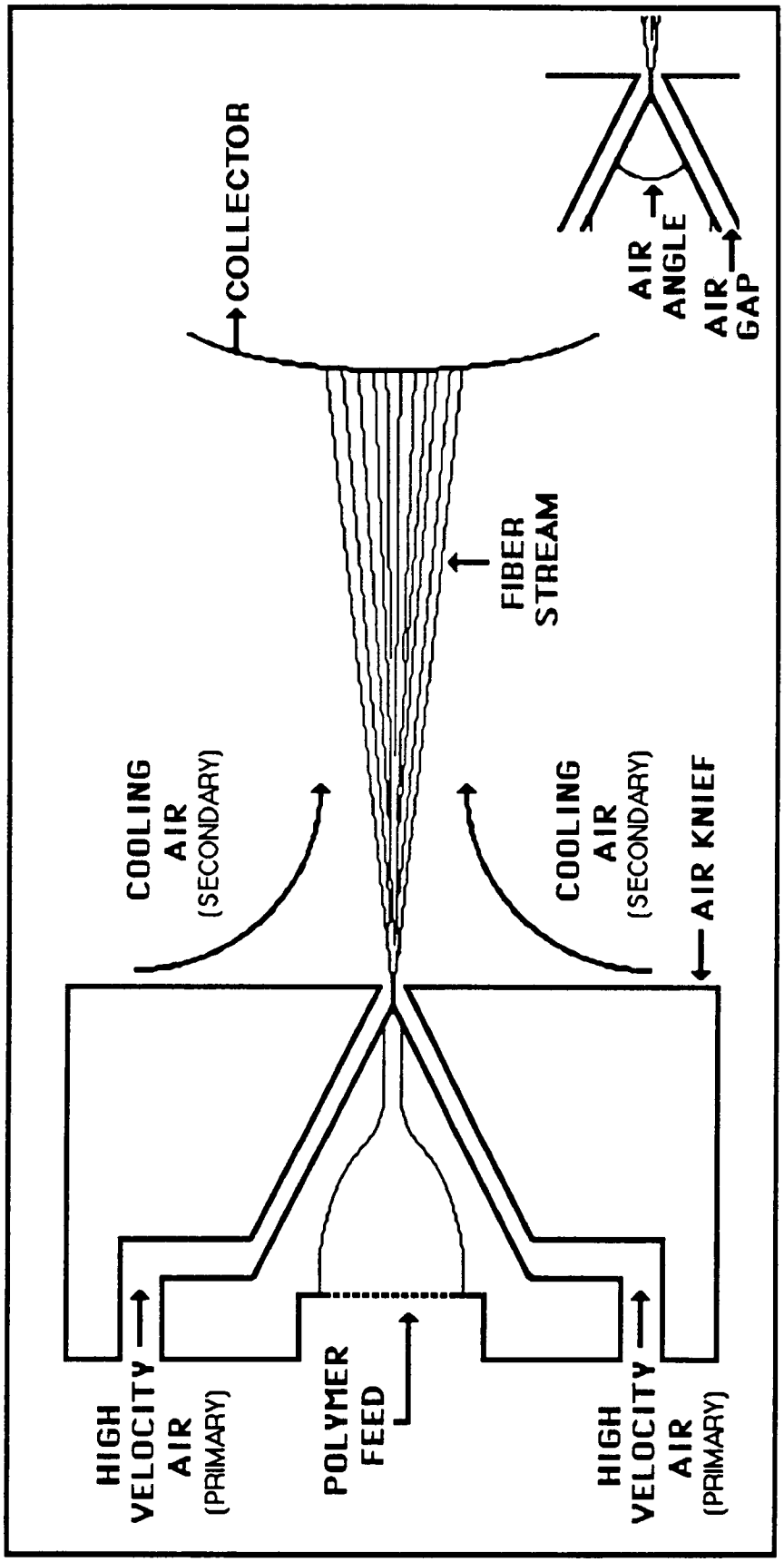

Figure 2.7. Schematic showing primary and secondary air flow and web formation.

vacuum is applied to the inside of the collector screen to suck the hot air and to enhance the fiber laying process.

Winding. The melt blown web is usually wound on a cardboard core and processed further according to the end-use requirements. The combination of fiber entanglement and fiber-to-fiber bonding generally produces enough web cohesion so that the web can be readily used without further bonding [14]. However, the webs may be subsequntly be thermally calendered with a smooth or patterned finish, or webs may be thermally laminated with other substrates.

Process Variables

The melt blowing process is quite complex and involves many operating variables. As shown in Figure 2.8, the operating variables can be divided into two categories: 1) **operational variables**, and 2) **material variables**. By manipulating the operational and the material variables one can produce a variety of melt blown fabrics with desired properties. Each of these variables plays a significant role in process economics and product reliability [24]. Therefore, it is essential that each of these variables be preciesly defined and understood in order to optimize the melt blown process.

Operational Variables. The operational variables can be classified as: a) **on-line variables**; and, b) **off-line variables**. The on-line variables are those variables which can be changed according to requirements during production, such as polymer and air throughput, polymer/die and air temperatures, die-to-collector distance, and quench environment. The off-line

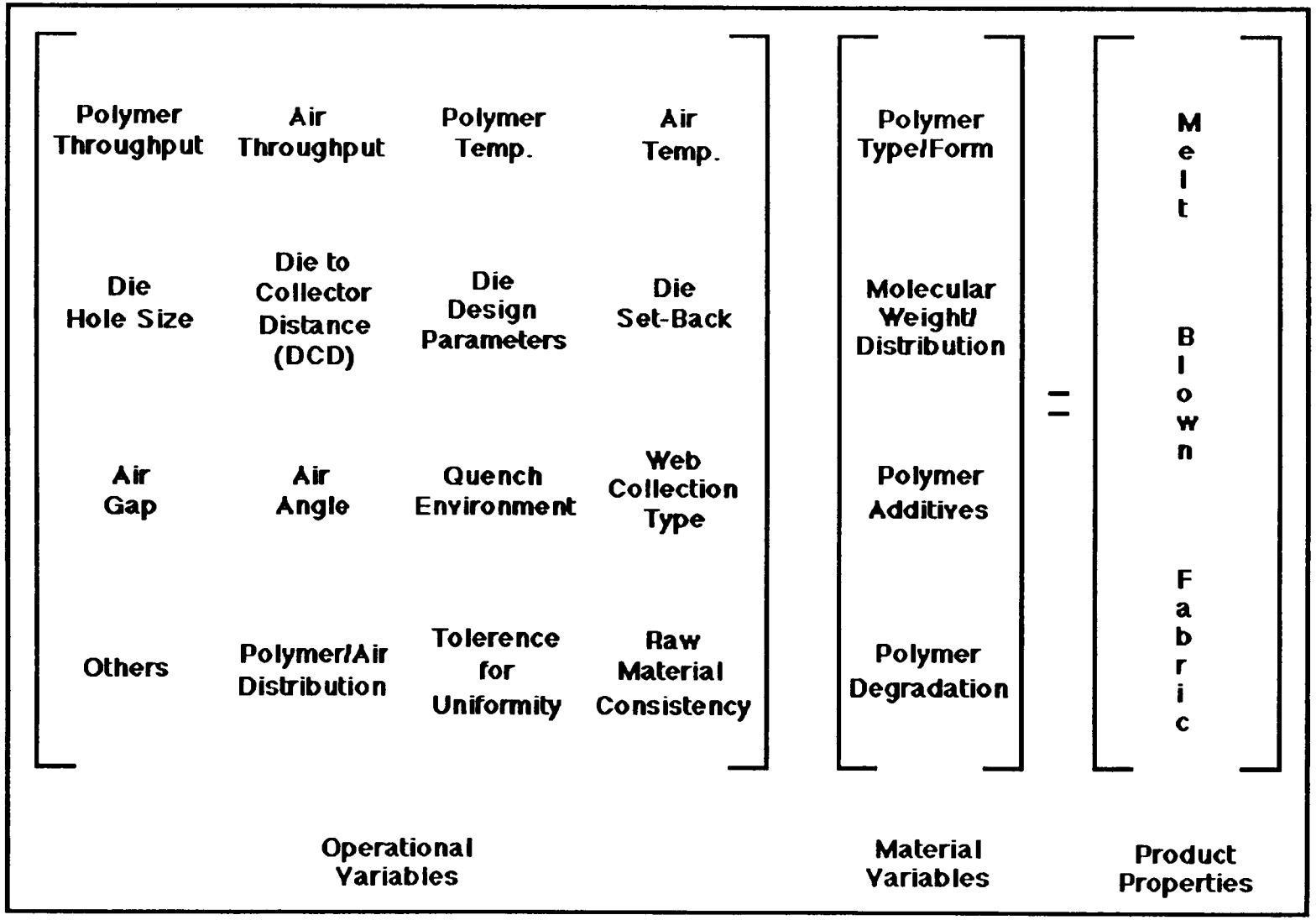

Figure 2.8. Melt blown process variables.

processing variables are those variables which can only be changed when the production line is not in operation, such as die hole size, die set-back, air gap, air angle, web collection type, and polymer/air distribution. Most of the off-line processing variables are set constant for a particular product line.

The polymer throughput rate, air throughput rate, polymer/die temperatures, air temperature, and die-to-collector distance are the five basic on-line operational variables. These variables are easy to change and dictate the major fabric properties. The polymer and air throughput rates basically control the final fiber diameter, fiber entanglements, and the extent of zone of attenuation. The polymer/die and air temperatures in conjunction with air flow rate affect the appearance and tactile hand of the fabric, fabric uniformity, and fabric defects during production, such as shot, rope, and fly formation. The die-to-collector distance generally affects the openness of the fabric and fiber-to-fiber thermal bonding.

The die hole size, die design parameters, and die set-back are believed to affect the fiber size. The die hole size should be large enough to pass the polymer melt without plugging. The back pressure generated by the polymer feed distribution type and the ratio of orifice length to diameter should be high enough to give good distibution and controllable flow of the polymer melt.

The air gap affects the air exit pressure and is also believed to affect the degree of fiber breakage. The air angle controls the nature of air flow. When the air angle approaches 90°, a high degree of fiber dispersion or turbulance results, and the most random fiber distribution is developed in the product [25]. An air angle of 30°, however, yields a high proportion of "roped" or paralleled fibers deposited as loosely coiled bundles, which are considered undesirable in a finished product. On the other hand, a 30° angle produces greater

attenuation in spite of discontinuities in the fiber length. An air angle of 60° is usually employed in the melt blowing process.

Material Variables. The material variables include polymer type, molecular weight, molecular weight distribution, polymer additives, polymer degradation, and polymer forms such as pellets or granules. One of the advantages of the melt blowing process is its ability to handle a variety of fiber forming polymers and blends of polymers [26,27]. Basically, any fiber forming polymer that can give an acceptably low melt viscosity at a suitable processing temperature and can solidify before landing on the collector screen can be melt blown into fine fibered webs [26]. A wide range of polymers have been melt blown. Polypropylene (PP) has been used predominantly in commercial production and has been thoroughly evaluated. The other successfully processed polymers are: polyesters, nylons, polyethylene, polystyrene, elastomers, ethylene copolymers, and many others.

The polymer molecular weight and molecular weight distribution (MWD) are important material variables. The melt blown process requires lower molecular weight and more narrow molecular weight distribution resins to produce uniform fine fibered webs. The polymer molecular weight is inversely proportional to the melt flow rate (MFR) and directly related to the melt viscosity. Thus, the lower the molecular weight, the higher the MFR and the lower the melt viscosity. Usually, the polyolefins such as polypropylene, polyethylene, and copolymers are designated by the MFR or MI (melt index), and the other polymers are designated by the melt viscosity or IV (intrinsic viscosity). Polypropylene and polyethylene polymers of various MFRs have been used successfully for the melt blown process. They range from 12 to 1500 MFR.

Although, the lower MFR resins result in good products, there has been a recent trend to use high MFR resins because they allow high throughput rates and much lower operating temperatures.

Polymer degradation is a helpful variable for tailoring polymer melt viscosity and MWD. There are three degradation mechanisms: chemical, mechanical shear, and thermal [28]. The controlled chemical degradation is achieved by using oxygen or peroxide additives during the melt blowing process or during an intermediate step prior to melt blowing. The mechancial shear and thermal degradation are achieved by increasing the extrusion rates and by increasing the heat and material residence time, respectively.

Status of Nonwovens Research

The nonwoven fabric industry is a relatively new field of textiles. Systematic research work on nonwoven fabrics began in the early 1950's when Cox [29], proposed a fiber-web theroy for the analysis of fibrous materials. Since then, a number of research studies have been published covering various aspects of nonwoven fabric technology. The published studies are a good blend of theoretical and experimental concepts. The most comprehensive treatments on the fundamentals of the nonwoven fabrics have been given by Brandt [30], Krama [1], Buresh [31], Hearle [6], and more recently by Lunenschloss and Albrecht [32].

Until the late 1960's, most of the nonwoven fabric research activities were based on the dry-laid adhesive bonded fabrics. A number of studies have been published concerning the structural and mechanical behavior of adhesive bonded nonwoven fabrics. In the late 1960's, due to the development of many

new manufacturing processes such as spunbonding, melt blowing, needle punching, and hydro-entanglement, the research activities were diverted to these new areas of nonwovens.

Melt Blowing

Despite the extensive research and development in the area of melt blowing, there is a paucity of published research studies mainly due to the secretive and competitive nature of the research and developmental work. However, there is a large body of patented literature available based on process enhancement and product development studies. An in-depth review of patents on the melt blowing process is given by Moore [33].

There are about twenty published research studies on the melt blowing process based on processing science. Also, theoretical concepts are being applied to the melt blowing process. The following is a review of literature on melt blowing. Due to the limited published studies, it was not possible to group the studies according to their specific findings. Therefore, each study is reviewed individually.

Wente and co-workers [25,34] first established the feasability of manufacturing submicron fibers from a variety of thermoplastic polymeric materials. The main objective of the study was to design an apparatus that would produce submicron fibers. It was thought that a nonwoven material composed entirely of submicron fibers would have great usefulness for aerosol filtration as well as for dielectric insulation. The study is thorough in its nature and describes the various aspects of the melt blown process ranging from

equipment design to the single fiber properties of a web. The major findings of the study were as follows:

- Fiber diameter is a function of air temperature, die temperature, air pressure, and polymer feed rate.
- Since the molten polymer issues from the die nose tip direclty into the confluence of the air streams, the greatest amount of attenuation occurs at the point of exit. Thus, the orifice size has little importance provided it is large enough to pass the melt without plugging.
- A steeper air angle gives a higher degree of fiber dispersion and random orientation. A slander air angle yields a greater number of parellel fibers, greater attenuation, and less fiber breakage.
- The ability of a polymer to attenuate to a fine fiber is dependent on its melting point, viscosity-temperature characteristics, and surface tension.
- The air resistance through a web is related to fiber diameter by the following expression:

$$\text{Resistance} = C / (\text{fiber diameter})^2$$

  where C is a constant whose value depends in part upon the porosity or density of the fiber mat.
- Below a certain melt temperature a given thermoplastic polymer forms a large granule of non-fibrous material called "shot."
- High air pressure generally yields uniform and shot free fibers but, at the same time, make difficult the separation of fiber and air because of the excess volume of the fibers.
- The melt blown webs derive their strength from mechanical entanglement and frictional forces.
- The unbonded webs acquire tensile strength rapidly as fiber diameter is decreased.

Buntin and Lohkamp [26], have described the development of the melt blowing process for converting polypropylene into low-cost fine fibrous webs. Two process design concepts of using multiple dies and a circular die were also discussed. The study found that, by using multiple dies, high production rates can be achieved without increasing polymer throughput rates above the optimum. Multiple dies also produced more uniform webs with less fabric defects. The main disadvantage of the multiple dies operation was that for heavy basis weight the bonding between layers was found to be unsatisfactory. In a circular die, a die with the orifices in a circle was used. The die was operated in such a way that the conical fiber blast from the orifices was focused roughly on a point where the fibers were formed into a continuous cylindrical roving. The technique was studied to make fine fibered cigarette filters.

Buntin and Lohkamp also made the following qualitative observations based on the processing of different thermoplastic polymers:

- Polyethylene was more difficult to melt blow into fine fibered web than polypropylene.
- Nylon 6 was easy to process and had less tendency to make shot than in the case of polypropylene.
- Most of the thermoplastics can be melt blown sucessfully into good finished products with few exceptions.

Jones [35], reported the effects of resin melt flow rate and polydispersity on the mechanical properties of the melt blown webs. The research was focused on the optimization of the process variables, particularly the extruder temperatures, in order to enhance the fabric properties. Several experimental resins with different melt flow rates and varying polydispersity indexes were melt blown under various conditions. In general, it was found that the strength

properties peaked with the melt flow rate of 300 and decreased as the melt flow rate increased significantly above that. The fabric strength was believed to be a combination of individual fiber strength and good thermal bonding and/or fiber entanglements.

Jones reported that the change in polydispersity of the polymers did not appreciably affect the mechanical properties. Only a slight downward trend of the fabric strength with increased degrees of polydispersity was observed. The elongation decreased with increased molecular weight distribution. The decrease in elongation was attributed to the larger diameter fibers and fewer fiber entanglements resulting from higher die swell of the broad molecular weight distribution resins.

Finally, the study showed that the effects of varying extruder temperatures and throughput rate on the strength properties were readily evident. The decreased extruder temperatures increased tenacity and bursting strength. The increased throughput rate decreased the bursting strength.

Wadsworth and Jones [36, 37] demonstrated the effects of die-to-collector distances, polymer throughput rates, and die orifice diameters on melt blown fabric properties. The study found that machine direction (MD) tenacity decreased with increased die-to-collector distance; whereas, the cross direction (CD) tenacity and bursting strength remained relatively constant. Fiber diameters increased slightly with increased die-to-collector distance. The MD tenacity increased with increased polymer throughput rates at corresponding collecting diatances. On the other hand, the CD tenacity changed little.

The study also showed that bursting strength decreased with increased throughput rates. The webs produced with the small orifice die were found to have slightly larger fiber diameters than the webs produced with standard

orifice die. It was hypothesized that greater die swell could have occured with small orifice die resulting in a net increase in filament diameter compared to the standard orifice die.

Eaton et al. [38], studied the effects of pigments on the physical properties of melt blown nonwovens. The objective of the work was to demonstrate the feasability of processing pigmented resins into melt blown webs. Different melt flow rate pigmented polypropylene resins were melt blown under different processing conditions. The physical properties of pigmented webs were compared with the properties of unpigmented webs. The study found that melt blown webs of uniform coloration were readily obtainable by the mass pigmentation of polypropylene resins. It was believed that the pigments acted as nucleating agents in the high melt flow rate (MFR) resins that were melt blown. The average fiber diameter decreased slightly with increased MFR for both pigmented and unpigmented webs. The apparent colors of the webs became lighter with increased resin MFR. This effect was attributed to the increased ratio of fiber surface area to the amount of pigment resulting with the finer fibers produced with the higher MFR resins. The photomicrogaphs showed no notable differences between the pigmented and unpigmented webs in terms of fiber and web structure. The pigmented webs generally exhibited higher stiffness than the unpigmented webs.

Eaton, Wadsworth and Potnis [39] studied the suitability of melt blown fabrics for healthcare applications. The study suggested that the process parameters could be carefully controlled to produce webs with physical properties designed to meet healthcare end-use requirements. The study found that the mean fiber diameters may be largely controlled by adjusting polymer throughput and air rates. Fabric flexural rigidity provided a good indication of

softness for optimized melt blown webs. In coarse, non-optimized webs, a high degree of fiber bunching was observed and there was poor agreement between tactile hand and flexural rigidity.

Wadsworth and Muschelewicz [40] reported the results of a study designed to produce extremely fine melt blown fibers using 35, 300 and 700 MFR resins. The study established the optimized melt blown processing conditions to produce fine fibered webs, with less than 2 μm fiber diameters. The study found that the small orifice die (with orifice diameter in the range of 0.2-0.3 mm) resulted in statistically smaller mean fiber diameters than the die with standard size orifices (approximately 0.4 mm diameter orifices). However, the actual difference was found to be minimal, considering the fact that the cross-sectional areas of the small die holes differed by a factor of greater thant two. The study also reported that increased air flow rates decreased mean fiber diameters. The air gap settings did not have any noticeable effects except that much larger diameters were obtained with the standard die tip and the smaller air gap setting with 300 and 700 MFR resins. Notably higher bursting strength values were achieved with the small die holes, indicating increased fiber strength with greater draw-down.

Wadsworth et al. [41] studied the relationships among the processing conditions, structure, and filtration efficiency of polypropylene melt blown webs. The structure of the melt blown webs was varied using different die-to-collector distances and smooth roll thermal calendering. The study found that the air permeability, and mean and maximum pore sizes increased with increased die-to-collector distance. The filtration efficiencies for water aerosols containing 0.5 and 0.8 μm latex spheres, and for bacteria (Staphylococcus aureus) were found to be dependent on mean pore diameter and the parameter of basis weight

divided by the square of the average fiber diameter. The calendering process decreased the web thickness, maximum pore diameter, and air permeability regardless of the original values.

Choi et al. [42], studied the strength properties of the melt blown webs. A method to obtain the tenacity and Young's modulus of melt blown webs without direct measurement of web thickness was proposed and tested using several series of web samples with different basis weight. The web tenacity and Young's modulus, which were, of course, normalized for weight, were found to be nearly independent of basis weight and gage length. However, these properties were greatly affected by the processing conditions. Tencity and Young's modulus decreased with increased die temperature, air pressure at the die, and die-to-collector distance.

Choi and co-workers also measured and compared the strength properties of single melt blown fibers with the strength of the web and the high-speed melt spun filaments prepared from the same resins. Single fiber strength tended to be intermediate between the strength of the web and that of the high-speed melt spun filaments. The low strength of the single fiber was attributed to low molecular orientation, irregular diameter profiles along the length of the fibers, and the existence of voids in the fibers.

Malkan et al. [15] reported the effects of increasing the throughput rate of polypropylene resins (300 and 1400 MFR) while maintaining constant air flow rate on the morphological and physical properties of the melt blown fibers and webs. It was found that as the throughput rate increased web elongation and bursting strength decreased. This decrease in web properties was attributed to more thermal fusing of the fibers and the presence of a greater number of larger diameter fibers.

Differential Scanning Calorimetry and X-ray diffraction studies on the web samples produced at high throughput rates in the above study indicated the presence of more than one morphological form of a single crystal structure. It is believed that this may be a significant finding that could have an important bearing on the understanding of the melt blown process.

Bodaghi [43] also reported many melt blown microfiber characterization techniques. The major finding of the study was that the water-quenched polypropylene fibers showed para-crystalline crystal structure. The air-quenched fibers showed regular monoclinic crystal structure.

Narasimhan and Shambaugh [44] attempted to model the melt blowing process. The study was based on a single die hole melt blowing process, with a circular air slot surrounding the melt blown spinnerette nozzle. Narasimhan and Shambaughs' process did not simulate the most commonly used melt blown die geometry, which consists of a row of spinnerette with sheets of hot air exiting from top and bottom sides of the die. Moreover, the study lacked specific exlanations of the modelling process and concepts involved.

Shambaugh continued this study [45, 46] and applied macroscopic energy balance and dimensional analysis concepts to the melt blowing process. These two concepts were analyzed using different die geometries. Shambaugh proposed the existence of three regions of operation for the melt blowing process. The three regions were classified according to the extent of the air flow rate as:

> Region I -- is the low gas velocity region, similar to the commercial melt spinning operation insofar as the fibers are continuous.

Region II -- is the unstable region, which occurs as the gas velocity is increased. In this region filaments break up into fiber segments and undesirable lumps.
Region III -- occurs at a very high air velocity with excessive fiber breakages.

Shambaugh concluded that the operation of the melt blown process using predominately the low air rate (region I) was inherently more energy efficient. Further, the author claimed that the monodisperse fiber distribution required less energy to produce than polydisperse fiber distribution. The dominant dimensionless groups in the melt blowing process were the gas Reynolds number, the polymer Reynolds number, fiber attenuation, and the ratio of the polymer viscosity to the gas viscosity.

Milligan and Haynes [47] studied the air drag on monofilament fibers. The aim was to study the air drag by simulating the actual melt blowing conditions. The experimental set-up closely simulated the actual melt blowing operation. The two differences between the experimental arrangement and actual arrangement were: cold air was used instead of hot, and a solid monofilament was fixed on one end to a tensiometer. The air drag was studied as a function of fiber length , upstream stagnation pressure, air injection angle, and gravity orientation. Four series of experiments were conducted as follows:

1. Determination of air drag for a fiber of constant length over a range of air stagnation pressures.
2. Determinatin of air drag for a range of fiber length at a constant value of stagnation pressure.
3. Determination of air drag for a fiber of known length and stagnation pressure using different injection angles (15°, 30°, and 45°).

4. Determination of air drag by changing the die orientation, with respect to gravity, using a 30° air injection angle with different fiber length and stagnation pressures.

The study concluded the following:

- The drag increased with fiber length when all other parameters were constant. The drag peaked at the length of 2.5 cm. This was due to large amplitude flapping of the fiber.
- The drag increased linearly with stagnation pressure for stagnation pressure up to 207 kPa.
- The drag increased with decreased air injection angle for any particular stagnation pressure. This finding was in basic agreement with the fundamental momentum consideration.
- Orientation of the die with respect to gravity using an injection angle of 30° (45° above the horizontal to 90° below the horizontal) showed no measureable difference in drag. It was concluded that the viscous and pressure forces on the filament far exceed the gravitational force for the flow conditions investigated.

Milligan [48] has analyzed several design concepts to minimize the energy cost in the melt blowing process. The study found that the pressure losses associated with air piping and the air heater were two of the principal energy cost areas. Several design rules have been presented to minimize the air cost. The design rules were developed using the Darcy pressure drop relationship as shown below:

$$\Delta P = \rho \frac{fv^2}{d}$$

The design rules are summarized as follows:

1. The piping between the air compressor and die assembly should be as short in length and as large in diameter as feasible.
2. The air heater should be as close as possible to the die assembly.
3. The number of pipe fittings should be minimized, and all piping should be well insulated.

The study also described the importance of the correct sizing of a compressor intended to serve a melt blown pilot line. The author derived equations to estimate the energy cost for a required air flow rate and discharge pressure. It was stated that, if a compressor operated at less than its designed or rated capacity, the energy cost per unit of air compressed would be increased. This increased cost was due to the fact that when the compressor was unloaded it still required a significant fraction of the rated power. Therefore, the required air flow rate and discharge pressure should be carefully established before preparing specifications for the air compressor.

Milligan, Wadsworth, and Cheng [49] investigated the energy requirements for the melt blowing of different polymers. The studied polymers were: polypropylene, linear low-density polyethylene, nylon and polyester. The energy requirements were reported in kW-HR per kg of polymer. It was apparent from the reported data that the energy cost per unit mass of the product greatly depended on the air flow rate, air temperature, polymer throughput rate, and polymer molecular weight. The results also showed that a large fraction (greater than 85% for all the materials investigated) of the energy required was associated with the hot air streams. The study also found that the difference in total energy consumed and the actual energy required at the die

can be attributed to improper compressor size, compressor cooling, and heat losses from the die and piping. The study suggested that substantially lower energy consumption is possible if a melt blowing line is carefully designed and operated with an objective of minimizing energy consumption.

Mechanical Properties of Nonwovens

The mechanical properties of nonwoven fabrics are largely dependent on fiber properties, orientation of fibers in the web, the type of bonding, and finishing treatments. Nummerous studies have been conducted on the mechanical properties of nonwoven fabrics with particular emphasis on tensile properties [50 - 62]. However, the other properties, such as bending and shear deformation, have also been studied to a limited extent. The following is a general review of some of the most important studies on mechanical properties of nonwoven fabrics.

Cusick et al. [63] compared the physical properties of several commercial nonwoven materials to woven fabrics. The nonwoven fabrics examined represented a variety of fiber types, web formation techniques, and binder types. The study found that the nonwoven fabrics had higher bending lengths and higher drape coefficient values than woven fabrics. The higher stiffness of a nonwoven fabric was considered the primary problem in replacing woven fabrics for apparel applications. The nonwovens displayed lower rupture strength and modulus. Anisotropy of fabrics was measured as the ratio of strength or modulus in the machine direction to the corresponding value in the cross-direction. The modulus anisotropies were higher and more variable than the strength anisotropies.

Theoretical analysis of the mechanics of a material may be based on either on a consideration of the forces involved or on a consideration of energy relations. In general, the analysis of forces has yielded more detailed information, especially on internal forces in the structure, but the energy method is simpler and can be applied to more complicated problems. The fiber network theory of Hearle and Newton [64] is the most successful attempt to predict mechanical responses of nonwovens by stress analysis; and their study [65] by energy analysis is simpler and also successful.

Petterson and Backer [66] stated that an ideal nonwoven structure would be one in which all components (fiber, binder, and geometry) are fully utilized. In a comparable study of synthetic fiber papers, Hentschel [67] stated that the physical properties of a sheet will be determined by the properties of the binder, strength proeprties of the fiber and structural arrangement of the fibers and binder. Petterson [68, 69] considered nonwovens as orthotropic materials. Petterson developed a fiber network theory in which the nonwoven fabric was treated as build-up of a series of unit cells. The unit cells were defined in such a way that the boundaries move in parallel under uniaxial stress. The tensile properties were predicted from the orientation and stress-strain properties of fibers in the unit cell. The unit cell was assumed to be large enough to allow each fiber to have a sufficient number of bonds to obviate any local variations in strain. Thus, the average strain developed in each fiber could be approximated by the strain that fiber would have if it were bonded only at the boundaries of the unit cell. The study was based on the following assumptions:

- Fiber deformation was Hookean until rupture.
- Fiber segments between bonds were considered straight.
- Bonds were inextensible and stronger than the fibers.

Petterson extended this theory and derived the stress-strain properties of nonwoven fabrics in different loading directions. The theory agreed well with the results of a wet laid viscose rayon web. This good agreement was mainly due to the straight fibers in wet laid fabrics. For a typical dry laid nonwoven, however, the prediction of initial modulus was higher by one order of magnitude. This was because of crimped fibers in dry laid nonwovens.

It is generally agreed that the assumption of straight fibers in nonwovens is not justifiable. Hearle and Stevenson [70] recognized this point and introduced a fiber curl factor in Petterson's fiber network theory, with following assumptions:

- Bond-to-bond distance is constant.
- Bond is at least as strong as the fiber.
- All of the fiber curl is allowed to be taken-up, and this operation is accompanied by a force that is negligible compared with that required to stretch the fiber.
- The extension of the binder at a bonding point is ignored.

Hearle [70] predicted the stress-strain properties using this new theory. The study found that the fiber curl factor applied to the theory improved agreement with actual results for extension up to 2%, beyond which the calculated stresses were greater. They also recognized that the contribution of binder had been ignored in studies of the fiber network. It was pointed out that bond failure and fiber slippage through the bonds occurs prior to fiber rupture. Allowances for bond failure were made by limiting fiber stress values in calculating the shape of the stress-strain curve. Hearle and Newton [70] further developed this concept of fiber stress limits for predicting tensile properties. The agreement

between theoretical and actual measurements was illustrated using several commercial nonwoven fabrics. Olson and Freeston [71] extended the Petterson's fiber network theory from two dimensional to three dimensional nonwoven fabrics in which cube shaped unit cells were considered.

The bending rigidity of nonwoven fabrics has been analyzed theoretically by Freeston and Platt [72], and Tayebi et al. [73]. They analyzed two cases: complete freedom and no freedom of relative fiber motion. They applied unit cell concept of Petterson's fiber network theory [68]. The study concluded that the bending rigidity can be predicted more closely by assuming no freedom of relative fiber motion. The study suggested three methods to improve nonwoven flexilbility: 1) placement of the fibers in the fabrics darting back and forth between the two surfaces and bonding only at the mid-plane; 2) increasing the distance between bond points; and 3) using binders with improved mechanical properties, i.e. with lower modulus and high elastic recovery.

Lee and Argon [73- 77] studied the mechanics of bending of spunbonded and print bonded fabrics. An analytical model, based on the structural features and using a composite materials approach, was employed to interpret the experimental measurements of the bending stiffness of the fabrics. The study concluded the following:

- Self-bonded nonwoven fabrics, requiring fiber segments to be strained in tension and compression when the fabric is bent, have quasi-continum properties and hence possess relatively high bending stiffness.
- Relative fiber motion is essential to impart flexibility to a fabric.
- In spot bonded nonwovens, optimum bending flexibility can be obtained for fabrics of a given diameter by incorporating some

crimp that gives then high effective axial extennsibility and considerable freedom of relative fiber motion.

- The experimental results coupled with the analytical model indicated that fabric bending flexibility requires: a) as much freedom of relative fiber motion as possible; and b) an optimum binder application not greater than what is necessary to keep the tensile properties within the desired range.
- The grouping of the fibers in the fabric into straight and severely curved ones permits freedom of relative fiber motion among curved fibers and requires only the straight fibers to resist the bending moment.

Failure Modes of Nonwovens

Nonwoven failure modes have been observed by many researchers. Most of the studies have been based on dry laid adhesive bonded fabrics. Recently, spunbonded and other types of nonwovens have also been studied. Thus far no studies have been published assessing the failure modes of melt blown fabrics. The following is a review on failure modes of nonwoven fabrics.

Tikhmirov [78] suggested three possible failure modes of nonwoven fabrics: 1) fiber breakage; 2) cohesive failure; and 3) interfacial failure of bonds between adhesive and fiber surface. The later is possible if fiber strength and cohesion of the adhesive are higher then the adhesion forces. Tikhmirov also suggested that the failure mechanism is mainly dependent upon the fiber properties, the binder properties, and the amount of binder. In spunbonded fabrics, the number of fiber-to-fiber bonds is an important factor.

Hearle [79] studied the deformation of nonwovens using scanning electron microscope techniques. Hearle observed that the binder failure was the mechanism of fabric rupture for adhesive bonded fabrics. Hearle and

Newton [80] also studied the bonding of fibers. The study determined that failure occured at the binder fiber interface or in the fiber. Binder rupture was not observed. Oszanlav [81] found that failure was invariably due to the breakdown of the binder component. Bond failure started at an early stage of the uniaxial deformation and increased progressively towards the fabric rupture point. No correlation was found between single bond strength and nonwoven web strength. However, Fredrick [82] indicated that the fabric breakdown was the result of fiber rupture.

Hubbell and Whitwell [83] studied the bonds of rayon and polyester fibers with vinyon and low melting polyester fibers as binder. The study found that the interfacial failure mechanism predominated, due to poor bonding between the base fiber and the binder fiber. The poor bond eventually promoted slippage and hence failure at the interface. The study also suggested that the physical entrapment of the base fibers by the binder fibers was the mechanism of bonding in this type of fiber/binder system.

Winchester and Whitwell [84, 85] defined three types of stress-strain curves with corresponding characteristic mechanisms of failure for nonwovens. The three types of curves are as follows:

- A type I curve was obtained from a poorly bonded web. The web exhibited low modulus, low tenacity, and high elongation. The web was very bulky and flexible. The test specimens from this type of web failed primarily as a result of fiber dis-entanglement and slippage within a large, ill-defined, but restricted region.
- A type II curve was obtained from a moderately bonded web. The web exhibited high modulus, tenacity, and elongation. The failure occured largely as a result of a combination of bond and

fiber breakge after the entire specimen had been considerably extended.

- A type III curve was obtained from strongly bonded web. The web exhibited a very high modulus, tenacity, and low elongation. The web was very stiff and had a high density. The failure occurred at a fairly well defined and restricted location. The failure was almost entirely due to fiber breakge originating at a weak point in the structure and propagating rapidly across the specimen.

Tikhmirov and Gusev [86] introduced the concept of "critical area of contact." The concept stated that the area of contact between the binder and the fiber at which the strength of the fiber-binder bond is equal to the strength of a single fiber. When the sum of the bond strengths along a single fiber is larger than the strength of the fibers, then fiber rupture occurs. Kallmes [87] introduced the concept of "critical degree of bonding," to represent the degree of bonding below which the web failure is increased by bond failure, and above which it is induced by fiber failure.

Vaughn and Brannon [88] studied the dynamics of the nonwoven deformation process. Failure mechanisms of fabrics made using three types of binders (soft, medium, and hard) were studied. The failure mechanism was highly dependent on the binder type. For the hard binder type webs, the fibers bent towards the bond axis during the initial defromation; the fibers stretched and the bonds remained rigid and cracked during the propagation stage; and, the fibers ruptured as the bonds ruptured from the bond edge and then peeld off from the fiber surface at failure. For the soft binder type webs, the bond rotated and deformed during initial deromation; the bonds stretched away from the fibers to initiate some holes during the propagation stage; and the bonds

ruptured and fibers separated from the binder at failure. For the medium binder type webs, the bonds ruptured from the bond edge and peeled off from the the fiber surface at failure.

According to Bikerman [89] and Kaeble [90], with the soft binder in the nonwovens, the rupture mechanism of the soft binder type nonwovens is mainly due to binder failure even at high binder content. This is due to the weak binder strength, low modulus, and high peel strength between binder and fiber. The rupture of a nonwoven web with a hard binder is caused by interfacial failure at lower binder content because of low peel strength and thin bonding. However, fiber failure occurs at high binder content due to the thick binder volume at fiber entanglements and high bond strength.

Polypropylene

The properties of steroregular polypropylene--more specifically, isotactic polypropylene--made it evident that this material offered vast possibilities in plastic industries as well as in melt blown fiber production. In the past thirty years, many research studies have been published concerning the structural characterstics of polypropylene, including specification of its molecular conformation and its various polymorhic forms.

Polypropylene is usually polymerized in one of the three different tacticities -- **isotactic**, **syndiaotactic**, and **atactic**. The isotactic and syndiotactic forms of polypropylene are partially crystalline, where the atactic form is necessarily amorphous, due to the lack of stereo-regularity along the molecule. Most commercial polypropylene resins are highly isotactic with a

high degree of crystallinity. The isotactic polypropylene is of particular interest in this research.

Polypropylene Crystalline Forms

Isotactic polypropylene is known to exhibit as many as four different crystalline forms: the **α-form**, which is **monoclinic** and generally the most predominant; the **β-form**, which is **hexagonal**; the **γ-form**, which is **triclinic**; and, the smectic form, which is believed to be associated with the amorphous phase. The development of various forms is dependent on the degree of isotacticity, molecular weights, and thermal and mechanical history of the specimen.

The α-form is the crystal form commonly observed when the isotactic polypropylene is crystallized form the melt [91]. X-ray diffraction studies on the α-form polypropylene by Natta and Corradini [92], established the monoclinic symmertry for the unit cell with following lattice constnat values:

$a = 6.65 \pm 0.05$ Å $b = 20.96 \pm 0.15$ Å

$c = 6.50 \pm 0.04$ Å $\beta = 99° 20' \pm 1°$

The identity period along the c-axis was found to be 6.5 Å, indicating the presence of a three-fold helical conformation of the molecules. The crystal lattice was found to be centered with the most probable space group C_c.

Hikosaka and Seto [93] and Corradini et al. [94] have stated that the α-modification of isotactic polypropylene may show various degrees of disorder in the up and down positioning of the chains. The degrees of disorder were assessed as: a) the limiting ordered structure, called as α2; and b) the limiting disordered structure, called as α1. It was also proposed that the presence of

two endothermic peaks in the calorimetric scan could be related to the melting of crystals having a structure closer to that of the α1-modification and to the melting of crystals having a structure closer to that of the α2-modification.

The β-form of polypropylene was first reported by Keith et al. [95]. Their study suggested that the β-form had the hexagonal unit cell, with following the lattice constant values:

$a = 12.71$ Å $\qquad\qquad$ $c = 6.35$ Å

Turner et al. [96] obtained the β-form by rapidly quenching the polypropylene melt to below 130°C. Addink and Beintema [97] observed the β-form in fractions with a high degree of isotacticity. The β-form is considered to be meta-stable in character and by recrystallization or deformation converts to an α-form. Lovinger et al. [98] stated that the β-form polypropylene obtained at a heating rate of 1°C/min using the DSC, showed the actual melting and recrystallization of the β-spherulites into the α-form.

The γ-form was discovered upon cooling fractionated polypropylene from the melt, as reported by Turner [96] and Sauer et al. [99]. Usually, the γ-form is present in small amounts. It is characterized by the presence of five strong x-ray diffraction peaks. Four of these peaks lie very close to four of the five peaks of the α-form. Kardos [100] reported the crystallization of the whole poylmer to the γ-form, when melts were solidified under pressure.

Natta and Corradini [92] reported the existence of a smectic phase when molten polymer was quenched in water. X-ray studies of the smectic form revealed two strong halos with d-spacings of 5.9 Å. Several investigators [101 - 104] suggested structural interpretations for the smectic form. They stated that the smectic form had a short range three-dimensional order with the molecular conformation being the same as the crystalline α-form. Several investigators

[105 - 107] also suggested a hexagonal crystal lattice for smectic polypropylene. It has also been suggested that the α-form can be converted to the smectic form by cold deformation, and the smectic form can be converted to the α-form by heating [108].

Recently, Wang et al. [109] reported the structural study of irradiated polypropylene by x-ray diffraction. The study found that electron irradiation did not change the total crystallinity of polypropylene but greatly influenced its crystal structure. The amount of the β-form increased, and the α-form decreased as the irradiation dose increased. The study also suggested that the β-form may be recrystallized into the α-form at higher temperature because the melting point of the β-form is much lower than that of the α-form of the polypropylene.

CHAPTER 3
EXPERIMENTAL DESIGN

Materials

The polymers used in this study were commercial grade Exxon homo-polypropylene resins with **nominal melt flow rate (MFR)** values ranging from **35** to **1000**. The resin characteristics are given in Table 3.1. The polymers were supplied in pellet form. The molecular weight, polydispersity index, and intrinsic viscosity of supplied polymers were determined at the Exxon Chemical Company, Baytown Polymers Center, using gel permeation chromatography (GPC). The molecular weights ranged from 91,000 to145,000 and the polydispersity index values ranged from 2.5 to 3.5. The 35 and 300 MFR polymers had similar polydispersity indexes but, of course, had a large difference in molecular weights. The 600 and 1000 MFR polymers had similar polydispersity indexes but the difference in molecular weights was minimal.

Web Preparation

Melt blown webs for this study were produced on the 508 mm (20 inch) melt blown pilot line at The University of Tennessee. The line featured a 508 mm state-of-the-art die, an electric furnace for heating the air, and an Ingersoll-Rand 18.4 m^3/min (650 ft^3/min) air compressor. A 50.8 mm (2 inch) extruder (30/1 L/D) was utilized for this study. Two mosepieces were utilized with the melt blowing die: the **standard nosepiece** had 20 orifices per inch with orifice diameter of approximately 0.4 mm (L/D=10), and the **small nosepiece**

Table 3.1
Characteristics of polymers

Properties / Polymer Type	Intrinsic Viscosity (dL/g)	Weight Average Molecular Weight (M_w)	Number Average Molecular Weight (M_n)	Polydispersity Index (M_w/M_n)
35 MFR	1.06	145200	58400	2.5
300 MFR	0.80	112000	37000	2.8
600 MFR	0.73	93300	26800	3.5
1000 MFR	0.72	91400	27200	3.4

had 21 orifices per inch with orifice diameter in the range of 0.2 - 0.3 mm (L/D=8). The process conditions were monitored and controlled through a microprocessor.

The **35, 300, 600** and **1000 MFR** polypropylene resins were melt blown according to the experimental flow chart shown in Figure 3.1. The web preparation was divided into three phases:

- In the first phase, the **35, 300, 600** and **1000 MFR** resins were melt blown using a **75% air valve opening** (from the compressor) corresponding to an air flow rate of 7.9 m^3/min at standard conditions and a **standard orifice die** (approximate diameter of 0.4 mm) at three throughput rates of **160, 320**, and **480 g/min** (**0.4, 0.8**, and **1.2 g/min/orifice**, respectively).
- In the second phase, the **35, 300** and **600 MFR** resins were melt blown using a **90% air valve opening** corresponding to an air flow rate of 11.7 m^3/min at standard conditions and a **standard orifice die** (approximate diameter of 0.4 mm) at two throughput rates of **160** and **320 g/min**. The throughput rate of 480 g/min was not attainable at 90% air flow rate conditions because the higher air temperatures required resulted in excessive fly and shot formation.
- In the third phase, the **300** and **1000 MFR** resins were melt blown using a **75% air valve opening** corresponding to an air flow rate of 7.9 m^3/min at standard conditions and a **small orifice die** (uniform diameters in the 0.2-0.3 mm range) at three throughput rates of **160, 320**, and **480 g/min**.

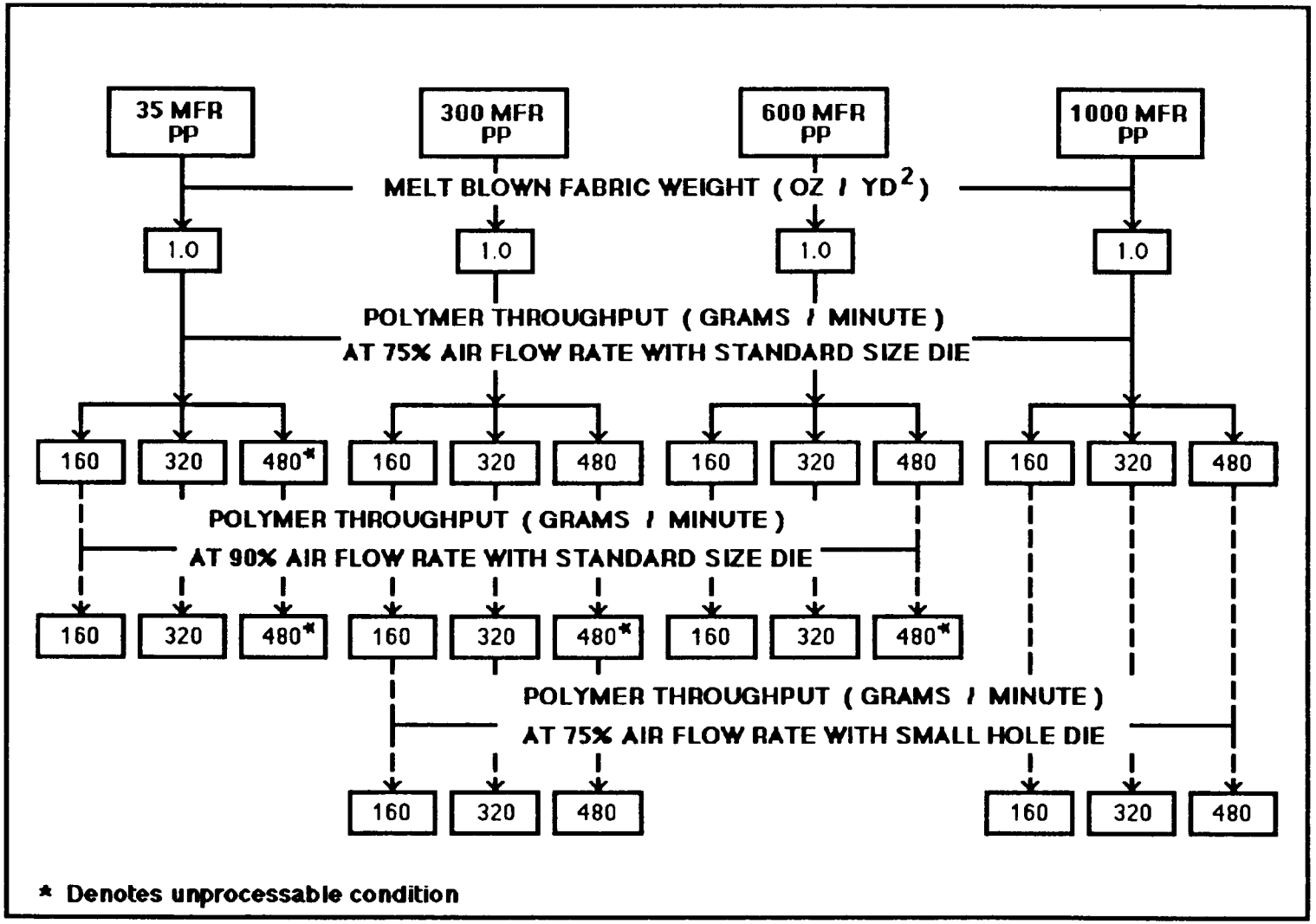

Figure 3.1. Flow diagram of experimental design.

The throughput rate of 160 g/min is often used in laboratory trial runs, while throughput rates of 320 g/min or greater (corresponding to this size extruder and die width) are usually employed in commercial processing. Generally, the lower the polymer throughput, the greater the latitude in adjusting the process parameters, such as air flow rate and temperatures of air and polymer, in order to achieve ultrafine fibers and optimum strength properties. The process conditions used for this study are given in Tables 3.2, 3.3, and 3.4.

There are a number of operating variables in the melt blowing process. Since the main focus of this research was to study the effects of polymer throughput rate, air flow rate, and die orifice diameter, the web basis weight was maintained at an average value of 33.9 g/m^2, and a die-to-collector distance of 300 mm was used for all the trial runs. The other **key process variables** -- **polymer** and **air temperatures** -- were changed as needed to produce web samples with similar tactile hand. For example, the 300 MFR resin has been shown in previous trials to result in much stiffer fabric and in large fiber diameters when processed at the same temperatures as 1400 MFR resin. Basically, the temperatures were controlled between the temperature where **shot** (resin beads resulting from prematurely broken filaments) was present and the temperature where excess **fly** (fiber fragments suspended in the air resulting from fiber breakage at excessive temperature and air flow rate) was generated.

For each trial run, the operating conditions were set and were allowed to equilibriate for 10 to15 minutes. Then, the polymer throughput rate was determined by weighing the web produced in one minute. The polymer throughput rate was checked three to five times for each trial runs. After determining the polymer throughput rate, the collcetor speed was adjusted in

Table 3.2

Melt blown processing conditions for webs processed at 75% air flow rate using standard orifice die

Sample ID		Properties	Melt Temp. (°C)	Die Temp. (°C)	Air Temp. at Die (°C)	Screw Speed (RPM)	Collector Speed (Meters/Min.)
75% Air Flow Rate Standard Orifice Die	35 MFR	160 g/min	294	321	341	20	7.9
		320 g/min	304	334	351	39	16.2
	300 MFR	160 g/min	251	254	282	20	8.8
		320 g/min	267	272	300	40	17.7
		480 g/min	276	287	317	66	28.0
	600 MFR	160 g/min	232	247	273	23	9.2
		320 g/min	246	258	284	42	16.5
		480 g/min	257	272	289	68	23.8
	1000 MFR	160 g/min	227	234	239	20	8.8
		320 g/min	243	244	250	46	17.7
		480 g/min	248	254	263	68	24.1

Table 3.3

Melt blown processing conditions for webs processed at 90% air flow rate using standard orifice die

Sample ID		Properties	Melt Temp. (°C)	Die Temp. (°C)	Air Temp. at Die (°C)	Screw Speed (RPM)	Collector Speed (Meters/Min.)
90% Air Flow Rate Standard Orifice Die	35 MFR	160 g/min	301	315	278	20	7.9
		320 g/min	316	332	285	39	16.2
	300 MFR	160 g/min	250	250	249	20	8.2
		320 g/min	271	271	260	40	17.4
	600 MFR	160 g/min	231	238	230	23	9.2
		320 g/min	248	249	237	42	16.5

Table 3.4

Melt blown processing conditions for webs processed at 75% air flow rate using small orifice die

Sample ID		Properties	Melt Temp. (°C)	Die Temp. (°C)	Air Temp. at Die (°C)	Screw Speed (RPM)	Collector Speed (Meters/Min.)
75% Air Flow Rate Small Orifice Die	300 MFR	160 g/min	246	251	281	20	8.8
		320 g/min	263	274	292	40	17.7
		480 g/min	264	278	292	66	28.1
	1000 MFR	160 g/min	233	232	237	22	8.8
		320 g/min	236	245	246	46	17.4
		480 g/min	232	240	241	68	24.1

order to maintain an average basis weight of 33.9 g/m^2. In order to determine the correct basis weight, five square specimens were cut during on-line processing. These specimens were weighed using an electronic balance, and an average weight of these specimens was converted to the basis weight.

The air flow rate for the trial runs was determined according to the American Society of Mechanical engineers Power Test Code. The procedure to determine the air flow rate is given in Appendix A.

CHAPTER 4
EXPERIMENTAL PROCEDURES

The specimens which were subjected to physical testing were first conditioned under standard textile testing conditions of 20 °C and 65% relative humidity for a minimum of 24 hours.

Physical Property Measurements

Basis Weight. The basis weight of the webs was determined according to ASTM Standard D-3776-79 [4]. The specimens for basis weight determination were selected randomly over a length of 50 meters but in a manner to ensure equal representation across the fabric width. Twenty-five (127 x 127 mm) specimens were cut for testing in the manner illustrated in Figure 4.1.

Stress-Strain Properties of Webs. The tensile stress-strain properties were measured in accordance with ASTM Standard D-1682 [4] using an Instron tensile tester. The tensile properties were measured in two fabric directions: machine direction (MD) and cross direction (CD). The test specimens were selected over a length of 50 meters at different locations across the fabric width. Two sets of twenty-five (25.4 x 175 mm) specimens were cut for testing, as shown in Figure 4.2.

The load-extension data were normalized according to the procedure explained in Appendix B. Twenty-five load-extension curves of each web type

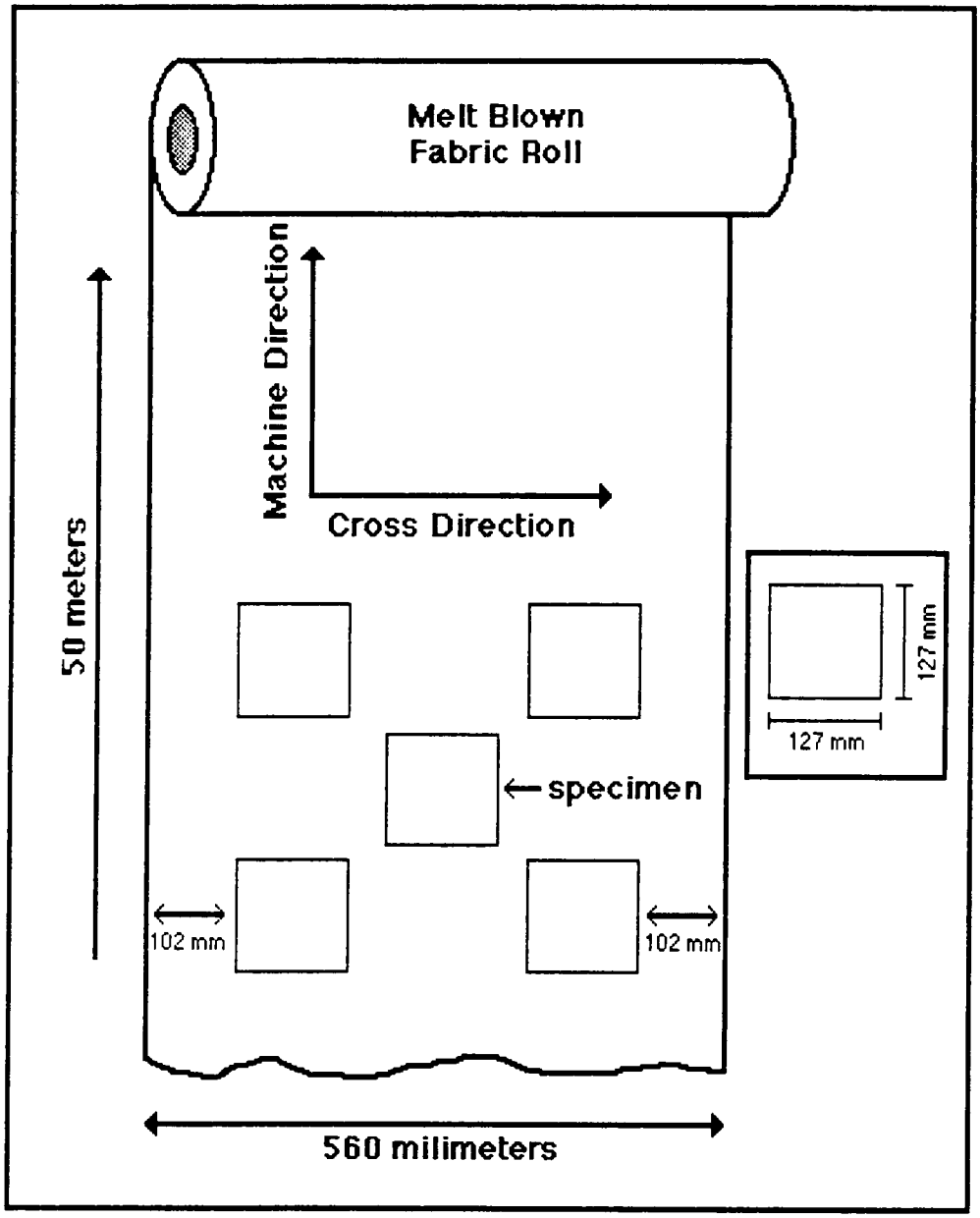

Figure 4.1. Schematic showing specimen cutting procedure for basis weight determination.

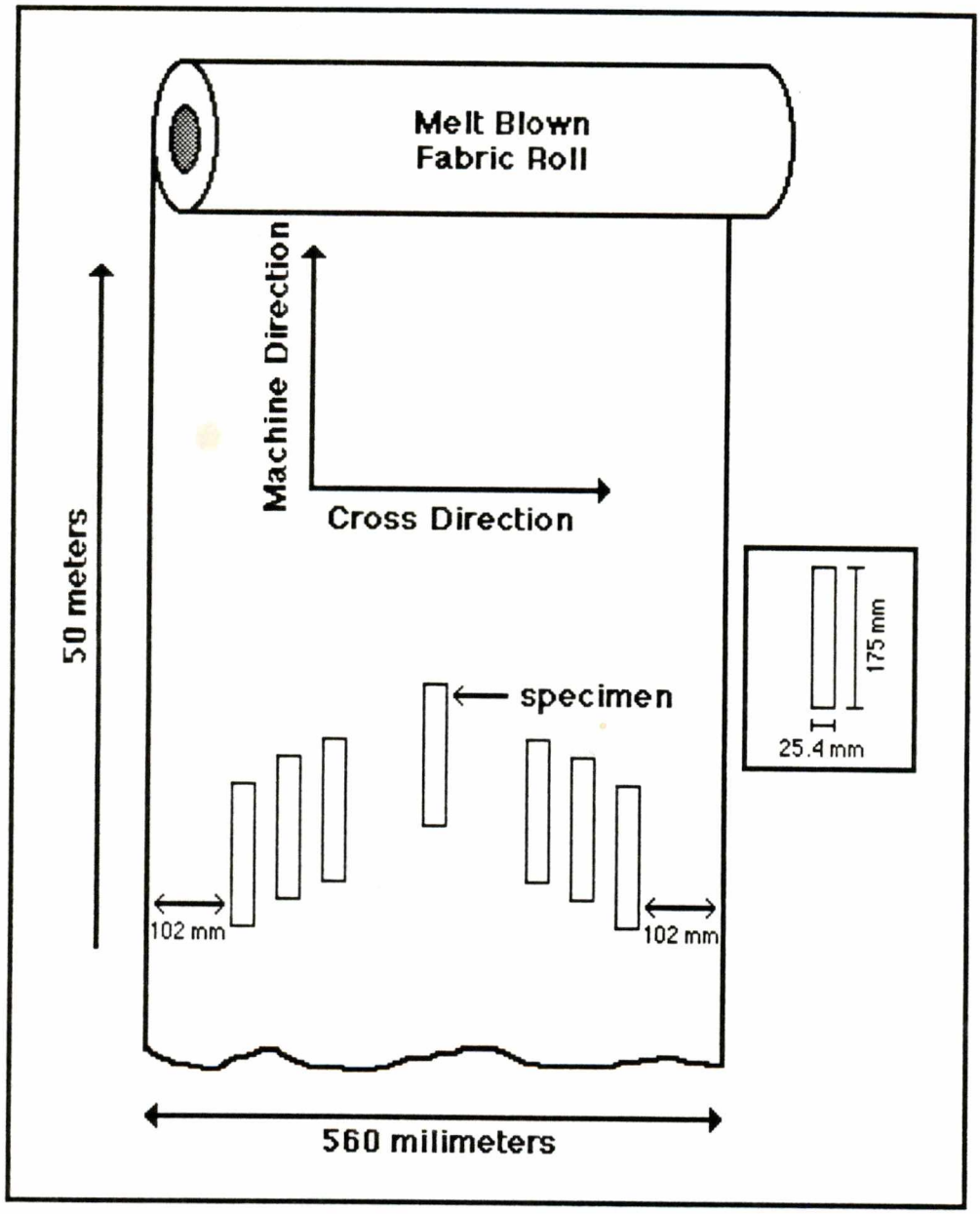

Figure 4.2. Schematic showing specimen cutting procedure for tensile testing.

were averaged to generate a composite stress-strain curve. Appendix C describes the technique for averaging the curves.

Stress-Strain Properties of Single Fibers. The stress-strain properties of single fibers were measured using a floor model Instron tensile tester. The method for mounting and testing the single fibers is described in sequential order below:

1. In order to facilitate the removal of a single fiber from a melt blown web, a web with very low basis weight (2 to 3 g/m^2) was prepared for each web type.
2. The low basis weight web was prepared by placing a wire screen between the die nosepiece and the collector, right below the fiber stream, as shown in Figure 4.3. The wire screen was then quickly pulled upward through the fiber stream. By doing so, a web with very low basis weight was collected onto the wire screen.
3. The low basis weight web was then carefully removed from the wire screen. A small portion of this web was cut and glued onto a piece of pre-cut construction paper, as shown in Figure 4.4. The pre-cut construction paper had a (2 x 5 mm) center hole.
4. All the fibers were removed from the hole area, except for a single fiber near the center of the hole, as shown in Figure 4.4. The fibers were removed using sharp tweezers under a lighted magnifying glass. Figure 4.5 shows a photomicrograph of a mounted single fiber.
5. The mounted single fiber was then placed under a microscope to measure the fiber diameter. The diameter of the single fiber was measured in order to calculate the breaking stress. The diameter of the single fibers for the test ranged from 3 to 25 μm.
6. The single fibers were tested using the following conditions:
   - a gauge length of 2 milimeters

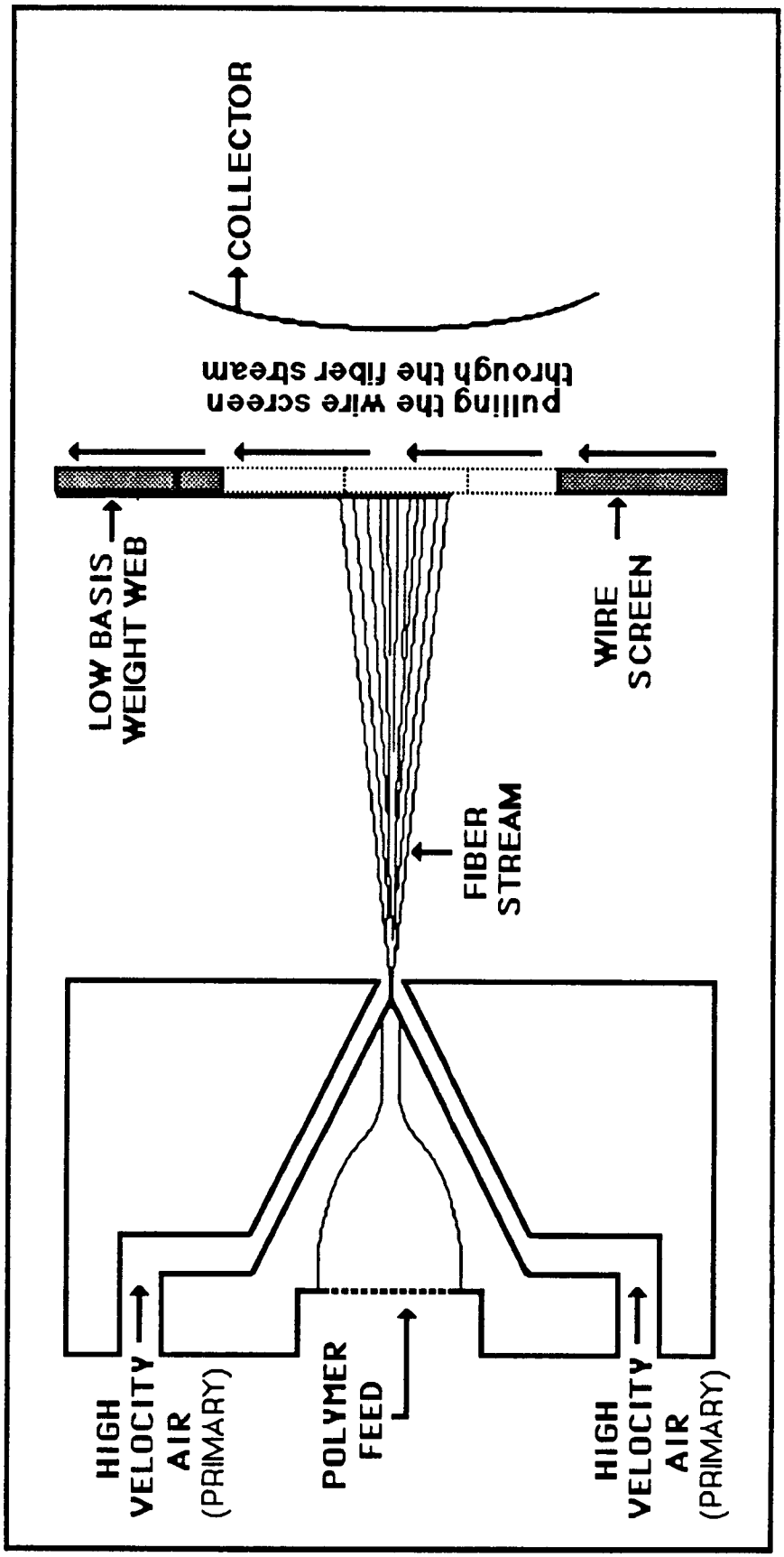

Figure 4.3. Schematic showing collection of low-basis weight melt blown web.

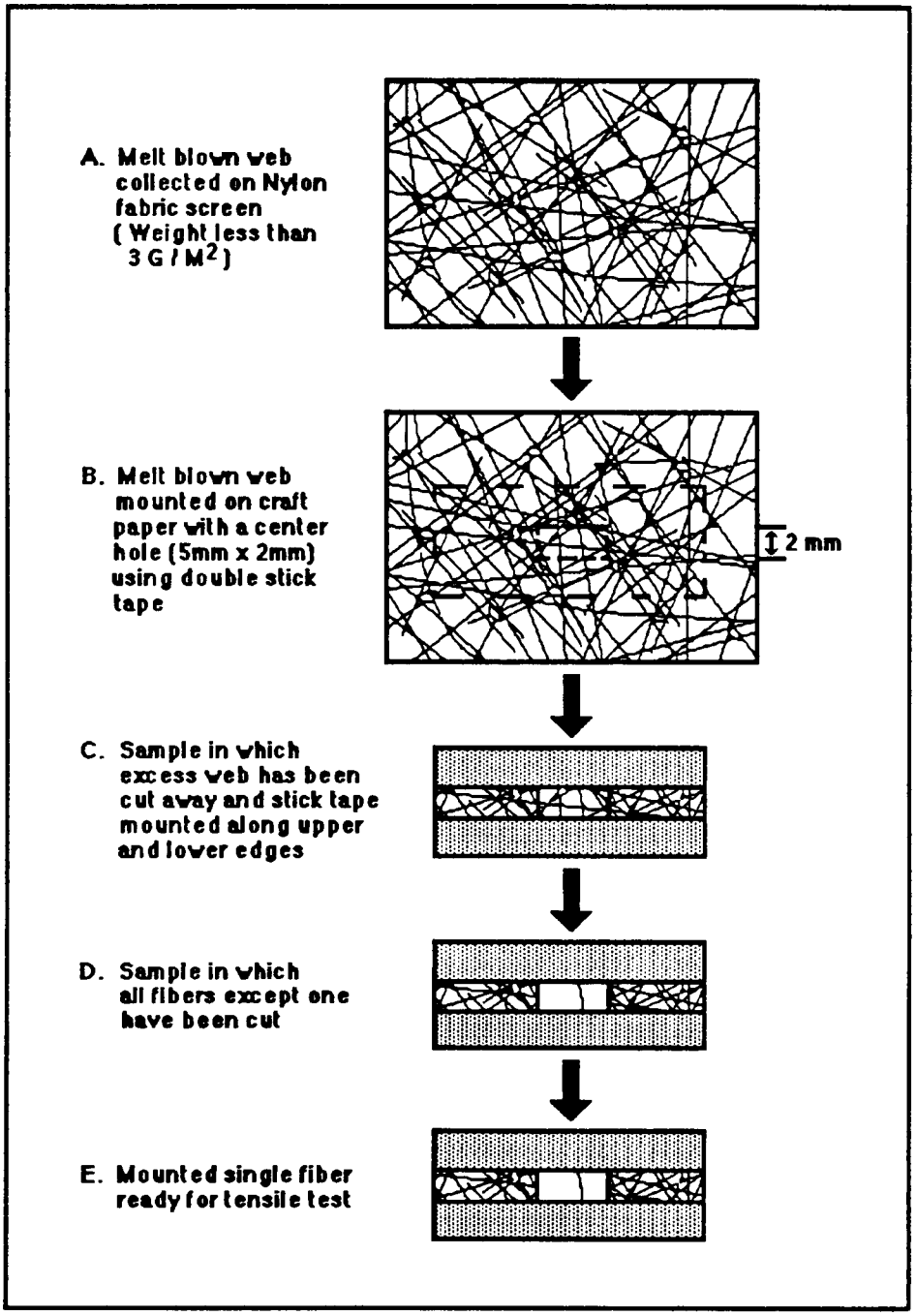

Figure 4.4. Schematic showing single fiber mounting procedure.

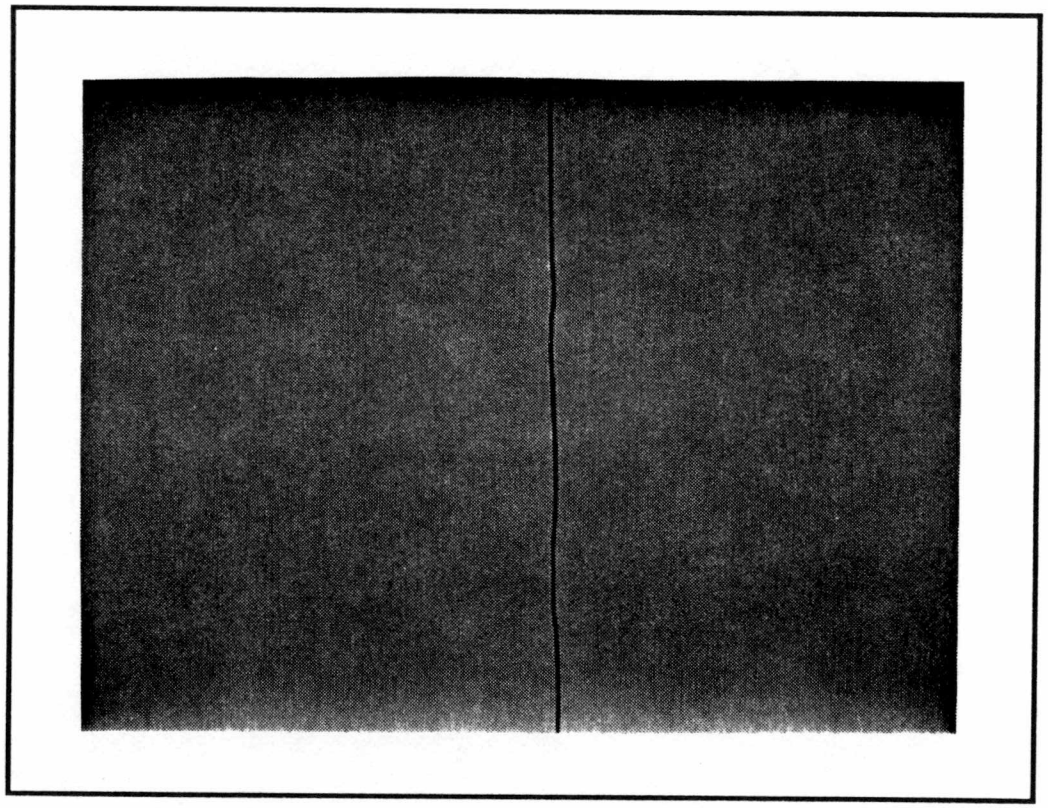

Figure 4.5. Optical photomicrograph of a single fiber.

- cross-head speed of 2 mm/min
- full-scale load of 50 grams

7. A total of eight single fiber samples were mounted and tested for each web type.
8. The single fiber load-extension data were normalized according the procedure shown in Appendix B.

Flexural Rigidity. The bending rigidity of the webs, as described in ASTM Standard D-1388 [4], was measured using the Cantilever Bending Tester. The specimens were prepared according to the procedure explained in the section entitled, "Stress-Strain Properties of Webs."

Bursting Strength. The bursting strength was measured using the Mullen Bursting Tester according to ASTM Standard D-3387 [4]. The test specimens were selected randomly over a length of 50 meters. Twenty-five (127 x 127 mm) specimens were cut for testing, as shown in Figure 4.1.

Shear Properties. Shear stiffness and shear hysteresis measurements were performed only on 300 MFR resin webs in the machine direction (MD). The shear properties were measured using the Kawabata Shear Test equipment. The shear tests were conducted on a contract basis by the Department of Chemical Engineering, Louisiana State University, Baton Rouge. Three (200 x 200 mm) specimens from each web type were cut. The specimens were sheared two degrees in one direction and two degrees in the opposite direction, as shown in Figure 4.6. The shear stiffness was calculated from the slopes of the foward and backward curves between 0.125 and 0.68 degrees, as shown in Figure 4.6, according to the following equation:

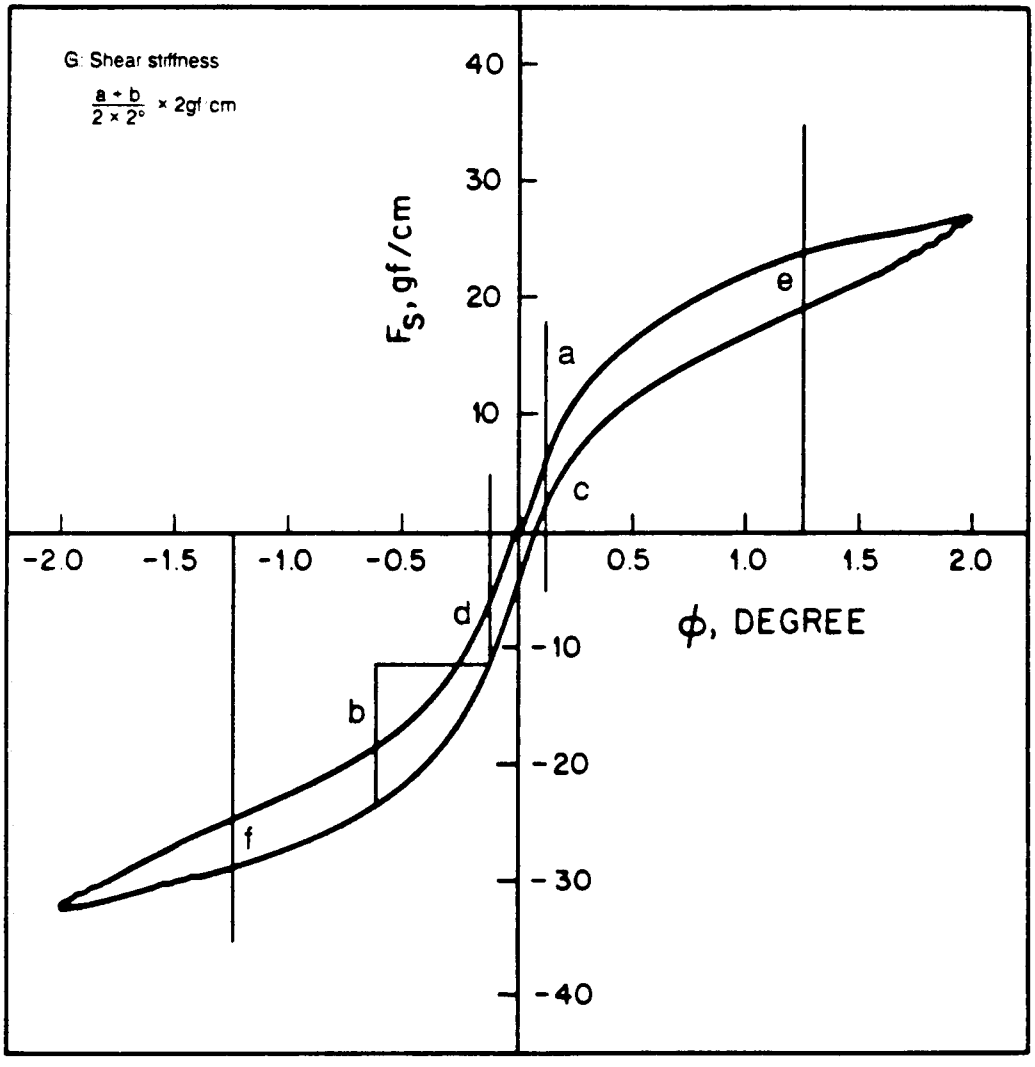

Figure 4.6. Schematic of a typical shear curve.

$$F_S = C + G\phi$$

where

F_S is the shearing force,

G is the shear stiffness,

ϕ is the angle of displacement of one edge of the specimen with respect to the other edge, and

C is a constant.

Three values of each web type were averaged to obtain shear stiffness. The shear hysterisis analysis was also performed on all specimens at 0.125 and 1.25 degrees of shear angle.

Air Permeability. The air permeability of the webs was determined according to the ASTM Standard D737-35 [4] at a pressure drop of 0.5 inches of water. A Gurley Permeometer, Model TY 1253, was used to perform the test. The specimens were prepared according to the procedure explained in the section entitled, "Basis Weight."

Web Density. Web density (g/m^3) was determined by dividing the basis weight of the web by the thickness of the web. The thickness of the web was measured using the Ames Thickness Gauge, Model 85-0071, in accordance with the ASTM standard D1777-64 [4]. The basis weight of the web was measured according to the ASTM standard D3776-79 [4]. The specimens were prepared according to the procedure explained in the section entitled, "Basis Weight."

Microscopical Analysis of Fibers

Fiber Diameter. Fiber diameters were determined from the photomicrographs of the webs. The photomicrographs were taken using the ETEC Auto Scan electron microscope. The specimens were selected from the left, middle, and right sides of the webs over a length of 5 meters. The specimens were cut in a circular form (0.8 cm^2) using a special cutter. All the specimens were coated with gold by a diode sputtering technique. The photomicrographs were taken at 15 kv accelerating setting in order to minimize the charging effects and the thermal degradation of the specimens. Eight photomicrographs were taken for each web type at 500x magnification.

In order to facilitate the fiber diameter measurement, two diagonal lines were drawn across each photomicrograph, as shown in Figure 4.7. The diameters of all the fibers at the points where the lines crossed were measured with a scale under a lighted magnifying glass (fibers which crossed the diagonal lines more than once were measured at only one cross-over point). Typically, an average of 200 fiber diameter values for each web type was reported.

Birefringence of Fibers. Birefringence measurements were performed only on 300 MFR resin fibers. The total birefringence of the melt blown fibers was determined using the Zeiss polorizing microscope equipped with the Berek compensator and a scaled eyepiece. A fifth order compensator was used to determine the phase difference or retardation (Γ) between two mutually perpendicular, plane polorized-light waves emerging from the fiber sample. The scaled eyepiece was used to determine the diameter of the fiber.

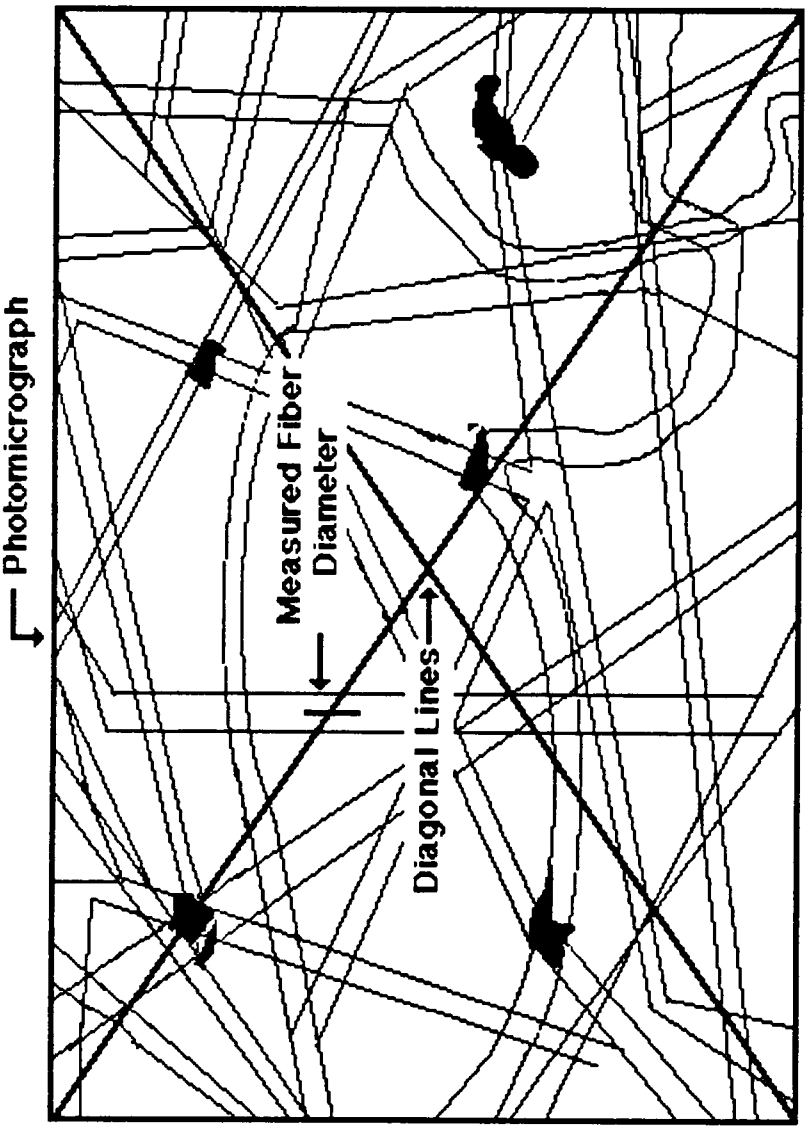

Figure 4.7. Schematic showing fiber diameter measurement.

The total birefringence was calculated using the following expression:

$$\eta = \frac{\Gamma}{d}$$

where

η is the birefringence,

Γ is the retardation, and

d is the fiber diameter

The single fibers for birefringence measurements were mounted according to the procedure explained in the section entitled, "Stress-Strain Properties of Single Fibers."

Differential Scanning Calorimetry

A Model DSC-7 Perkin Elmer Differential Scanning Calorimeter was used to measure the experimental heat of fusion, ΔH_f^* of resins and webs. A temperature range of 50 °C to 200 °C was used with a heating rate of 10 °C/min. Indium was selected as the standard to calibrate the measurements. The resin and web specimens were weighed in an aluminum pan using an electrically operated balance. The weight of the specimen ranged from 3.5 to 4 mg with an accuracy of 0.001 mg. The DSC curves were normalized and evaluated using TAS7 Perkin Elmer software.

The percent crystallinity was calculated from the heat of fusion data by using the following equation:

$$X_c = (\Delta H_f / \Delta H_f^*) \times 100\ \%$$

where

ΔH_f is the heat of fusion of the sample, and

ΔH_f^* is the heat of fusion of 100% crystalline material.

The value of heat of fusion of 100% crystalline polypropylene used in this work was 146.5 J/g [133].

The specimens were selected from the left, middle, and right sides of the webs over a length of 5 meters. A total of ten specimens were tested for each web type.

Wide Angle X-Ray Diffraction

The wide angle x-ray diffractograms were obtained using a Rigaku diffractometer with copper radiation in reflection mode. The diffractograms (two-theta scans) were obtained over the angular range of 5 to 35°. Specimens were prepared by cutting webs into small square pieces and pressing them on a glass disk to form a mat of 2 mm in thickness, as shown in Figure 4.8.

The wide angle x-ray diffraction (WAXD) patterns for the webs were obtained using a Philips Norelco x-ray generator and flat plate camera. Nickel filtered, copper radiation (wavelength 1.542 Å) was used. The schematic of the

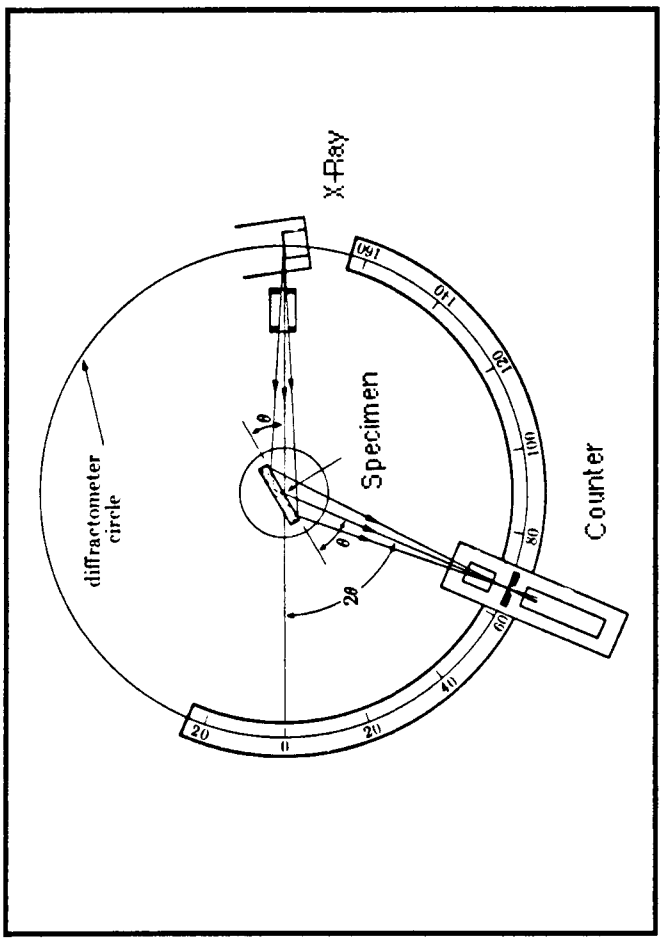

Figure 4.8. Schematic of an x-ray diffractometer.

experimental set-up is shown in Figure 4.9. The x-ray films were exposed for 20 hours with a generator setting of 35 kV and 20 mA.

The specimens were selected from the left, middle, and right sides of the webs over a length of 5 meters. A total of five specimens were tested for each web type.

Gel Permeation Chromatography

The gel permeation chromatography (GPC) analysis of the web and resin specimens was conducted at the Exxon Chemical Company, Baytown Polymers Center, according to ASTM Standard D3593 [4].

Melt Flow Rate

The resin and web melt flow rates were determined at the Exxon Chemical Company, Baytown Polymers Center according to ASTM Standard D1238 [4].

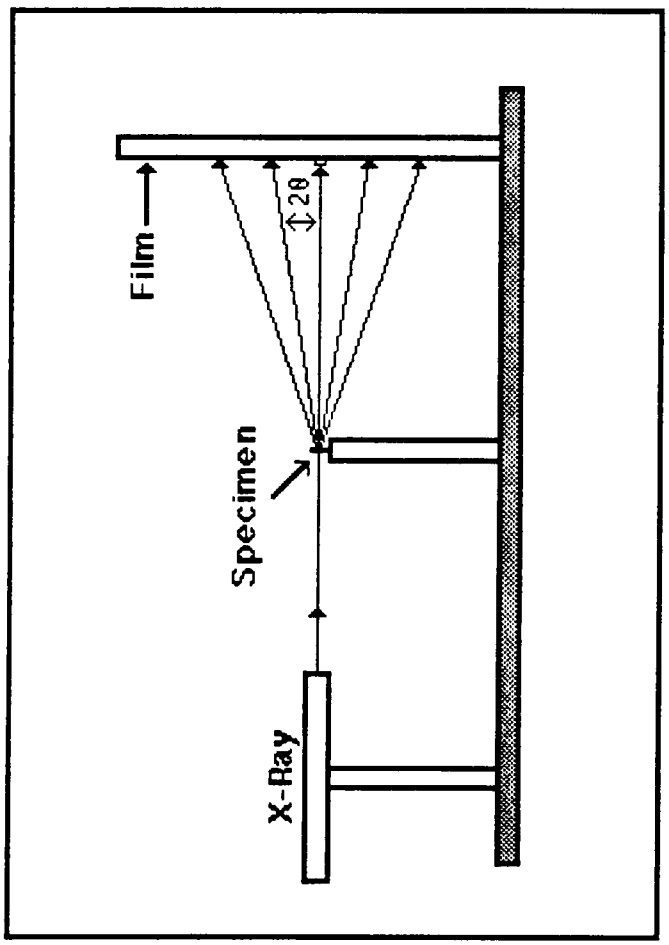

Figure 4.9. Schematic of an x-ray flat plate camera set-up.

CHAPTER 5
RESULTS AND DISCUSSION

In this chapter, the results of the study are presented. The discussion has been focused on the effects of polymer throughput rates of different molecular weight polypropylene resins on melt blown nonwoven web properties because among the process variables studied, polymer throughput rate appeared to have the most notable effects on the physical and morphological properties of melt blown webs. The effects of other process variables on melt blown web properties are also discussed.

Process Conditions

The key melt blown line conditions for each of the runs are given in Tables 3.2 - 3.4 (Chapter 3). Generally, all of the resins processed well under the different operating conditions. The melt blown runs resulted in webs that were uniform in appearance across the width.

The polymer melt temperatures ranged from 230°C to 310°C, the die temperatures ranged from 230°C to 335°C, and the air temperatures ranged from 230°C to 350°C. At normal air flow rate of 75% (7.9 m^3/min), the air temperatures were maintained higher than the die temperatures for the following reasons:

1) to increase softness and tactile hand of the web;
2) to increase drawing time before quenching of the fibers; and
3) to avoid cooling of the die below the set temperature.

At the higher air flow rate of 90% (11.7 m^3/min) the air temperatures were kept lower than the die temperatures in order to reduce **rope** and **fly** formation. For the small orifice die the temperatures were kept slightly higher in order to reduce the melt pressure efffect on the polymer throughput rate. Usually, the difference between the die and air temperatures at all processing conditions ranged from one to 60°C.

As the throughput rate increased from 160 to 480 g/min, the extruder and air temperatures were raised to the values shown in Tables 3.2 - 3.4 (Chapter 3). The increase in temperatures at higher throughput rates was necessary for two reasons: 1) to achieve optimum tactile hand of the webs, that were obtained at the lower throughput rate; and 2) to reduce shot formation. As the throughput rate increased, it was more difficult to maintain similar tactile hand of the webs because the air temperatures could not be raised high enough above the die temperatures before **rope** and **fly** became noticeable [40]. Therefore, processing was not attainable at 480 g/min for 35 MFR resin using 75% air flow rate and for 35, 300, and 600 MFR resins using 90% air flow rate.

At higher throughput rates, three types of web defects were observed: **shot** , **rope**, and **fly**. The probable causes and solutions for these defects are given in Tables 5.1-5.2 [23]. The webs defects can be defined as follows:

> **Shot.** Shot is defined as **a globule of polymer considerably larger in diameter than the fibers, formed by the elastic "snap-back" of the fiber ends upon breaking** [26]. Shots imparted "sandy" feel to the web. Figure 5.1 shows a photomicrograph of a typical shot. Shot usually occurs when processing temperatures are low and throughput rates are high. The phenomenon of shot formation can be attributed to **periodic melt fracture or melt instability**, which depend on such

Table 5.1

Probable causes and solutions for "shot"

Source: Anonymous : Melt Blowing Nonwoven Web Technology, Exxon Chemical Company, 1982.

Web Defect	Cause	Solution
Shot		
• Uniform shot across total web width.	Most likely:	
	• Temperatures too low.	• Raise temperatures or lower throughput rate.
	• Air rate too low for conditions.	
	Less likely:	
	• Throughput rate too high for product.	• Reduce throughput rate or reset conditions.
	• Die adjustments incorrect.	• Improve set back or air gap.
	• Air pressures uneven.	• Balance primary air flow.
• Shot in one or several streaks.	Most likely:	
	• Damaged die tip or pour set back or gap adjustment.	• Shut down and correct.
	• Blocked or partially blocked holes.	• Clear or replace die nosepiece.
	Less likely:	
	• Air slightly unbalanced.	• Balance air flow, streaks are most evident where holes are off centered.
	• Nonuniform hole size.	• Replace die nosepiece.

Table 5.2

Probable causes and solutions for "rope and fly"

Source: Anonymous : Melt Blowing Nonwoven Web Technology, Exxon Chemical Company, 1982.

Web Defect	Cause	Solution
Rope and Fly		
• Rope and fly across web width.	Most likely:	
	• Temperatures too high.	• Lower temperatures or increase screw speed.
	• Air rate too high for conditions.	• Lower air rate or change conditions.
	Less likely:	
	• Air gap settings, DCD or secondary air streams not in normal position.	• Check for cause and correct.
	• Air gap settings different on two sides.	• Correct the settings.
• Rope and fly at one location.	Most likely:	
	• Tight spot on air gap.	• Shutdown and correct.
	• Hot spot or section in die assembly.	• Analyze the cause and correct settings.
	• Air leak or extraneous air current.	• Analyze and correct.

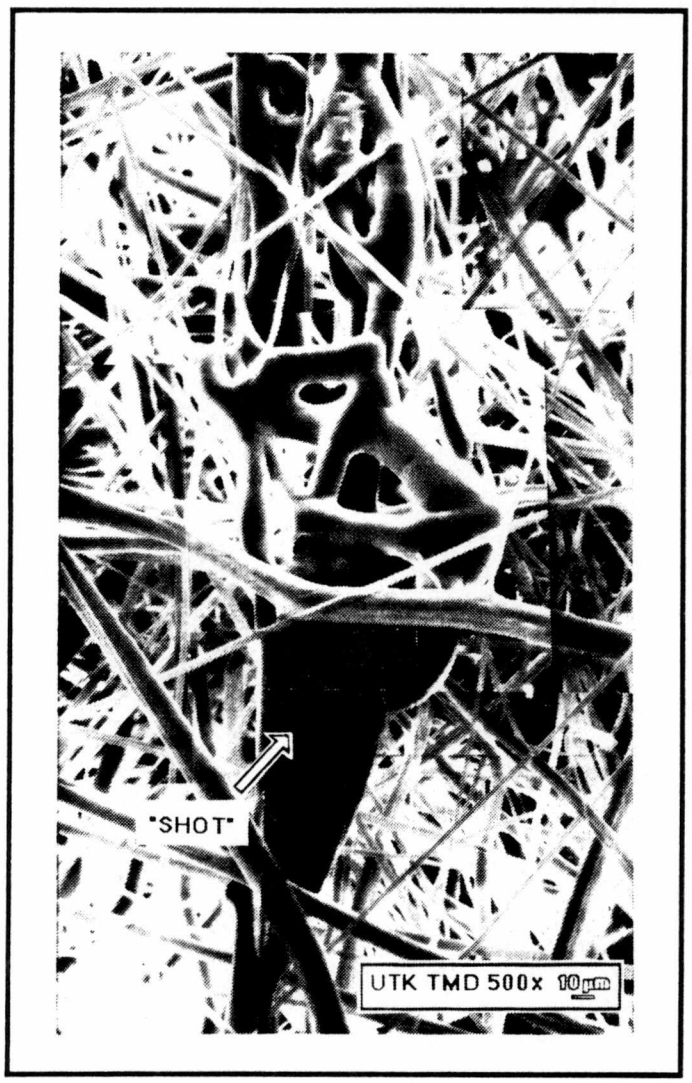

Figure 5.1. Photomicrograph showing "shot."

factors as processing temperatures, shear rate, air flow rate, and die configuration.

Rope. Rope is defined as **multiple fibers twisted together** and get deposited onto the web. Figure 5.2 shows a typical rope found on the melt blown web.

Fly. Fly is defined as **short broken fibers formed upon breaking from polymeric streams**. Fly usually move away from the primary air stream and get deposited away from the collector. Figure 5.3 shows fly collected during a production run.

Based on observed melt blown line conditions, a **process condition window** was established for polypropylene resins as a function of die and air temperatures, polymer throughput rate, and air flow rate (reference scale only) as shown in Figure 5.4. Within this process condition window, there exist the two extreme conditions: **shot conditions** and, **rope and fly conditions**. The conditions between these two extreme conditions were **favorable** for processing, and all other conditions were **unfavorable** for processing. The favorable conditions resulted in webs with a **good balance of tactile** and **strength properties**, while unfavorable conditions resulted in webs which were ropy and excessively soft or in stiff webs which contained a great deal of shot. It is to be noted that the favorable conditions did not preclude the occassional formation of shot, rope, and fly. From Figure 5.4 it was evident that as the throughput rate increased, the processing window of operation (favorable conditions) became more narrow, hence there was less lattitude for optimizing web properties at higher throughput rates. Moreover, at much higher throughput rates (640 g/min and above), shot and rope conditions were observed at the same time, and thus there was no region of satisfactory operation at these throughput rates.

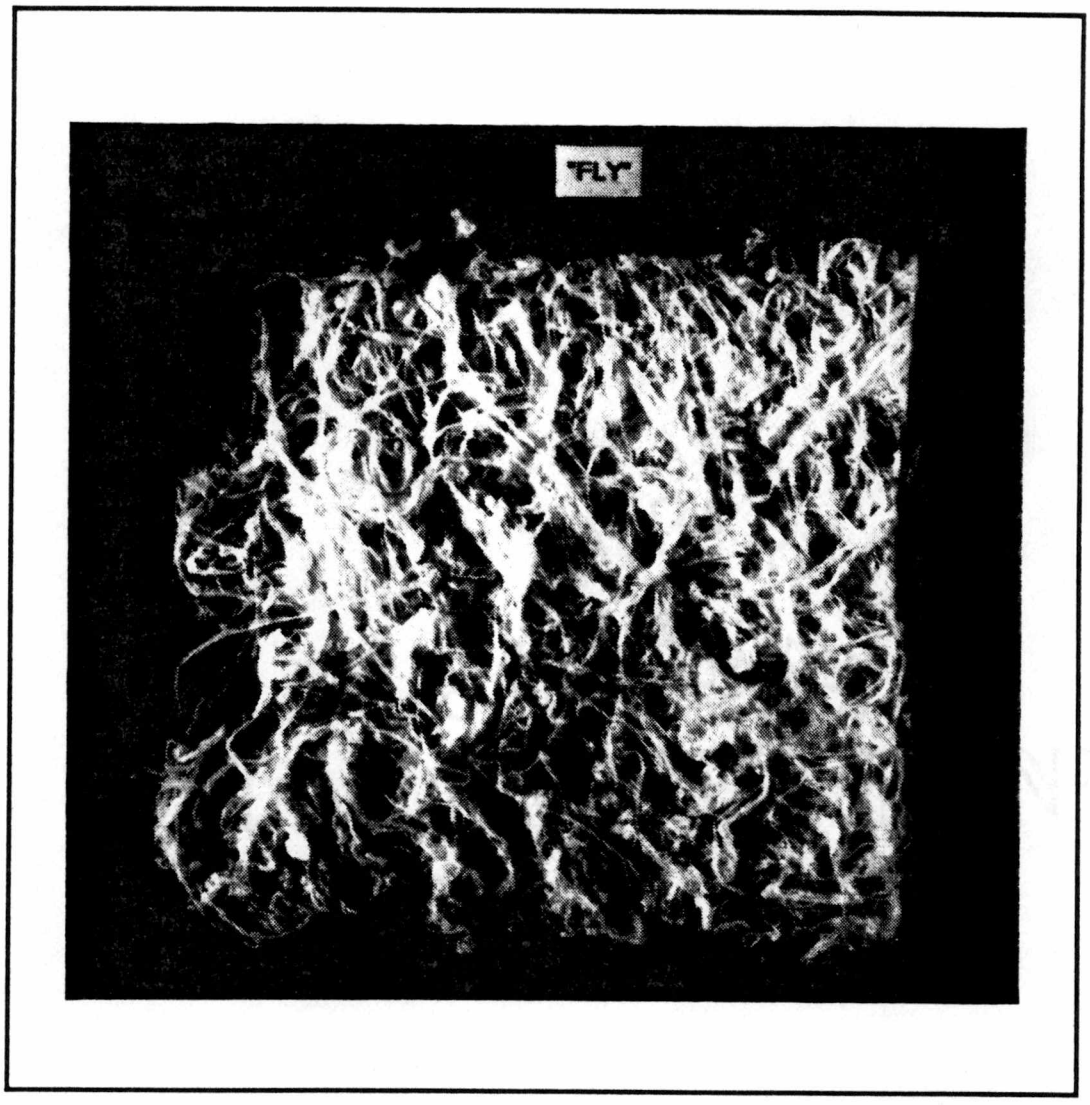

Figure 5.2. Photograph showing "fly."

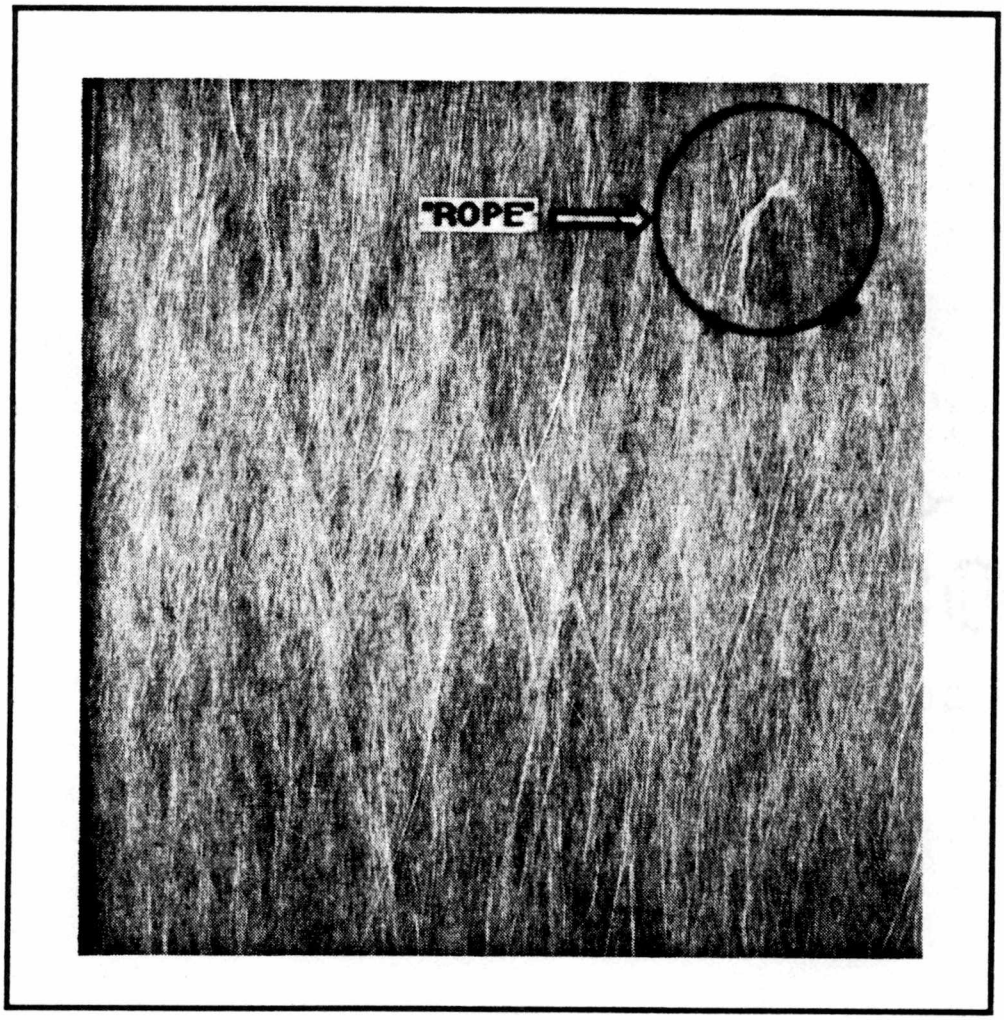

Figure 5.3. Photograph showing "rope."

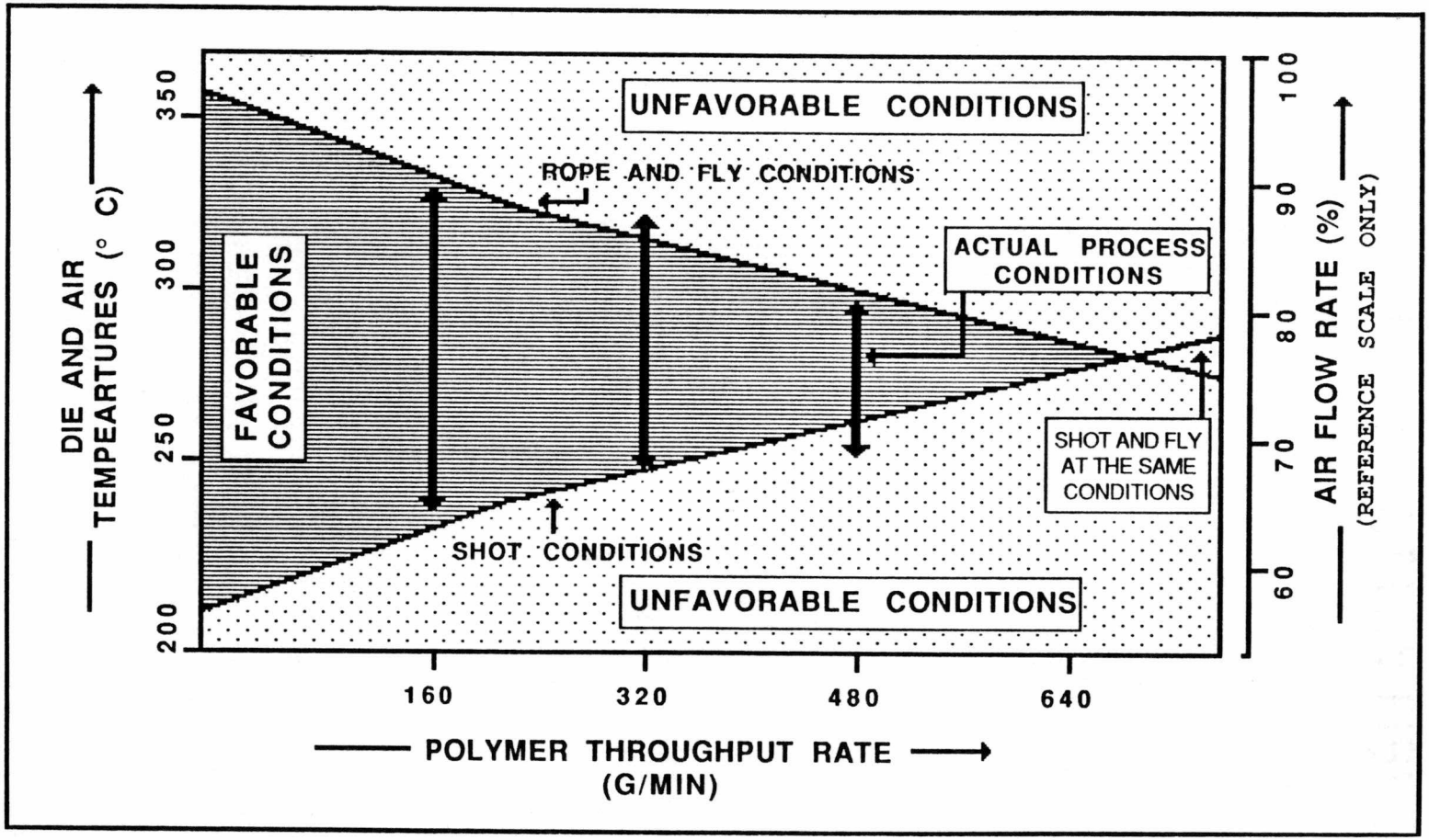

Figure 5.4. **Perceived process condition window for 35, 300, 600, and 1000 MFR polypropylene resins.**

Figure 5.4 also shows the actual processing temperature ranges for different throughput rates (**solid vertical arrows**). The vertical arrows indicate the overall processing temperature range for processed polypropylene resins at different throughput rates. The processing temperature range for 160 g/min throughput rate was within the two extreme conditions and no problem was encountered during the processing. At the 320 g/min throughput rate with the 35 MFR resin, the upper limit of the processing temperature range was in the region of rope and fly formation; therefore, rope and fly were observed. At 480 g/min throughput rate with the 1400 MFR resin, the lower limit of the processing temperature range was in the shot formation region; therefore, a great deal of shots were visible in the webs.

Polymer melt pressures (between the screen pack and the die) ranged from 1400 to 4700 kPa. Melt pressure increased as the polymer throughput rate increased. For 35 MFR polymer, melt pressure was higher at all processing conditions than any other polymers. As expected, back pressure was higher for the small orifice die than for standard orifice die.

Processing conditions had a notable effect on the texture of the web. The webs produced at the lowest throughput rate of 160 g/min were thicker and loftier than the webs produced at 320 and 480 g/min. The higher throughput webs had a harsher hand and were thin. The increased air rate made the webs softer, bulkier, and relatively shot free.

During the trial runs, the melt blowing process was observed closely. The following two visual observations were made:

- **There was one main polymer strand per die hole, which may or may not join to other polymer strands away from the die tip.**

- **The polymer strands left the die in fairly straight and parallel pattern, but developed waviness in all radial directions after about 3 inches from the die tip.**

Effects of Process Variables on Melt Blown Fibers

Fiber Diameter

The average fiber diameter values as a function of processing conditions are given in Tables D.1 - D-3 (Appendix D), and shown schematically in Figure 5.5. The average fiber diameters ranged from 2.8 to 6.7 μm. Figure 5.6 and Figures E.1 - E.8 (Appendix E) show typical photomicrographs of webs as a function of processing conditions.

The overall trend for the average fiber diameter was that as the throughput rate increased the average fiber diameter **increased**. The same trend has been observed in previous studies [35-40]. The increase in fiber diameter may be attributed to the **die swell** and the **change in polymer-to-air ratio for a given air flow rate**.

- It seems likely that the lower **polymer-to-air ratio** at low throughput conditions means more air and drag force per amount of polymer melt, which should increase draw-down of the fibers, resulting in a greater number of small diameter fibers in the webs. On the other hand, the higher **polymer-to-air ratio** at high thoughput conditions means less air and drag force per amount of polymer melt, which should decrease draw-down of the fibers, resulting in a greater number of large diameter fibers in the web [15, 110].
- **Die swell**, which is a result of viscoelastic nature of the polymeric material, is another factor believed to have an affect on

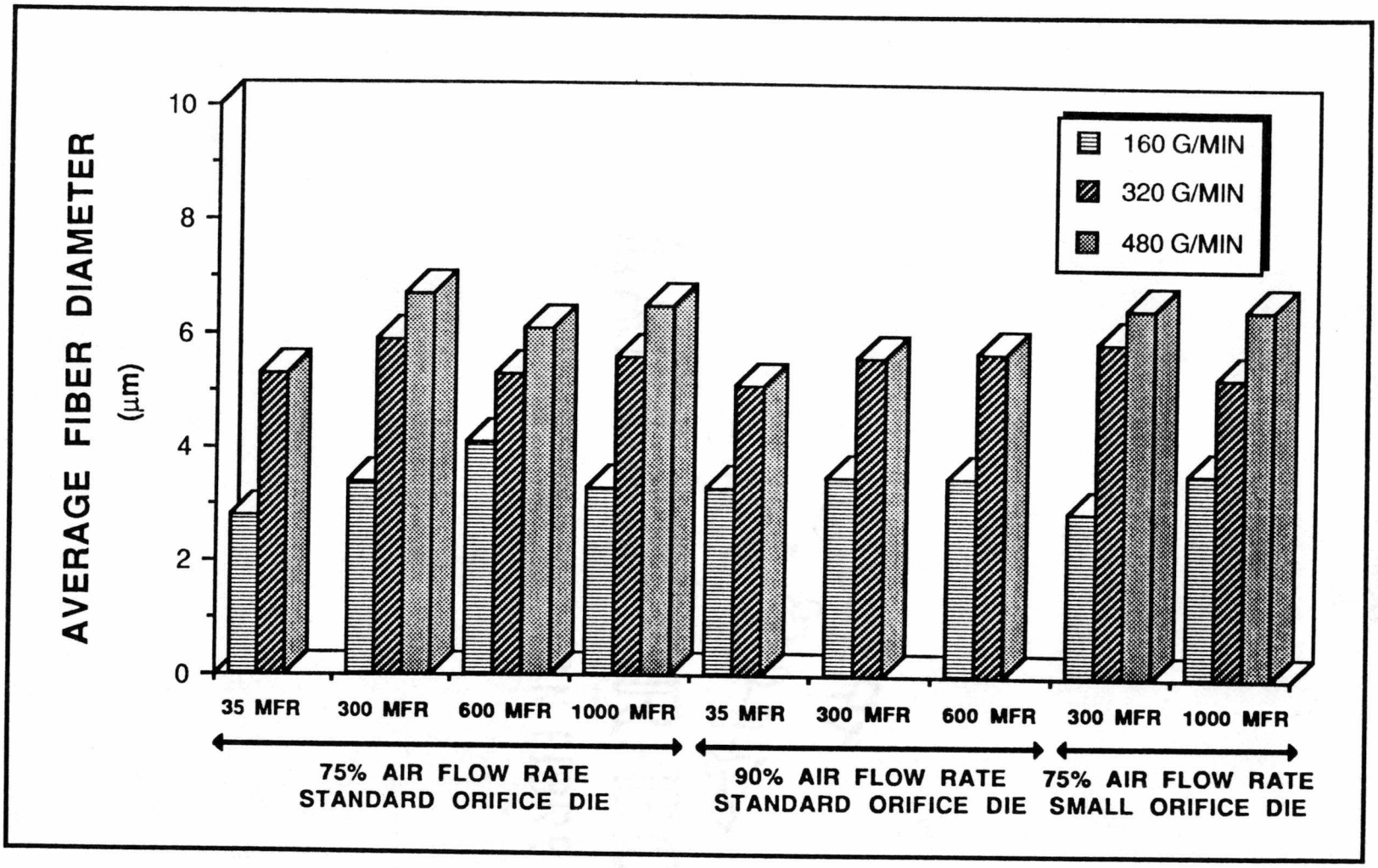

Figure 5.5. **Effect of MFR and process variables on average fiber diameter.**

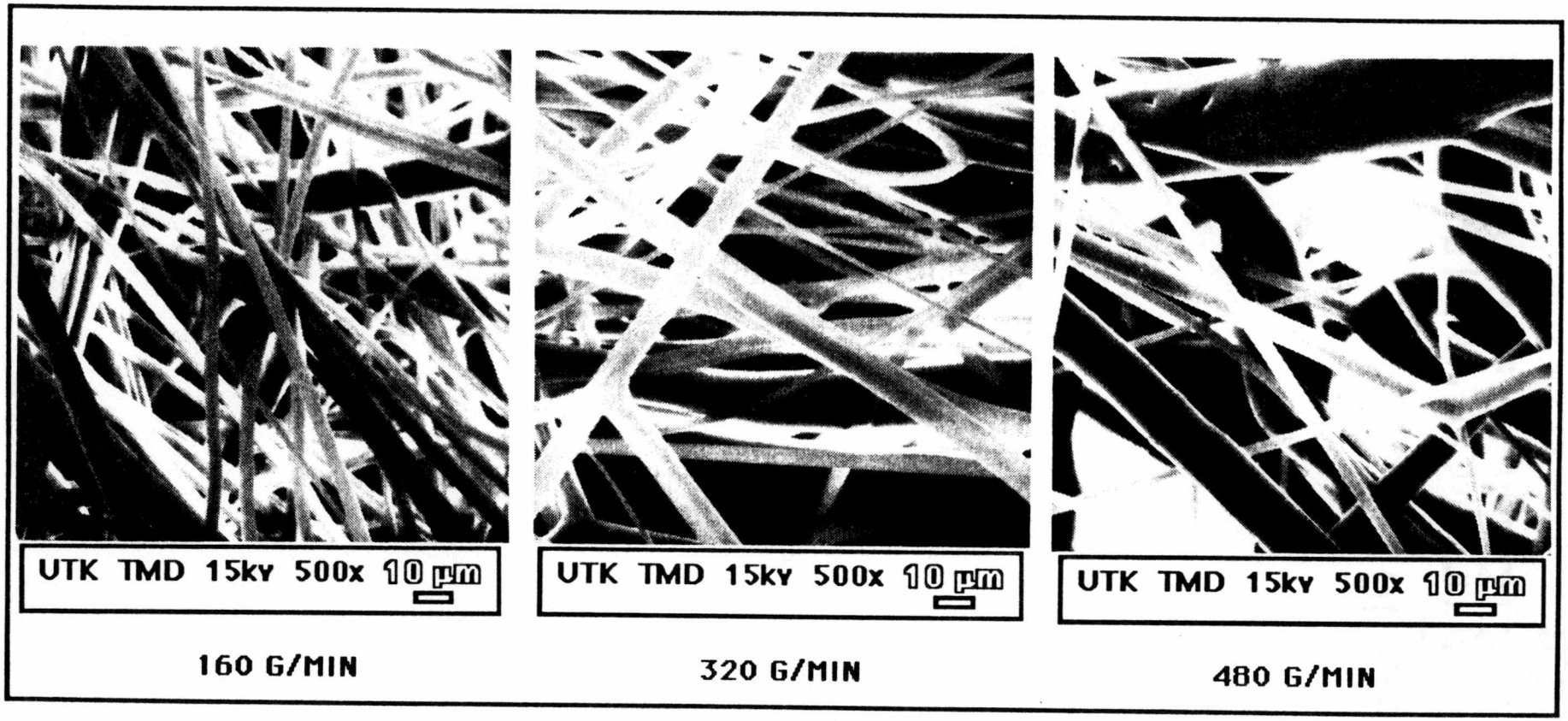

Figure 5.6. Photomicrographs of 1000 MFR webs processed at 75% air flow rate using standard orifice die.

the final fiber diameter. In an extrusion process, the energy, stored as pressure in the melt, is released on exiting from the die orifice and exhibits as die swell. In other words, the polymer melt as it leaves the die capillary **'remembers'** the large die entrance cross-section and tries to return to it by swelling.

The magnitude of the die swell directly depends on the entrance pressure in the die, which in turn depends directly on the throughput rates. As the throughput rate increases, the die entrance pressure increases; hence the die swell increases. Due to this increased die swell at high throughput rate, the starting diameter is larger compared to the low throguhput rate. Therefore, less draw-down polymer melt, which in turn results in increased final diameter.

The average fiber diameter increased with increased polymer MFR at the lower air flow rate of 75%, but the resin MFR appeared to have little effect at the 90% air flow rate. A study by Wadsworth and Jones [36] has shown a similar trend. Smaller average fiber diameter values were obtained with the 35 MFR resin. This may be explained by the fact that both the polymer melt and air attenuation temperatures were approximately 60°C higher for the 35 MFR resin runs. This additional heat could have more than offset the greater non-Newtonian viscosity behavior of the 35 MFR resin. Furthermore, the greater melt strength of the 35 MFR resin possibly could withstand more filament strand thinning prior to breaking or deposition onto the collector [40].

The diameter of the die orifices had minimal effects on the average fiber diameter. The study by Wadsworth and Jones [36] also showed the similar results. The differences in fiber diameter were smaller than expected initially, considering the fact that the cross-sectional area of the standard orifice die was

over twice that of the small orifice die. Several factors, many of them interacting, could have contributed to these results as follows:

First, with the larger orifices, there would be more than twice the amount of molten polymer in each polymer strand, which would provide proportionally more heat from the polymer melt for thread line thinning. Second, since the molten polymer streams exit from the die orifices directly into the confluence of the two air streams (top and bottom), it would appear that the greatest amount of attenuation should occur at the point of convergence of the air streams. Thus, the die orifice size should have little effect, provided it is large enough to pass the melt without plugging [25]. Finally, it is probable that the greater die swell could have occured with the smaller die orifices resulting in a proportionally greater increase in fiber diameter. It has been shown by many investigators [111], that in conventional melt spinning of polypropylene, a decreased spinneret diameter increased the die swell.

With the standard orifice die, increasing the air flow rate from 75 to 90% had little effect on the average fiber diameter at corresponding resin MFR and throughput rate values. However, the results did not agree with the results reported by Wadsworth and Muschelewicz [40] in which the polymer throughput rate of only 80 g/min (0.2 g/min/orifice) was utilized. In their study, they reported that significantly (statistically) smaller fiber diameter were obtained at 90% air flow rate than at 85% air flow rate.

In this study, the effect of change in air flow rate on the final diameter was not as noticeable because of the following reasons:

- It is probable that the lower primary air temperatures (necessary to reduce rope and fly formation) at higher air flow rate may have

reduced the effect of increased draw-down of polymer streams due to increased air at a given throughput rate.

- Due to lower die temperatures at higher air flow rate, the induced normal stress and the left elastic memory are ususally more on the extrudate, so that a higher die swell results. The increased die swell may have offset the effect of increased draw-down due to higher air flow rate at a given throughput rate.
- As the air flow rate increases, the drag force on the polymer streams increases [112], and this should result in smaller diameter. However, it is probable that the effect of increase in air drag may have been reduced by the rheological force (due to lower processing temperatures).

Fiber Attenuation

In melt blowing process, the factors that are responsible for the final melt blown fiber diameter of 2 to 8 μm has been a perplexity to researchers. From the visual observation of the process, it seems intuitive that as soon as the polymer streams are extruded from the die orifices, the air continuously impinges on the polymer streams to form micro-fibers and carries them to the collector. If this concept is true than ***a greater dependence of final diameter as a function of the change in air flow rate would be obvious***. Apparently it is not the case for the results found in this study. The effects of change in air flow rates on the final diameter was minimal at a given throughput rate. Therefore, it is logical to say that the fiber attenuation is a function of **air flow rate** as well as the **"other mechanisms"** which take place between the die and the collector after fibers travel certain distance from the die. The most probable **"other mechanisms"** are: 1) the **flapping motion** of the fibers proposed by Milligan and co-workers [112]; and, 2)

drawing of fiber segments between entanglement points as **fiber network is stressed** during its flight, by Bresee and Wadsworth [113].

The **flapping motion** of the fibers is believed to occur in many directions [112]. The exact cause of flapping motion is not clearly understood, but it is **this author's opinion** that the flapping motion (in conjunction with local phase change due to fiber microstructure development) promotes change in local fiber velocities which in turn help attenuate the fibers.

Fiber Characteristics

The following are some of the general observations based on mircroscopic examination of melt blown fibers:

- The fibers had smooth surface texture and appeared to be circular in cross section.
- There was extensive variations in fiber diameter along a single fiber, as shown in Figure 5.7.
- The close examination of approximately 800 photomicrographs showed no **"fiber ends"** (except a few near "shot" area). Therefore, it was belived that the fibers were continuous in length.
- The fibers showed **thermal branching**, as shown in Figure 5.8. The exact cause of thermal branching is not known, but it is **this author's opinion** that the branching of the fibers occur when propagating fibers collide with another propagating fibers, which in turn, stripe off portions of polymer streams as fine branches (filaments). Richardson [135] pointed out that when the velocity of the liquid jet relative to air jet increases, portions of the liquid are stripped off as filaments. Bresee and Wadsworth [113] stated that **fiber splitting**

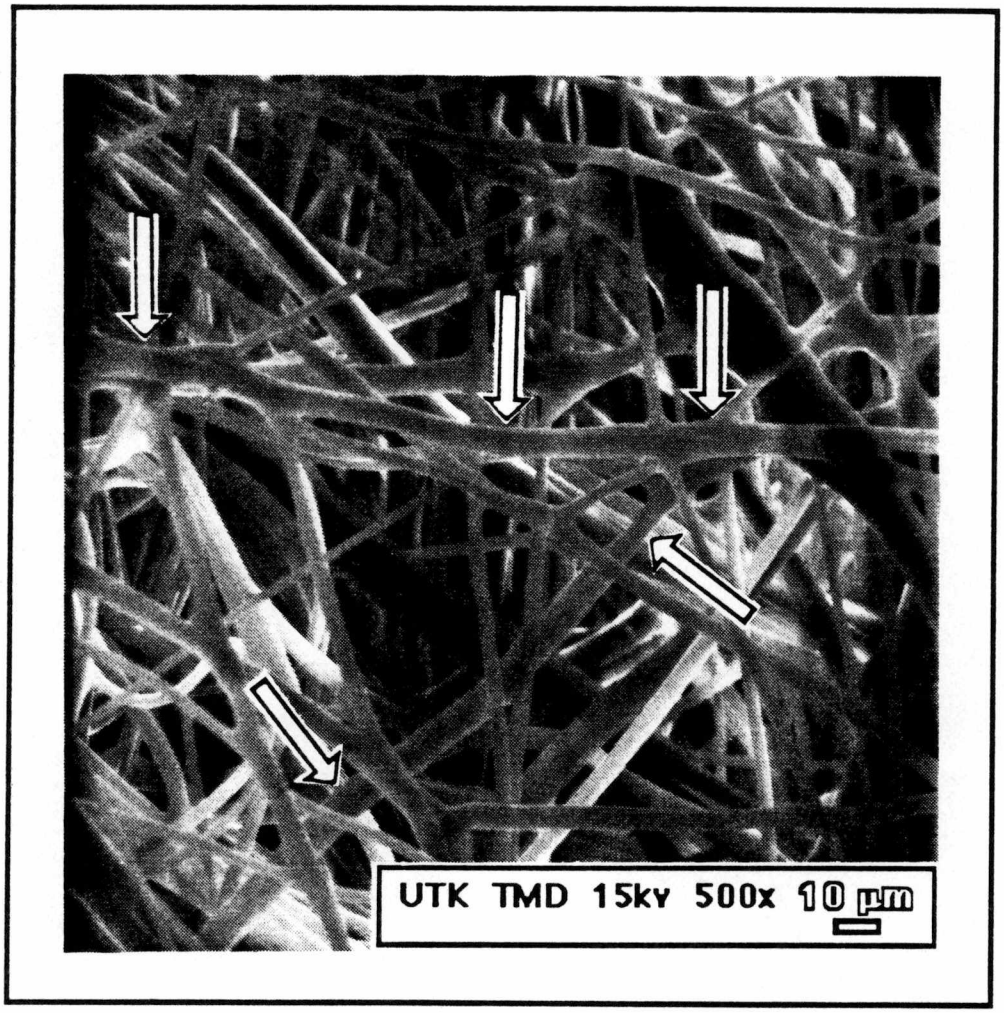

Figure 5.7. Photomicrograph showing variation in fiber diameter along a single fiber.

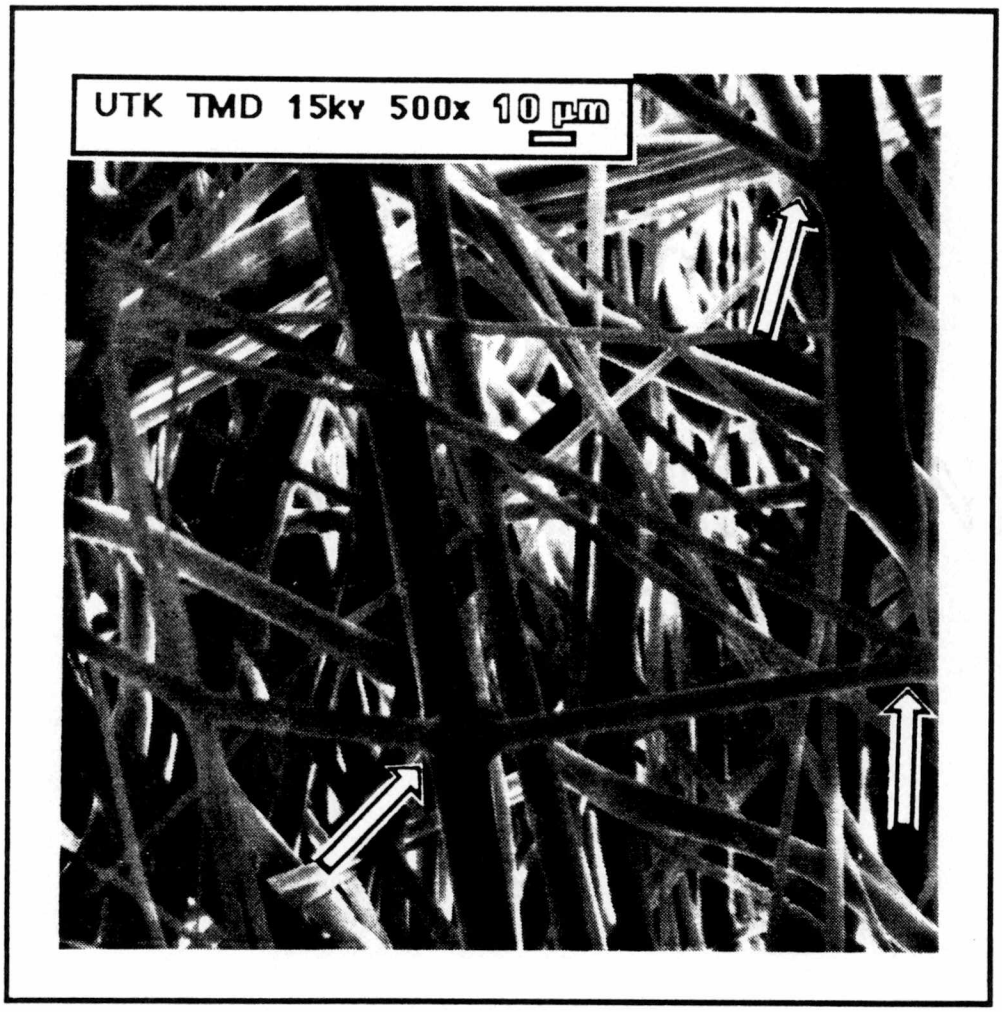

Figure 5.8. Photomicrograph showing thermal branching.

(branching) occurs when extrudate is **stressed in complex ways in flight** towards the collector.

Fiber Diameter Distribution

Figures 5.9 - 5.11 show fiber diameter distribution as a function of processing conditions. All the 160 g/min throughput fibers showed a sharp peak at 2 to 4 μm with a narrow distribution. The 320 and 480 g/min throughput rates fibers processed at 75% air rate using standard orifice die showed peaks at 4 to 6 μm with a slightly broader distribution. The 320 g/min throughput rate fibers processed at 90% air rate using the standard orifice die, and the 320 and 480 g/min throughput rate fibers processed at 75% air rate using small orifce die showed peaks at 2 to 4 μm with a slightly broader distribution.

Fiber birefringence

The measured birefringence is an indicator of molecular orientation in the fibers. The values of birefringence as a function of processing conditions are given in Table 5.3. The birefringence values ranged between 15.2×10^{-3} and 26.1×10^{-3}. The birefringence values decreased as throughput rate increased for fibers processed at 75% air flow rate using standard orifice die. The values peaked at 320 g/min for the fibers processed at 75% air flow rate using the small orifice die.

The birefringence values were higher and were comparable to the values of regular melt spun fibers as reported by Lu and spruiell [115-116]. Choi et al. [42] reported lower values than the values obtain in this study. The birefringence values certainly indicated that the melt blown fibers have

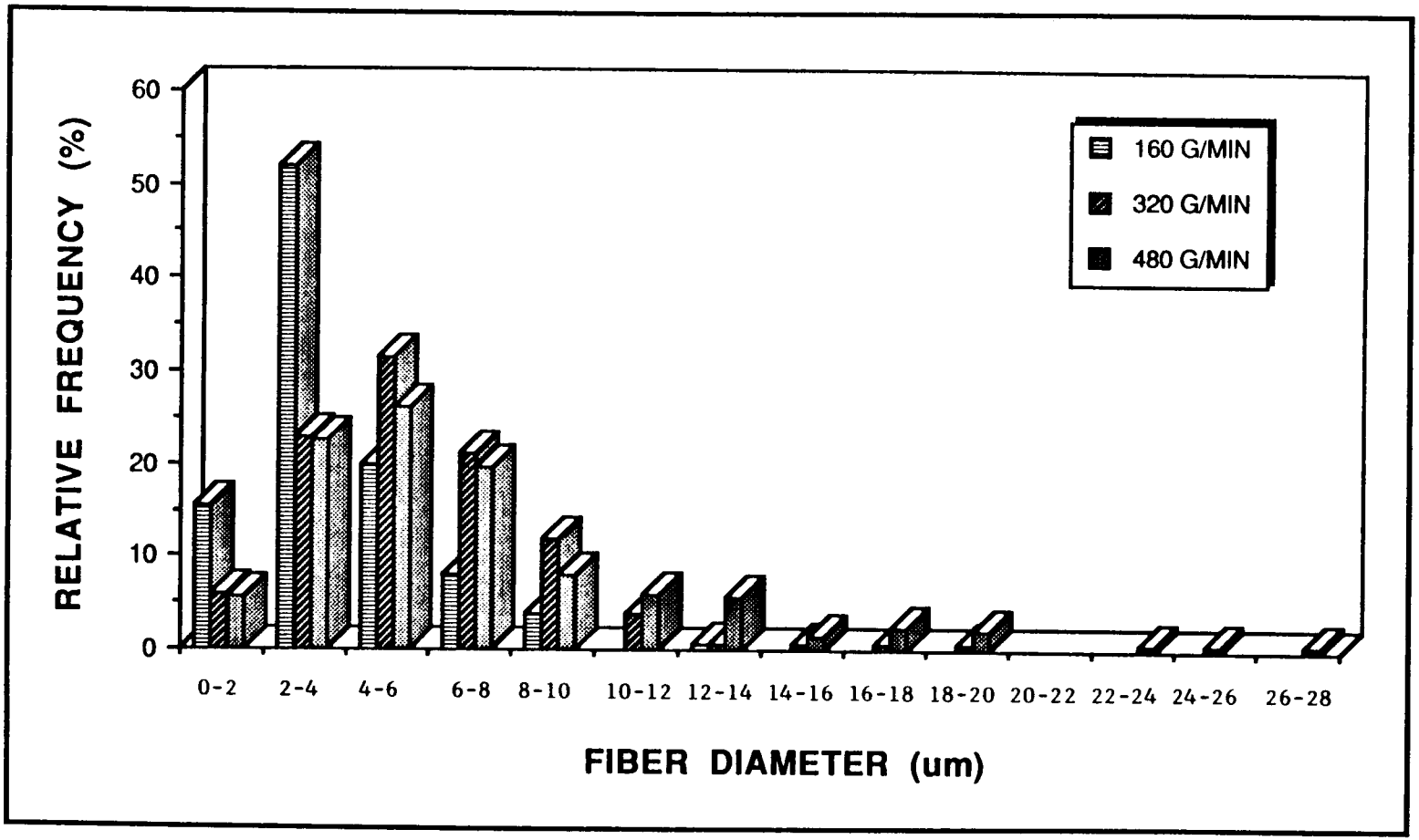

Figure 5.9. **Fiber diameter distribution of melt blown webs processed at 75% air flow rate using standard orifice die.**

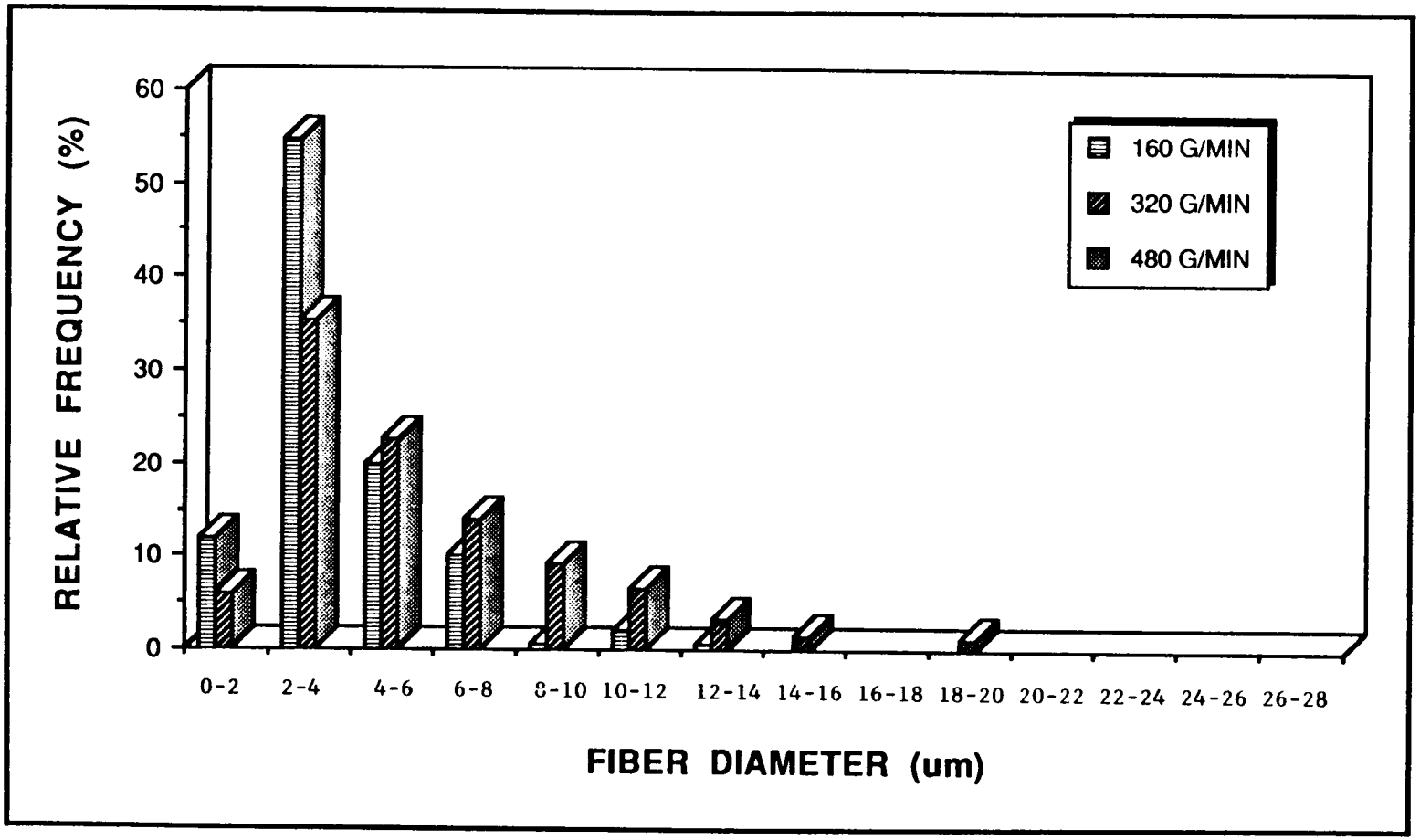

Figure 5.10. Fiber diameter distribution of melt blown webs processed at 90% air flow rate using standard orifice die.

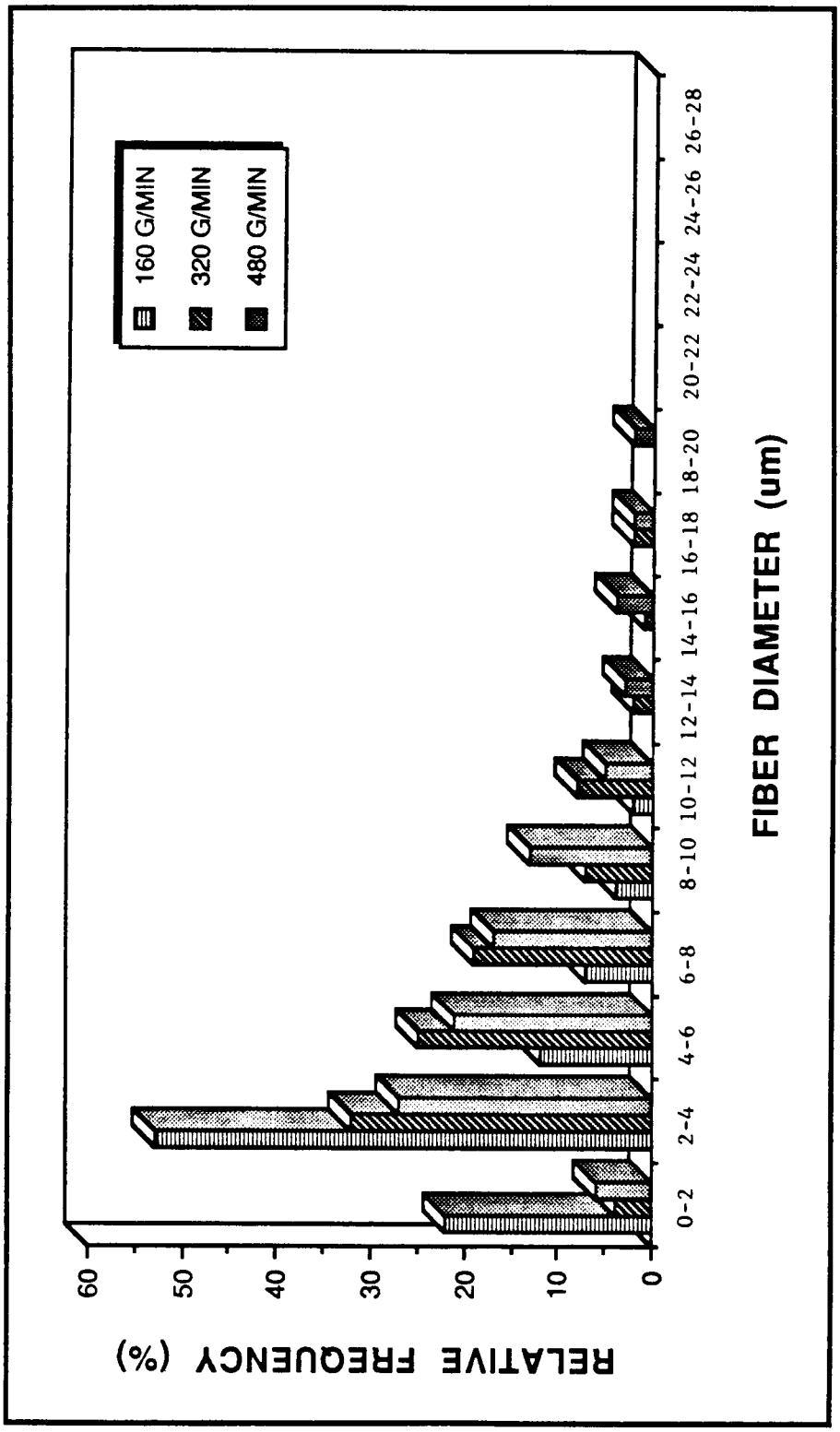

Figure 5.11. Fiber diameter distribution of melt blown webs processed at 75% air flow rate using small orifice die.

Table 5.3
Birefringence of melt blown fibers

Sample ID	Properties	Birefringence ($\Delta n \times 10^3$)
A	160 g/min	25.6
	320 g/min	21.8
	480 g/min	15.2
B	160 g/min	20.2
	320 g/min	24.1
C	160 g/min	24.7
	320 g/min	26.1
	480 g/min	20.5

A -- 75% air flow rate, standard orifice die
B -- 90% air flow rate, standard orifice die
C -- 75% air flow rate, small orifice die

orientation; however, the mechanism for molecular orientation in melt blown fibers was not clear.

Effects of Process Variables on Molecular Weight

The molecular weight of resins and webs were determined through GPC in order to assess the change in molecular parameters after processing. The intrinsic viscosity, molecular weight, and polydispersity index of "as recieved" resins and webs as a function of processing conditions are given in Tables D.4 - D.6 (Appendix D), and molecular weight values are shown in Figure 5.12. Figures E.9 - E.16 (Appendix E) show the GPC chromatograms as a function of processing conditions.

There was a notable **decrease** in intrinsic viscosity, molecular weight, and polydispersity index between the **resin** and the **webs**. The decrease in molecular weight and intrinsic viscosity was about 22 to 25%. This indicated thermal breakdown of polymer chains. The decrease in polydispersity index indicated that the polymer molecular weight distribution became narrow after processing (Figure 5.13). This was anticipated because of breakdown of longer polymer chains.

The difference in molecular weights and other parameters among different throughput rate webs was minimal. This indicated that the polymer did not experience severe thermal degradation at higher throughput rates. This was rather surprising because it is imperative that at higher temperatures and throughput rates, polymer degradation is usually more. The possible explanation for this is that at higher throughput rates, polymer residence time in

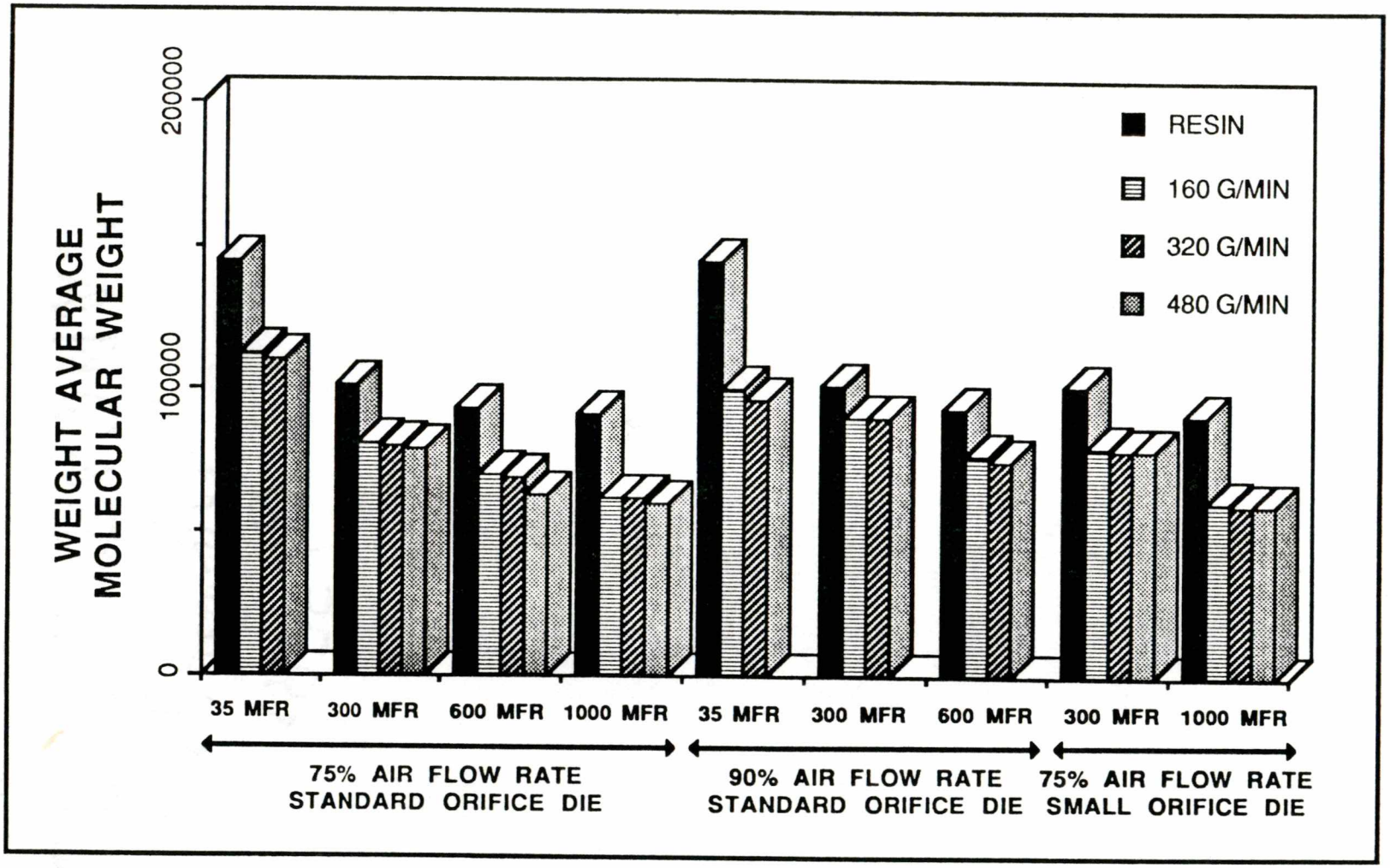

Figure 5.12. **Effect of MFR and process variables on weight average molecular weight of the webs.**

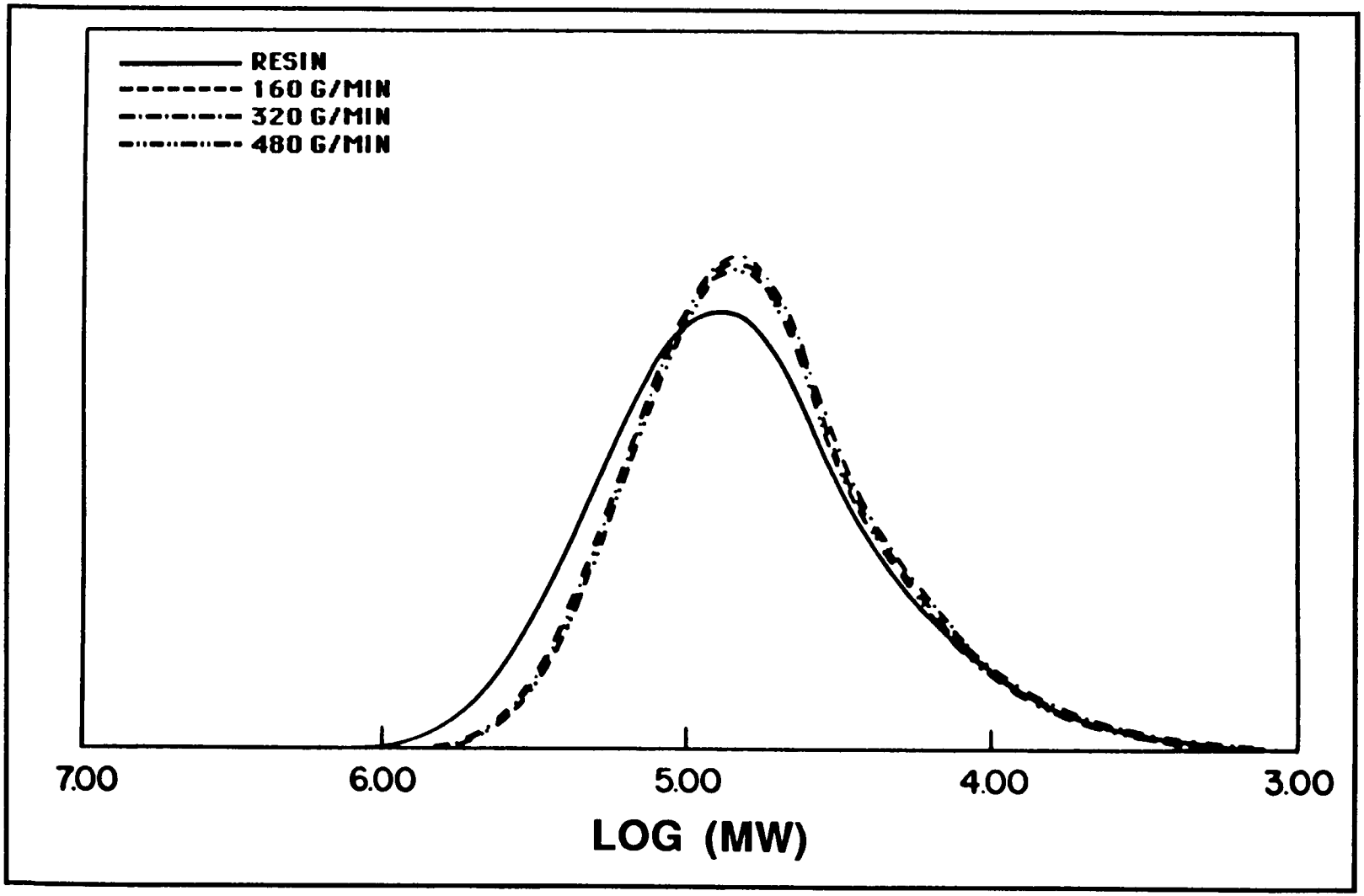

Figrue 5.13. GPC chromatograms of 300 MFR resin and webs processed at 75% air flow rate using standard orifice die.

the extruder is shorter which may have reduced the effects of higher temperatures; therefore, minimal change in molecular weights among webs.

The change in molecular weight between the standard orifice die and small orifice die webs at correponding throughput rate was minimal, even though the smaller orifice die had higher shear rate at the die tip due to higher mass velocity. This trend, in conjunction with the minimal change in molecular weight among webs, indicated that the shear rates were not high enough to cause notable changes in molecular weights of the webs as a fucntion of throughput rate. The 90% air flow rate webs showed less molecular degradation than 75% webs processed using the standard orifice die. This was attributed to lower processing temperatures at 90% air flow rate.

The measured melt flow rate values of resins and webs as a function processing conditions are given in Tables D.7 - D.9 (Appendix D), and shown schematically in Figure 5.14. There was a notable increase in MFR between the resin and webs which corresponded to simultaneous decrease in molecular weights. The increase was more greater for 35 MFR resin compared with 300, 600, and 1000 MFR resins at all processing conditions. This may be due to the fact that the 35 MFR resin had higher starting molecular weight with higher percentage of longer molecular chains and the numerical proprotional melt flow rate difference between 35 MFR and other resins was more than '8 times'. This indicated that the 35 MFR should degrade proprotionatly more than 300, 600, and 100 MFR resins.

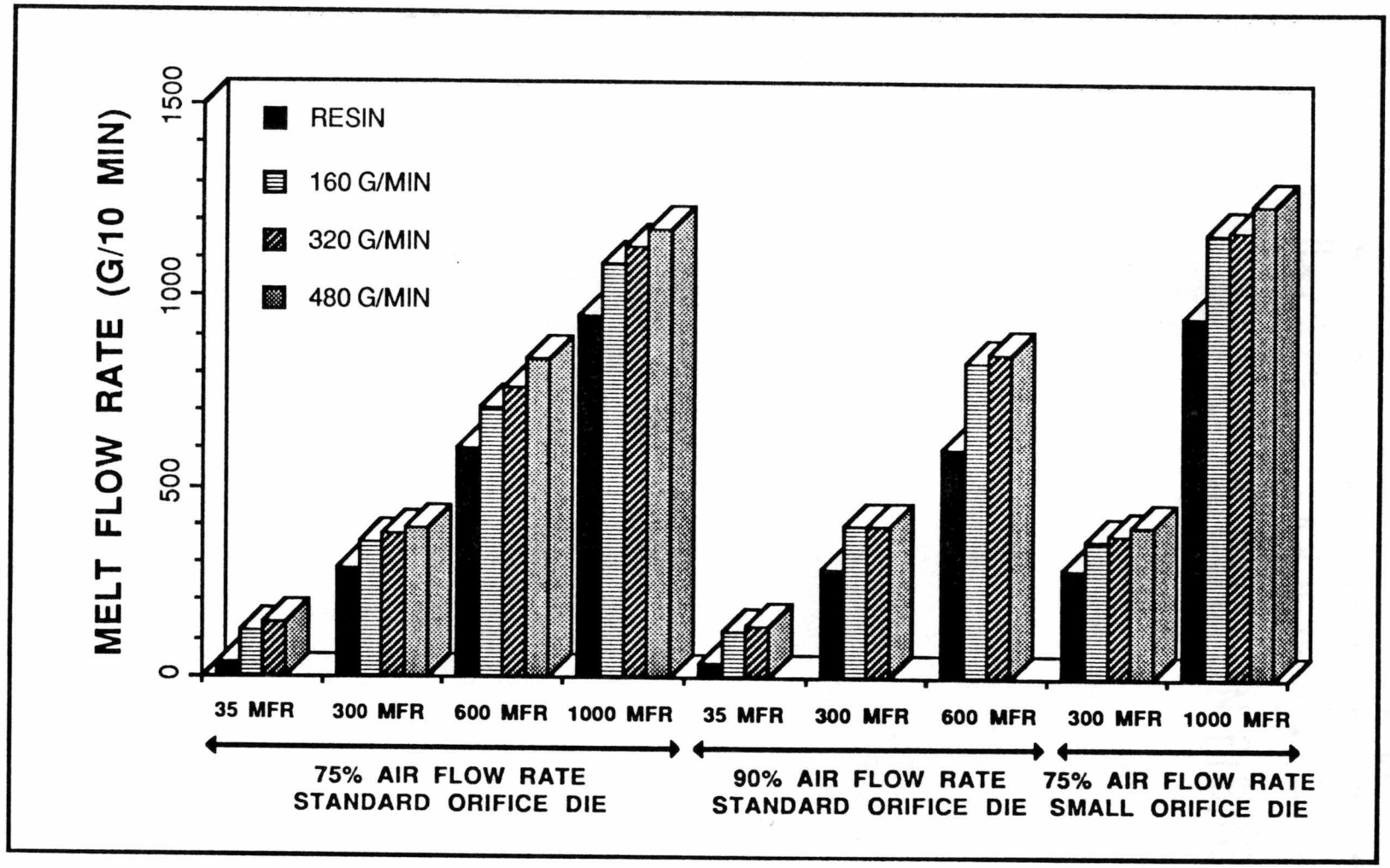

Figure 5.14. Effect of MFR and process variables on melt flow rate of the webs.

Effects of Process Variables on Physical Properties

The physical properties of conventional nonwovens are a manifestation of fiber properties and web structure. However, the melt blown web physical properties were found to be primarily dependent on processing conditions. The following is a discussion on effects of resins and process variables on physical properties.

Tensile Properties

The tensile properties of 35, 300, 600, and 1000 MFR PP melt blown webs as a function of processing conditions are given in in Tables D.10 - D.12 (Appendix D), and shown schematically in following six Figures.

Breaking Stress. The breaking stress values at which failure occured ranged between 3.5 and 20.7 mN/tex (Figures 5.15 - 5.16). The MD breaking stress was higher than the CD breaking stress. This was mainly due to anisotropy in orientation. In cross direction, the fibers are predominantly perpendicular to the test direction. So, the fiber "ends" are free and not gripped between the jaws. This results in lower resistance to deformation, even though some resistance is provided by the fiber entanglements and fiber bonding. Hence, the CD breaking stress is usually lower than MD breaking stress.

The maximum MD web breaking stress was obtained at a throughput rate of 320 g/min, with the exception of the 35 MFR resin webs and 300 MFR resin webs, processed using a small orifice die. Wadsworth and Jones [36] also

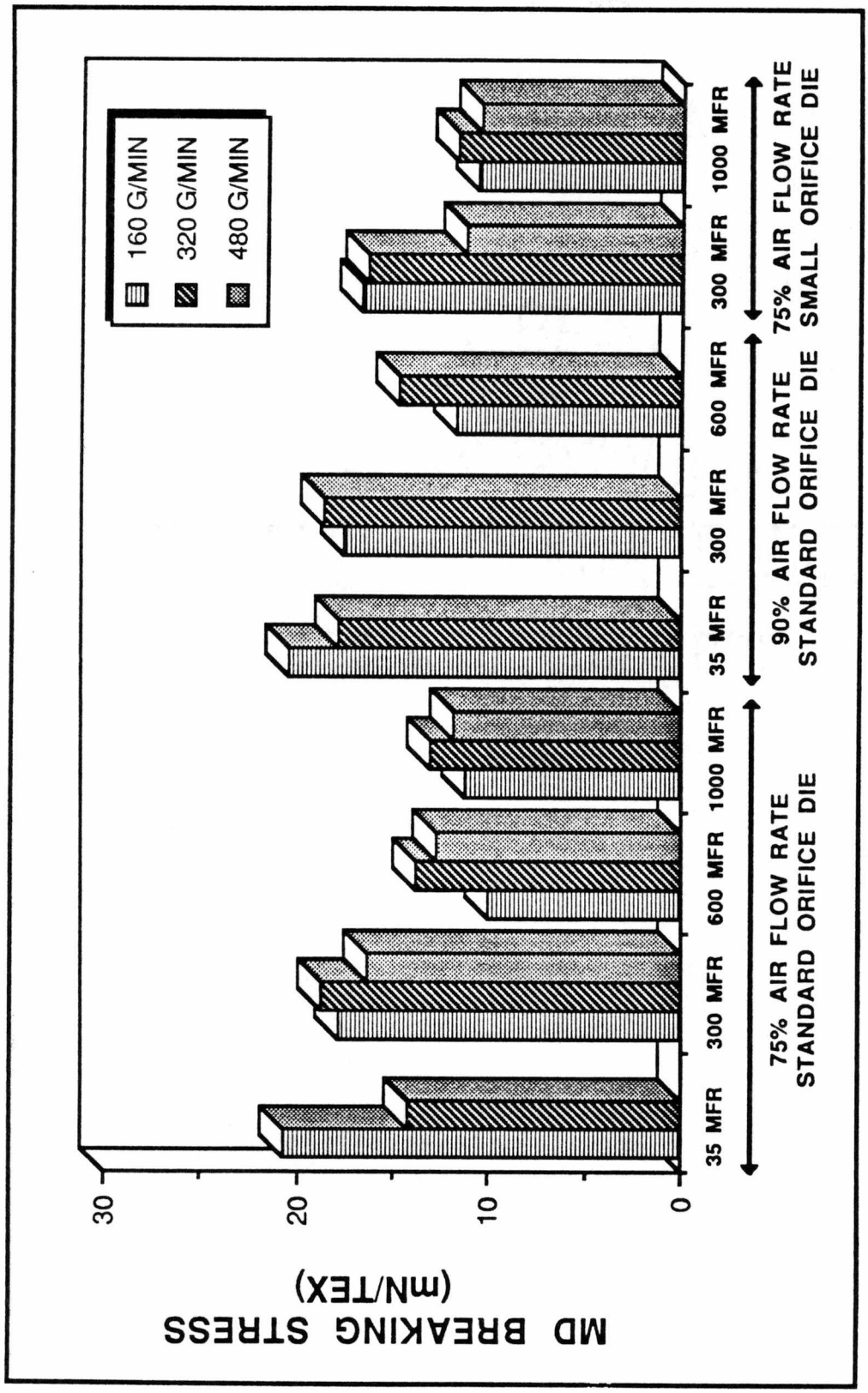

Figure 5.15. Effect of MFR and process variables on MD breaking stress.

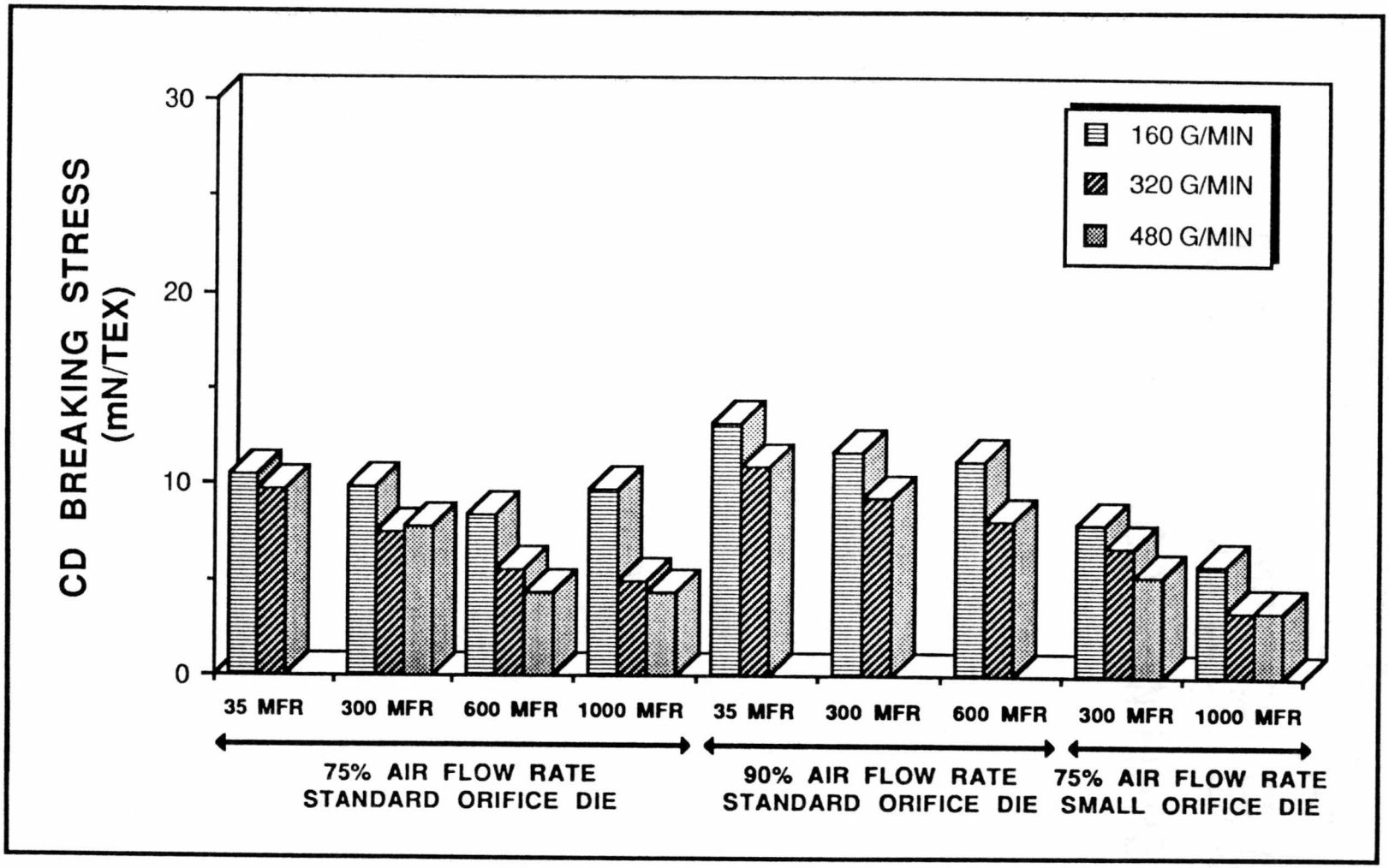

Figure 5.16. Effect of MFR and process variables on CD breaking stress.

reported higher MD breaking stress at higher throughput rates. The increase in MD breaking stress can be explained as folllows:

- the molecular weights of the higher throughput rate webs were almost the same as the lower throughput rate webs. Thus, the web strength should remain relatively constant; and,
- the quenching of the greater mass of the polymer at higher throughput rate may be less efficient due to slow heat transfer (lower cooling rate) from the resin (resulting in more residual heat), and hence more **fiber-to-fiber thermal bonding** (Figure 5.17). The fiber-to-fiber thermal bonding restricts the fiber shear movements during tensile deformation. Therefore, the deromation process requires more force.

Thus, this increased fiber-to-fiber thermal bonding, in conjunction with minimal change in molecular weight between higher throughput and lower throughput webs, resulted in higher breaking stress at higher throughput rate.

The CD breaking stress decreased as the throughput rate increased. This was mainly to the web structure. The **openess of web structure** in high throughput rate webs, in conjunction with less fiber orientation in the test direction, resulted in lower resistance to deformation even with increased fiber-to-fiebr thermal bonding. Therefore, decrease in CD breaking stress with increase in throughput rate.

Breaking stress decreased non-linearly with the increased melt flow rate in both MD and CD. Jones [35] reported that the breaking stress increases initailly with MFR, peaks, and then decreases considerably at the higher melt flow rates. The decrease in breaking stress was expected because of decrease in molecular weight, since polymer strength is directly proportional to molecular weight.

Figure 5.17. Photomicrograph showing fiber-to-fiber thermal bonding.

The change in air flow rate from 75 to 90% had minimal effects on MD breaking stress, but the CD breaking stress increased with the air flow rate. The ratios of MD to CD breaking stress of the webs processed at 90% air flow rate were less anisotropic than the webs processed at other conditions. This indicated that at higher air flow rate more random orientation results.

The 300 and 1000 MFR webs processed using small orifice die had slightly lower breaking stress values than the webs processed using standard orifice die. It is probable that in small orifice die due to hihger shear rate at the die tip, more fiber branching would have occured; therefore, lower overall breaking stress.

Breaking Strain. The breaking strain values at breaking stress ranged between 1.6 and 65.2% (Figures 5.18 - 5.19). The MD breaking strain was lower than the CD breaking strain due to higher fiber orientation in MD which inhibits extension. The breaking strain dramatically decreased as the polymer throughput rate increased in both MD and CD. The similar trend has been reported by [35-40].

It was hypothesized that the decrease in breaking strain was largely due to the increased **fiber-to-fiber thermal bonding** with the higher throughput rate webs as was indicated by SEM photomicrographs (Figure 5.17). This increased fiber-to-fiber thermal bonding would be expected to restrict the fiber shear movements resulting in low strain. The increased fiber-to-fiber thermal bonding can be attributed to **residual heat** due to **lower cooling rates** of polymer streams at high throughput rates.

The breaking strain increased slightly with increased air flow rate at corresponding MFR and air flow rate. This can be attributed to the reduced

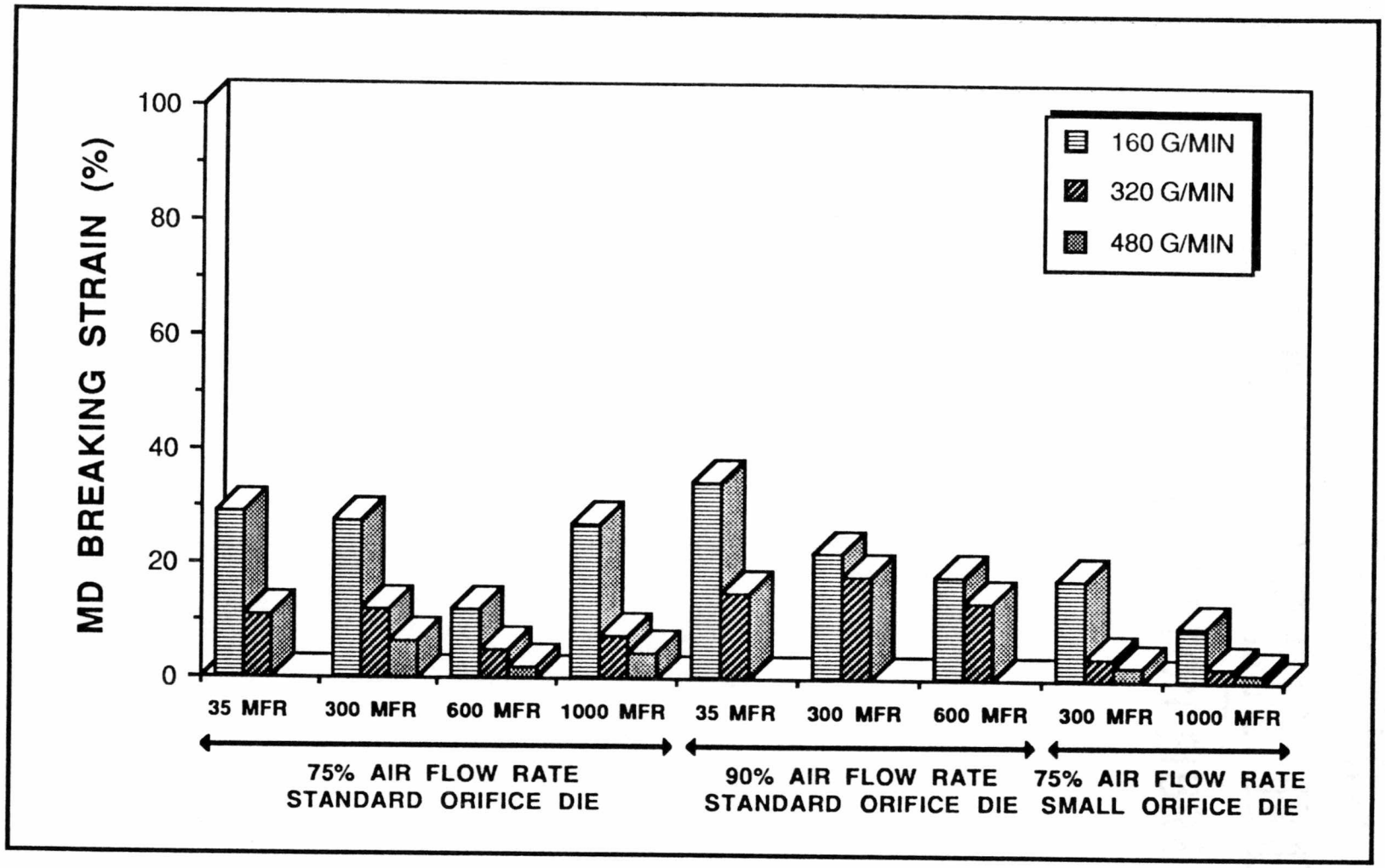

Figure 5.18. Effect of MFR and process variables on MD breaking strain.

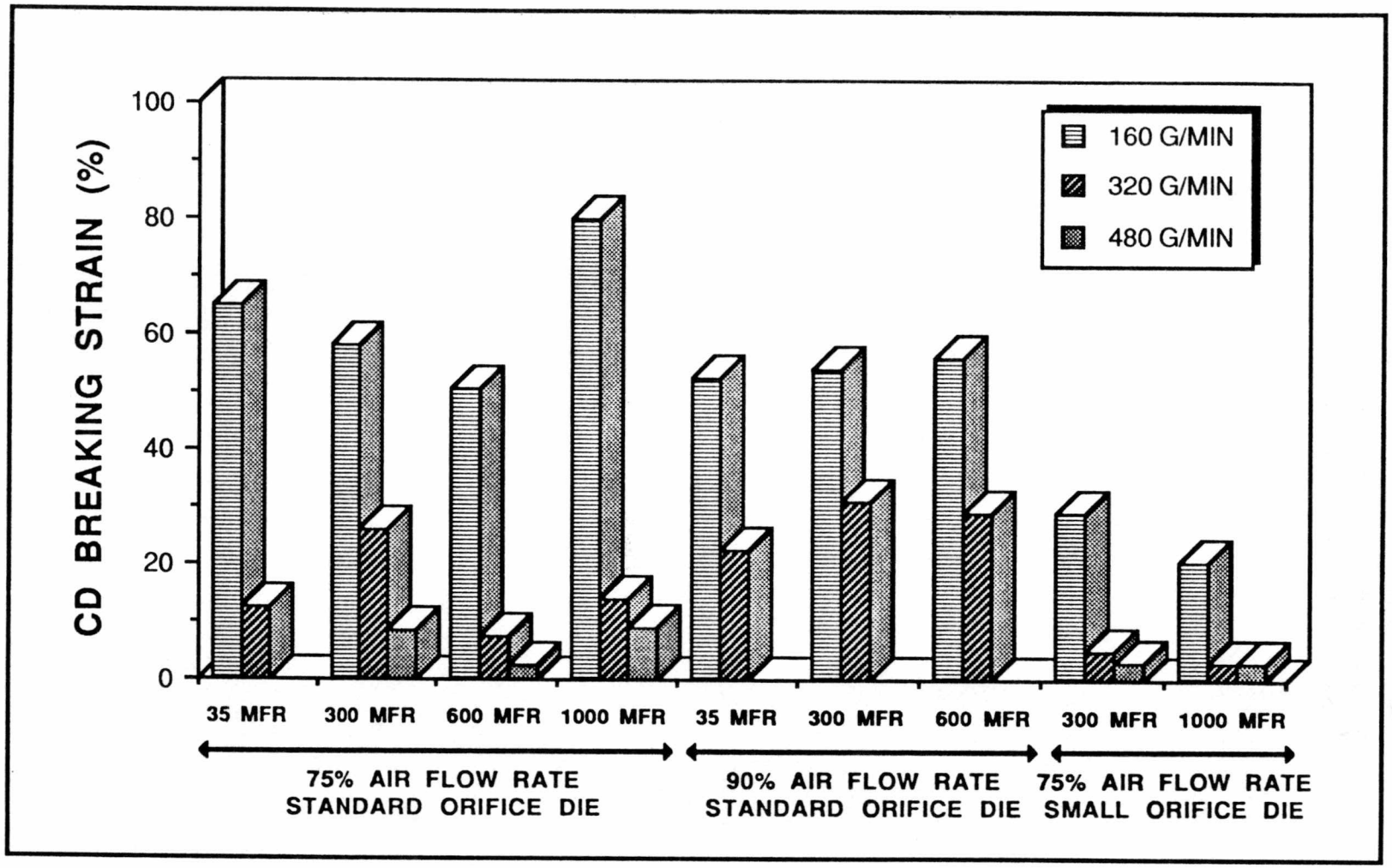

Figure 5.19. Effect of MFR and process variables on CD breaking strain.

fiber-to-fiber thermal bonding because of lower air temperatures at high air flow rate conditions. The reduced bonding **increases the fiber freedom**; hence, higher breaking strain. Overall, ther breaking strain decreased as the MFR increased at all processing conditions due to simultaneous decrease in molecular weight. The breaking strain values of webs processed using small orifice die were lower, especially for 320 and 480 g/min webs, than the webs processed at other conditions. This may be due to higher processing temperatures for small orifice die than standard oriifce die; which in turn may have increased fiber-to-fiber thermal bonding. Hence, lower breaking strain.

Initial Modulus. The initial modulus values ranged between 49 and 574 mN/tex (Figures 5.20 - 5.21). The MD modulus was higher than the CD because of higher fiber orientation in MD. The initial modulus increased as the polymer throughput rate increased in both MD and CD (except in 35 MFR resin webs (MD) processed at 75% air flow rate using standard orifice die). The increase in modulus corresponded to the simultaneous decrease in breaking strain. The increase in initial modulus may have been due to was due to **high fiber-to-fiber thermal bonding** and **large diameter fibers**.

Overall, the modulus decreased as the MFR increased at all three throughput rates due to decrease in molecular weight. The webs processed at 90% air flow rate using the standard orifice die showed lower modulus than the webs processed at 75% air flow rate using standard orifice die. This can attributed to **soft** and **bulky web structure** resulting in low initial resistance during tensile deformation. The effect of change in die orifice die was minimal for the webs processed at 160 g/min. However, the effect was noticeable for 320 and 480 g/min webs at corresponding MFR. This was attributed to

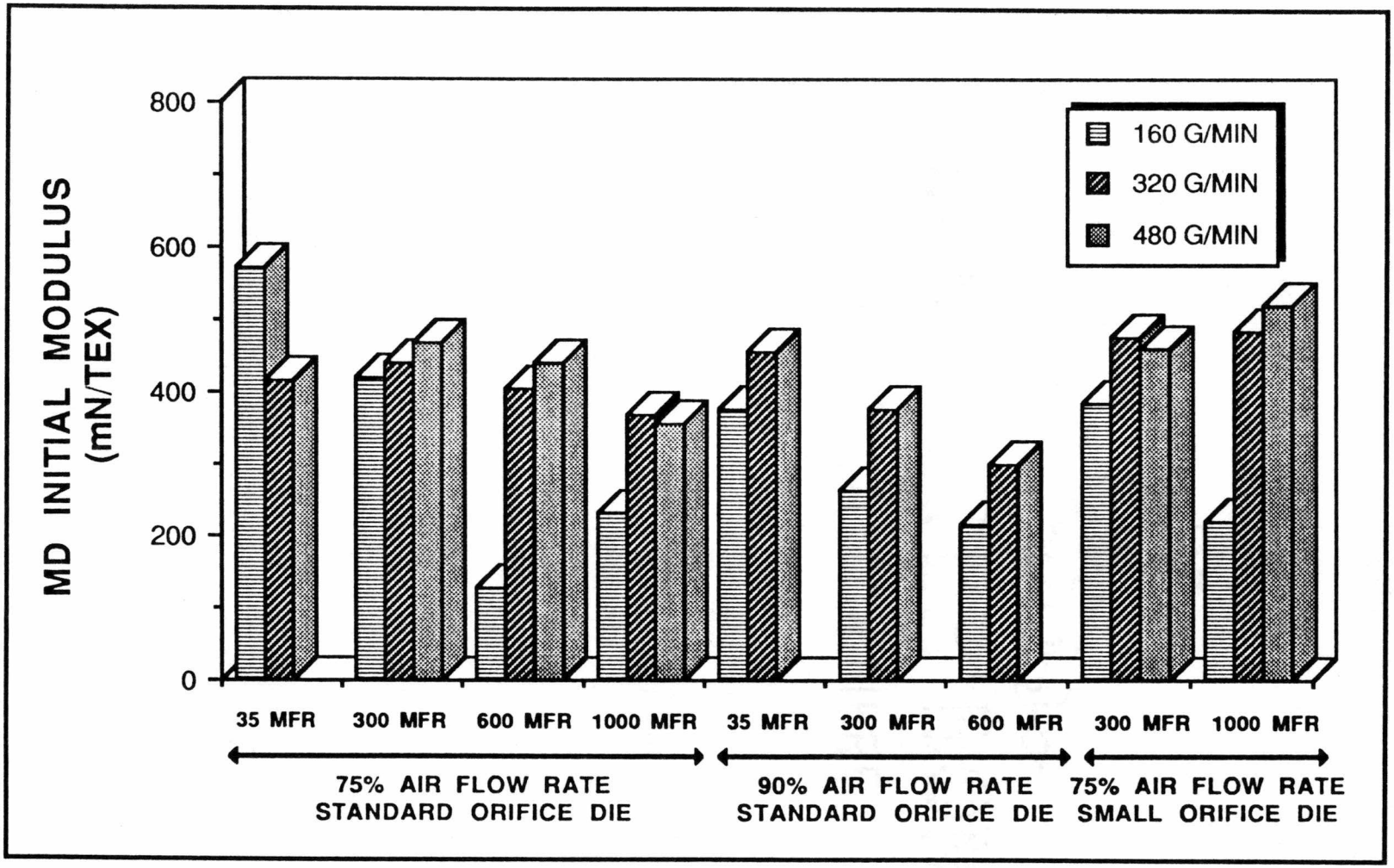

Figure 5.20. Effect of MFR and process variables on MD initial modulus.

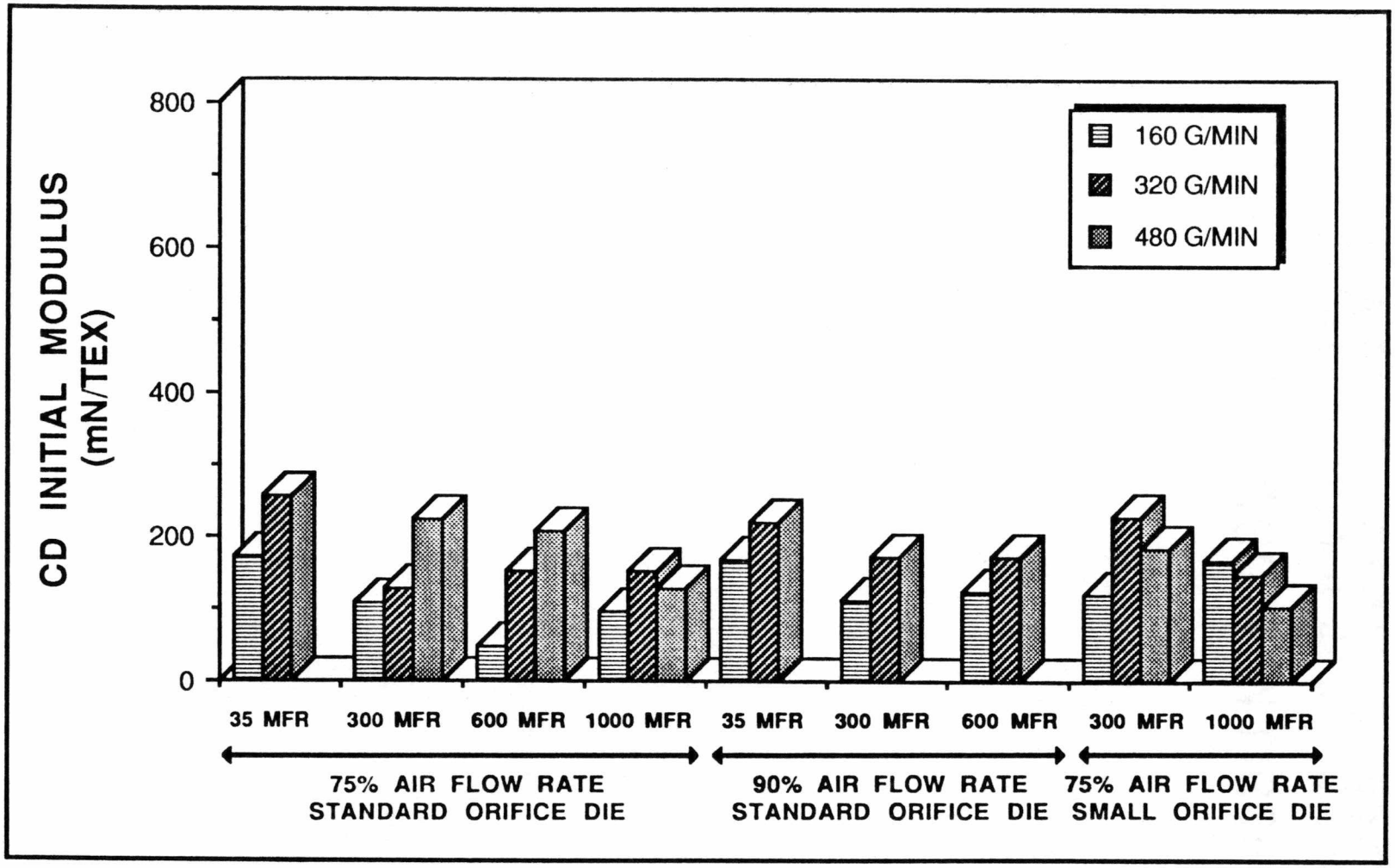

Figure 5.21. Effect of MFR and process variables on CD initial modulus.

increased brittle characterisitcs of the webs (since the breaking strain was lower).

Stress-Strain Curves. Figure 5.22 and Figures E.17 - E.24 (Appendix E) show typical tensile stress-strain curves as a function of processing conditions. The tensile stress-strain curves showed **two distinct regions of deformation**. The **initial region** showed a steep rise in stress with a small increase in strain, and was followed by a **second region** with a more gradual rise in slope. The second region was more dominant in the 160 g/min throughput webs than 320 and 480 g/min throughput webs. This indicated a more ductile behavior of 160 g/min throughput webs. The low throughput web, stress-strain curves showed an inflection point between 7 to 10% strain, beyond which the curves were concave downward. The MD and CD stress-strain curves followed the same general trend. The curvature of the stress-strain curves was smooth, except in a few cases where the data discrepancy made it slightly irregular.

Single Fiber Properties. The single fiber breaking stress and strain values are given in Tables D.10 - D.12 (Appendix D), and are shown in Figures 5.23 and 5.24. The breaking stress values ranged between 26 and 42 MPa and breaking strain values ranged between 17 and 70%.

In a majority of the cases, as the throughput rate increased, the fiber breaking stress increased first and then decreased. This trend was similar to the trend found for web breaking stess. This peak in breaking stress with polymer throughput rate may have been due to the change in morphological properties of single fibers. The breaking strain decreased with increased

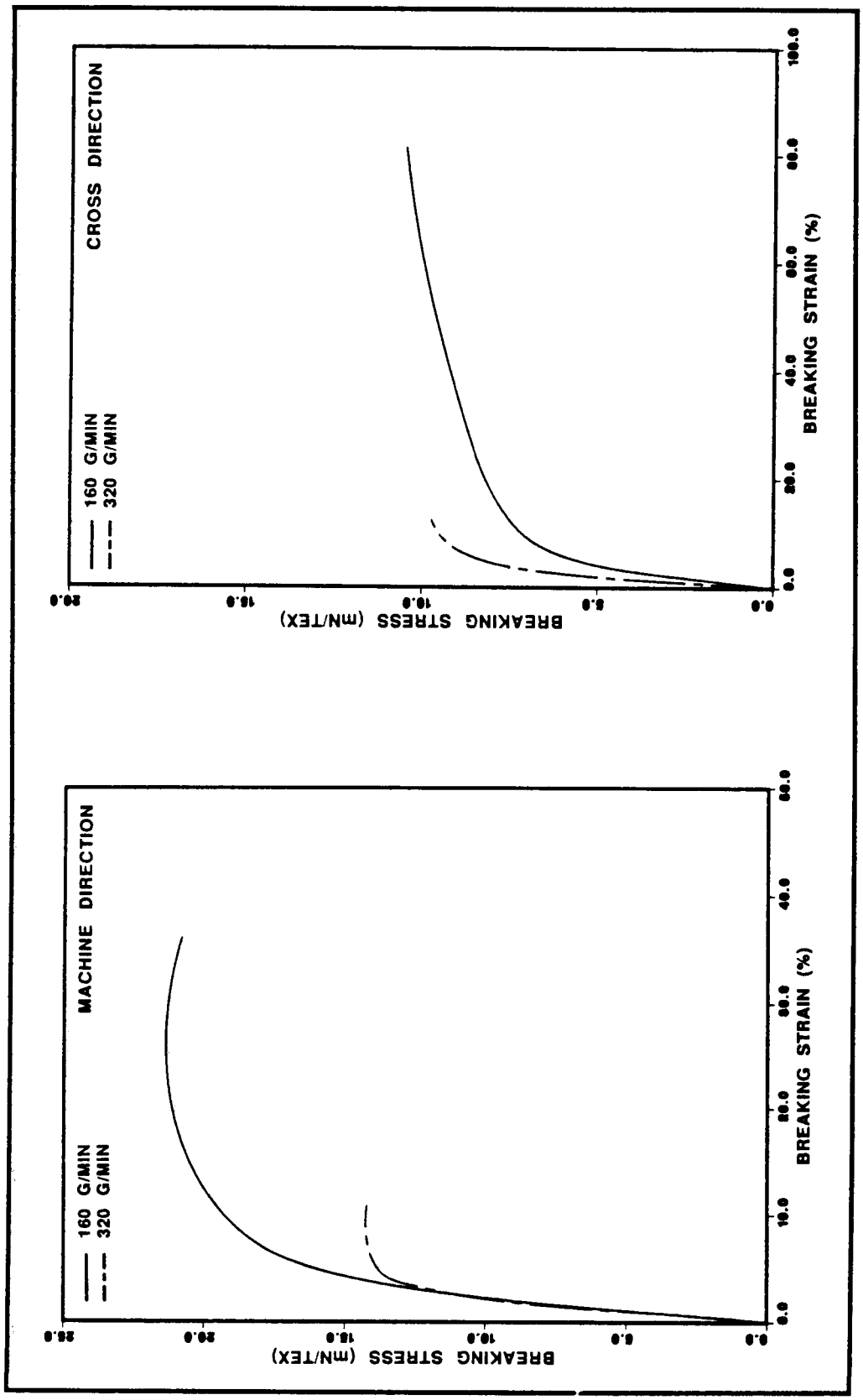

Figure 5.22. Average MD and CD stress-strain curves of 35 MFR webs processed at 75% air flow rate using standard orifice die.

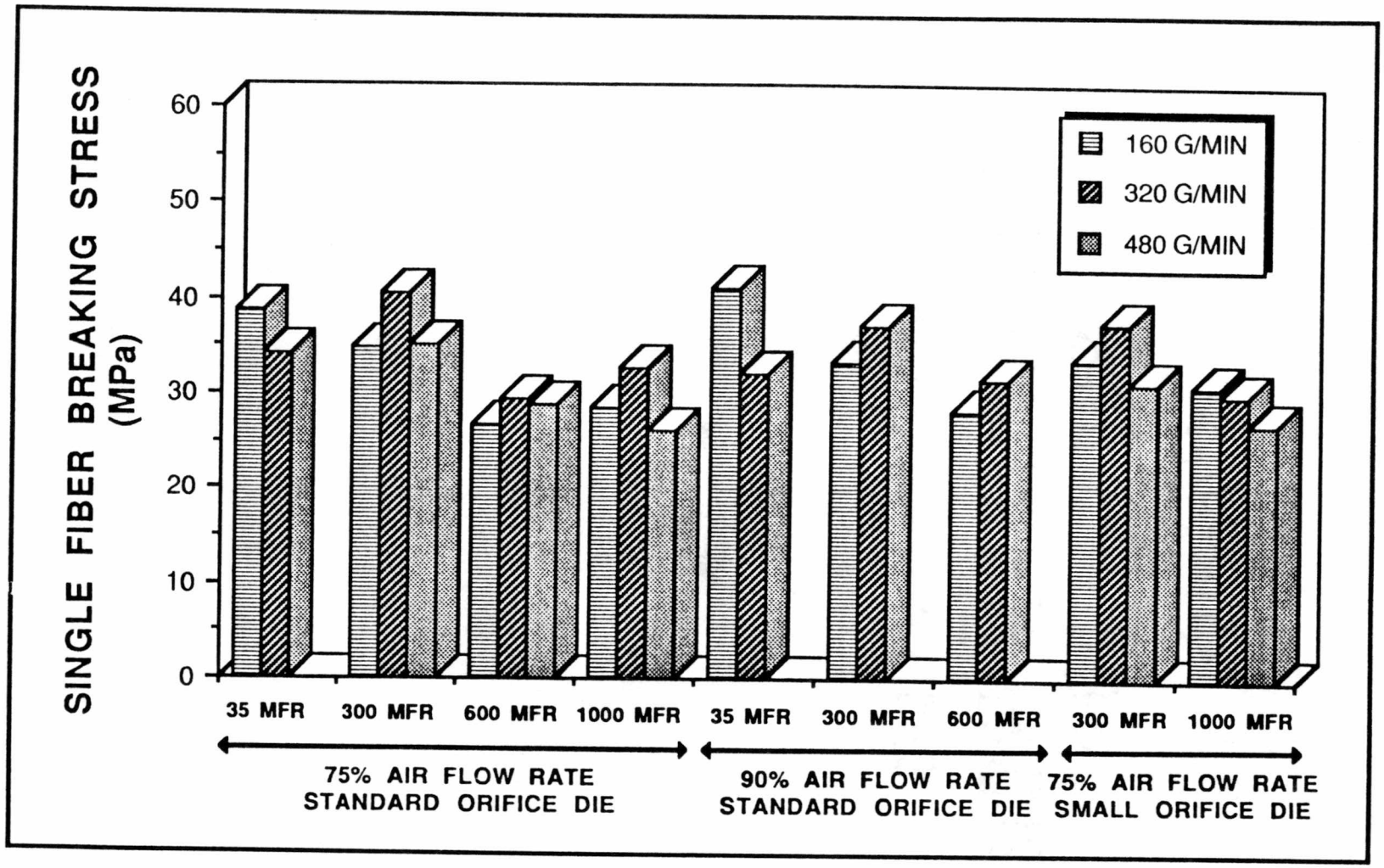

Figure 5.23. Effect of MFR and process variables on single fiber breaking stress.

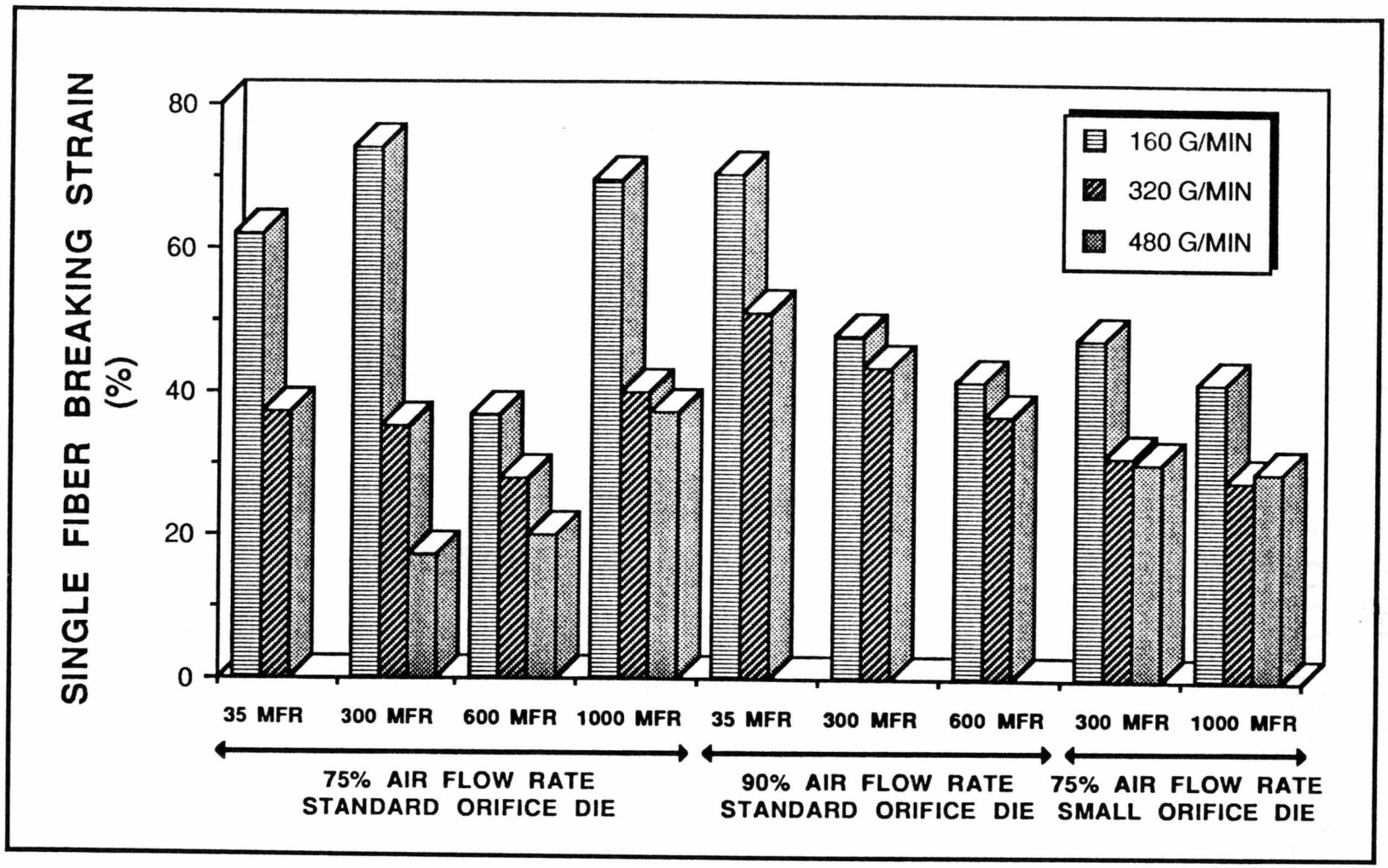

Figure 5.24. Effect of MFR and process variables on single fiber breaking strain.

throughput rate at all conditions. This decrease can be attributed to the brittle characteristics of single fibers imparted propbably by partial change in crystal structure as indicated by DSC and WAXD analysis. The single fiber breaking strain decreased with increased MFR at all processing conditions except for the fibers processed at 75% air flow rate using standard orifice die.

Single Fiber--Web Co-relationship. The single fiber breaking stress and strain were higher than the web breaking stress and strain (Table D.13 - D.15, Appendix D). The single fiber breaking stress was approximately twice than that of web and breaking strain was approximately three to five times than that of web. The higher single fiber properties than the web properties is a usual trend in nonwovens. This is because, in nonwoven webs, the single fiber properties **tend to loose some of their effectiveness** (or translational efficiency) due to **angular distribution** of fibers in the web, and **stress concentration** arising at fiber cross-over points during deformation [136]. In a melt blown web, fibers make substantial angels with any given direction and to the applied loading; hence, load borne by the fibers during tensile deformation is uneven. Furthermore, **stress concentrations** at the **fiber cross-over points** are believed to promote **premature failure**. This would result in, less tranlation of single fiber properties to web properties. The comparision of single fiber properties with web properties indicated that the web property is a function of single fiber strength as well as web structure (fiber entanglements and fiber-to-fiber bonding).

Failure Modes

The typical tensile failure modes of melt blown webs are shown in Figure 5.25. Typically, three types of failure modes were observed: **ductile**, **brittle**, and **laminar**. Ductile failure infers a reduction in web cross-sectional area during deformation, brittle failure infers cohesive failure involving instantaneous break, and laminar failure infers separation of face and back of the web near the fracture zone during deformation. All the failure modes were a result of different web structures with different deformation mechanisms.

The **ductile** failure was associated with the soft low polymer throughput (160 g/min) webs processed at 75% air flow rate using standard and small orifice dies. The ductile failure was believed to be due to fiber dis-entanglements and slippage within a restricted region in the webs [85]. Fiber pull-out (a characteristics of a non-brittle failure [117]) was also observed at the rupture zone, as shown in Figure 5.26. The **brittle** failure was mainly associated with higher polymer throughput rate webs. The webs produced with 90% air flow rate were less brittle at all polymer throughput rates. The brittle failure can be attributed to high degree of **fiber-to-fiber thermal bonding**, resulting in high modulus and low strain. The brittle failure was instantaneous and was belived to have occured at the fiber cross-over points or due to fiber rupture. The brittle failure zones were fairly well-defined and restricted (as shown in Figure 5.27), and individual fiber failure was observed at the fracture zones as shown in Figure 5.28. The **laminar** failure was mainly associated with the low polymer throughput webs processed at 90% air flow rate and was believed to be due to **bulkiness of the webs**. The bulkiness of the web may

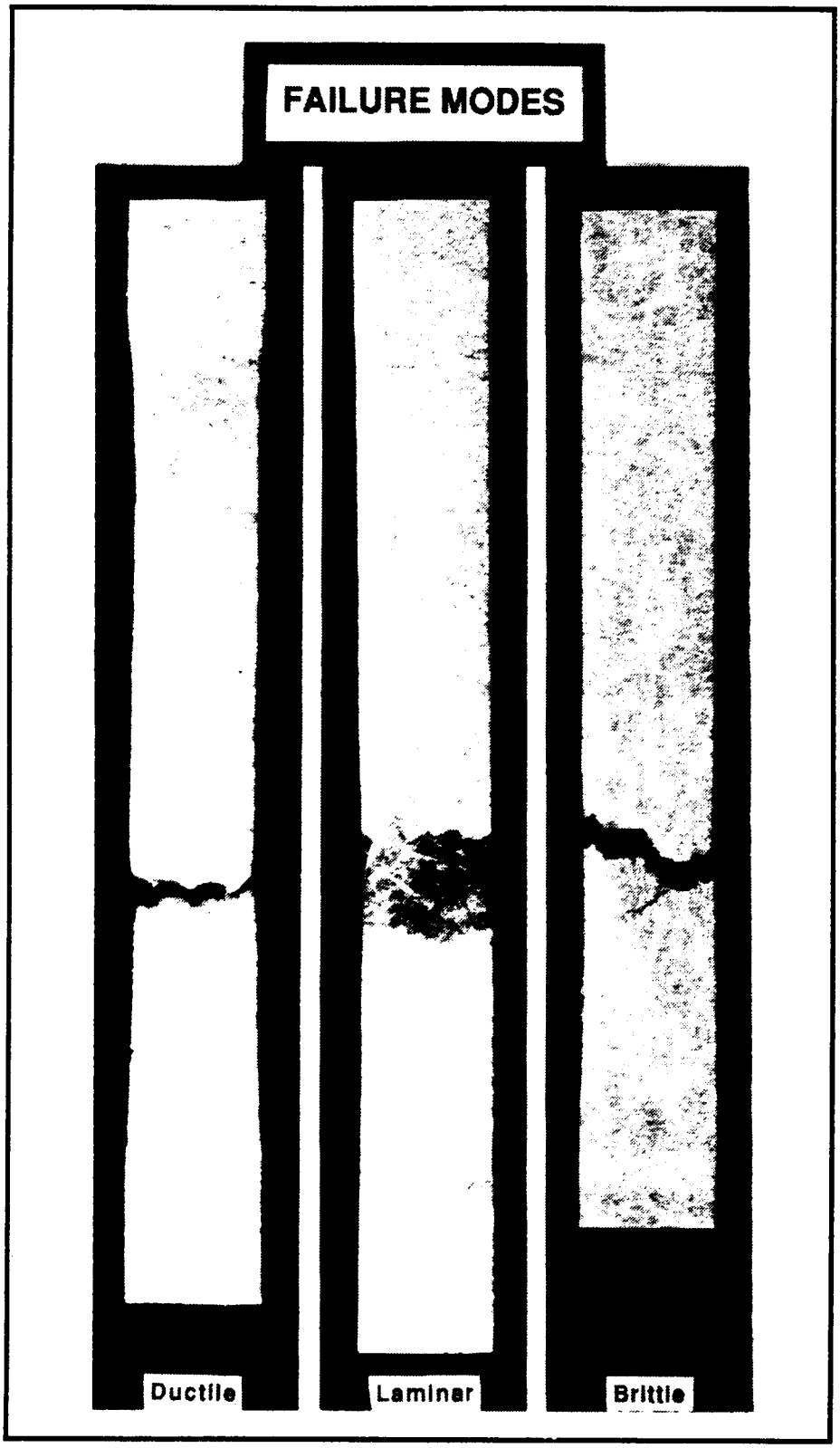

Figure 5.25. Photograph showing melt blown web failure modes.

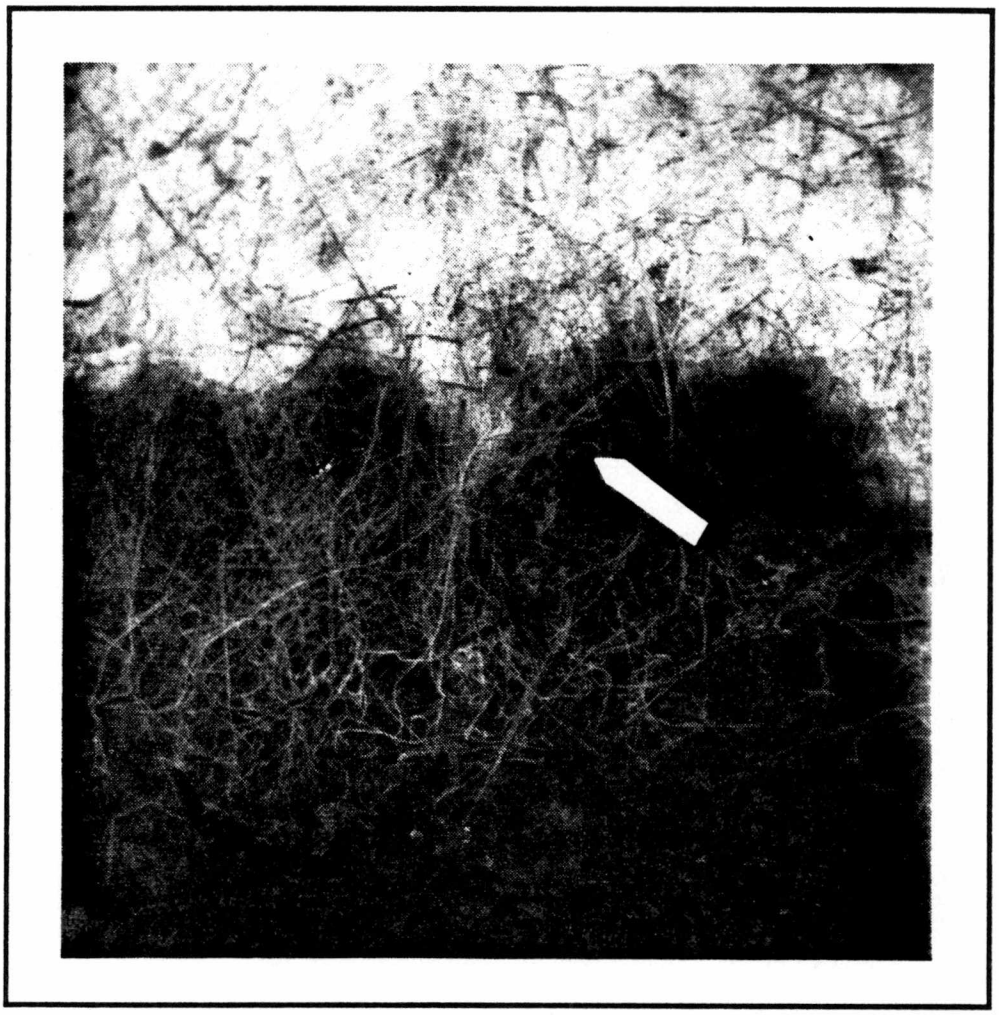

Figure 5.26. Photomicrograph showing fiber pull-out zone.

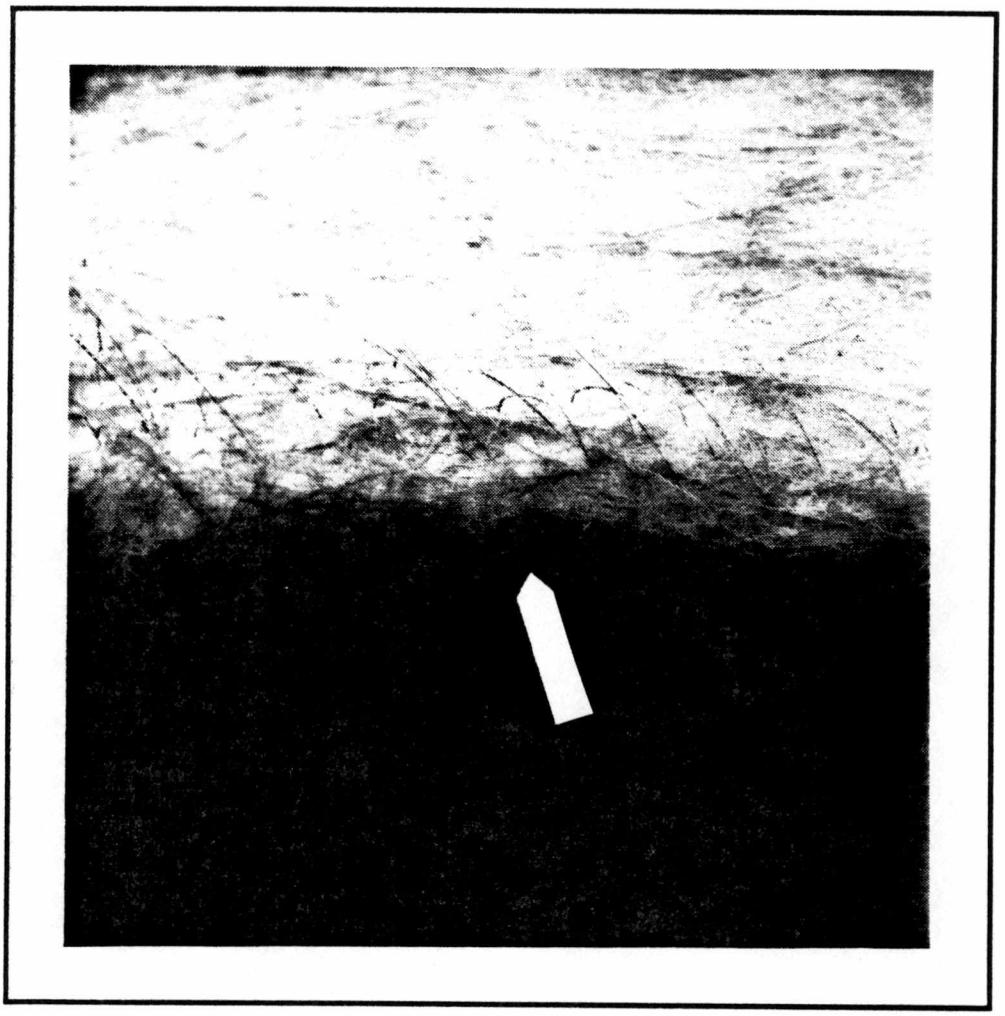

Figure 5.27. Photomicrograph showing brittle failure zone.

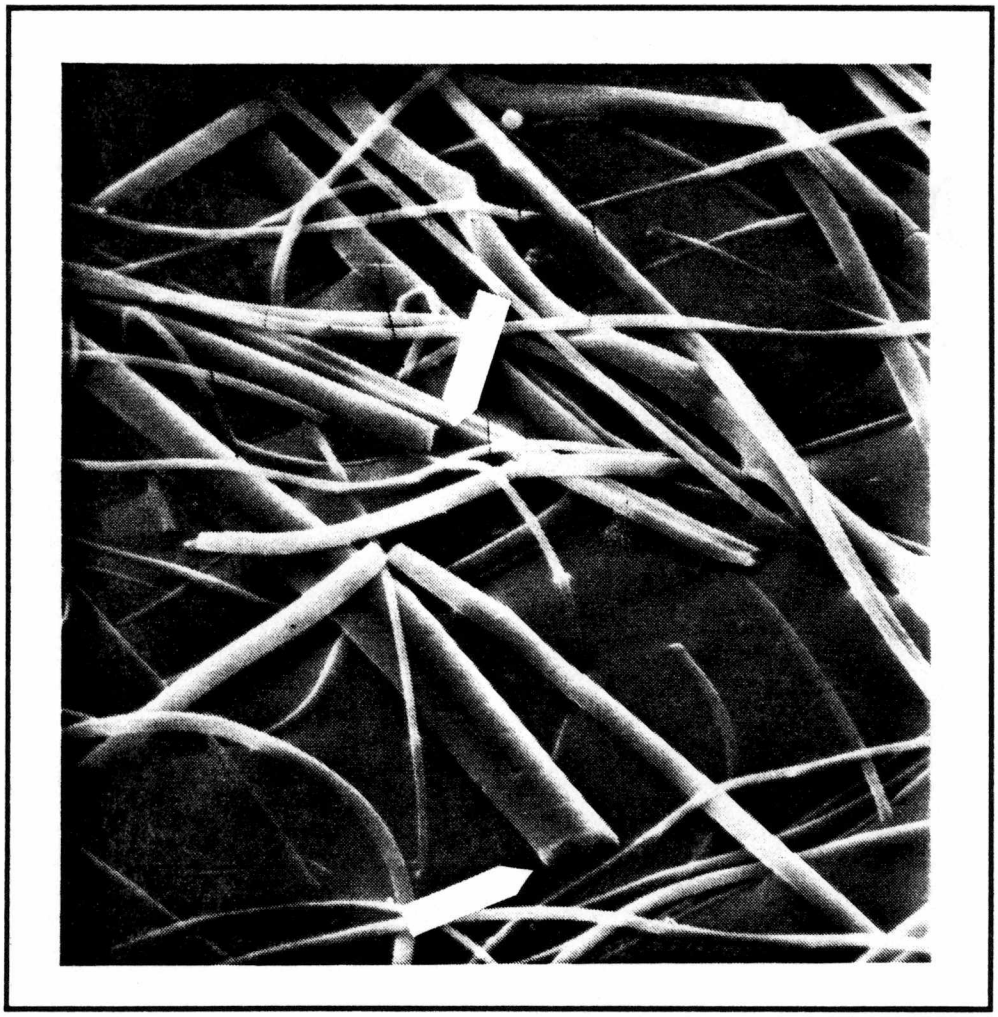

Figure 5.28. Photomicrograph showing fiber fracture.

have given rise to slippage of fibers between the face and back of the web during deformation, resulting in a laminar failure.

Most of the web specimens failed at the **mid-length** of the gauge length during testing (Figure 5.29). However, some of them failed near the **jaw**. The jaw break may have been due to misalignment of the jaws with the Instron tensile tester load cell.

Bursting Strength

Bursting strength is a measure widely used for nonwovens where the web construction do not lend themselves to tensile tests [118]. Bursting strength is defined as a force required to rupture a web by distending it with a force applied at right angle to the plane of the fabric under specified conditions [118]. Bursting strength values as a function of procesing conditions are given in Tables D.16 - D.18 (Appendix D), and are shown schematically in Figure 5.30.

Bursting strength decreased dramatically as the throughput rate increased. The sharp decrease in bursting strength values was due to the brittle characteristics of the higher throughput webs imparted by a high degree of **fiber-to-fiber thermal bonding, openness of the web structure**, and **single fiber properties**. The open web structure of high throughput rate webs, in conjunction with brittle charcterstics, may have provided less resistance to the applied force; hence, decrease in bursting strength. Bursting strength followed the same trend as breaking strain. The same trend has been shown by Wadsworth et al. [36].

The bursting strength also decreased with increased MFR for 160 and 320 and 480 g/min g/min throughput rate webs processed at 75% air flow rate

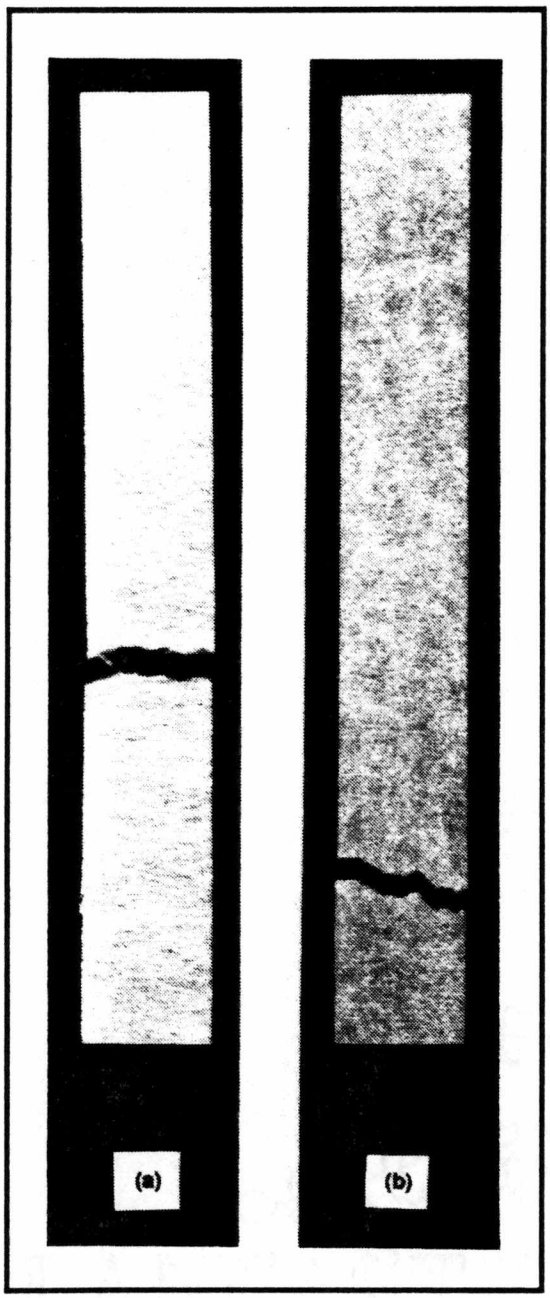

Figure 5.29. Photograph showing positions of specimen break.

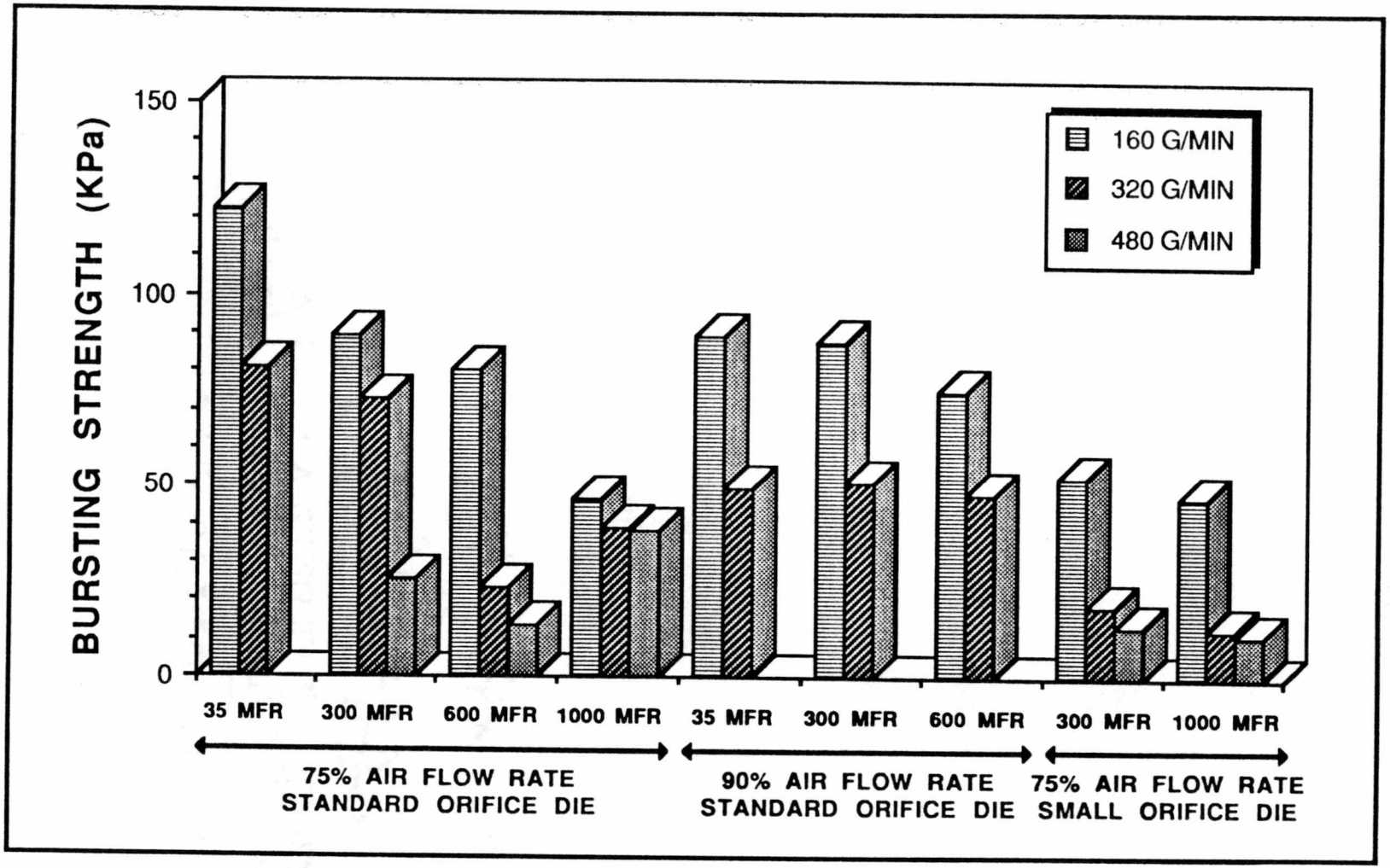

Figure 5.30. Effect of MFR and process variables on bursting strength.

using the standard and small orifice die . This decrease was expected since polymer strength is greatly proportional to molecular weight. The similar trend has been shown by Jones [35] for 35, 325, and 840 MFR polypropylene resins. The change in bursting strength as a function of MFR was minimal for webs processed at 90% air flow rate using the standard orifice die.

As the air flow rate increased from 75 to 90%, the bursting strength decreased at corresponding throughput rates for 35, 300, and 600 MFR resin webs. The decrease was more noticeable in 35 MFR resin webs than 300 and 600 MFR resin webs. This may have been due to softness and less fiber-to-fiber thermal bonding in 90% air flow rate webs. The 300 and 1000 MFR resin webs processed using the small orifice die had the lowest bursting strength values.

Flexural Rigidity

Flexural rigidity values as a function of processing conditions are given in Tabels D.16 - D.18 (Appendix D), and are shown schematically in Figures 5.31 and 5.32. The MD flexural rigidity was higher than the CD flexural rigidity. This was due to higher fiber orientation in the MD which results in more stiffness. The flexural rigidity as a function of throughput rate and MFR did not show any clear trend. In some cases it decreased and in some it increased. A study by Wadsworth and Jones [36] has shown that the flexural rigidity increases as the throughput rate increases.

Generally, the flexural rigidity should increase with the increased throughput rate. This is because the higher throughput rate webs have larger fiber diameters which are stiffer than the smaller fiber diameters. The flexural

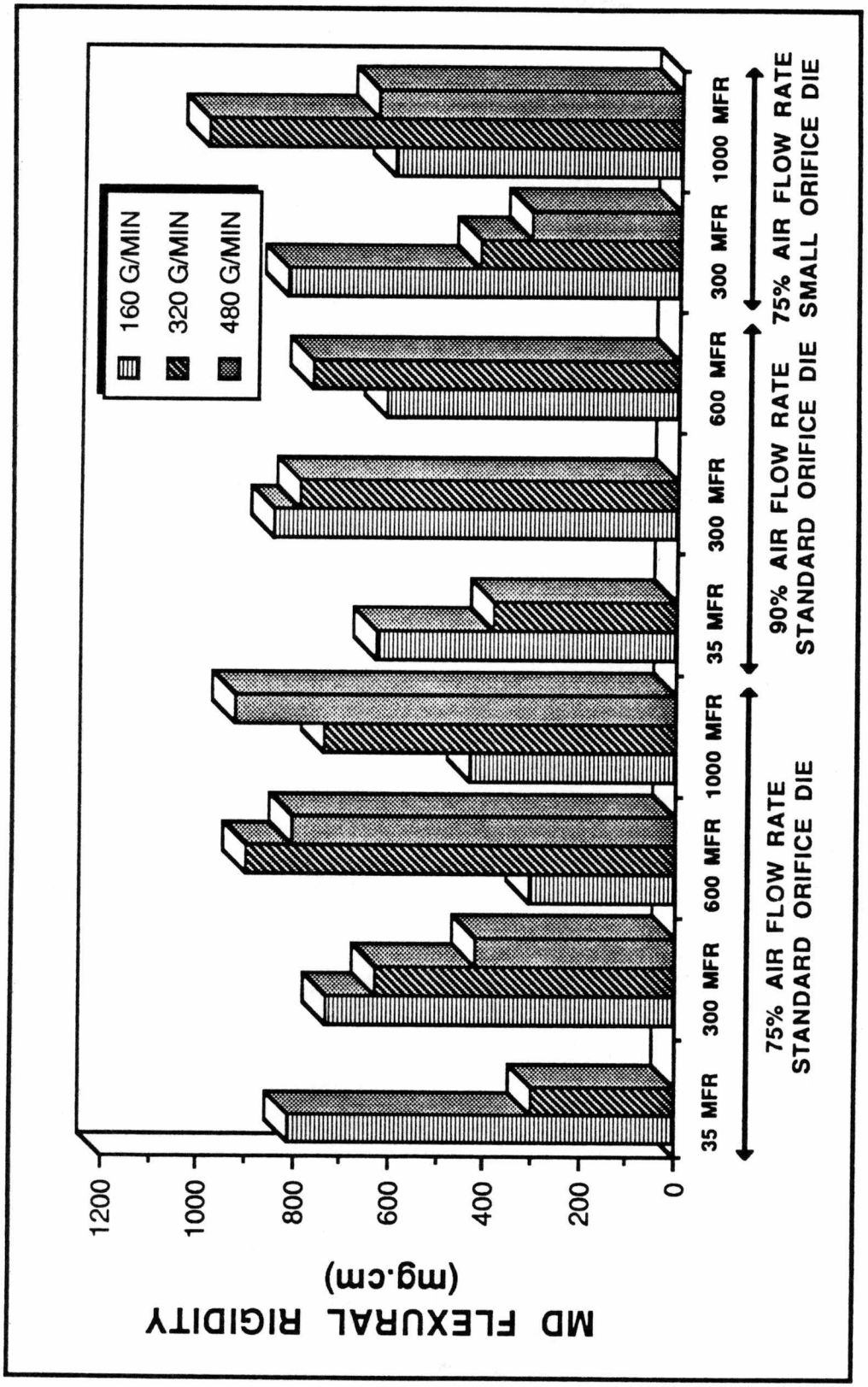

Figure 5.31. Effect of MFR and process variables on MD flexural rigidity.

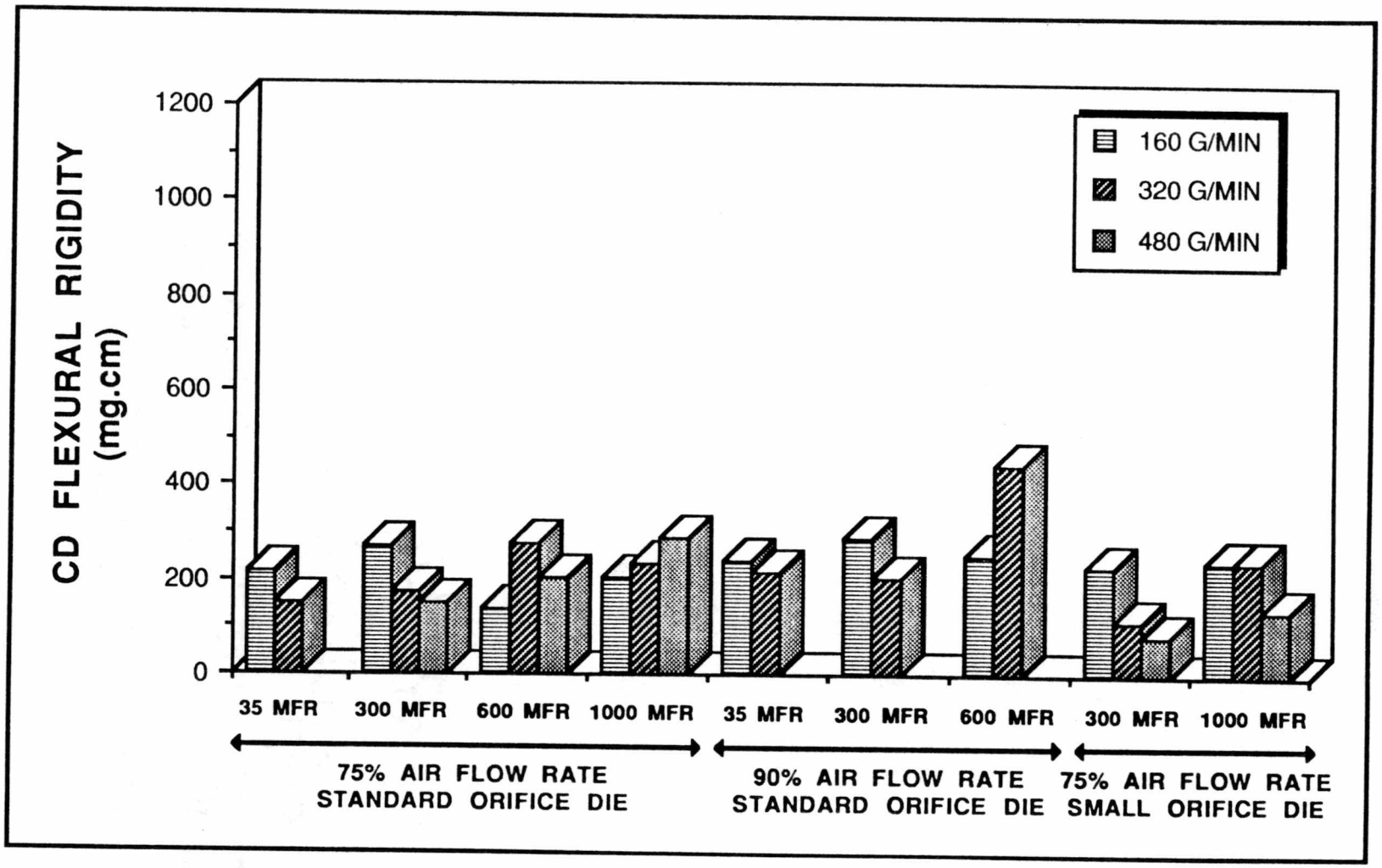

Figure 5.32. Effect of MFR and process variables on CD flexural rigidity.

rigidity of webs is also dependent on the web structure. The higher fiber-to-fiber thermal bonding in high throughput rate webs should provide more stiffness.

Shear Stiffness

The shear stiffness was determined using the KES equipment at the point of buckling for all 300 MFR webs. The shear stiffness values as a function of processing conditions are listed in Table 5.4, and shear stifness curves are shown in Figures E.25 - E.27 (Appenxid E). The shear stiffness values ranged from 22.6 to 28.3 gf/cm·degree. The 160 g/min throughput webs showed lower shear stiffness than 320 and 480 g/min throughput webs.

It is generally agreed that the shear stiffness of nonwoven fabric is mainly dependent on the **web construction** and **fiber diameter**. When a nonwoven fabric is subjected to shearing, the fibers in the webs slip over each other in order to conform to the imposed extensions and changes in curvature. The relative ease of the fiber slippage and the degree of fiber freedom usually dictate the resistance to shearing of nonwoven webs. The **tight** (good fiber-to-fiber thermal bonding) **web construction** and **large fiber diameter** should provide more resistance to shearing, and **loose** (poor fiber-to-fiber thermal bonding) **web construction** and **small fiber diameter** should povide less resistance to shearing.

The lower shear stiffness of the 160 g/min webs was probably due to **less fiber-to-fiber thermal bonding** and the presence of a larger number of **small diameter fibers**. The higher shear stiffness values of the 320 and 480 g/min webs may be attributed to **more fiber-to-fiber thermal bonding** (as indicated by SEM photomicrographs), **large diameter fibers**, and presence

Table 5.4

Shear properties of melt blown webs

Sample ID	Properties	Shear Stiffness G (gf/cm•degree)	Shear Hysterisis at 0.125° Shear Angle 2HG (gf/cm)	Shear Hysterisis at 1.25° Shear Angle 2MG5 (gf/cm)
A	160 g/min	22.6	4.7	4.1
	320 g/min	27.6	4.8	4.7
	480 g/min	26.2	4.5	4.3
B	160 g/min	23.9	4.6	4.8
	320 g/min	28.3	5.5	4.9
C	160 g/min	23.9	3.4	3.6
	320 g/min	27.8	4.9	4.9
	480 g/min	28.2	4.4	4.5

A -- 75% air flow rate, standard orifice die

B -- 90% air flow rate, standard orifice die

C -- 75% air flow rate, small orifice die

of **shot**. It is believed that the shot actually fuse the cross-over points of 3 to 4 fibers, hence inhibiting the fiber movements during shearing.

Another property that is related to the shear stiffness behavior is the hysterisis loss [119]. In nonwoven fabrics, the hysterisis is a measure of frictional losses at fiber cross over points and at fiber entanglements. The shear hysterisis was studied at 0.125 and 1.25 degrees of shear angle. There were no notable differences in shear hysterisis values among these specimens mainly because the test shear angle was **too low** to measure a **web response**. Above a test shear angle of 1.25°, the shear hysterisis was not measurable because of **buckling** of relatively soft web specimens.

Air Permeability and Web Density

The air permeability values as a function of processing conditions are given in Tables D.19 - D.21 (Appendix D), and are shown schenatically in Figure 5.33. In almost every case the air permeability increased as the polymer throughput rate increased. The similar trend has been reported by Wente and co-workers for polystyrene webs [25], and by Davis for woolen felts [120]. The trend also agreed with the empirical relationship between air resistance and fiber diameter proposed by Wente [25]. The increase in air permeability was mainly due to **larger fiber diameters** in higher throughput webs and more **open web structure**.

The web air permeability is a **geometric phenomenon** closely related to the **fiber diameter** and **web structure**. As the fiber diameter increases, the mean pore size increases because of less efficient packing of larger diameter fibers, as shown in optical photomicrogaphs in Figure 5.34. This in

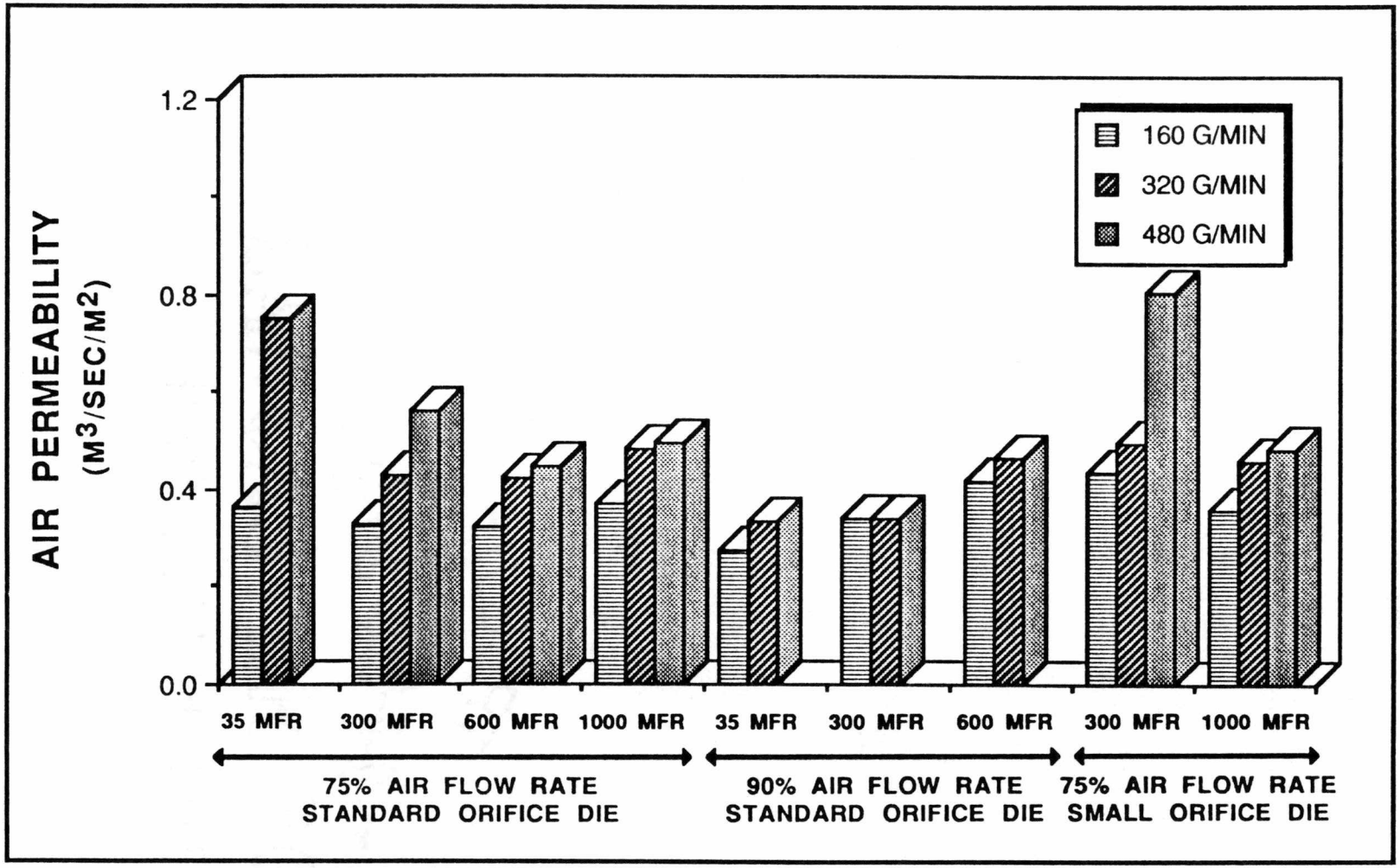

Figure 5.33. Effect of MFR and process variables on web air permeability.

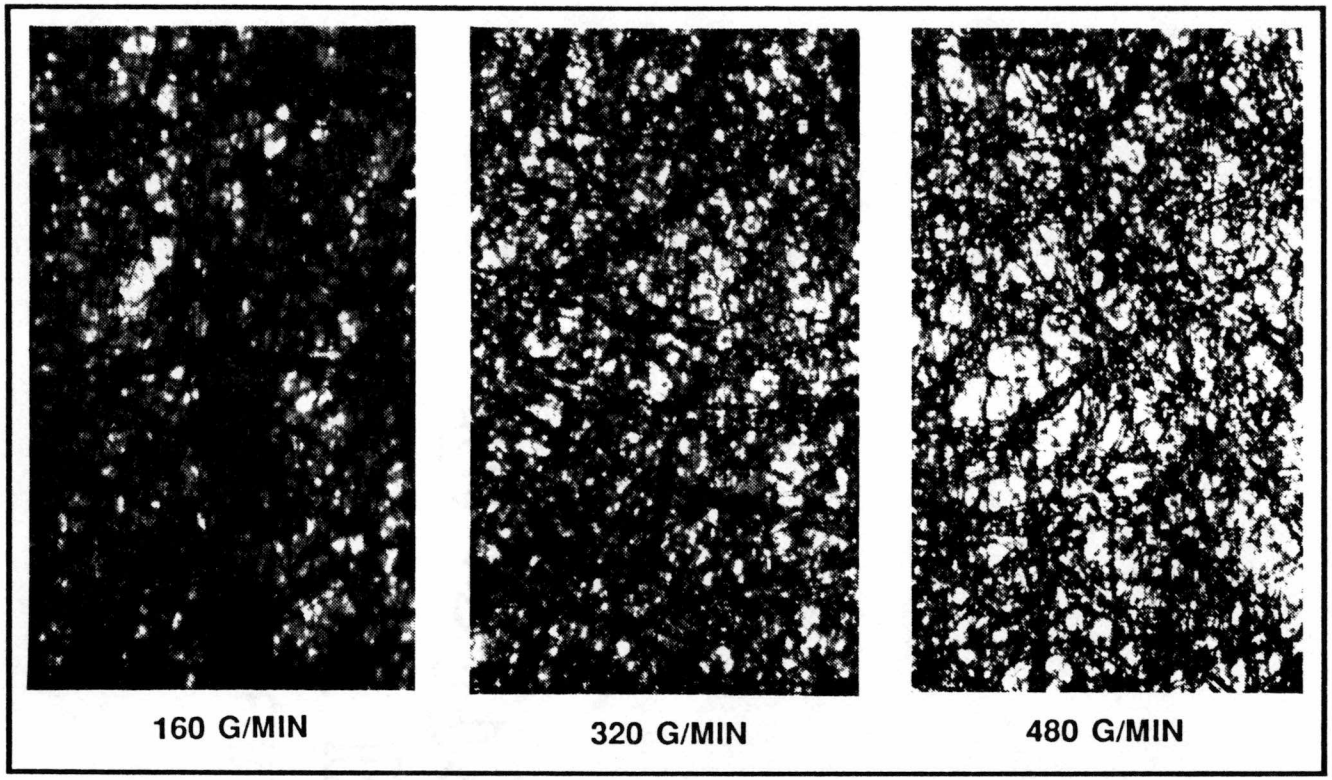

Figure 5.34. Photomicrographs showing "openness" of the webs as a function of polymer throughput rate.

turn increases the web air permeability. Therefore, the web air permeability increased as the throughput rate increased. The **bulky web structure** (with small diameter fibers at low throughput rate) provide higher air resistance than **less bulky web structure** (with large diamter fibers at high throughput rate) at constant pressure drop which in turn decreases the web air permeability. Therefore, higher air permeability results as the web structure becomes more open.

The web density values as a function of processing conditions are given in Tables D.22 - D.24 (Appendix D), and are shown schenatically in Figure 5.35. In almost every cases the web density increasd as the throughput rate increased. The increase in web density was due to a decrease in web thickness (since the basis weight of the web was a constant parameter) and a change in fiber packing density. The decrease in web thickness was probably due to the **fiber-to-fiber thermal bonding**. The fiber-to-fiber thermal bonding made **two or more fibers to stick together** thus reducing the **bulkiness** and/or **fluffiness** of the web; hence reduction in thickness.

The web density slightly decreased as the MFR increased at corresponding throughput rate at all processing conditions. However, the decrease was very minimal, therefore, the effect is considered to be negligible. The effect of change in air flow rate was noticeable only in 35 MFR webs. This may be due to bulkiness of the webs imparted by higher air flow rate.

Air Permeability--Web Density Co-relationship. The air permeability values normalized for the web basis weight (in order to reduce any variations in weight) are plotted versus web density in Figure 5.36. It can be seen that the air permeability increased as the density of the web increased.

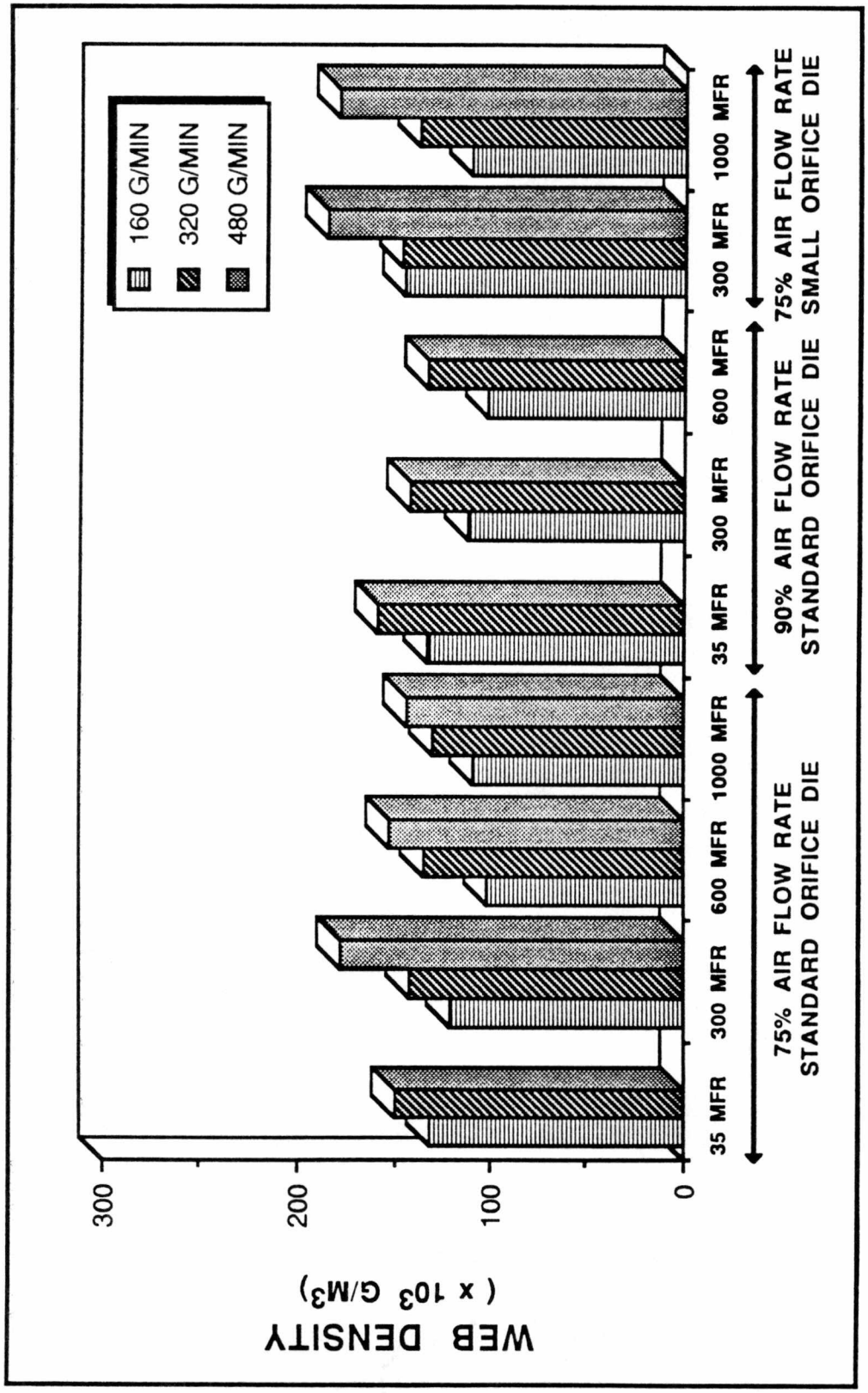

Figure 5.35. Effect of MFR and process variables on web density.

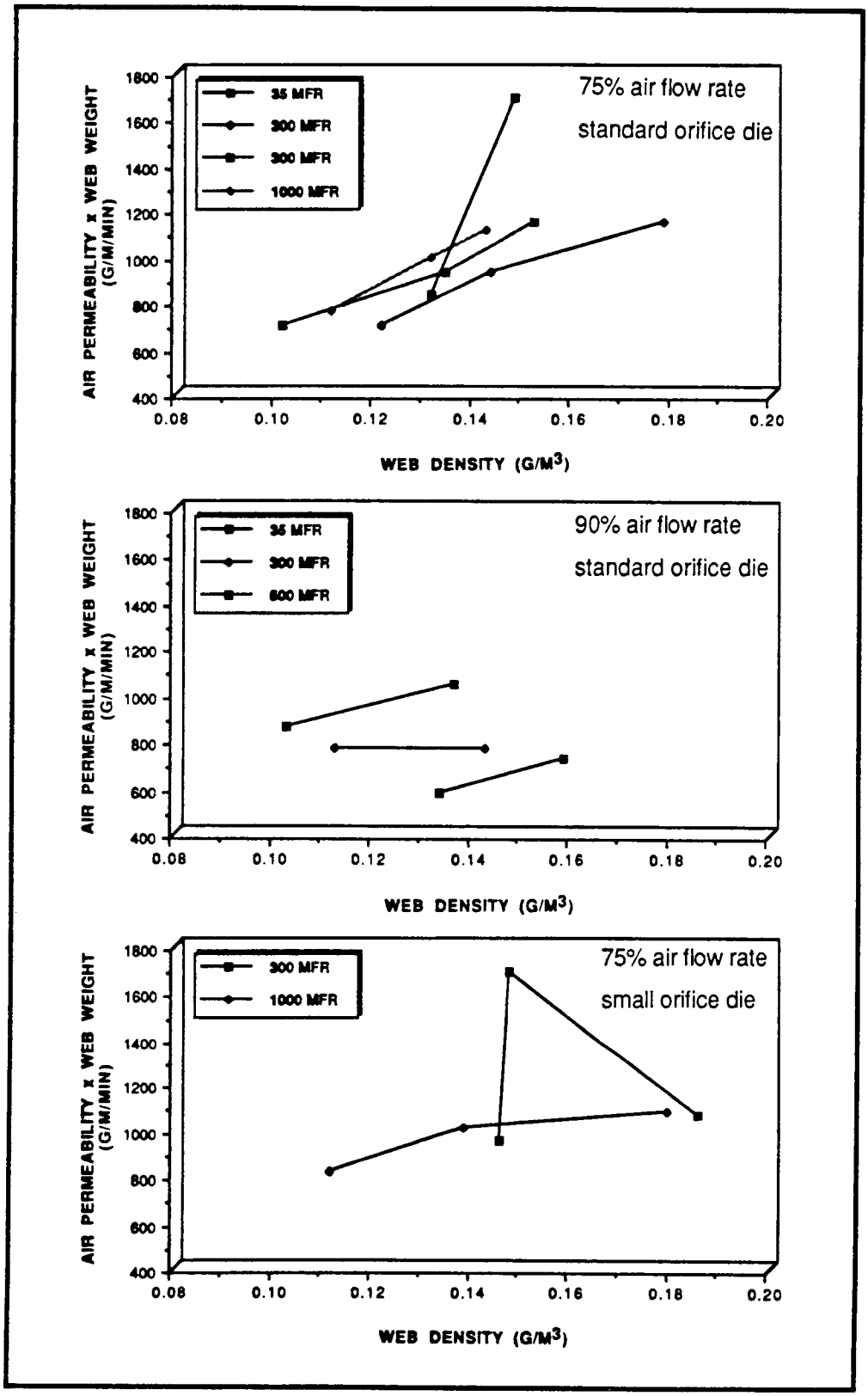

Figure 5.36. Web air permeability versus web density.

However, a closer appraisal of the grahps reveals an unusual trend and fact. It is generally known that denser fabrics have lower air permeability [120-127]. The results under discussion showed the opposite trend. The possible explanation for this is that the web density increased because of decreased thickness. And, the effect of change in fiber diameter and fiber packing density (openness of the structure) on air permeability was greater than the web density.

Web Uniformity

The uniformity of nonwoven webs exerts a strong influence on the properties of finished nonwoven products. The uniformity of melt blown web is a function of processing conditions and resin characterisitcs; and, therefore, it is essential to study the uniformity of the melt blown webs processed under different conditions. Web uniformity can be assessed in two ways: **macroscopically** and **microscopically**. Macroscopic web uniformity can be assessed in terms of basis weight variations over a specified area of the fabric; and, microscopic web uniformity can be assessed in terms of morphological changes. In this study, web uniformity was characterized in terms of basis weight variations using a **cut-and-weigh technique**.

The calculated mean weight and pooled weight variance data in terms of standard deviation and percent coefficient of variation are given in Tables 5.5-5.7. The coefficient of variation calculated from the pooled weight variance ranged from 1.5 to 7%. There was practically no difference found in weight variation between the right side and left side of the fabric. However, there was a difference in weight between the middle side and left or right side of the fabric.

Table 5.5

Basis weight of webs processed at 75% air flow rate using standard orifice die

Sample ID		Properties	Basic Weight (oz/yd^2)		
			Mean	S.D.	% C.V.
75% Air Flow Rate Standard Orifice Die	35 MFR	160 g/min	1.10	0.016	1.7
		320 g/min	1.10	0.024	2.8
	300 MFR	160 g/min	1.02	0.041	5.5
		320 g/min	1.05	0.064	7.7
		480 g/min	1.00	0.055	7.1
	600 MFR	160 g/min	1.04	0.052	6.3
		320 g/min	1.04	0.036	4.4
		480 g/min	1.10	0.055	6.3
	1000 MFR	160 g/min	1.00	0.056	7.0
		320 g/min	1.00	0.052	6.5
		480 g/min	1.10	0.053	6.1

Table 5.6

Basis weight of webs processed at 90% air flow rate using standard orifice die

Sample ID		Properties	Basic Weight (oz/yd^2)		
			Mean	S.D.	% C.V.
90% Air Flow Rate Standard Orifice Die	35 MFR	160 g/min	1.06	0.044	5.3
		320 g/min	1.04	0.048	5.9
	300 MFR	160 g/min	1.03	0.045	6.1
		320 g/min	1.10	0.066	7.5
	600 MFR	160 g/min	1.10	0.067	8.0
		320 g/min	1.10	0.041	4.7

Table 5.7
Basis weight of webs processed at 75% air flow rate using small orifice die

Sample ID		Properties	Basic Weight (oz/yd^2)		
			Mean	S.D.	% C.V.
75% Air Flow Rate Small Orifice Die	300 MFR	160 g/min	1.02	0.037	4.6
		320 g/min	1.05	0.047	5.7
		480 g/min	1.10	0.037	4.3
	1000 MFR	160 g/min	1.10	0.043	4.9
		320 g/min	1.0	0.037	4.6
		480 g/min	1.1	0.047	5.4

This was expected because of the air convergence to the middle of the die during melt blowing. During the trial runs for this study, the processing conditions, especially temperatures of the die and extruder zones, were closely monitored and kept constant through out the run for a particular type of web; hence, the dependence of the web uniformity on the processing conditions was not noticeable.

Effects of Process Variables on Morphological Properties

Differential Scanning Calorimetry

In order to study the structure-property-process relationship of the melt blowing process in terms of morphological properties, Differential Scanning Calorimertry (DSC) analysis was carried out. Tables D.25 - D.26 (Appnedix D) show ΔH, percent crystallinity, peak and onset temperature values of different MFR polypropylene resins and webs as a function of processing conditions. The percent crystallinity values of resins and webs are shown in Figure 5.37. The values ranged between 52 and 60%.

The percent crystallinity values of resins and webs increased with increased MFR. This may be due to faster crystallization rates of higher melt flow rate polypropylene resins (a study on kinetics of crystallization of 35, 300, 600, and 100 MFR polypropylene resin is described in Appendix F). There was a notable difference in percent crystallinity values between resin and webs, but only in 35 and 300 MFR resins and webs. However, there were minimal differences in percent crystallinity values between low and high throughput rate webs except for 35 and 300 web MFR specimens. This indicated that the higher

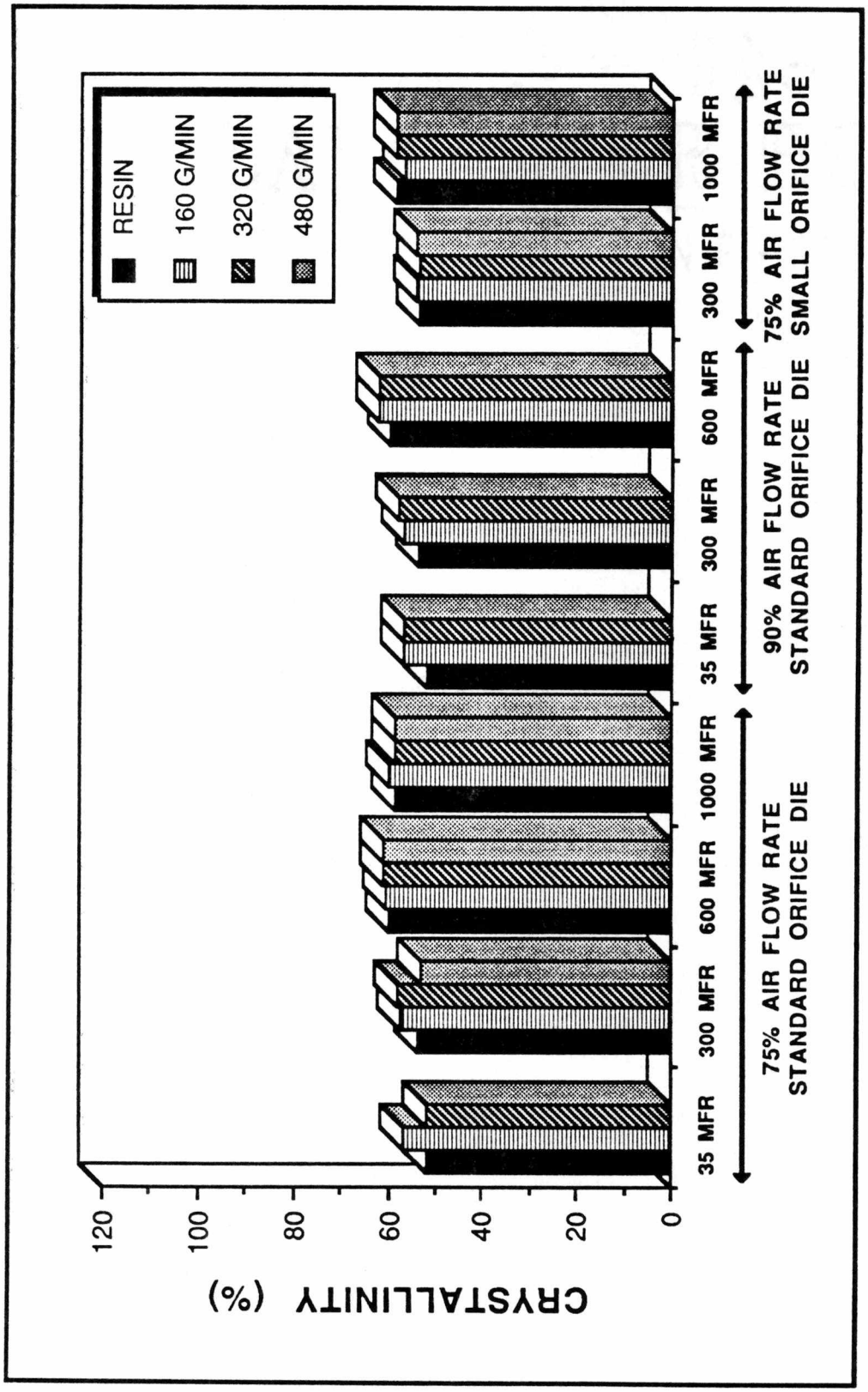

Figure 5.37. Effect of MFR and process variables on web crystallinity.

molecular weight resin degraded more proportionately than the lower molecular resin during processing although the final molecular weights of the former are still higher. The effects of air flow rate and die orifice size on percent crystallinity of webs were minimal.

Figure 5.38 and Figures E.28 - E.35 (Appendix E) show typical DSC fusion curves as a function of processing conditions. The general shape of the melting endotherms did not change much with the processing conditions and resin MFR. There were minimal differences in peak temperatures and onset temperatures. The higher throughput web samples showed **double endothermic peaks** (especially in 35 and 300 MFR resin webs), suggesting the presence of **two distinct melting species**. The first peak was located in the tempearture range of 145° C - 155° C and the second, higher melting peak, in the temperature range of 160° C - 170° C.

The appearence of two endothermic maxima in the DSC fusion curves in some polymers is a point of interest for many investigators. The origin of the double endothermic peak for isotactic polypropylene has been discussed by Samuels [128], Katayama [129], Cooper [130], Harrison [131], and Keith and Padden [132]. There are many conflicting opinions about the assessment of double endothermic peaks in α-form isotactic polypropylene. However, the complex thermal behaviour exhibited by polypropylenes and other polymers has been ascribed to the existence of different crystalline forms with different unit cell dimensions or to the presence of more than one morphological form of a single crystal structure [133]. The different crystalline forms can be: **α-form (monoclinic)**, **β-form (hexagonal)**, and **γ-form (triclinic)** with corresponding melting point at about **170°**, **160°**, and **130° C** [134]. The different morphologies can be: **extended** or **folded chain crystals**.

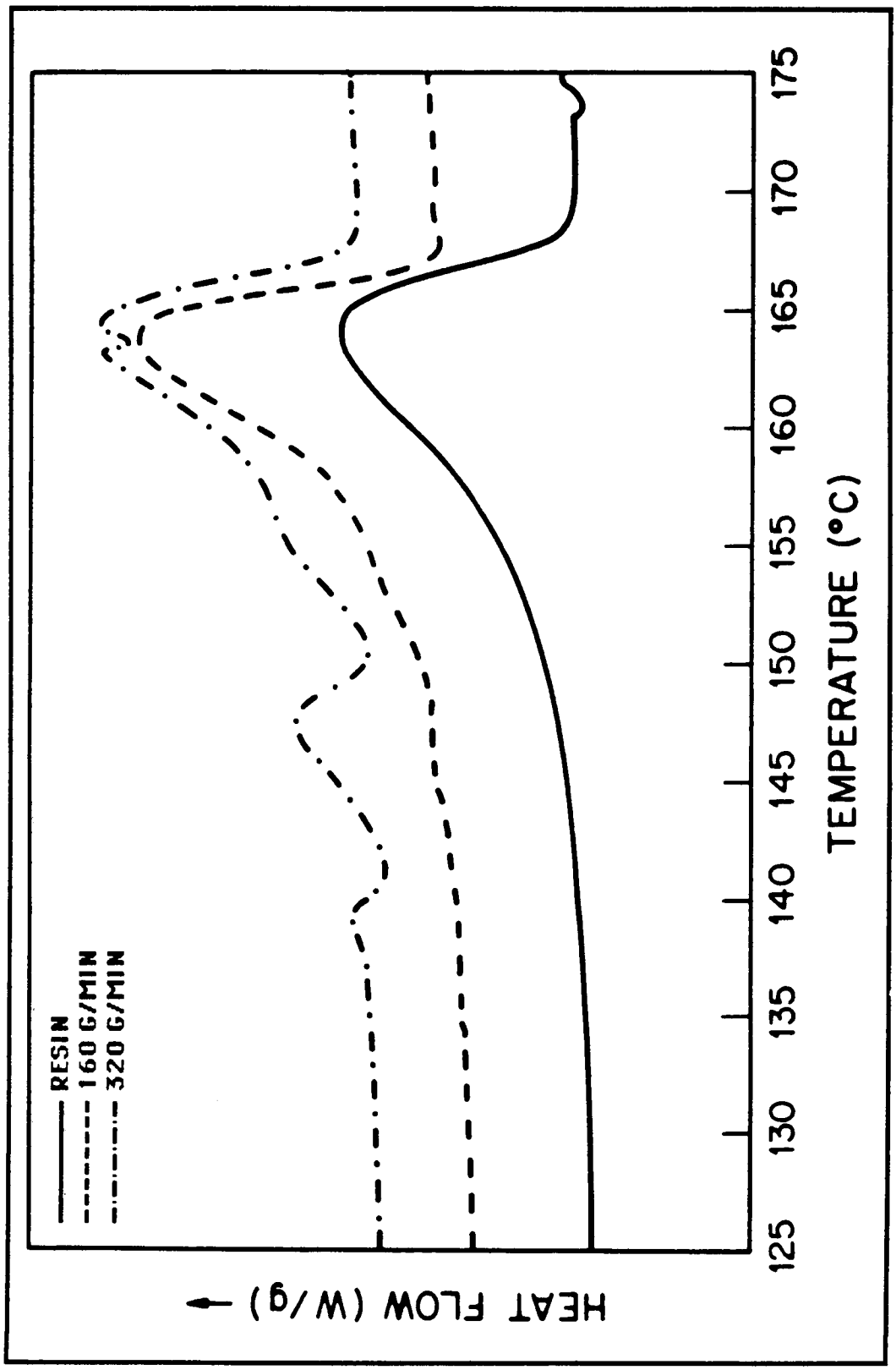

Figure 5.38. DSC thermograms of 35 MFR resin and webs processed at 75% air flow rate using standard orifice die.

Samuels [128] rejected the hypothesis of different morphologies (folded chains or extended chains) based on the fact that the double endotherms are produced at an isothermal crystallization temperature as low as 130° C. Crystallization half-times of only 18 minutes seem to preclude the possibility of extended chain crystal formation. Samuels [128] concluded that even if the source of double endothermic behaviour in istotactic polypropylene in the α-form is still unresolved, obviously two crystalline species are involved, either different disordered crystals, different crystal sizes, or different crystal types.

The comparision of DSC curves with the results obtained from the WAXD patterns of high thoughput webs indicated that the presence of double endothermic peaks was probably due to different crystal forms, namely: α-**form** (monoclinic) and β-**form** (hexagonal). There are many arguments presented in the literature on the growth of the β-**phase** in polypropylene. The following argument seems to be relavent to the results of this study.

The growth of the β-**phase** can be attributed to higher processing temperatures and lower cooling conditions at higher throughput rates. The increase in temperatures would ordinarily force the molecular chains to crystallize at the reduced rate, and that is precisely what happens in a material such as poly(ethylene oxide), which is monomorphic [98]. However, polypropylene, because of its polymorphic characteristics, can preserve the mode of growth by altering the rate; or can continue at this rate by converting into the **faster growing** β-**form** [98]. It appears that there exists a certain kinetic momentum to the packing of the chains into a unit cell, which makes substitution of the unit cell more favorable kinetically than the sudden decelartion of the growth rate [98]. It has also been shown that at a high heat (250° C) nucleation is suppresed in polypropylene melt, which enhances the

the growth of β-**phase**, because β-**phase** is faster growing than α-pahse [98].

Wide Angle X-Ray Diffraction

Wide angle X-ray diffraction techniques were used to assess the morphological changes in the melt blown webs and single fibers. It has been suggested by many researchers [96] that the isotactic polypropylene can show varied reflection patterns based on different crystalline forms. The generic diffractograms of the most common crystalline forms are shown in Figure 5.39. These crystalline forms can exist independently or as a mixture of two or more. Figure 5.40 and Figures E.36 - E.43 (Appendix E) show typical diffractograms of webs as a function of processing conditions.

The diffractograms of low polymer throughput webs showed α-form crystalline structure with four distinct peaks at **14°**, **16.8°**, **18.5°**, and **21°**. The diffractograms of 320 and 480 g/min web samples (especially in 35 and 300 MFR webs) also showed α-form crystalline structure but with an extra peak at about **16°** (which is between the 110 and 040 peaks). This extra peak was ascribed to β-**form** crystalline structure [96]. The intensity of β-**form** peak varied slightly with resin MFR. The peak intensity was higher in 35 and 300 MFR resin webs.

The presence of the β-**form** in higher throughput webs was believed to be due to change in molecular weight, the degree of isotacticity, higher processing temperatures, and lower cooling rate at higher throughput rates. Many researchers have shown that the variation in external environments (such as temperatures) can cause this type of crystal transformation [109]. At present

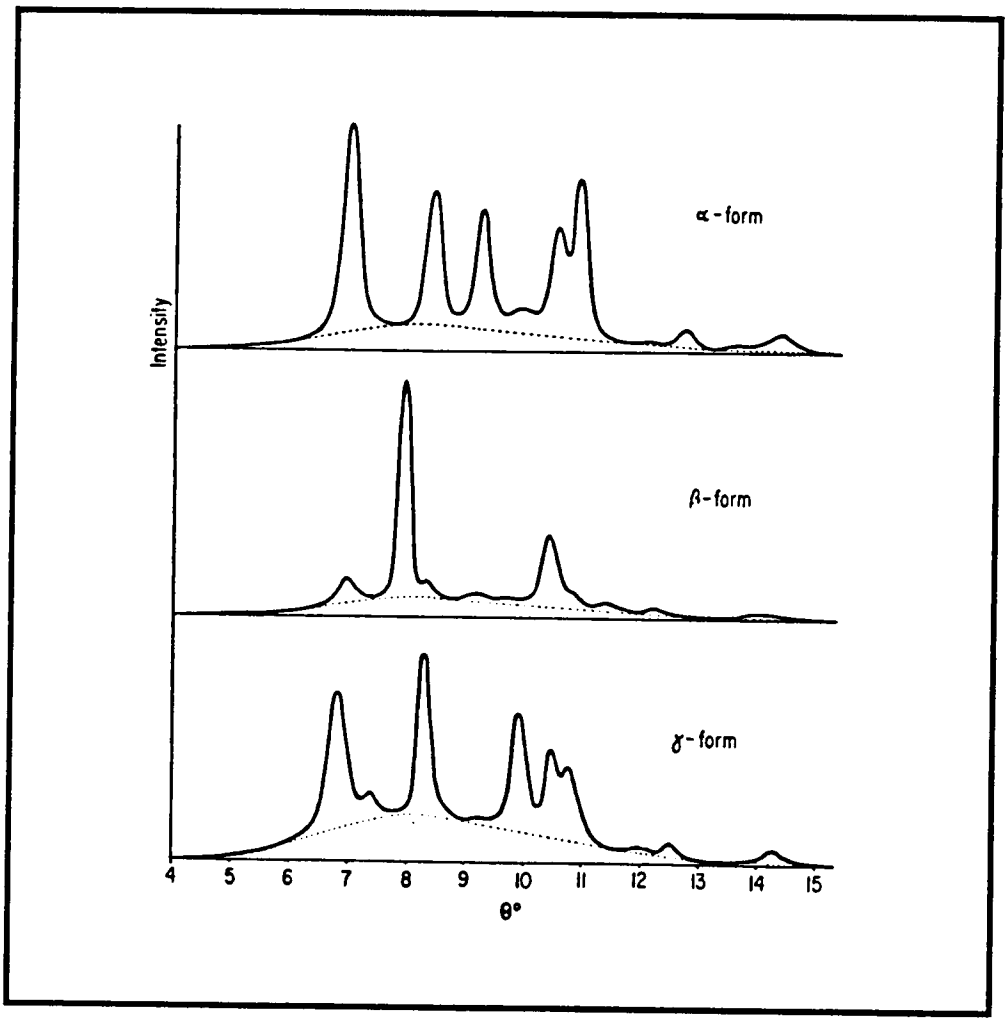

Figure 5.39. X-ray diffractograms of various crystalline forms of polypropylene.
Source: Turner, J. A. et al. : Die Makromol. Chem., Volume 75, 1964, pp. 134 - 158.

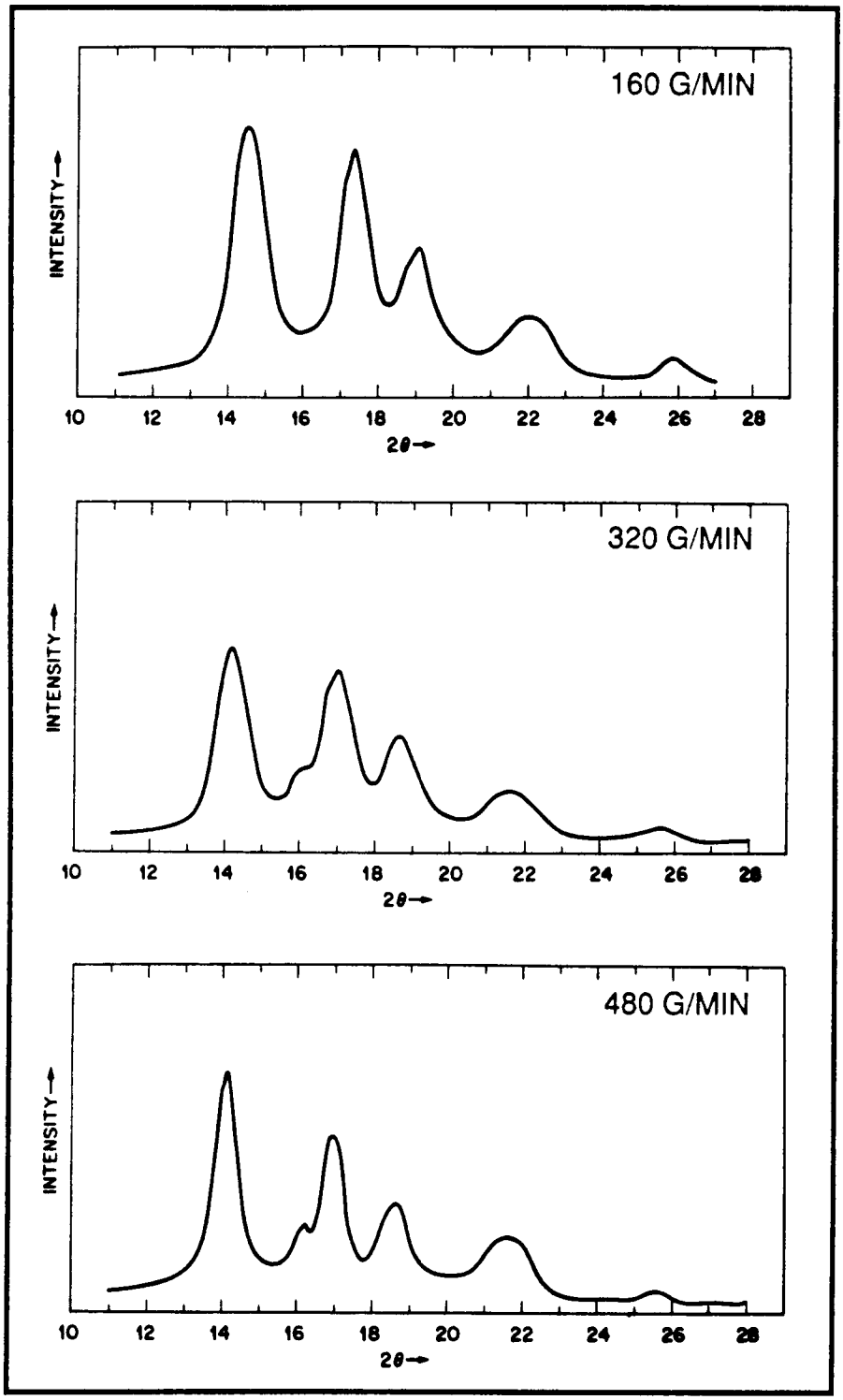

Figure 5.40. X-ray diffractograms of 300 MFR webs processed at 75% air flow rate using standard orifice die.

it is uncertain that the presence of β-**form** is due only to the thermal history a polymer experiences. Nevertheless, the present results indicated that the thermal processing history of polypropylene can cause a change in melt blown fiber morphology.

The **relative peak intensities** were about the **same among low** and **high throughput webs** for each MFR resin, and therefore, the crystallinity in low and high throughput webs were probably similar. In lower MFR web diffractograms, the peaks of **{110}**, **{040}**, and **{130}** planes were sharper than the higher MFR web samples. This indicated the possibility of having a higher degree of crystallinity and larger crystallite size in the lower MFR webs. However, the difference in percent crystallinity values (as determined from DSC analysis) between low and high MFR webs was not much.

An attempt to show molecular orientation by flat plate x-ray camera was unsuccessful because of **unsufficient material mass of a single fiber**. However, an attempt was made to assess orientation within the fibers by taking flat film patterns of webs. Figure 5.41 shows WAXD flat film patterns of 300 and 1400 MFR webs (160 and 320 g/min) processed at 75% air flow rate using standard orifice die. There was no significant difference in any of the four patterns. Four or more relatively broad ring patterns with dark background around the origin indicated that the orientation in fibers is in all directions with a moderate degree of crystalline monoclinic structure and possibly a low degree of smectic structure [42].

Both the DSC and WAXD analyses indicated the presence of two crystalline forms in high throughput webs. The relavance significance of the presence of two crystalline forms to the web properties was not possible to assess. However, from the characteristics of higher throughput webs, it is

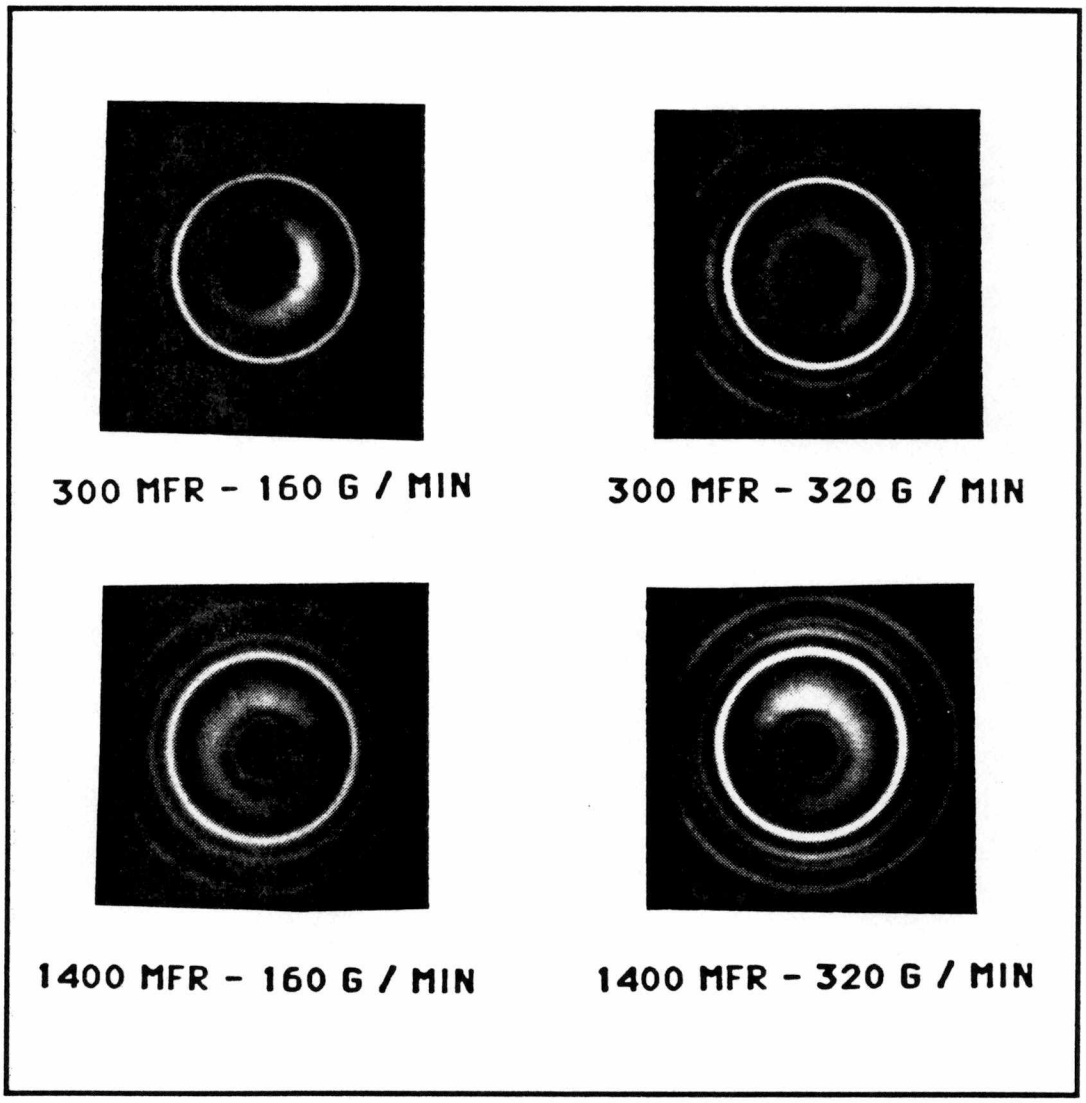

Figure 5.41. X-ray diffraction patterns of 300 and 1000 MR webs (160 and 320 g/min) processed at 75% air flow rate using standard orifice die.

probable that the presence of β-**form** may have imparted some brittleness to the webs. This is because, the β-**form** has hexagonal crystal structure, which is brittle in nature.

CHAPTER 6
CONCLUSIONS AND RECOMMENDATIONS

A fundamental study was carried out to assess the **process-structure-property** relationships in the melt blown nonwoven fabrics. The study encompassed many aspects of the melt blowing process, ranging from process and polypropylene resin varibles to the characterization of web and single fiber properties. The results of this study have shown a strong realtionships among the process conditions and the final fiber and web properties. The **primary conclusion of this study was that among the process and polypropylene resin variables studied, polymer throughput rate had the most notable effects on the physical and morphological properties of the melt blown webs**. Based on the results presented in this dissertation, the conclusions drawn are summarized below:

1. This study has established a set of **optimum** melt blown processing conditions for **35, 300, 600**, and **1000 melt flow rate (MFR)** polypropylene resins as a function of polymer throughput rate, air flow rate, and attenuation air temperatures.
2. The **shot conditions** and, **rope and fly conditions** were the two **limiting factors** for establishing the processing temperature range for a given polymer. For this reason, as the throughput rate increased, the processing window of operation (favorable conditions) became narrow, hence there was **less latitude for optimizing web properties** at the higher throughput rates.
3. It was hypothesized that the increase in fiber diameter with increase in throughput rate was due to the **die swell** and the **change in polymer-to-air ratio for a given air flow rate**.
4. The fiber attenuation process is a function of **air flow rate** as well as **"other mechanisms"**. The primary air attenuates the fiber up

to a certain distance form the die. Then the **"other mechanisms"**, in conjunction with the air flow, attenuate the fibers to the final fiber diameter in the range of 2 to 8 μm.

5. The melt blown fibers were **smooth**, **circular**, and **continuous** in length. However, the fibers showed extreme variation in fiber diameter along the fiber axis and occassional evidence of **thermal branching**.
6. **Fiber-to-fiber thermal bonding** was an important factor in controlling the physical properties of the web. The high degree of fiber-to-fiber thermal bonding was responsible for imparting brittle characteristics to the higher throughput rate webs. The fiber-to-fiber thermal bonding had a greater effect on breaking strain and bursting strength than any other physical properties.
7. The tensile failure modes of melt blown fabrics are **dependent** on the processing variables.
8. The effect of change in fiber diameter and fiber packing density (**openness of the web structure**) on air permeability was greater than the web density. Both, the air permeability and web density were a function of throughput rate.
9. Both the web molecular weight and web crystallinity were **dependent** on the starting resin MFR and processing temperatures. However, molecular weight and crystallinity appeared to be **independent** of shear rate at a given web MFR.
10. Based on DSC and x-ray results, it was hypothesized that the high throughput rate condition causes a change in polypropylene melt blown fiber morphological or crystal structure.

Based on the results obtained from this study and in order to expand the basic understanding of the melt blowing process, the following studies are recommended:

1. A more detailed analysis of the preliminary DSC and WAXD results is necessary in order to better understand the process-structure-property relationships.
2. Effect of polymer molecular weight and throughput rate on die swell and its effects on the final fiber diameter should be throughly studied.
3. One of the drawbacks of the melt blown process is the phenomena of shot, rope, and fly formation. Therefore, an in-depth analysis of these phenomena and their effects on the final web properties is most improtant.

LIST OF REFERENCES

LIST OF REFERENCES

1. Krcma, R. : "Manual of Nonwovens," Textile Trade Press, Manchester, England, 1971.

2. Guide to Nonwoven Fabrics, INDA, New York, NY, 1978.

3. Porter, K. : Physics in Technology, Volume 8, No. 9, 1977, pp. 204-212.

4. American Society for Testing and Materials : Annual Book of Standards, Philadelphia, Pennsylvania, 1989.

5. Goldstein, G. : Tappi Journal, Volume 67, No. 10, 1984, pp. 44-48. TS1080.T3

6. Hearle, J. W. S. : Textile Institute and Industry, Volume 5, No. 8, 1967, pp. 232-261.

7. Dahlstorm, N. : Melliand Textilberichte, Volume 68, No. 6, 1987, pp. 381-383.

8. Nutter, W. : Textile Month, No. 5, 1970, pp. 94-100.

9. Ahmed, M. : Polypropylene Fibers--Science and Technology, Elsevier Scientific Publishing Company, New York, 1982, pp. 434-448. TS1548.7.P6A36

10. Till, D. E. : Modern Textiles Magazine, No. 10, 1959, pp. 36-44.

11. Mansfield, R. G. : Textile World, No. 2, 1979, pp. 83-84.

12. Newton, A. and Ford, J. E. : Textile Progress, Volume 5, No. 3, 1973, pp. 57-59.

13. Wadsworth, L. C. and MuCulloch, W. J. G. : Meltblown Technolgy Today, Miller Freeman Publications, San Francisco, 1989, pp. 28-40.

14. Anonymous : Meltblown Technolgy Today, Miller Freeman Publications, San Francisco, 1989, pp. 7-12. TS1828.M55

15. Malkan, S. R. et. al. : Nonwovens : An Advanced Tutorial, Turbak, A. F. and Vigo, T. L., Editors, Tappi Press, Atlanta, USA, 1989, p. 101-129.

16. McCrum, N. G. : Principles of Polymer Engineering, Oxford University Press, New York, 1988, pp. 264-265.

17. Rodriguez, F. : Principles of Polymer Engineering, McGraw Hill, New York, 1982, pp. 330-331. TA455.P58M2

18. Mastubara, Y. : US Paternt # 4,285,655, 1981.

19. Mastubara, Y. : Polymer Engineering and Science, Volume 19, No.3, 1979, pp. 169-172.

20. Mastubara, Y. : Polymer Engineering and Science, Volume 20, No.3, 1980, pp. 212-214.

21. Mastubara, Y. : Polymer Engineering and Science, Volume 20, No.11, 1980, pp. 716-719.

22. Mastubara, Y. : Polymer Engineering and Science, Volume 23, No.1, 1983, pp. 17-19.

23. Anonymous: Melt Blowing Nonwoven Web Technology, Exxon Chemical Company, 1982.

24. Johnston, M. : Book of Papers, INDA-TEC, Fort Lauderdale, Florida, USA, May 16-19, 1988, pp. 67-86.

25. Went, V. A. et. al. : United States Department of Commerce, Office of Technical Services Report No. PB111437, NRL 4364, April 15, 1954.

26. Buntin, R. R. and Lohkamp, D. T. : Tappi, Volume 56, No. 4, 1973, pp. 74-77.

27. Anonymous: Melt Blowing Nonwoven Web Technology, Exxon Chemical Company, 1982.

28. Cheng, C. Y. and Kwalik, K. M. : Meltblown Technology Today, Miller Freeman Publications, San Francisco, 1989, pp. 64-68.

29. Cox, H. L. : British Journal of Applied Physics, Volume 3, No. 3, 1952, pp. 72-79.

30. Brandt, C. M. (Editior) : Nonwoven Fabrics, An Unbiased Appraisal, A comprehensive report for industry, prepared by graduates of the Harvard Business School, published by Nonwoven Associates, June, 1959.

31. Buresh, F. M. : Nonwoven Fabrics, Reinhold Publications, New York, USA, 1962.

32. Lunenschloss, J. and Albrecht, W. (Editors) : Non-Woven Bonded Farics, John Wiley and Sons, New York, USA, 1985.

33. Moore, G. K. : Meltblown Technology Today, Miller Freeman Publications, San Francisco, 1989, pp. 150.158.

34. Went, V. A. : Industrial and Engineering Chemistry, Volume 48, 1956, pp. 1342-1346.

35. Jones, A. M. : Book of Papers, Fourth International Conference on Polypropylene Fibers and Textiles, Nottingham, England, September 23-25, 1987, pp. 47.1-47.10.

36. Wadsworth, L. C. and Jones, A. M. : Book of Papers, INDA-TEC, Philadelphia, Pennsylvania, June 2-6, 1986, pp. 312-320. TS1828.I52

37. Jones, A. M. and Wadsworth, L. C. : TAPPI Proceeddings, Atlanta, Georgia, April 21-24, 1986, pp. 23-30.

38. Eaton, G. M. et al. : Book of Papers, INDA-TEC, Hilton Head, South Carolina, USA, May 18-21, 1987, pp. 221-231.

39. Eaton, G. M. et al. : Book of Papers, The Pira Paper and Board Fibramerics Programme, Volume 1, International Conference on Nonwovens in Medial and Healthcare Applications, Brighton, England, November 10-12, 1987, pp. 1-19.

40. Wadsworth, L. C. and Muschelewicz, A. O. : Book of Papers, Fourth International Conference on Polypropylene Fibers and Textiles, Nottingham, England, September 23-25, 1987, pp. 47.11-47.20.

41. Wadsworth, L. C. et al. : Book of Papers, INDA-TEC, Philadelphia, Pennsylvania, USA, May 30 - June 2, 1989, pp. 585 - 600.

42. Choi, K. J. et al. : Polymer Engineering and Science, Volume 28, No. 2, 1988, pp. 81-89.

43. Bodaghi, H. : Book of Papers, INDA-TEC, Philadelphia, Pennsylvania, USA, May 30 - June 2, 1989, pp. 535-571.

44. Narasimahan, K. M. and Shambaugh, R. L. : Book of Papers, INDA-TEC, Hilton Head, South Carolina, USA, May 18 - 21, 1987, pp. 189-205.

45. Shambaugh, R. L. : Industrial Engineering Chemistry Research, Volume 27, No. 12, 1988, pp. 2363-2372.

46. Shambaugh, R. L. : Book of Papers, 58th Annual Meeting, Society of Rheology, Tulsa, Oklahoma, 1986, pp.

47. Milligan, M. W. et al. : Nonwovens : An Advanced Tutorial, Turbak, A. F. and Vigo, T. L., Editors, Tappi Press, Atlanta, USA, 1989, p. 101-129.

48. Milligan, M. W. et al. : Book of Papers, INDA-TEC, Philadelphia, Pennsylvania, USA, May 30 - June 2, 1989, pp. 573-583.

49. Milligan, M. W. and Haynes, B. : American Society of Mechanical Engineers, Volume 54, pp. 47 - 50.

50. Hearle, J. W. S. : Theory and Design of Wood and Fiber Composite Materials, Edited by Jayne, B. A., Syracuse University Press, 1972, pp. 327 - 351.

51. Orr, R. S. and Grant, J. N. : Textile Research Journal, Volume, 1953, pp. 505 - 509.

52. Sinha, A. K. et al. : The Indian Textile Journal, October 1981, pp. 57- 65.

53. Purdy, A. T. : Filtration and Separation, Volume 17, No. 2, 1980, pp. 134 - 136.

54. Mohamad, M. H. and Herring, S. H. : Book of Papers, INDA-TEC, 1983, pp. 113 -128.

55. Sengupta, A. K. et al. : Indian Journal of Textile Research, Volume 10, No. 9, 1985, pp. 91 -96.

56. Danforth, P. A. and Jarvis, C. W. : Book of Papers, INDA-TEC, Kissimmee, Florida, USA, March 1980, pp. 207 - 223.

57. Treiber, E. E. : Tappi, Volume 61, No. 4, 1978, pp. 87 - 90.

58. Shivers, J. C. et al. : Book of Papers, INDA-TEC, Atlanta, March 1976, pp. 150 - 172.

59. Wyatt, N. E. and Goswami, B. C. : Journal of Coated Fabrics, Volume 14, No. 10, 1984, pp. 100 - 123.

60. Wei, K Y. et al. : Journal of Applied Polymer Science, Volume 30, 1985, pp. 1523 - 1534.

61. Trosesch, J. and Hoffman, G. : Tappi, Volume 59, No. 8, 1976, pp. 133-136.

62. Ko, F. K. and Scardino, F. L. : Book of Papers, INDA-TEC, 1983, pp. 129-145.

63. Cusick, G. E. et al. : Journal of Textile Institute, Proceedings, Volume 54, 1963, pp. 52 - 74.

64. Hearle, J. W. S. and Newton, A. : Textile Research Journal, Volume 37, 1967, pp. 778 - 797.

65. Hearle, J. W. S. and Newton, A. : Textile Research Journal, Volume 38, 1968, pp. 343 - 351.

66. Petterson, D. R. and Baker, S. : Textile Research Journal, Volume 33, 1963, pp. 809 - 816.

67. Hentschel, R. A. : Tappi, Volume 42, No. 12, 1959, pp. 979 - 982.

68. Petterson, D. R. : Ph. D. Dissertation, Massachusetts Institute of Technology, 1958.

69. Baker, S. and Petterson, D. R. : Textile Research Journal, Volume 30, 1960, pp. 704 - 711.

70. Hearle, J. W. S. and Stevenson, P. J. : Textile Research Journal, Volume 34, 1964, pp. 181 - 191.

71. Olson, L. H. and Freeston, W. D. : Book of Papers, INDA-TEC, 1976, pp. 60 - 70.

72. Freeston, W. D. and Platt, M. M. : Textile Research Journal, Volume 35, 1965, pp. 48 - 57.

73. Tayebi, A. et al. : Book of Papers, Washington, D.C., 1977, pp. 7 - 16.

74. Lee, S. M. and Argon, A. S. : Journal of Textile Institute, Volume 74, No. 1, 1983, pp. 1 - 11.

75. Lee, S. M. and Argon, A. S. : Journal of Textile Institute, Volume 74, No. 1, 1983, pp. 12 - 18.

76. Lee, S. M. and Argon, A. S. : Journal of Textile Institute, Volume 74, No. 1, 1983, pp. 19 - 30.

77. Lee, S. M. and Argon, A. S. : Journal of Textile Institute, Volume 74, No. 1, 1983, pp. 31 - 37.

78. Tikhomirov, V. R. : Technology of the Textile Industry, USSR, Volume 5, 1969, pp. 22-25.

79. Hearle, J. W. S. : Nonwovens'71, Edited by P. Lennox-Kerr, Textile Trade Press, Manchester, England, 1971, pp. 91- 102.

80. Hearle, J. W. S and Newton, A. : Textile Research Journal, Volume 38, 1968, pp. 488 - 496.

81. Oszanlav, V. : Ph.D. Dissertation, University of Manchester, England, 1971.

82. Fredricks, P. : Svensk Papperstidning, Volume 74, No. 8, 1971, pp. 233-237.

83. Hubbel, D. and Whitwell, J. C. : Textile Research Journal, Volume 40, 1970, pp. 521- 529.

84. Winchester, S. C. and Whitwell, J. C. : Journal of Engineering for Industry, ASME Transactions Series B, Volume 89, Febuary, 1967, pp. 1 - 10.

85. Winchester, S. C. and Whitwell, J. C. : Textile Research Journal, Volume 40, No. 5,1970, pp. 458 - 471.

86. Tikhomirov, V. R. and Gusev, V. E. : Technology of the Textile Industry, USSR, Volume 103, 1966, pp.

87. Kallmes, O. J. : Theory and Design of Wood and Fiber Composite Materials, Edited by Jayne, B. A., Syracuse University Press, 1972, pp. 177 - 196.

88. Vaughn, E. A. and Branon, R. C. : Book of Papers, INDA-TEC, Washington, D. C., 1977, pp. 149 -170.

89. Bikerman, J. J. : Journal of Applied Physics, Volume 28, 1957, pp. 1484 - 1485.

90. Kaeble, D. H. : Journal of Colloid and Interface Science, Volume 19, 1964, pp. 413 - 424.

91. Morrow, D. R. : Journal of Macromolecular Science, Physics edition, Volume B3, No. 1, 1969, pp. 53 - 65.

92. Natta, G. and Corradini, P. : Nuovo Cimento, Supplement, Volume 15, 1960, pp. 40-51.

93. Hikosaka, M and Seto, T. : Polymer Journal, Volume 5, 1973, pp. 111 - 121.

94. Corradini, P. et al. : Gazz. Chim. Ital., Volume 110, 1980, pp. 413 - 418.

95. Keith, H. D. et al. : Journal of Applied Physics, Volume 30, 1959, pp. 1485 - 1488.

96. Turner, J. A. et al. : Die Makromol. Chem., Volume 75, 1964, pp. 134 - 158.

97. Addink, E. J. and Beintema, J. : Polymer, Volume 2, 1961, pp. 185 - 193.

98. Lovinger, A. J. et al. : Journal of Polymer Science, Polymer Physics Edition, Volume 15, 1977, pp. 641 - 656.

99. Sauer, J. A. et al. : Journal of Applied Physics, Volume 36, 1965, pp. 3017 - 3021.

100. Kardos, J. L. et al. : Journal of Polymer Science, A2, Volume 4, No. 5, 1966, pp. 777 - 788.

101. Hosemann, R. J. : Journal of Applied Physics, Volume 34, 1963, pp. 25 - 41.

102. Ashby, G. E. and Hoeg, D. F. : Journal of Polymer Science, Volume 39, 1959, pp. 535 - 538.

103. Natta, G. et al. : Accad Maze Lincer, Volume 26, 1959, pp. 14 - 23.

104. Wyckoff, H. W. : Journal of Polymer Science, Volume 62, 1962, pp. 83 - 114.

105. Gezorich, D. M. and Geil, P. H. : Polymer Engineering and Science, Volume 8, No. 3, 1968, pp. 202 - 209.

106. Statton, W. O. : Journal of Polymer Science, Volume 58, 1962, pp. 205 - 220.

107. Sze, G. M. et al. : Journal Applied Polymer Science, A, Volume 20, 1976, pp. 1823 - 1847.

108. Miller, R. K. : Polymer, Volume 1, 1960, pp. 135 - 143.

109. Wang, G. H. et al. : Zeitschrift Fuer Physik. B Condensed, Volume 65, No. 3, 1987, pp. 347 - 351.

110. Private Communications with Dr. Bogue, Department of Materials Science and Engineering, The University of Tennessee, Knoxville, 1988.

111. Galanti, A. V. and Mantell, C. L. : Polypropylene Fibers and Films, Plenum Press, New York, 1965, pp. 13 -70.

112. Milligan, M: Unpublished Research, The University of Tennessee, Knoxville, 1990.

113. Bressee, R. R. and Wadsworth, L. C. : Book of Papers, Exxon Melt Blown Seminar, Baytown, Texas, September 15-16, 1988.

114. Private Communications with Mr. Rajen Patel, Department of Materials Science and Engineering, The University of Tennessee, Knoxville, 1990.

115. Lu, F. and Spruiell, J. E. : Journal of Applied Polymer Science, Volume 34, 1987, pp. 1521 - 1539.

116. Lu, F. and Spruiell, J. E. : Journal of Applied Polymer Science, Volume 34, 1987, pp. 1541 - 1556.

117. Puslow, D. : Composites, Volume 12, No. 10, 1981, pp. 241-247.

118. Anonymous : Man-MAde Fiber and Textile Dictionary, Celanese Corporation, New York, 1978.

119. Goswami, B. C. : Journal of Applied Polymer Science, Applied Polymer Symposium, Volume 33, 1978, pp. 245 - 259.

120. Davis, N. C. : Textile Research Journal, Volume 28, 1958, pp. 318 - 324.

121. Lamb, G. E. R. et al. : Textile Research Journal, Volume 45, 1975, pp. 452 - 463.

122. Lamb, G. E. R. and Costana, P. D. : Textile Research Journal, Volume 49, 1979, pp. 79 - 87.

123. Madhusoothanan, V. S. and Debnath, C. R. : Textile Research Journal, Volume 58, 1988, pp. 677 - 678.

124. Igwe, G. J. I. et al. : Melliand Textilberichte, No. 9, Volume 67, 1986, pp. 624 - 626.

125. Igwe, G. J. I. et al. : Melliand Textilberichte, No. 10, Volume 67, 1986, pp. 703 - 705.

126. Kothari, V. K. and Newton, A. : Journal of the Textile Institute, Volume 65, 1974, pp. 525 - 531.

127. Dent, R. W. : Journal of the Textile Institute, Volume 67, 1976, pp. 220 - 224.

128. Samuels, R. J. : Journal of Polymer Science, Polymer Physics Edition, Volume 13, 1975, pp. 1417 - 1446.

129. Katayama, K. et al. : Kolloid Z u Z Polymere, Volume 226, 1968, pp. 125 - 128.

130. Cooper, W. et al. : Polymer, Volume 8, 1967, pp. 273 - 277.

131. Harrison, I. R. : Journal of Polymer Science, Polymer Physics Edition, Volume 11, 1973, pp. 991 - 995.

132. Padden, F. J. and Keith, H. D. : Journal of Applied Physics, Volume 44, 1973, pp. 1217 - 1223.

133. Huda, M. N. et al. : Colloid and Polymer Science, Volume 263, 1985, pp. 730 - 737.

134. Urabe, Y. et al. : Reports on Progress in Polymer Physcis in Japan, Volume 8, 1965, pp. 151 - 154.

135. Richardson, E. G. : Flow Properties of Disperse Systems, Chapter VI, Edited by Hermans, J. J., North-Holland Publication Corporation, Amsterdam, 1953, pp. 266 - 298.

136. Van Den Akker, J. A. et al. : Tappi, Volume 41, No. 8, 1958, pp. 416 - 425.

137. Anonymous : Flow Measurement, American Society of Mechanical Engineers, Power Test Code, PTC 19.5;4-1959.

138. Mandelkern, L. : Crystallizatin of Polymers, McGraw-Hill: New York, 1964.

139. Pratt, C. E. and Hobbs, S. Y. : Polymer, 17, 1976, pp. 12.

140. Godovsky, Y. K. and Slonimsky, G. L. : Journal of Polymer Science, Polymer Physics Ed., 12, 1974, pp. 1053.

APPENDICES

APPENDIX A

DETERMINATION OF AIR FLOW RATE

DETERMINATION OF AIR FLOW RATE

The air mass flow rate was determined according to the American Society of Mechanical Engineers (ASME) standard procedure [137]. The following equation was used to determine the air mass flow rate[112]:

$$W_h = 359\ C\ F\ d^2\ \sqrt{Y\ h_w} \qquad \text{(A-1)}$$

Where

W_h is the air mass flow rate in lbs/hr,

C is the discharge coefficient

d is the diameter of the orifice in inches,

h_w is the differential pressure in "H_2O,

Y is the weight of air in lbs/ft^3 entering the orifice, and

F is the velocity of approach factor and is expressed as

$$F = \frac{1}{\sqrt{1 - \beta^4}}\ ;\ \beta = \frac{d}{D} \qquad \text{(A-2)}$$

where d is the orifice plate diameter and D is the pipe diameter.

The orifice diameter, d, is 1.335 in. and the inside pipe diameter,D, is 2.9 in. This gives a diameter ratio of 0.46. Evaluation of Equation (2) gives a velocity of approach factor, F = 1.023. Thus, the Equation (1) becomes:

$$W_h = 654.64\ C\ \sqrt{Y\ h_w} \qquad \text{(A-3)}$$

The specific weight of the air entering the orifice, Y, can be determined from the ideal gas equation of state:

$$Y = \frac{P}{R\,T} \qquad \text{(A-4)}$$

Where

P is the absolute pressure in lb/ft^2,

T is the absolute temperature in °R, and

R is the gas constant of air, 53.34 ft-lb/lbm-°R.

The absolute pressure upstream of the orifice is given by:

$$P_1 = P_2 + \rho g h_w + P_\infty \qquad \text{(A-5)}$$

Where

P_1 is the pressure upstream of orifice in psia,

P_2 is the pressure downstream of orifice in psig,

ρg is the specific weight of H_2O in 0.0361 lb/in^3, and

P_∞ is the ambient pressure in psia.

The coefficient of discharge, C, is a function of B and the Reynolds number, Re, based on the inside pipe diameter. The expression for the Reynolds number is given by:

$$Re = \frac{Y\,V\,D}{\mu} \qquad \text{(A-6)}$$

Where

V is the air velocity in ft/s,

μ is the dynamic viscosity in lb/ft-s, and

D is the inside diameter of pipe in ft.

The viscosity of air is a function of the temperature. The following expression, derived from the Sutherland equation is useful to determine the viscosity in terms of the absolute temperature

$$\mu = 1.3183 \times 10^{-6} \frac{T^{1.5}}{(T + 200)} \text{ in } \frac{\text{lb}}{\text{ft - sec}} \qquad \text{(A-7)}$$

Equation (8) gives the air velocity in the pipe:

$$V = \frac{W_h}{Y \frac{\pi D^2}{4}} \frac{1}{3600} \text{ in } \frac{\text{ft}}{\text{sec}} \qquad \text{(A-8)}$$

The flow rate, Equation (3), can be converted to standard cubic feet per minute (SCFM) using a standard density, , evaluated at P = 14.7 psia and T = 68°F. The standard density is = 0.07516 lb/ft^3. The volumetric flow rate in SCFM is given by:

$$Q = \frac{W_h}{60\, Y_s} \text{ in SCFM} \qquad \text{(A-9)}$$

Sample Calculation

The following is a sample calculation to determine air mass flow rate at a given air valve opening. The following measured values (Figure A.1) at a given air valve opening will be used in this sample calculation [112]:

P_2 = 25 psig

T_1 = 90°F

h_w = 10.5 in. H_2O

P_∞ = 14.5 psia (pressure drop across the orifice)

Step 1 Determine the pressure upstream of the orifice using Equation (5)

P_1 = 25 + 0.0361 (10.5) + 14.5 = 39.88 psia

Step 2 Evaluate the air density using Equation (4). To be consistent with units, the pressure should be converted to lb/ft^2 and the temperature to °R.

P_1 = (39.88) (144) = 574.26 lb/ft^2

T_1 = 90 + 460 = 560 °R

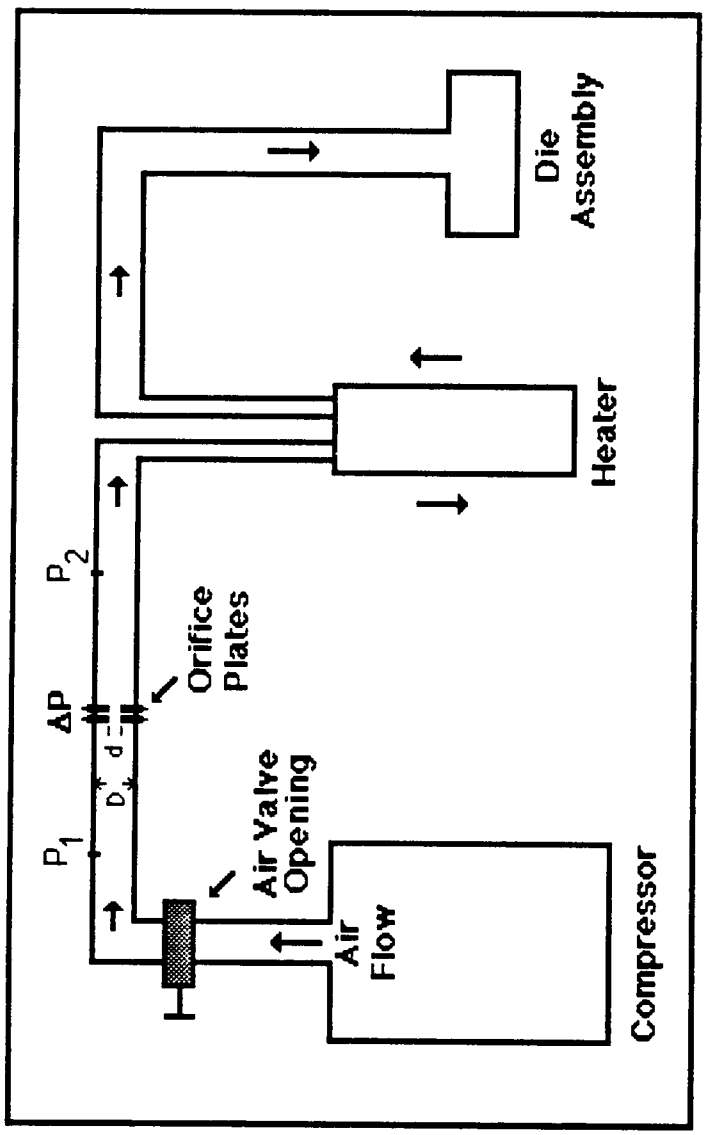

Figure A.1. Schematic of air delivery system.

$$Y = \frac{5742.61}{53.34(550)} = 0.20 \frac{lb}{ft^3}$$

Step 3 Assume a value of the discharge coefficient (a value of 0.61 will be close) and calculate the flow rate using the equation (3). The assumed value of C will be checked after calculating the Reynolds number and determining C from Table A.1 [137]. For C = 0.61, the Equation (3) becomes:

$$W_h = 654.64(0.61)\sqrt{10.5(0.20)} = 578.7 \frac{lb}{hr}$$

Step 4 Determine the air velocity in the pipe using Equation (8). The cross sectional area should be in the units of ft^2.

$$\frac{\pi D^2}{4} = \frac{\pi(2.9)^2}{4} \frac{1}{144} = 0.0459 \text{ ft}^2$$

Equation (8) becomes:

$$V = \frac{578.7}{0.2(0.0459)} = 63,039 \frac{ft}{hr} \text{ or } 17.5 \frac{ft}{sec}$$

Step 5 Evaluate the Reynolds number. The dynamic viscosity for the given temperature, Equation (7), is given by:

$$\mu = 1.3183 \times 10^{-6} \frac{(550)^{1.5}}{550 + 200} = 2.26 \times 10^{-5} \frac{lb}{ft - sec}$$

The Reynolds number, Equation (6), becomes

Table A.1

Flow coefficients

Source: Anonymous : Flow Measurement, American Society of Mechanical Engineers, Power Test Coce, PTC 19.5;4-1959.

Values of the Flow Coefficient, K, Velocity of Approach Factor Included, as a Function of the Pipe Reynolds Number, R_D, and Diameter Ratio, β

For 3 In. Pipe, $D = 3.068$ In.

R_D \ β	5,00	1,000	2,000	3,000	4,000	5,000	6,000	8,000	10,000	15,000	20,000	25,000	50,000	100,000	500,000	10^6
0.100	0.6190	0 6112	0 6057	0.6032	0 6017	0 6007	0 6000	0.5990	0 5983	0 5972	0 5965	0.5961	0 5950	0 5942	0 5931	0.5929
.150	.6208	.6124	.6064	.6037	.6021	.6010	.6002	.5991	.5984	.5972	.5965	.5960	.5948	.5940	.5928	.5925
.200	.6242	.6145	.6082	.6052	.6035	.6023	.6014	.6002	.5993	.5980	.5972	.5967	.5954	.5944	.5932	.5929
.250	.6290	.6185	.6110	.6077	.6058	.6044	.6034	.6020	.6011	.5996	.5987	.5981	.5966	.5956	.5942	.5939
.300	.6356	.6236	.6152	.6115	.6092	.6077	.6066	.6050	.6039	.6022	.6013	.6006	.5989	.5977	.5961	.5957
.325	.6396	.6269	.6179	.6139	.6115	.6099	.6087	.6070	.6058	.6040	.6030	.6023	.6001	.5992	.5975	.5971
.350	.6443	.6306	.6210	.6167	.6142	.6125	.6112	.6094	.6081	.6062	.6051	.6043	.6024	.6010	.5992	.5988
.375	.6495	.6349	.6246	.6201	.6174	.6155	.6141	.6122	.6109	.6089	.6076	.6068	.6048	.6033	.6014	.6009
.400		.6398	.6288	.6240	.6211	.6191	.6176	.6156	.6142	.6120	.6107	.6098	.6076	.6060	.6040	.6035
.425		.6454	.6337	.6285	.6254	.6232	.6217	.6195	.6180	.6157	.6143	.6133	.6110	.6093	.6071	.6066
.450		.6518	.6392	.6336	.6303	.6281	.6264	.6241	.6225	.6200	.6185	.6175	.6150	.6132	.6108	.6103
.475		.6589	.6455	.6396	.6360	.6336	.6318	.6293	.6276	.6250	.6234	.6223	.6196	.6177	.6152	.6146
.500			.6527	.6461	.6426	.6400	.6381	.6354	.6336	.6308	.6291	.6279	.6251	.6230	.6203	.6197
.520			.6591	.6524	.6484	.6457	.6437	.6409	.6390	.6360	.6342	.6330	.6300	.6279	.6250	.6244
.540			.6662	.6591	.6549	.6521	.6500	.6470	.6450	.6419	.6400	.6387	.6355	.6333	.6303	.6296
.560			.6740	.6666	.6622	.6591	.6569	.6538	.6517	.6484	.6464	.6451	.6417	.6394	.6362	.6355
.580			.6826	.6748	.6701	.6670	.6646	.6613	.6591	.6556	.6535	.6521	.6486	.6461	.6428	.6420
.600				.6839	.6790	.6756	.6732	.6697	.6673	.6636	.6614	.6599	.6562	.6536	.6501	.6492
.620				.6940	.6888	.6853	.6827	.6790	.6765	.6726	.6702	.6686	.6647	.6619	.6582	.6573
.640				.7054	.6999	.6961	.6933	.6894	.6867	.6825	.6800	.6783	.6741	.6712	.6672	.6663
.660				.7182	.7123	.7082	.7052	.7010	.6981	.6937	.6910	.6892	.6847	.6815	.6772	.6762
.680				.7328	.7264	.7220	.7187	.7142	.7111	.7062	.7033	.7014	.6965	.6930	.6884	.6873
.700					.7427	.7378	.7342	.7292	.7258	.7205	.7173	.7151	.7098	.7060	.7009	.6997
.720					.7617	.7563	.7523	.7467	.7428	.7369	.7333	.7309	.7249	.7206	.7150	.7136
.740					.7845	.7783	.7737	.7672	.7628	.7560	.7519	.7492	.7423	.7374	.7309	.7293
.750					.7976	.7909	.7859	.7790	.7742	.7669	7625	.7594	.7520	.7467	.7397	.7380
.760						.8049	.7995	.7919	.7867	.7787	.7739	.7706	.7625	.7568	.7491	.7473
.780						.8377	.8312	.8221	.8158	.8061	.8003	.7963	.7865	.7796	.7703	.7681
.800	TAPS AT 1 D AND $\frac{1}{2}$ D—					.8791	.8710	.8596	.8518	.8397	.8325	.8276	.8154	.8067	.7952	.7925

$$Re = \frac{(0.20)\ (17.51)}{(0.0000226)}\ \frac{2.9}{12} = 37,447$$

Step 6 Determine the value for the discharge coefficient using Table A.1. The discharge coefficient cn be obtained by dividing the flow coefficient, given in the table, by the velocity of approach factor. For Re = 37447 and a diameter ratio of 0.46 Table A.1 gives a flow coefficient of approximately 0.62. This gives a discharge coefficient of:

$$C = \frac{0.62}{1.023} = 0.606$$

As can be seen, the calculated value of C agrees well with the assumed value of 0.61. If the calculated value does not agree with the assumed value then the calculated value would be used in Step 3 and a new flow rate calculated.

Step 7 The volumetric flow rate is given by Equation (9):

$$Q = \frac{578.85}{60(0.07516)} = 128.36 \text{ SCFM}$$

APPENDIX B

PROCEDURE FOR NORMALIZING LOAD-EXTENSION DATA

PROCEDURE FOR NORMALIZING LOAD-EXTENSION DATA

A typical load-extension curve obtained from Instron is shown in Figure B.1. Distance A is the breaking load, distance B is the breaking extension, and distances C and D are selected load and extension level, respectively, to calculate initial modulus.

In order to claculate the web breaking stress, distance A was determined from the load-extension curve in terms of load(g). The following expression was used to calculate web breaking stress:

$$\text{Breaking Stress (g/den)} = \frac{\text{load (g)}}{\text{9000 m x width of specimen (m) x basis weight (g/m}^2\text{)}}$$

Breaking stress in g/den is a traditional textile unit. In order to express breaking stress in engineering SI unit, following conversion factor was used:

Breaking Stress (mN/tex) = Breaking Stress (g/den) x 88.3

The web breaking strain was calculated as follows:

$$\text{Breaking Strain (\%)} = \frac{\Delta L}{\text{gauge length}} \times 100$$

Where ΔL is the change in length of the specimen at the break. ΔL was claculated using following expression:

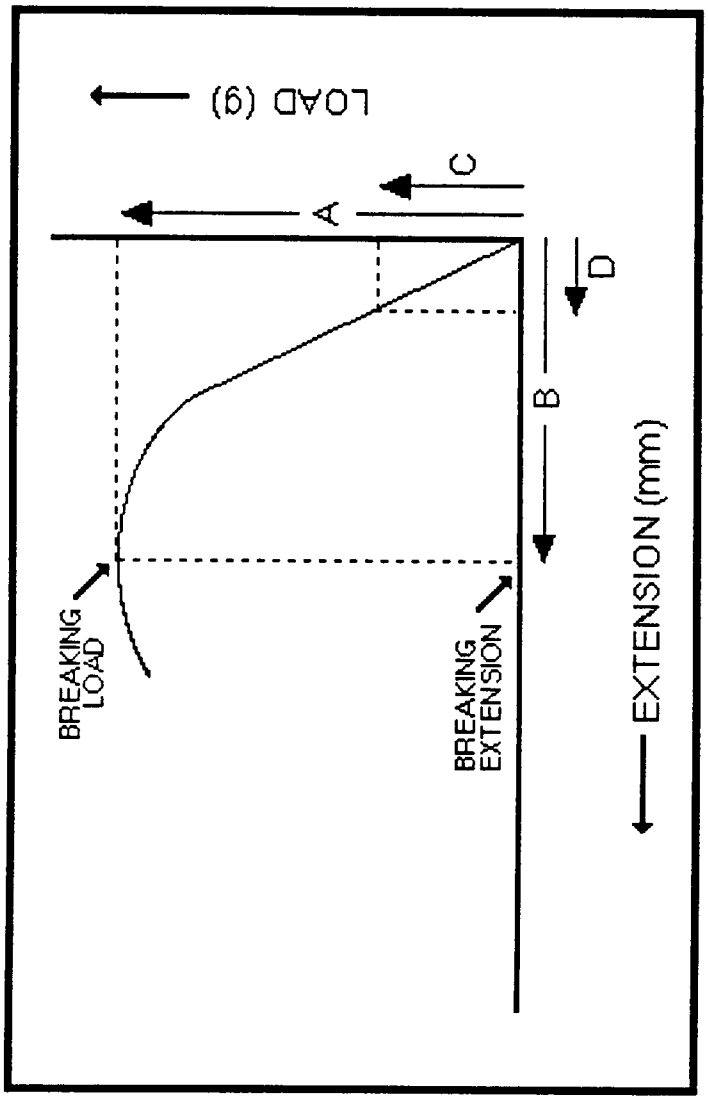

Figure B.1. Schematic of a typical load-extension curve.

$$\Delta L = \frac{\text{length stretched at the break (mm) (distance B in the above Figure)}}{\text{Instron chart speed (mm/min)}} \times \text{cross head speed (mm/min)}$$

For initial modulus, distances C and D were determined from the load-extension curve, in terms of load(g) and extension(mm). The following expression was used to calculate the initial modulus:

$$\text{Initial Modulus (g/den)} = \frac{\text{Load (g)} \times \text{gauge length (mm)}}{\text{width of specimen (m)} \times \text{basis weight (g/m}^2\text{)} \times \text{stretched length (mm) (distance D in above Figure)}}$$

The g/den unit was conversted to mN/tex unit as follows:

$$\text{Initial Modulus (mN/tex)} = \text{Initial Modulus (g/den)} \times 88.3$$

In order to calculate the breaking stress of a single fiber, first diameter of a single fiber was measured using a scaled microscope. The breaking stress was calculated as follows:

$$\text{Breaking Stress (Pa)} = \frac{\text{load (kg)} \times 9.8\ \text{m/sec}^2}{3.14 \times (\text{fiber diameter})^2/4}$$

The single fiber breaking strain was determined using the same expression used for the web breaking strain.

APPENDIX C

PROCEDURE FOR AVERAGING LOAD-EXTENSION CURVES

PROCEDURE FOR AVERAGING LOAD-EXTENSION CURVES

Step 1 According to the nature of the load-extension curve, a certain number of load levels with corresponding extensions were selected as data points, as shown in Figure C.1. For each selected load level the corresponding extension values (for twenty-five curves) were averaged as follows:

$$\text{Extension (mm) at load level 1} = \frac{1 + 2 + 3 + \ldots\ldots + 25}{25}$$

$$\text{Extension (mm) at load level 2} = \frac{1 + 2 + 3 + \ldots\ldots + 25}{25}$$

$$\vdots \qquad\qquad \vdots$$

$$\text{Extension (mm) at breaking load} = \frac{1 + 2 + 3 + \ldots\ldots + 25}{25}$$

Step 2 After determining the extension, the data were tabulated as follows:

Load Level	Extension
level 0	extension 0
level 1	extension 1
level 2	extension 2
⋮	⋮
breaking level	breaking extension

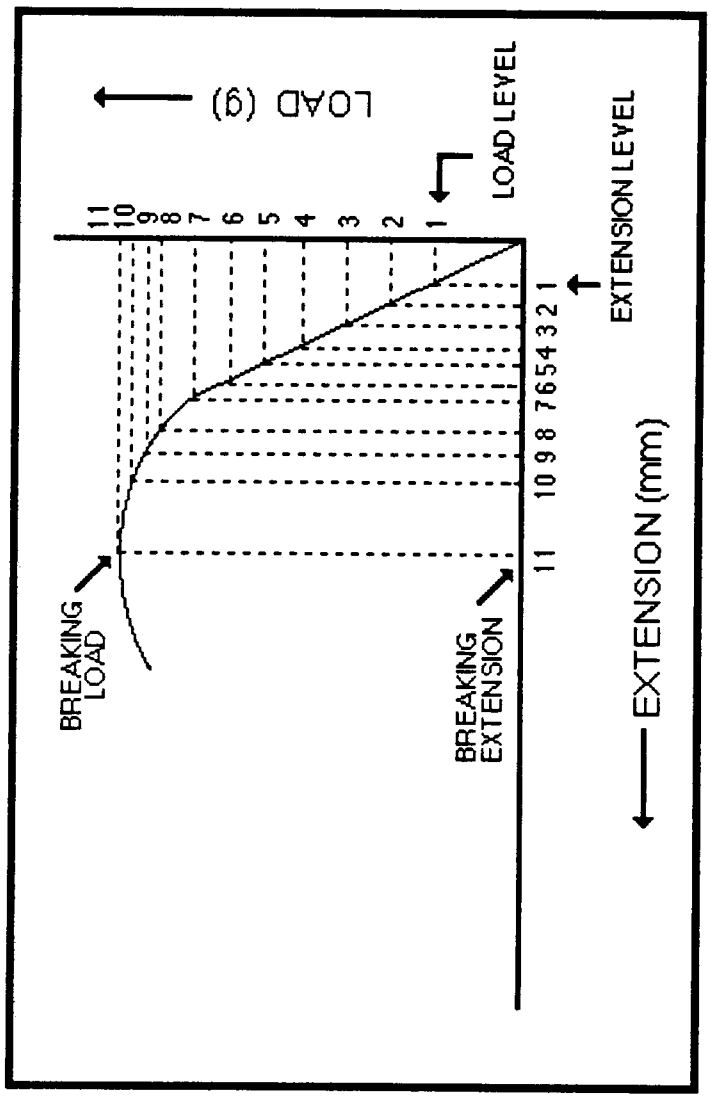

Figure C.1. Schematic of a typical load-extension curve with selected load levels.

Step 3 Load level and corresponding extension values were then noramlized to obtain stress in mN/tex and extension in percent, according to the procedure explained in preceeding section.

Stress (mN/tex)	Strain (%)
stress 0	strain 0
stress 1	strain 1
stress 2	strain 2
⋮	⋮
breaking stress	breaking strain

Step 4 The above obtained stress-strain data for each web type was then plotted using DISSPLA graphic software package; a cubic spline function was used to interpolate the curves.

APPENDIX D

TABLES

Table D.1

Average fiber diameter of webs processed at 75% air flow rate using standard orifice die

SAMPLE ID		PROPERTIES	AVERAGE FIBER DIAMETER (μm)	AIR VALVE OPENING (%)
75% Air Flow Die Standard Orifice Die	35 MFR	160 g/min	2.8	75
		320 g/min	5.3	75
	300 MFR	160 g/min	3.4	75
		320 g/min	5.9	75
		480 g/min	6.7	75
	600 MFR	160 g/min	4.1	75
		320 g/min	5.3	75
		480 g/mim	6.1	75
	1000 MFR	160 g/min	3.3	75
		320 g/min	5.6	75
		480 g/min	6.5	75

Table D.2
Average fiber diameter of webs processed at 90% air flow rate using standard orifice die

SAMPLE ID		PROPERTIES	AVERAGE FIBER DIAMETER (μm)	AIR VALVE OPENING (%)
90% Air Flow Die Standard Orifice Die	35 MFR	160 g/min	3.3	90
		320 g/min	5.1	90
	300 MFR	160 g/min	3.5	90
		320 g/min	5.6	90
	600 MFR	160 g/min	3.5	90
		320 g/min	5.7	90

Table D.3
Average fiber diameter of webs processed at 75% air flow rate using small orifice die

SAMPLE ID		PROPERTIES	AVERAGE FIBER DIAMETER (μm)	AIR VALVE OPENING (%)
75% Air Flow Rate Small Orifice Die	300 MFR	160 g/min	2.9	75
		320 g/min	5.9	75
		480 g/min	6.5	75
	1000 MFR	160 g/min	3.6	75
		320 g/min	5.3	75
		480 g/min	6.5	75

Table D.4

Intrinsic viscosity, molecular weight, and polydispersity index of resins and webs processed at 75% air flow rate using standard orifice die

Sample ID	Properties	Intrinsic Viscosity (dL/g)	Weight Average Molecular Weight (M_w)	Number Average Molecular Weight (M_n)	Polydispersity Index (M_w/M_n)
75% Air Flow Rate Standard Orifice Die	Starting 35 MFR Resin	1.06	145200	58400	2.5
	160 g/min web	0.87	112500	48700	2.3
	320 g/min web	0.86	111000	50000	2.2
	Starting 300 MFR Resin	0.80	112000	37000	2.8
	160 g/min web	0.67	81200	33900	2.4
	320 g/min web	0.67	80300	33900	2.4
	480 g/min web	0.66	79500	33000	2.4
	Starting 600 MFR Resin	0.73	93300	26800	3.5
	160 g/min web	0.59	69900	23500	3.0
	320 g/min web	0.59	69200	25700	2.7
	480 g/min web	0.58	63700	24900	2.7
	Starting 1000 MFR Resin	0.72	91400	27200	3.4
	160 g/min web	0.54	62500	25000	2.5
	320 g/min web	0.54	62000	24500	2.5
	480 g/min web	0.53	60300	24600	2.4

Table D.5

Intrinsic viscosity, molecular weight, and polydispersity index of resins and webs processed at 90% air flow rate using standard orifice die

Sample ID	Properties	Intrinsic Viscosity (dL/g)	Weight Average Molecular Weight (M_w)	Number Average Molecular Weight (M_n)	Polydispersity Index (M_w/M_n)
90% Air Flow Rate Standard Orifice Die	Starting 35 MFR Resin	1.06	145200	58000	2.5
	160 g/min web	0.80	100000	53600	1.9
	320 g/min web	0.78	96900	51300	1.9
	Starting 300 MFR Resin	0.92	112000	38000	3.2
	160 g/min web	0.73	90600	42100	2.2
	320 g/min web	0.73	90400	42800	2.1
	Starting 600 MFR Resin	0.73	93300	26800	3.5
	160 g/min web	0.64	77300	25300	3.1
	320 g/min web	0.63	75700	28800	2.6

Table D.6

Intrinsic viscosity, molecular weight, and polydispersity index of resins and webs processed at 75% air flow rate using small orifice die

Sample ID	Properties	Intrinsic Viscosity (dL/g)	Weight Average Molecular Weight (M_w)	Number Average Molecular Weight (M_n)	Polydispersity Index (M_w/M_n)
75% Air Flow Rate Small Orifice Die	Starting 300 MFR Resin	0.80	112000	37000	2.8
	160 g/min web	0.66	80000	35200	2.3
	320 g/min web	0.66	79100	34400	2.3
	480 g/min web	0.66	79100	33900	2.3
	Starting 1000 MFR Resin	0.72	91400	27200	3.4
	160 g/min web	0.53	61500	21600	2.9
	320 g/min web	0.53	60800	23500	2.6
	480 g/min web	0.53	60400	24000	2.5

Table D.7

Measured melt flow rate of resins and webs processed at 75% air flow rate using standard orifice die

SAMPLE ID	PROPERTIES	Measured Melt Flow Rate (MFR) (g/10 minutes)
75% Air Flow Rate Standard Orifice Die	Starting 35 MFR Resin	34
	160 g/min web	120
	320 g/min web	141
	Starting 300 MFR Resin	290
	160 g/min web	355
	320 g/min web	376
	480 g/min web	391
	Starting 600 MFR Resin	600
	160 g/min web	710
	320 g/min web	762
	480 g/min web	840
	Starting 1000 MFR Resin	950
	160 g/min web	1083
	320 g/min web	1131
	480 g/min web	1173

Table D.8

Measured melt flow rate of resins and webs processed at 90% air flow rate using standard orifice die

SAMPLE ID / PROPERTIES		Measured Melt Flow Rate (MFR) (g/10 minutes)
90% Air Flow Rate Standard Orifice Die	Starting 35 MFR Resin	34
	160 g/min web	124
	320 g/min web	134
	Starting 300 MFR Resin	290
	160 g/min web	400
	320 g/min web	401
	Starting 600 MFR Resin	600
	160 g/min Resin	830
	320 g/min Resin	853

Table D.9

Measured melt flow rate of resins and webs processed at 75% air flow rate using small orifice die

SAMPLE ID	PROPERTIES	Measured Melt Flow Rate (MFR) (g/10 minutes)
75% Air Flow Rate Small Orifice Die	Starting 300 MFR Resin	290
	160 g/min web	363
	320 g/min web	376
	480 g/min web	397
	Starting 1000 MFR Resin	950
	160 g/min web	1167
	320 g/min web	1175
	480 g/min web	1247

Table D.10

Tensile properties of webs and single fibers processed at 75% air flow rate using standard orifice die

Sample ID			Breaking Stress (mN/tex)		Breaking Strain (%)		Initial Modulus (mN/tex)		Single Fiber	
			MD	CD	MD	CD	MD	CD	Breaking Stress (MPa)	Breaking Strain (%)
75% Air Flow Rate Standard Orifice Die	35 MFR	160 g/min	20.7	10.5	28.9	65.2	573.9	170.7	38.7	62.1
		320 g/min	14.2	9.7	10.9	12.4	418.0	258.0	34.1	37.4
	300 MFR	160 g/min	17.8	9.9	27.7	58.0	420.8	108.7	34.9	74.0
		320 g/min	18.7	7.5	12.0	26.0	420.8	127.1	40.6	35.2
		480 g/min	16.3	7.8	6.5	8.7	469.4	225.5	35.1	17.1
	600 MFR	160 g/min	10.1	8.4	11.8	50.3	129.6	48.9	26.7	36.6
		320 g/min	13.8	5.5	5.0	7.7	405.6	150.7	29.4	28.0
		480 g/min	12.7	4.3	2.2	2.4	441.3	208.2	28.9	20.1
	1000 MFR	160 g/min	11.3	9.8	27.1	80.2	234.0	97.5	28.5	69.4
		320 g/min	13.1	5.0	7.3	13.8	367.7	152.0	32.7	40.0
		480 g/min	11.9	4.4	4.4	9.2	356.9	126.8	26.1	37.1

Table D.11

Tensile properties of webs and single fibers processed at 90% air flow rate using standard orifice die

Sample ID			Breaking Stress (mN/tex)		Breaking Strain (%)		Initial Modulus (mN/tex)		Single Fiber	
			MD	CD	MD	CD	MD	CD	Breaking Stress (MPa)	Breaking Strain (%)
90% Air Flow Rate Standard Orifice Die	35 MFR	160 g/min	20.4	13.2	34.5	52.3	378.0	167.7	41.2	70.4
		320 g/min	17.8	10.9	14.8	22.4	454.2	220.2	32.1	51.2
	300 MFR	160 g/min	17.6	11.7	21.8	53.9	264.1	111.9	33.4	47.8
		320 g/min	18.6	9.3	17.9	31.1	376.4	172.5	37.1	43.5
	600 MFR	160 g/min	11.7	11.3	17.9	55.9	215.4	125.2	28.2	41.6
		320 g/min	14.7	8.1	13.3	28.9	301.5	170.8	31.4	37.0

Table D.12
Tensile properties of webs and single fibers processed at 75% air flow rate using small orifice die

Sample ID			Breaking Stress (mN/tex)		Breaking Strain (%)		Initial Modulus (mN/tex)		Single Fiber	
			MD	CD	MD	CD	MD	CD	Breaking Stress (MPa)	Breaking Strain (%)
75% Air Flow Rate Small Orifice Die	300 MFR	160 g/min	16.6	7.9	17.6	29.1	383.9	121.6	33.7	47.5
		320 g/min	16.3	6.8	3.9	5.2	476.1	229.2	37.4	31.2
		480 g/min	11.2	5.3	2.7	3.1	460.4	182.0	31.2	30.4
	1000 MFR	160 g/min	10.7	5.9	9.3	20.7	220.4	166.1	30.8	41.7
		320 g/min	11.7	3.5	2.3	3.1	484.1	147.2	29.9	28.2
		480 g/min	10.5	3.5	1.6	3.2	521.2	104.0	27.1	29.3

Table D.13

Breaking stress of webs and single fibers processed at 75% air flow rate using standard orifice die

Sample ID			Web Breaking Stress (mN/tex)		Single Fiber Breaking Stress (mN/tex)
			MD	CD	
75% Air Flow Rate Standard Orifice Die	35 MFR	160 g/min	20.7	10.5	42.6
		320 g/min	14.2	9.7	37.5
	300 MFR	160 g/min	17.8	9.9	38.4
		320 g/min	18.7	7.5	44.7
		480 g/min	16.3	7.8	38.6
	600 MFR	160 g/min	10.1	8.4	29.4
		320 g/min	13.8	5.5	32.3
		480 g/min	12.7	4.3	31.8
	1000 MFR	160 g/min	11.3	9.8	31.4
		320 g/min	13.1	5.0	36.0
		480 g/min	11.9	4.4	28.7

Table D.14
Breaking stress of webs and single fibers processed at 90% air flow rate using standard orifice die

Sample ID		Properties	Web Breaking Stress (mN/tex)		Single Fiber Breaking Stress (mN/tex)
			MD	CD	
90% Air Flow Rate Standard Orifice Die	35 MFR	160 g/min	20.4	13.2	45.3
		320 g/min	17.8	10.9	35.3
	300 MFR	160 g/min	17.6	11.7	36.7
		320 g/min	18.6	9.3	40.8
	600 MFR	160 g/min	11.7	11.3	31.0
		320 g/min	14.7	8.1	34.5

Table D.15
Breaking stress of webs and single fibers processed at 75% air flow rate using small orifice die

Sample ID		Properties	Web Breaking Stress (mN/tex)		Single Fiber Breaking Stress (mN/tex)
			MD	CD	
75% Air Flow Rate Small Orifice Die	300 MFR	160 g/min	16.6	7.9	37.1
		320 g/min	16.3	6.8	41.1
		480 g/min	11.2	5.3	34.3
	1000 MFR	160 g/min	10.7	5.9	33.9
		320 g/min	11.7	3.5	32.9
		480 g/min	10.5	3.5	29.8

Table D.16

Flexural rigidity and bursting strength of webs processed at 75% air flow rate using standard orifice die

SAMPLE ID / PROPERTIES			FLEXURAL RIGIDITY (mg•cm)		BURSTING STRENGTH (kPa)
			MD	CD	
75% Air Flow Rate Standard Orifice Die	35 MFR	160 g/min	810.9	219.0	122.2
		320 g/min	297.9	151.1	81.1
	300 MFR	160 g/min	733.2	269.5	89.0
		320 g/min	630.9	172.6	72.4
		480 g/min	418.3	148.0	25.2
	600 MFR	160 g/min	306.0	138.3	80.2
		320 g/min	901.7	278.6	23.2
		480 g/mim	802.8	201.4	13.3
	1000 MFR	160 g/min	434.3	201.2	46.4
		320 g/min	739.4	235.8	38.7
		480 g/min	921.9	289.1	38.2

Table D.17

Flexural rigidity and bursting strength of webs processed at 90% air flow rate using standard orifice die

SAMPLE ID		PROPERTIES	FLEXURAL RIGIDITY (mg•cm)		BURSTING STRENGTH (kPa)
			MD	CD	
90% Air Flow Rate Standard Orifice Die	35 MFR	160 g/min	632.0	242.6	88.9
		320 g/min	381.2	214.8	49.4
	300 MFR	160 g/min	848.2	285.0	87.4
		320 g/min	794.4	205.2	51.1
	600 MFR	160 g/min	611.3	254.0	74.9
		320 g/min	770.9	445.4	47.7

Table D.18

Flexural rigidity and bursting strength of webs processed at 75% air flow rate using small orifice die

SAMPLE ID / PROPERTIES			FLEXURAL RIGIDITY (mg•cm)		BURSTING STRENGTH (kPa)
			MD	CD	
75% Air Flow Rate Small Orifice Die	300 MFR	160 g/min	820.7	228.3	52.3
		320 g/min	418.0	111.8	18.5
		480 g/min	309.8	81.7	13.3
	1000 MFR	160 g/min	597.5	239.0	47.5
		320 g/min	990.4	240.1	12.8
		480 g/min	633.4	137.1	10.9

Table D.19
Air permeability of webs processed at 75% air flow rate using standard orifice die

SAMPLE ID		PROPERTIES	AIR PERMEABILITY ($M^3/S/M^2$)
75% Air Flow Rate Standard Orifice Die	35 MFR	160 g/min	0.366
		320 g/min	0.752
	300 MFR	160 g/min	0.330
		320 g/min	0.432
		480 g/min	0.559
	600 MFR	160 g/min	0.320
		320 g/min	0.422
		480 g/mim	0.447
	1000 MFR	160 g/min	0.371
		320 g/min	0.483
		480 g/min	0.493

Table D.20
Air permeability of webs processed at 90% air flow rate using standard orifice die

SAMPLE ID		PROPERTIES	AIR PERMEABILITY ($M^3/S/M^2$)
90% Air Flow Rate Standard Orifice Die	35 MFR	160 g/min	0.274
		320 g/min	0.335
	300 MFR	160 g/min	0.340
		320 g/min	0.340
	600 MFR	160 g/min	0.417
		320 g/min	0.463

Table D.21
Air permeability of webs processed at 75% air flow rate using small orifice die

SAMPLE ID		PROPERTIES	AIR PERMEABILITY ($M^3/S/M^2$)
75% Air Flow Rate Small Orifice Die	300 MFR	160 g/min	0.437
		320 g/min	0.498
		480 g/min	0.803
	1000 MFR	160 g/min	0.361
		320 g/min	0.457
		480 g/min	0.483

Table D.22

Basis weight, web thickness, and web density of webs processed at 75% air flow rate using standard orifice die

SAMPLE ID		PROPERTIES	WEB WEIGHT (g/m^2)	WEB THICKNESS (cm)	WEB DENSITY ($x10^3$ g/m^3)
75% AIR FLOW RATE STANDARD ORIFICE DIE	35 MFR	160 g/min	37.3	0.0284	131.3
		320 g/min	37.3	0.0251	148.6
	300 MFR	160 g/min	34.6	0.0287	120.6
		320 g/min	35.6	0.0250	142.4
		480 g/min	33.9	0.0191	177.5
	600 MFR	160 g/min	35.3	0.0350	100.9
		320 g/min	35.3	0.0263	134.2
		480 g/min	37.9	0.0250	151.6
	1000 MFR	160 g/min	33.9	0.0310	109.4
		320 g/min	33.9	0.0260	130.4
		480 g/min	37.3	0.0260	143.5

Table D.23

Basis weight, web thickness, and web density of webs processed at 90% air flow rate using standard orifice die

SAMPLE ID		PROPERTIES	WEB WEIGHT (g/m^2)	WEB THICKNESS (cm)	WEB DENSITY ($x10^3$ g/m^3)
90% AIR FLOW RATE STANDARD ORIFICE DIE	35 MFR	160 g/min	34.6	0.0261	132.6
		320 g/min	35.6	0.0225	158.2
	300 MFR	160 g/min	37.3	0.0334	111.7
		320 g/min	37.3	0.0262	142.4
	600 MFR	160 g/min	33.9	0.0333	101.8
		320 g/min	37.3	0.0280	133.2

Table D.24

Basis weight, web thickness, and web density of webs processed at 75% air flow rate using small orifice die

SAMPLE ID		PROPERTIES	WEB WEIGHT (g/m^2)	WEB THICKNESS (cm)	WEB DENSITY ($x10^3$ g/m^3)
75% AIR FLOW RATE SMALL ORIFICE DIE	300 MFR	160 g/min	35.9	0.0248	144.8
		320 g/min	35.3	0.0190	185.8
		480 g/min	34.9	0.0238	146.6
	1000 MFR	160 g/min	37.3	0.0336	111.0
		320 g/min	36.3	0.0263	138.0
		480 g/min	37.0	0.0207	178.7

Table D.25
Crystallinity of resins and webs processed at 75% air flow rate using standard orifice die

Sample ID	Properties	Heat of Fusion, ΔH (J/g)	Crystallinity (%)	Peak Temperature (°C)	Onset Temperature (°C)
75% Air Flow Rate Standard Orifice Die	Starting 35 MFR Resin	76.1	52.0	164.3	154.3
	160 g/min web	83.3	56.8	163.7	155.4
	320 g/min web	76.1	52.0	164.1	161.3
	Starting 300 MFR Resin	78.2	53.3	162.4	152.1
	160 g/min web	83.6	57.1	161.6	152.6
	320 g/min web	84.9	57.9	162.0	153.9
	480 g/min web	77.5	52.9	161.3	154.6
	Starting 600 MFR Resin	87.1	59.5	165.1	157.1
	160 g/min web	88.5	60.4	163.0	156.2
	320 g/min web	89.6	61.2	163.5	157.1
	480 g/min web	89.0	60.8	163.7	155.9
	Starting 1000 MFR Resin	85.2	58.2	165.7	159.2
	160 g/min web	87.8	59.9	161.8	153.4
	320 g/min web	85.9	58.6	162.7	156.8
	480 g/min web	85.5	58.4	162.9	158.5

Table D.26
Crystallinity of resins and webs processed at 90% air flow rate using standard orifice die

Sample ID	Properties	Heat of Fusion, ΔH (J/g)	Crystallinity (%)	Peak Temperature (°C)	Onset Temperature (°C)
90% Air Flow Rate Standard Orifice Die	Starting 35 MFR Resin	76.1	52.0	164.3	154.3
	160 g/min web	82.8	56.5	163.4	153.5
	320 g/min web	83.4	56.9	163.4	151.8
	Starting 300 MFR Resin	78.2	53.3	162.4	152.1
	160 g/min web	83.2	56.8	161.8	154.6
	320 g/min web	97.1	58.1	162.0	154.3
	Starting 600 MFR Resin	87.1	59.5	165.1	157.1
	160 g/min web	91.0	62.1	163.0	155.8
	320 g/min web	90.9	62.0	163.6	155.8

Table D.27
Crystallinity of resins and webs processed at 75% air flow rate using small orifice die

Sample ID	Properties	Heat of Fusion, ΔH (J/g)	Crystallinity (%)	Peak Temperature (°C)	Onset Temperature (°C)
75% Air Flow Rate Small Orifice Die	Starting 300 MFR Resin	78.2	53.3	162.4	152.1
	160 g/min web	79.4	54.2	162.3	153.1
	320 g/min web	78.8	53.8	162.1	154.7
	480 g/min web	79.1	54.0	162.2	155.6
	Starting 1000 MFR Resin	85.2	58.2	165.7	159.2
	160 g/min web	85.9	56.6	163.0	157.8
	320 g/min web	85.7	58.5	163.6	157.7
	480 g/min web	85.9	58.6	163.4	157.6

APPENDIX E

FIGURES

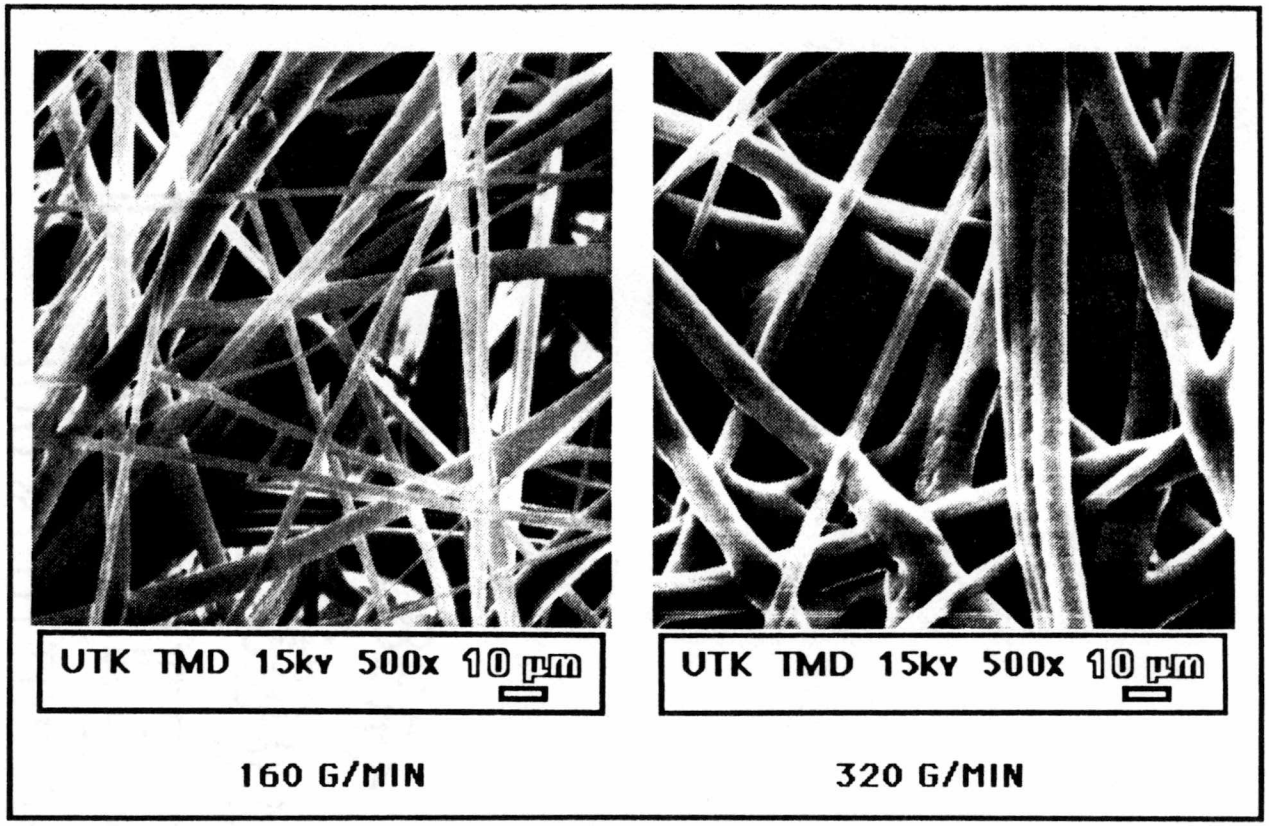

Figure E.1. Photomicrographs of 35 MFR webs processed at 75% air flow rate using standard orifice die.

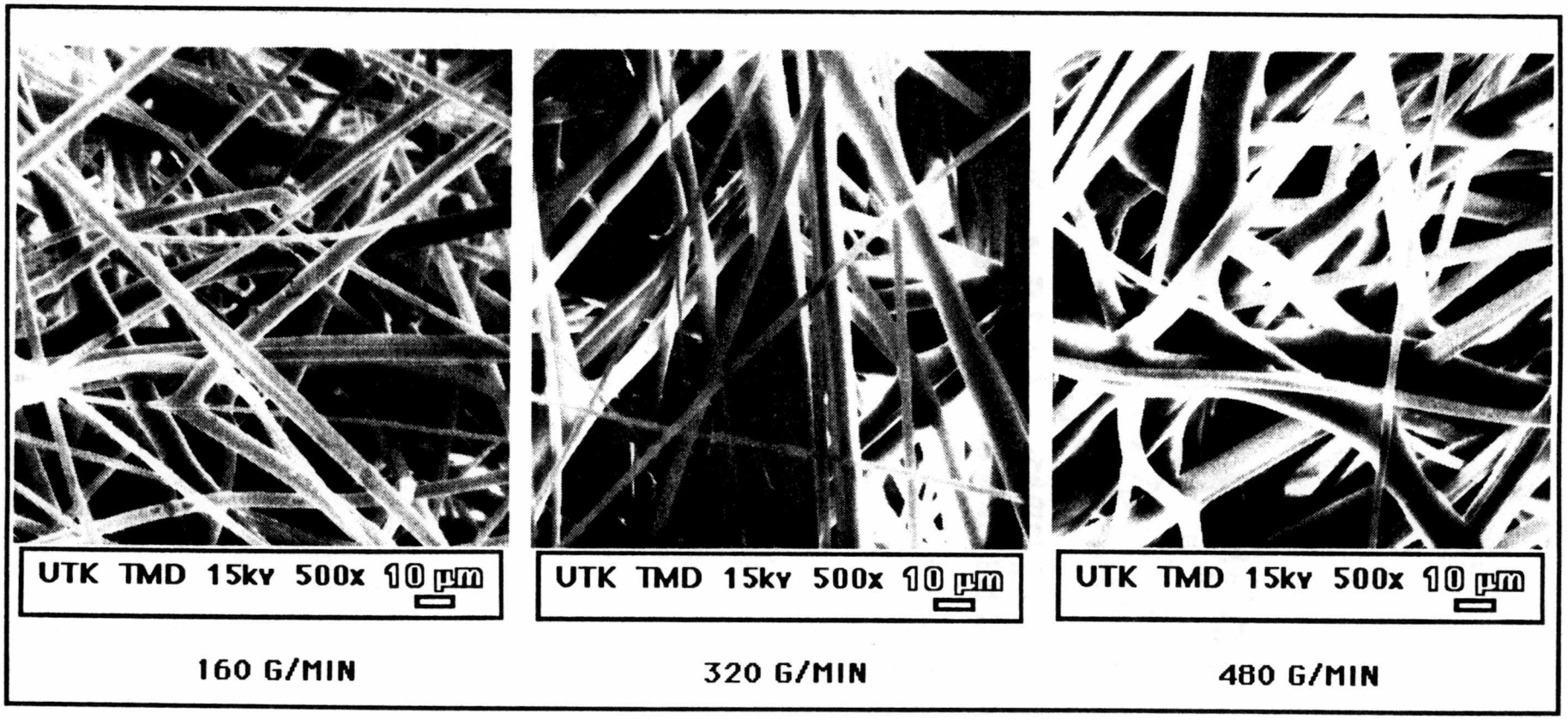

Figure E.2. Photomicrographs of 300 MFR webs processed at 75% air flow rate using standard orifice die.

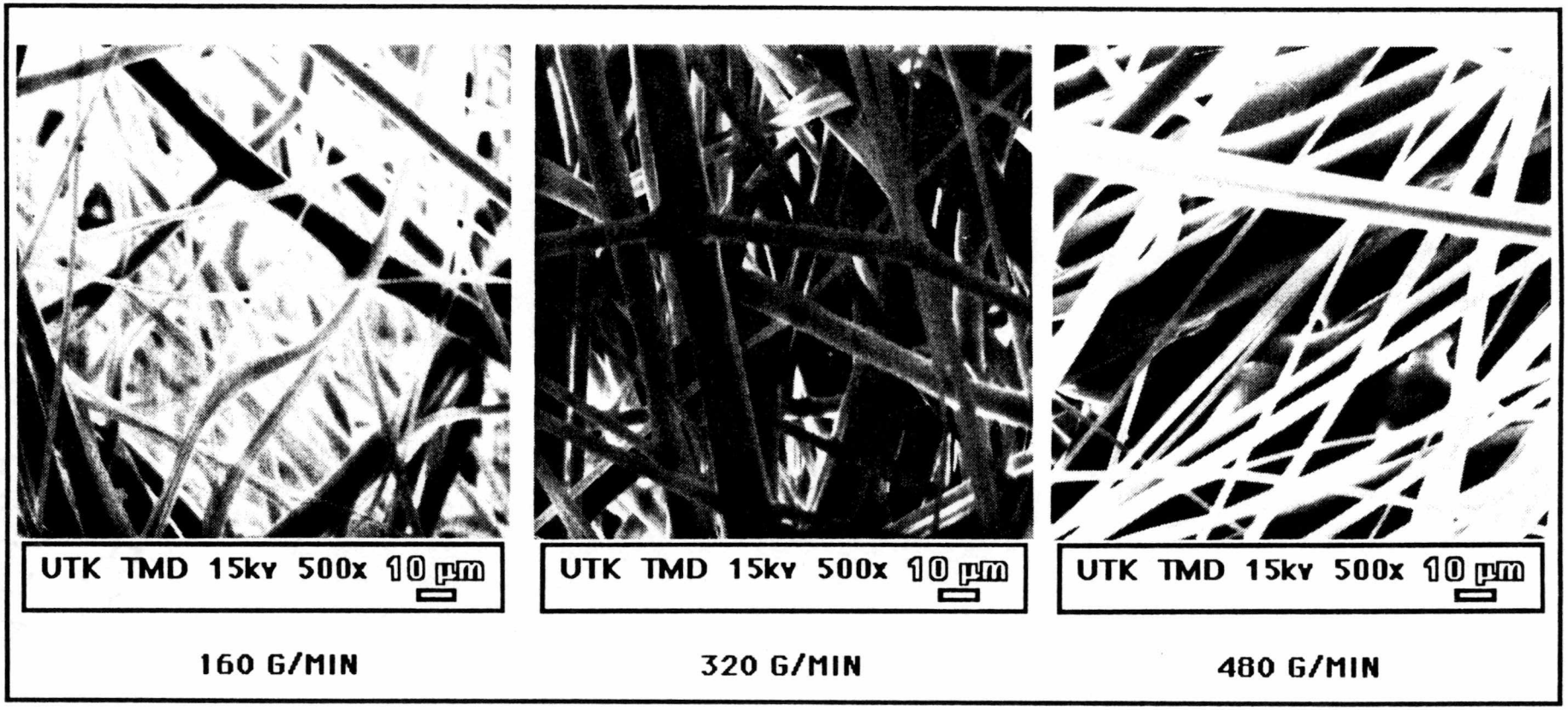

Figure E.3. Photomicrographs of 600 MFR webs processed at 75% air flow rate using standard orifice die.

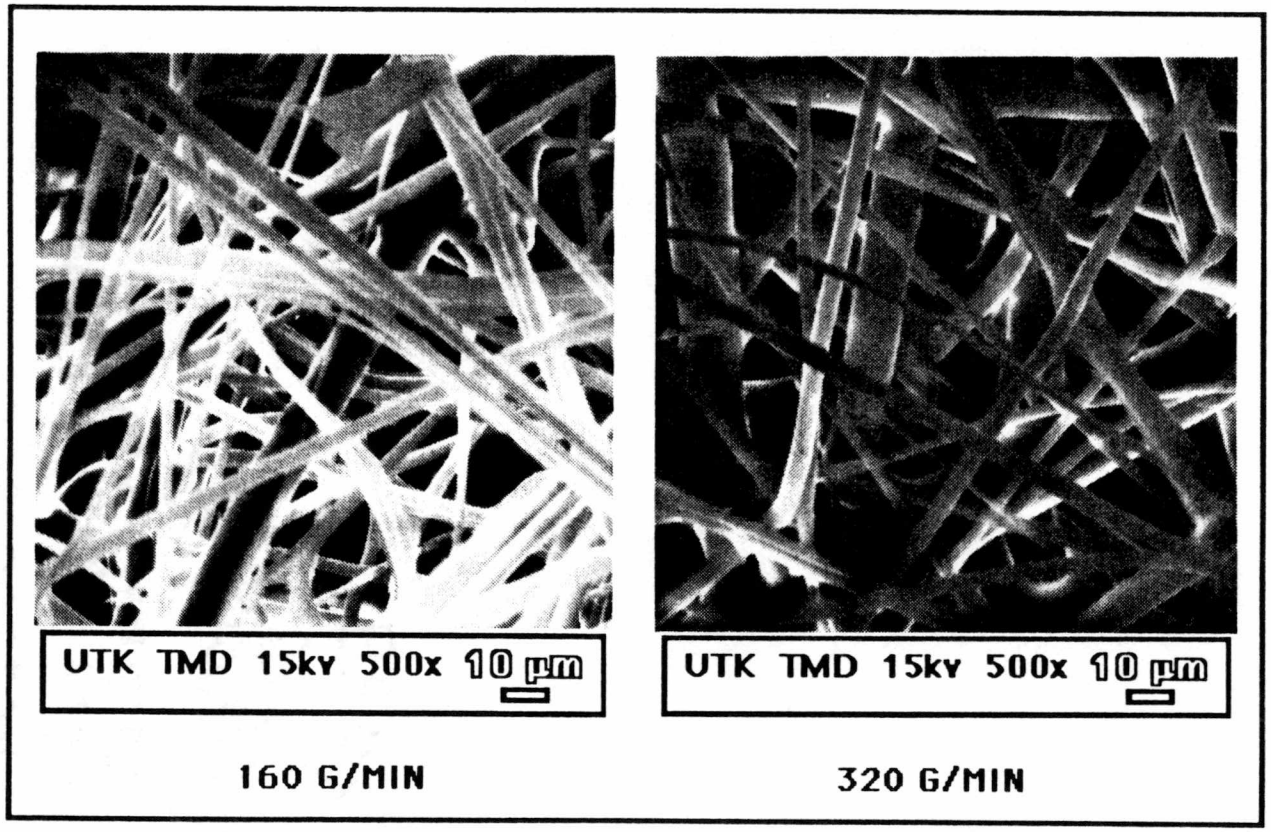

Figure E.4. Photomicrographs of 35 MFR webs processed at 90% air flow rate using standard orifice die.

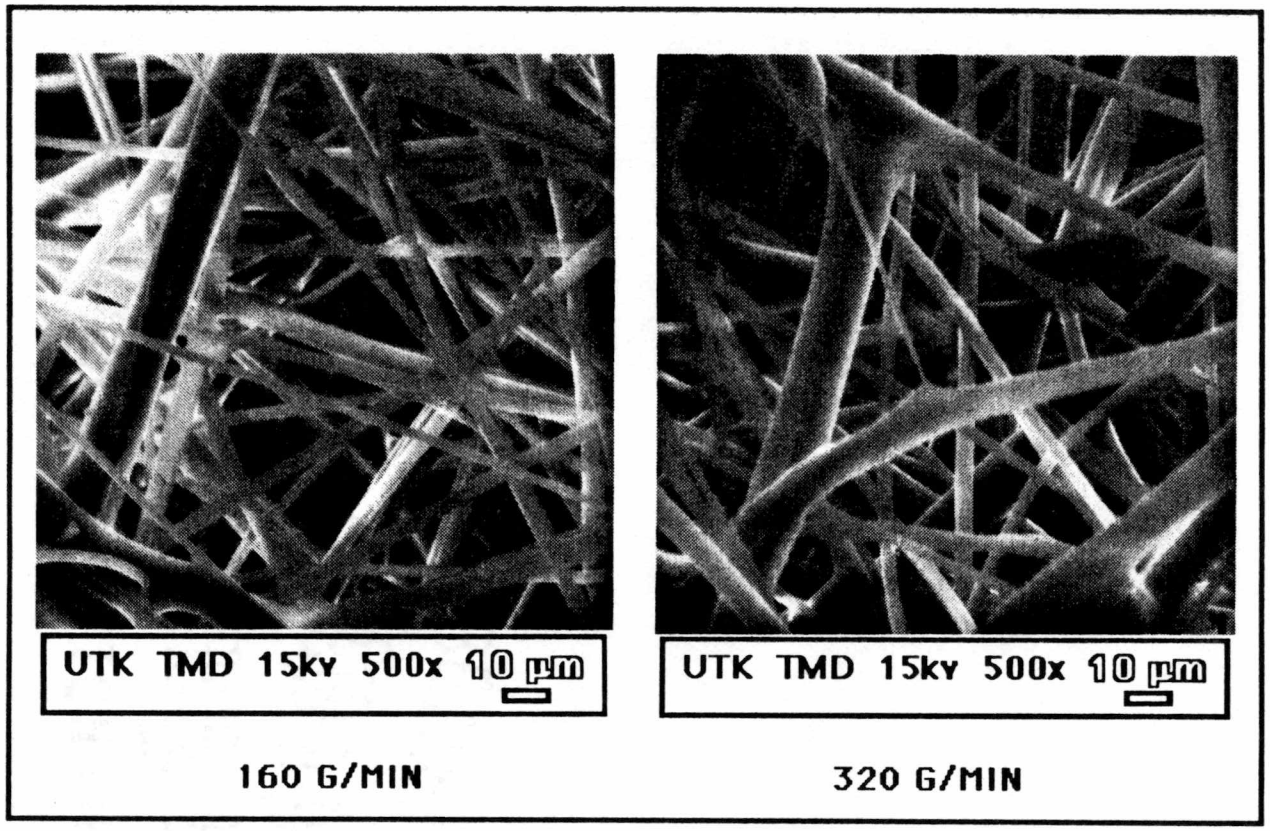

Figure E.5. Photomicrographs of 300 MFR webs processed at 90% air flow rate using standard orifice die.

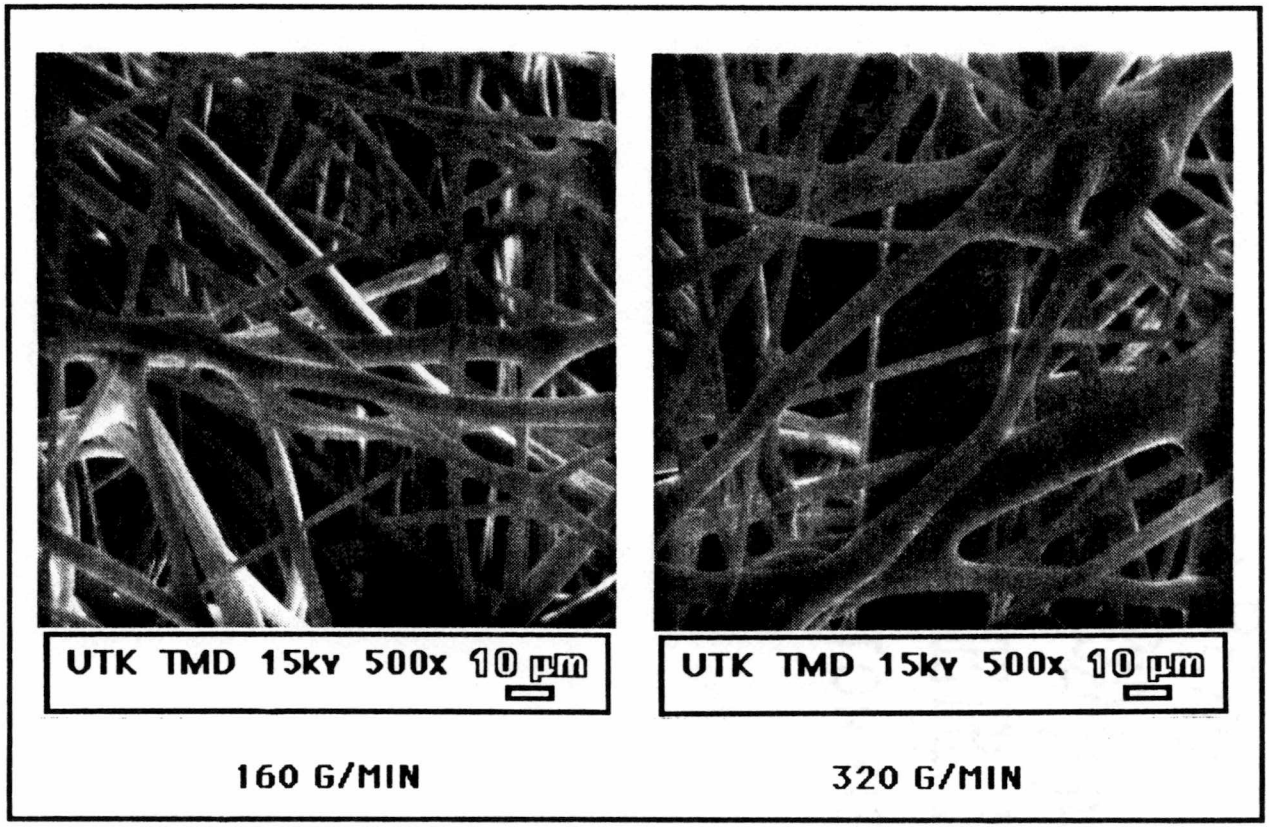

Figure E.6. Photomicrographs of 600 MFR webs processed at 90% air flow rate using standard orifice die.

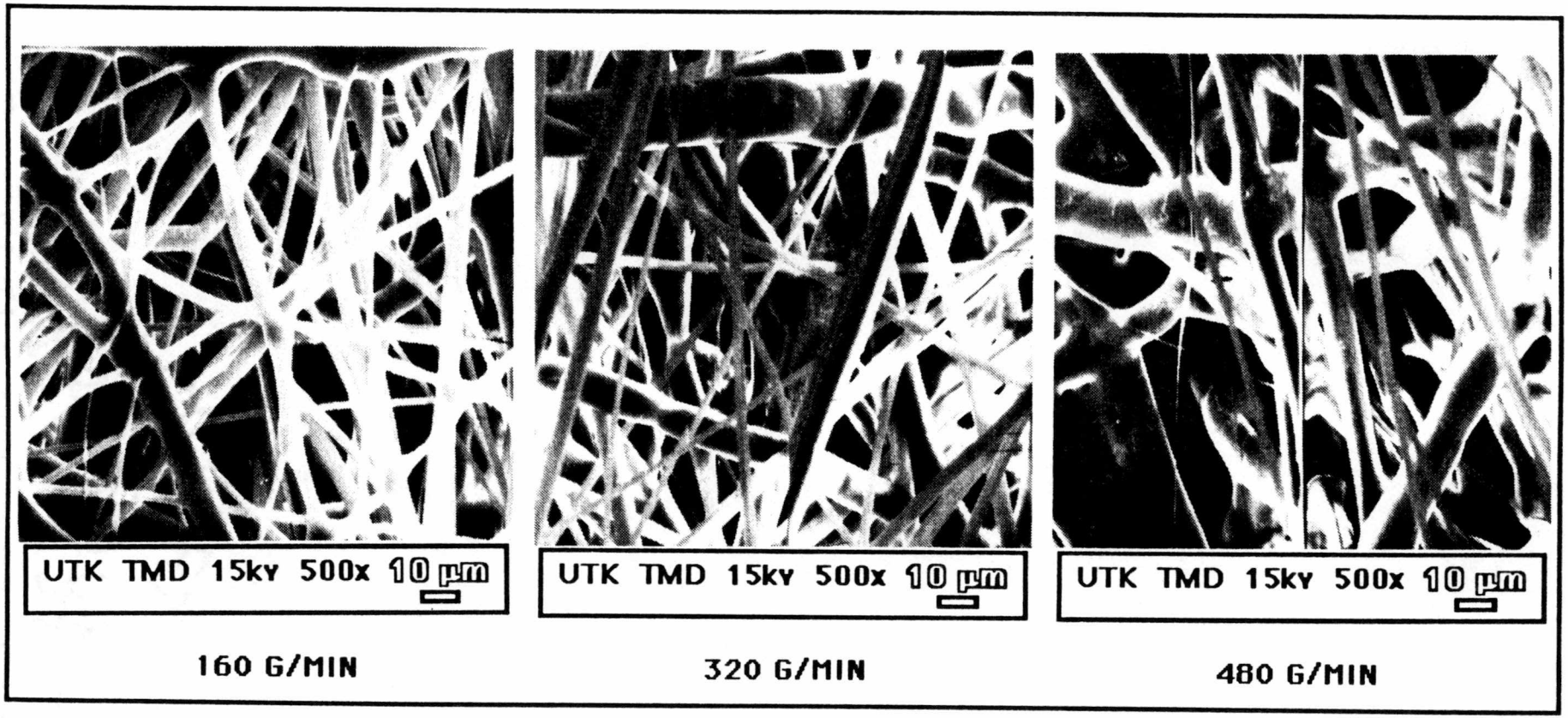

Figure E.7. Photomicrographs of 300 MFR webs processed at 75% air flow rate using small orifice die.

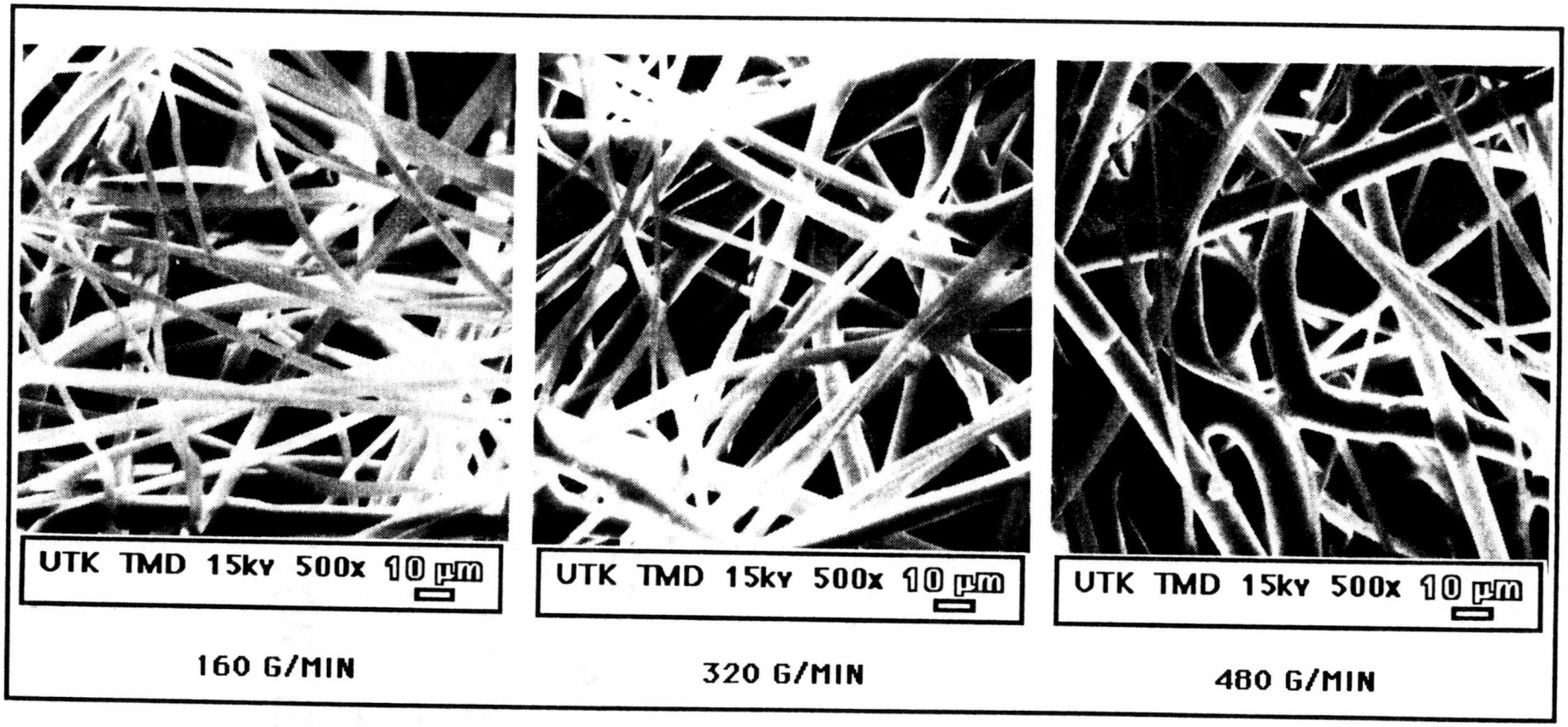

Figure E.8. Photomicrographs of 1000 MFR webs processed at 75% air flow rate using small orifice die.

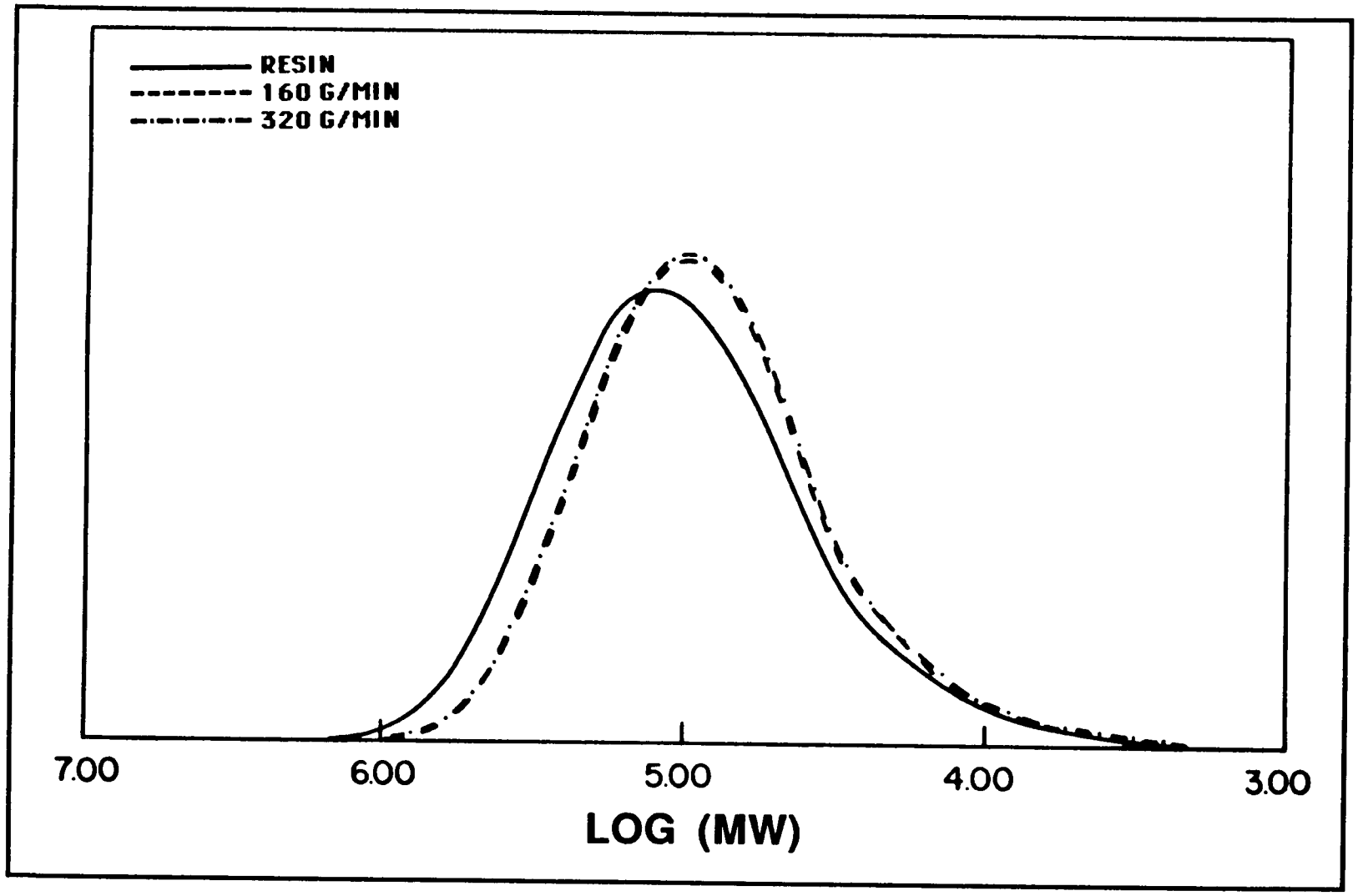

Figure E.9. GPC chromatograms of 35 MFR resin and webs processed at 75% air flow rate using standard orifice die.

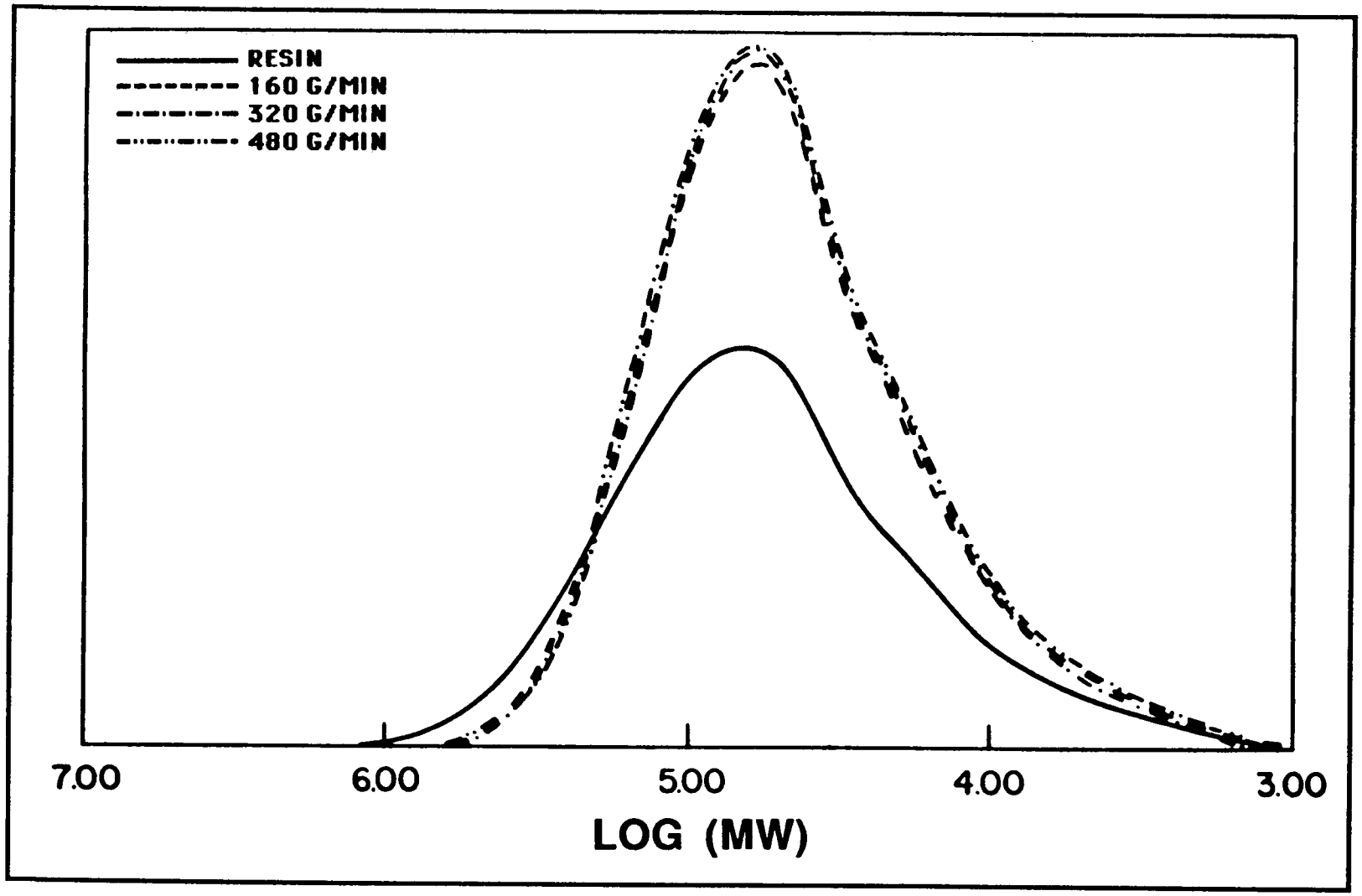

Figure E.10. GPC chromatograms of 600 MFR resin and webs processed at 75% air flow rate using standard orifice die.

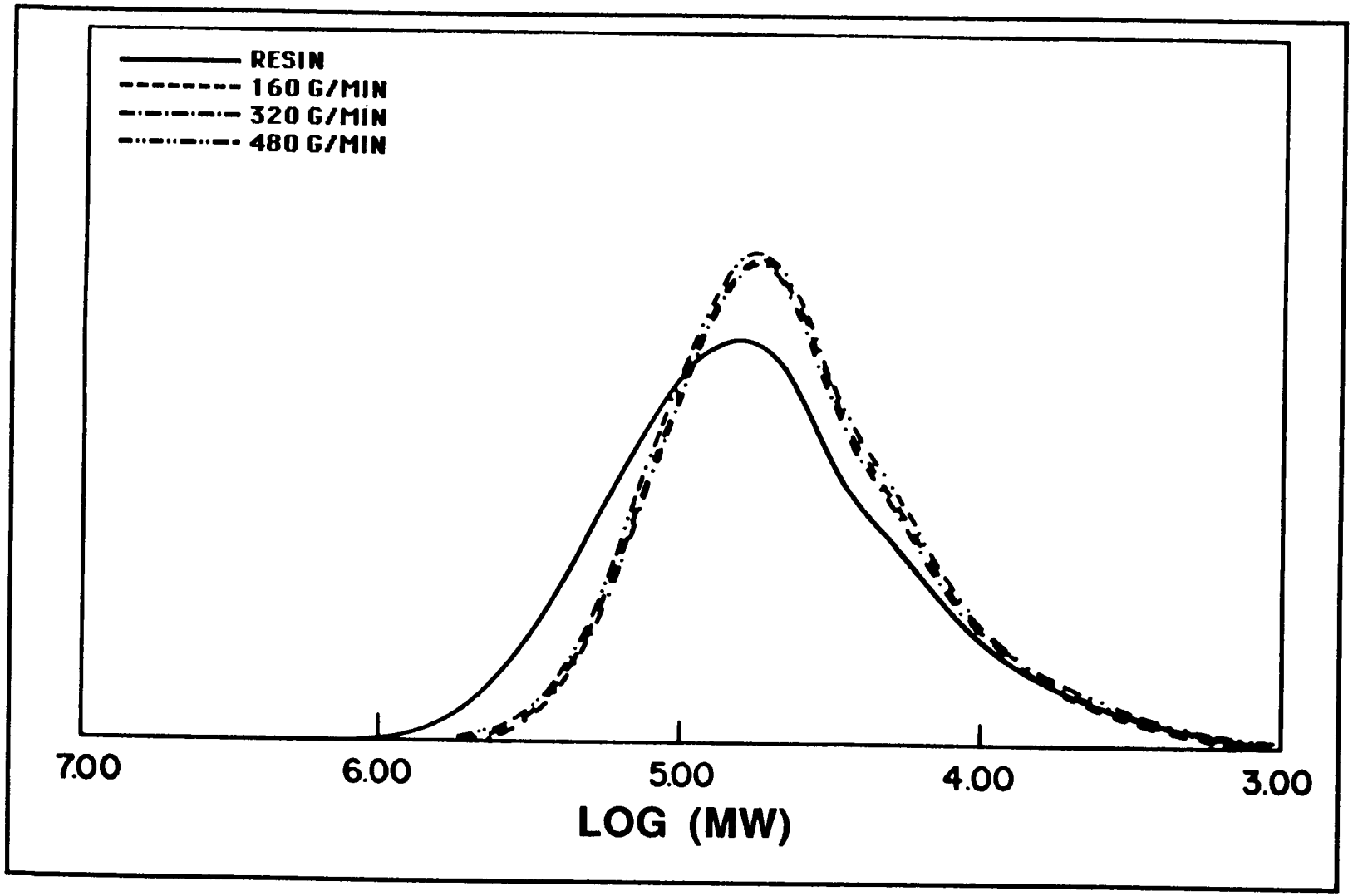

Figure E.11. GPC chromatograms of 1000 MFR resin and webs processed at 75% air flow rate using standard orifice die.

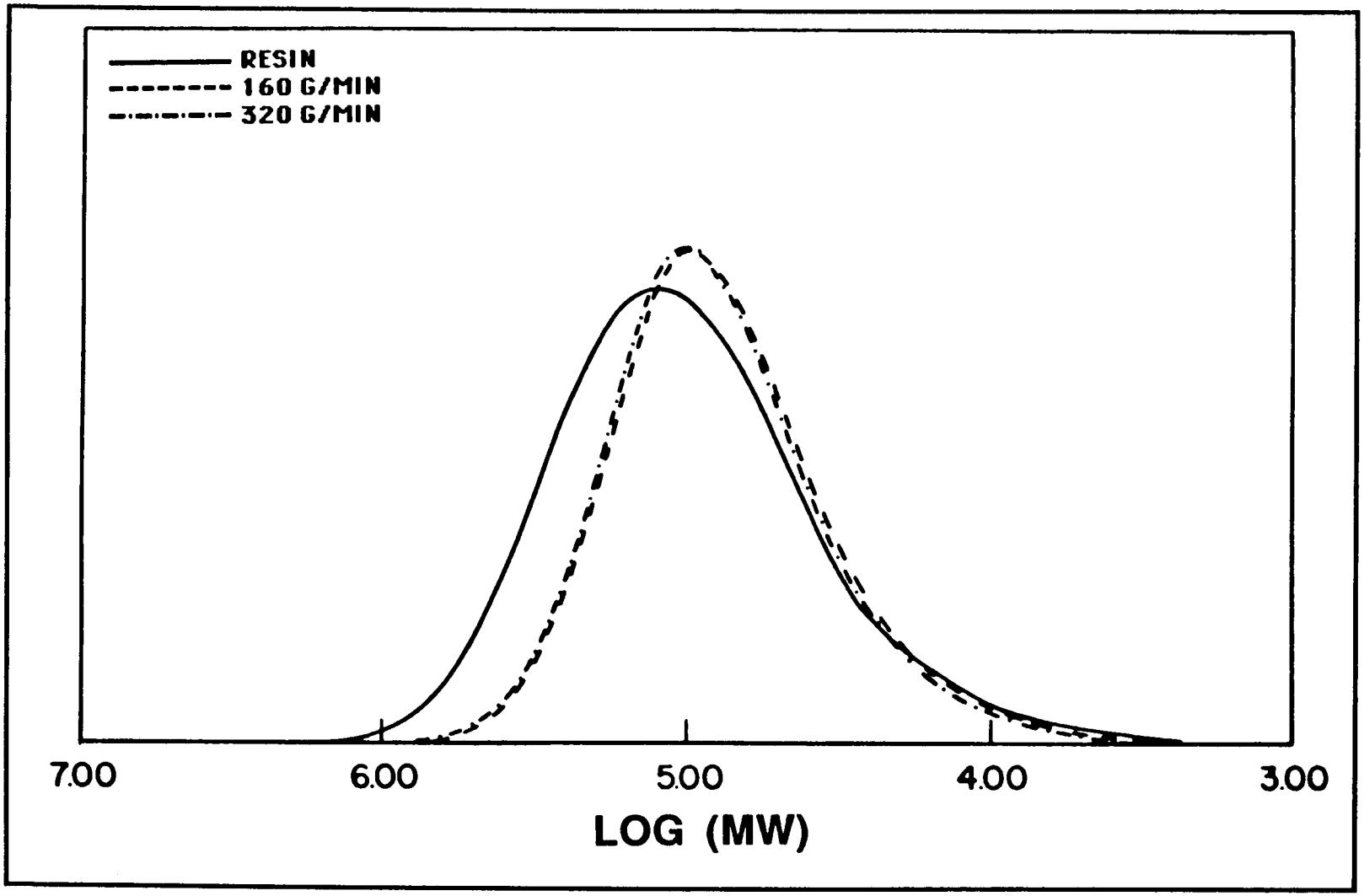

Figure E.12. GPC chromatograms of 35 MFR resin and webs processed at 90% air flow rate using standard orifice die.

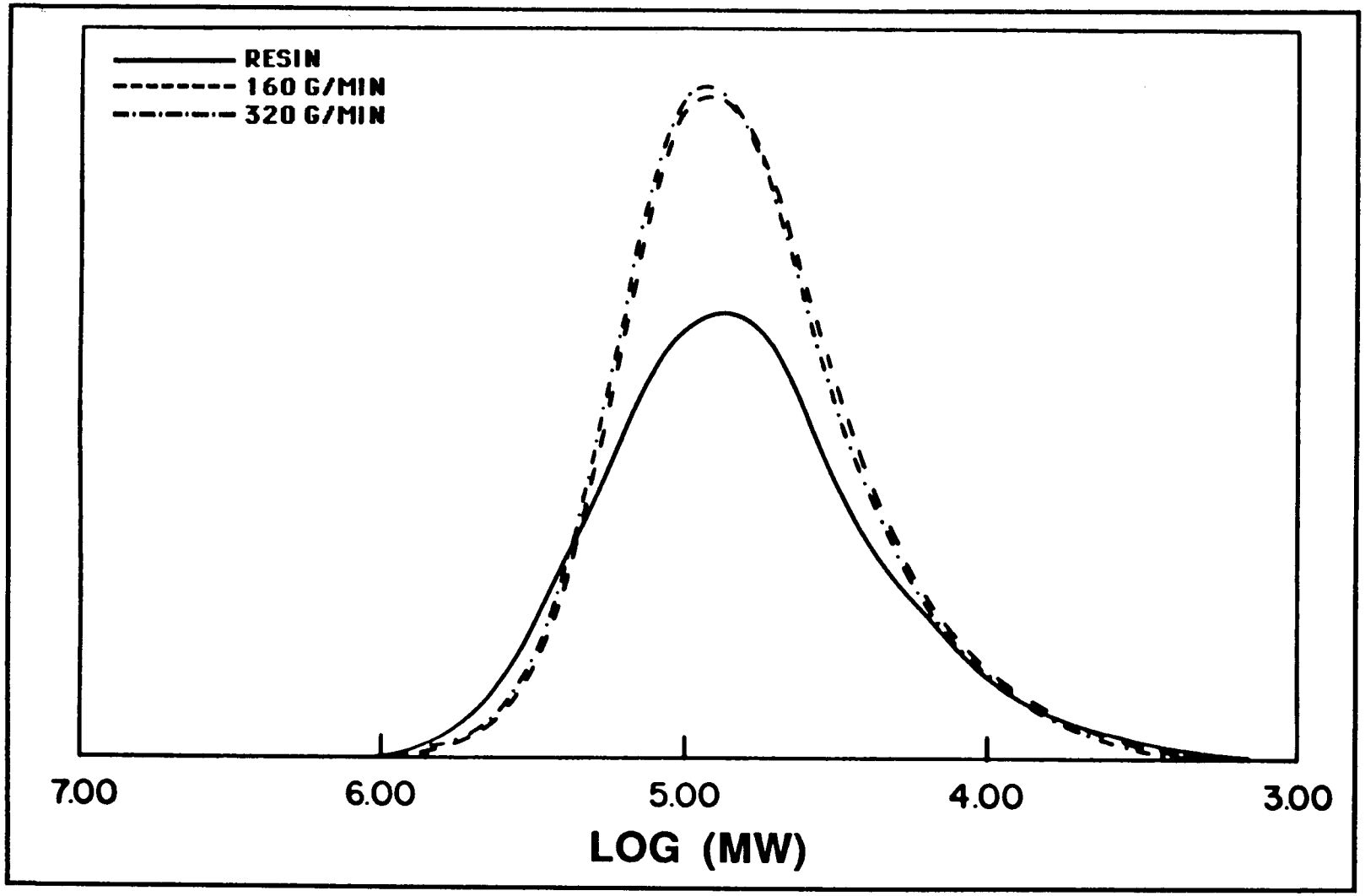

Figure E.13. GPC chromatograms of 300 MFR resin and webs processed at 90% air flow rate using standard orifice die.

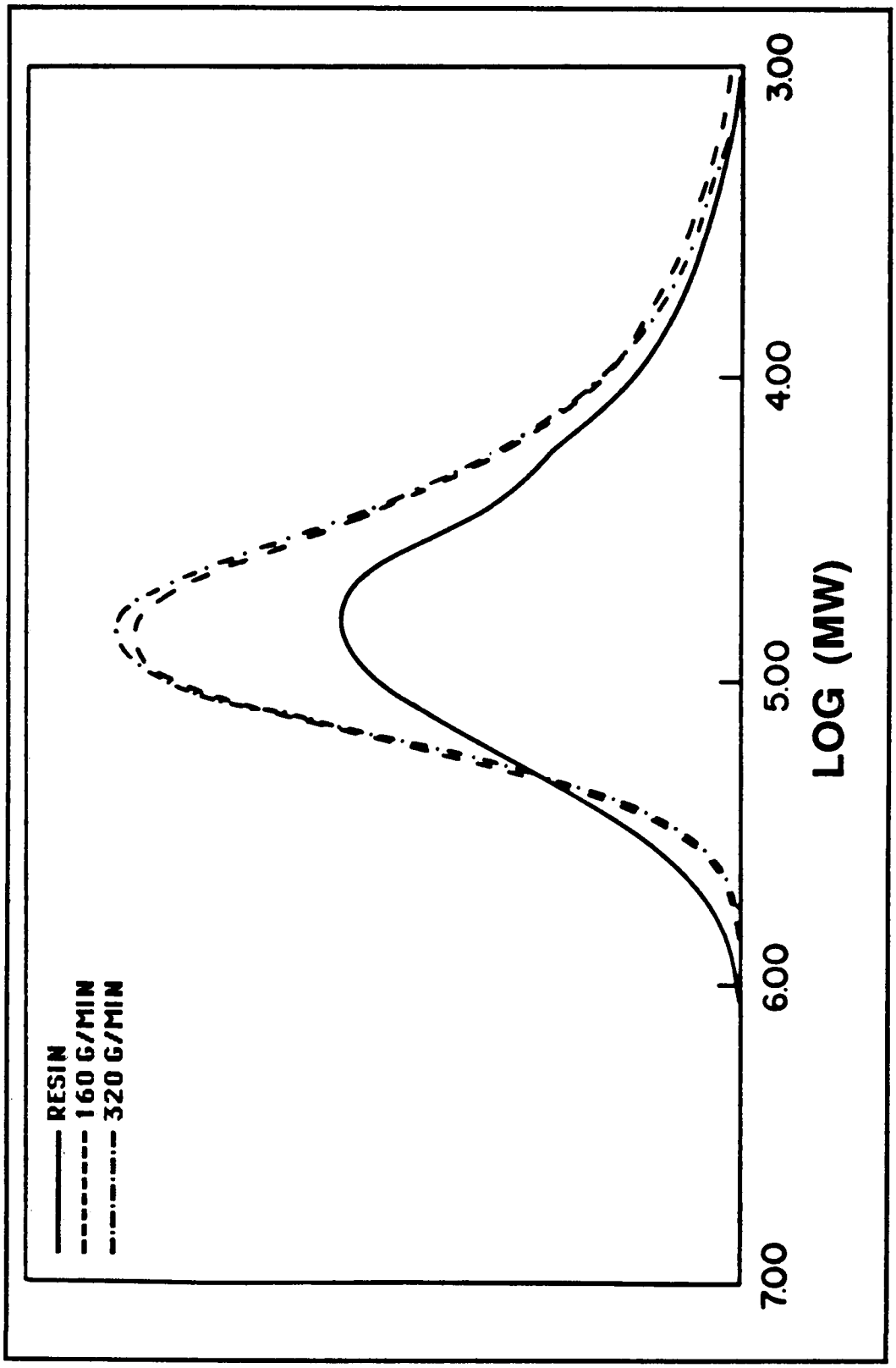

Figure E.14. GPC chromatograms of 600 MFR resin and webs processed at 90% air flow rate using standard orifice die.

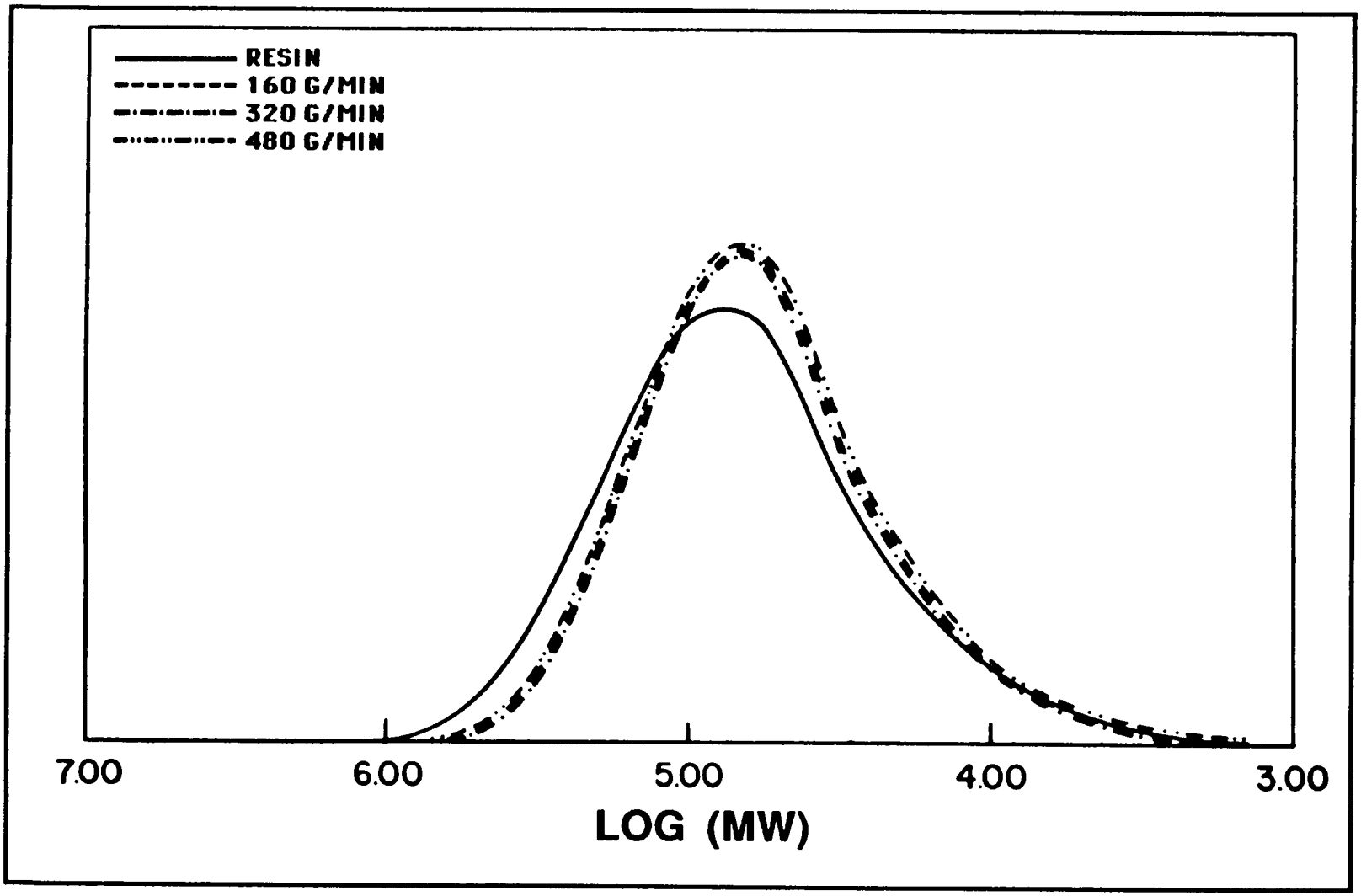

Figure E.15. GPC chromatograms of 300 MFR resin and webs processed at 75% air flow rate using small orifice die.

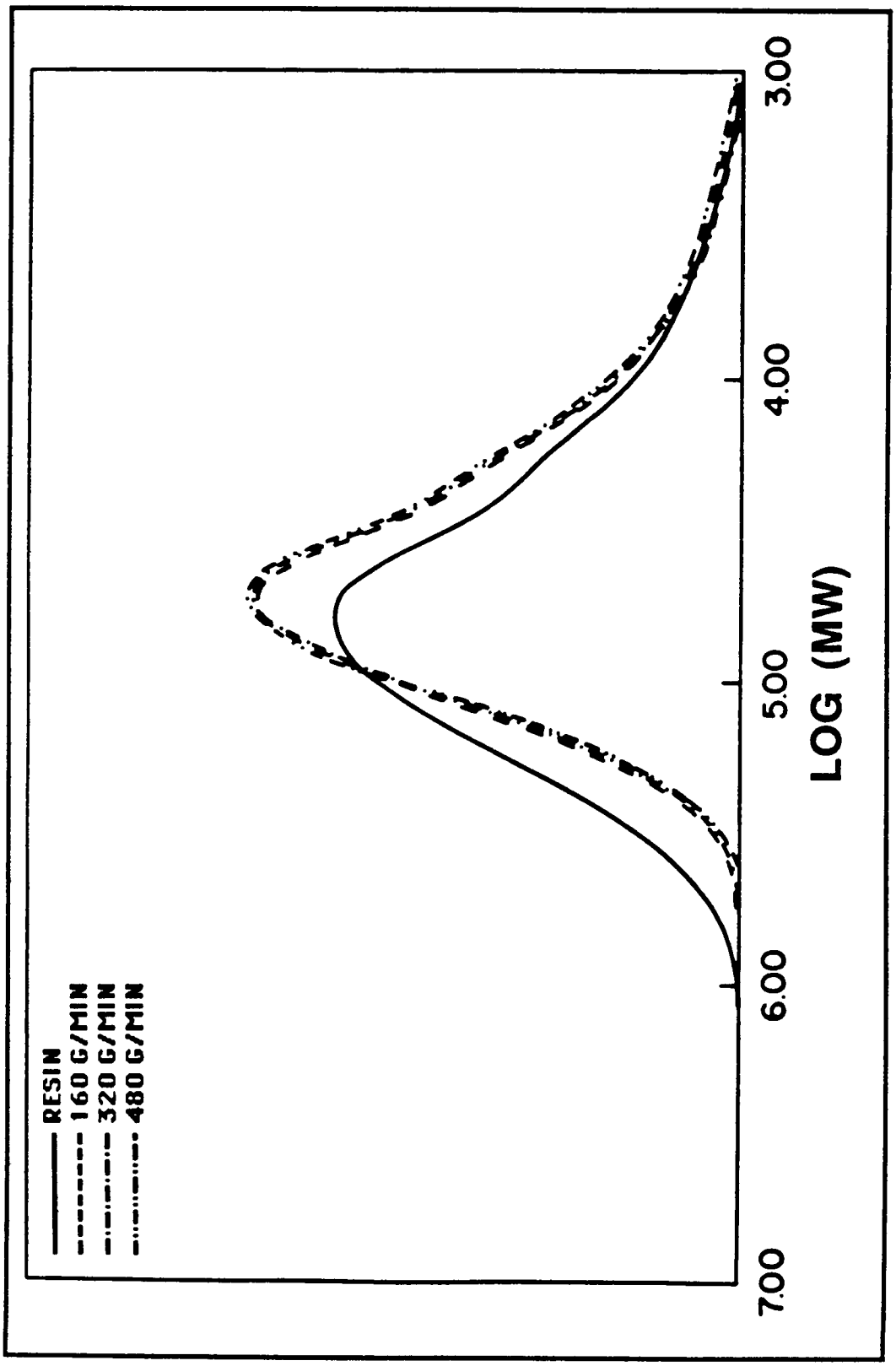

Figure E.16. GPC chromatograms of 1000 MFR resin and webs processed at 75% air flow rate using small orifice die.

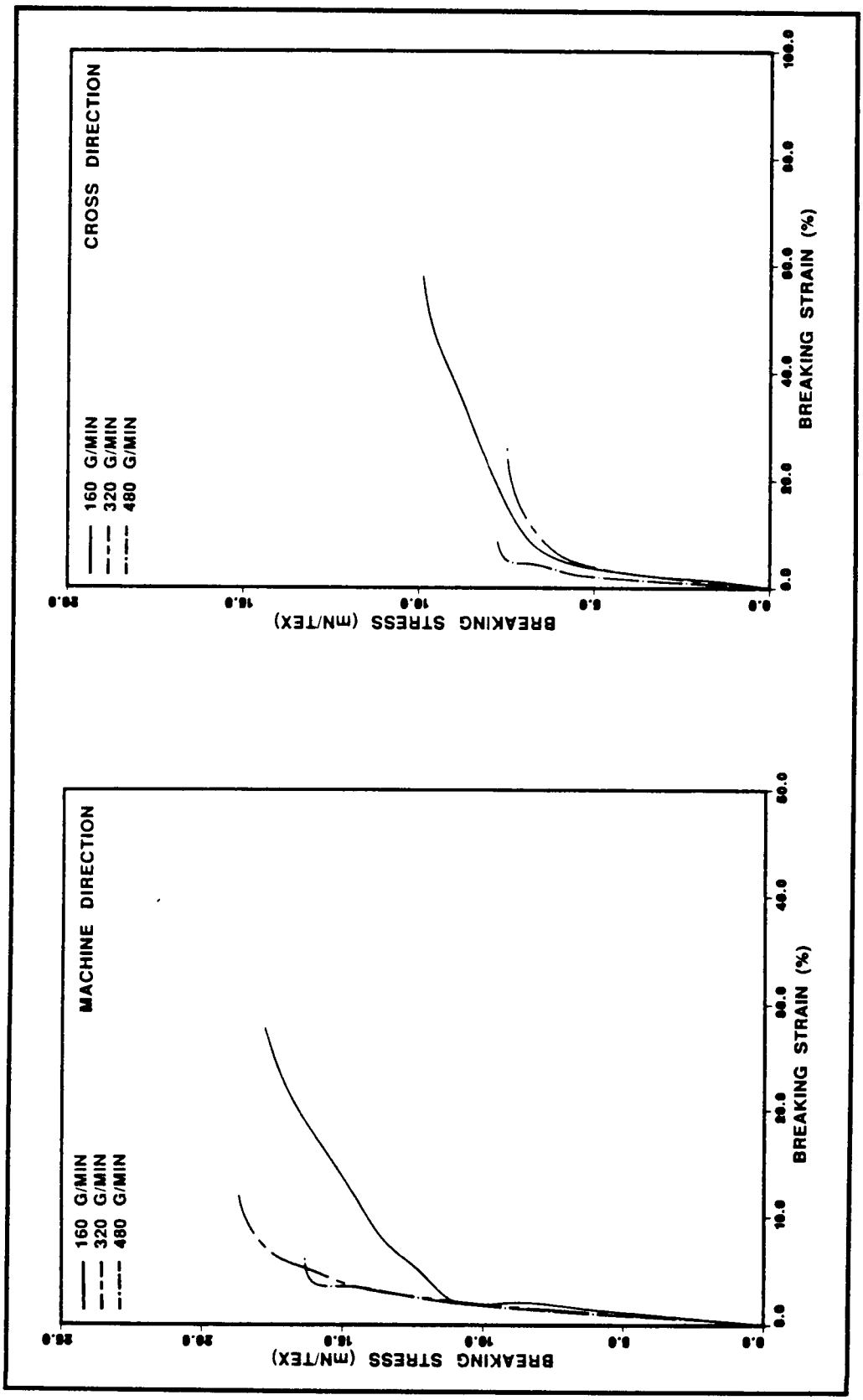

Figure E.17. Average MD and CD stress-strain curves of 300 MFR webs processed at 75% air flow rate using standard orifice die.

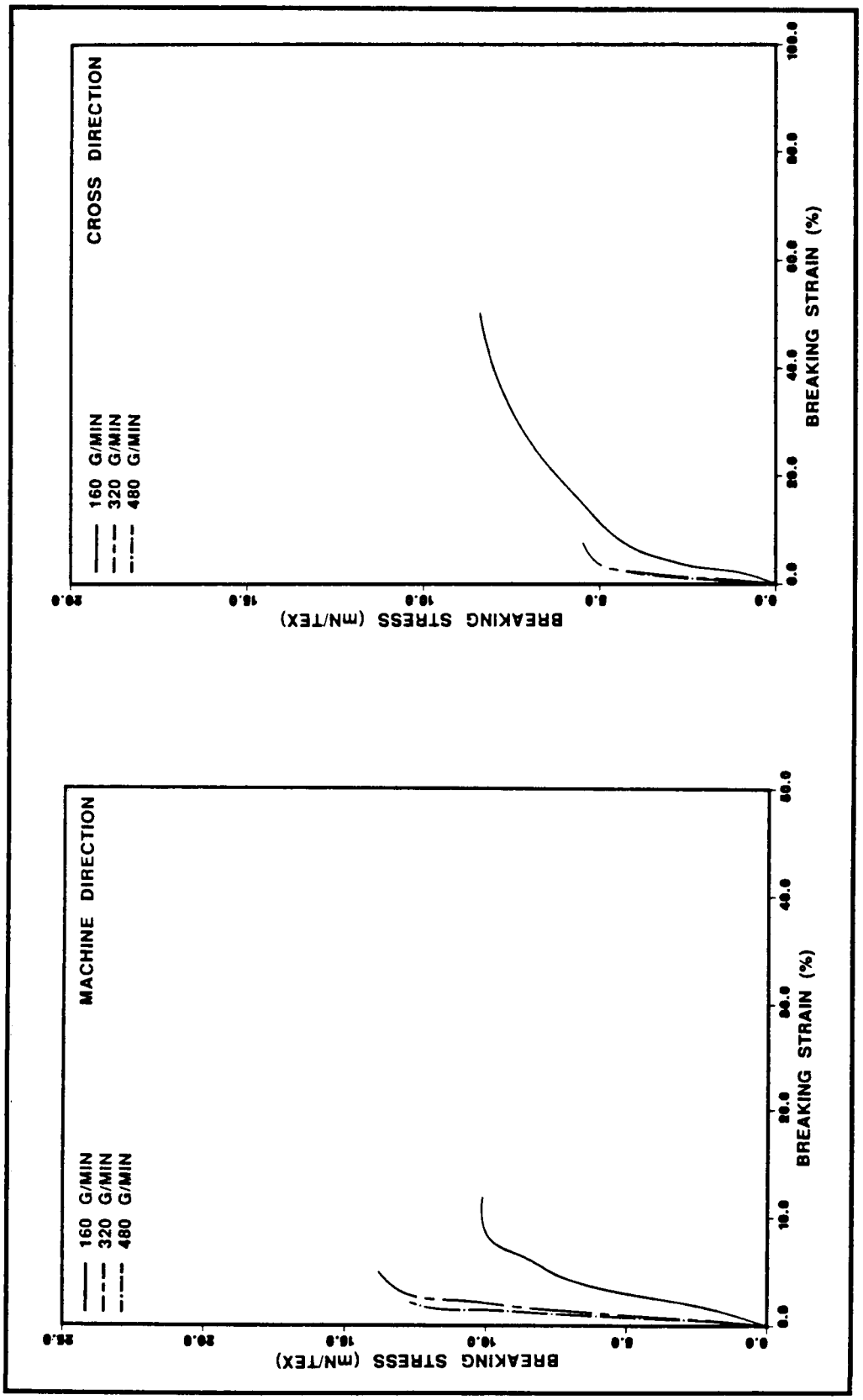

Figure E.18. Average MD and CD stress-strain curves of 600 MFR webs processed at 75% air flow rate using standard orifice die.

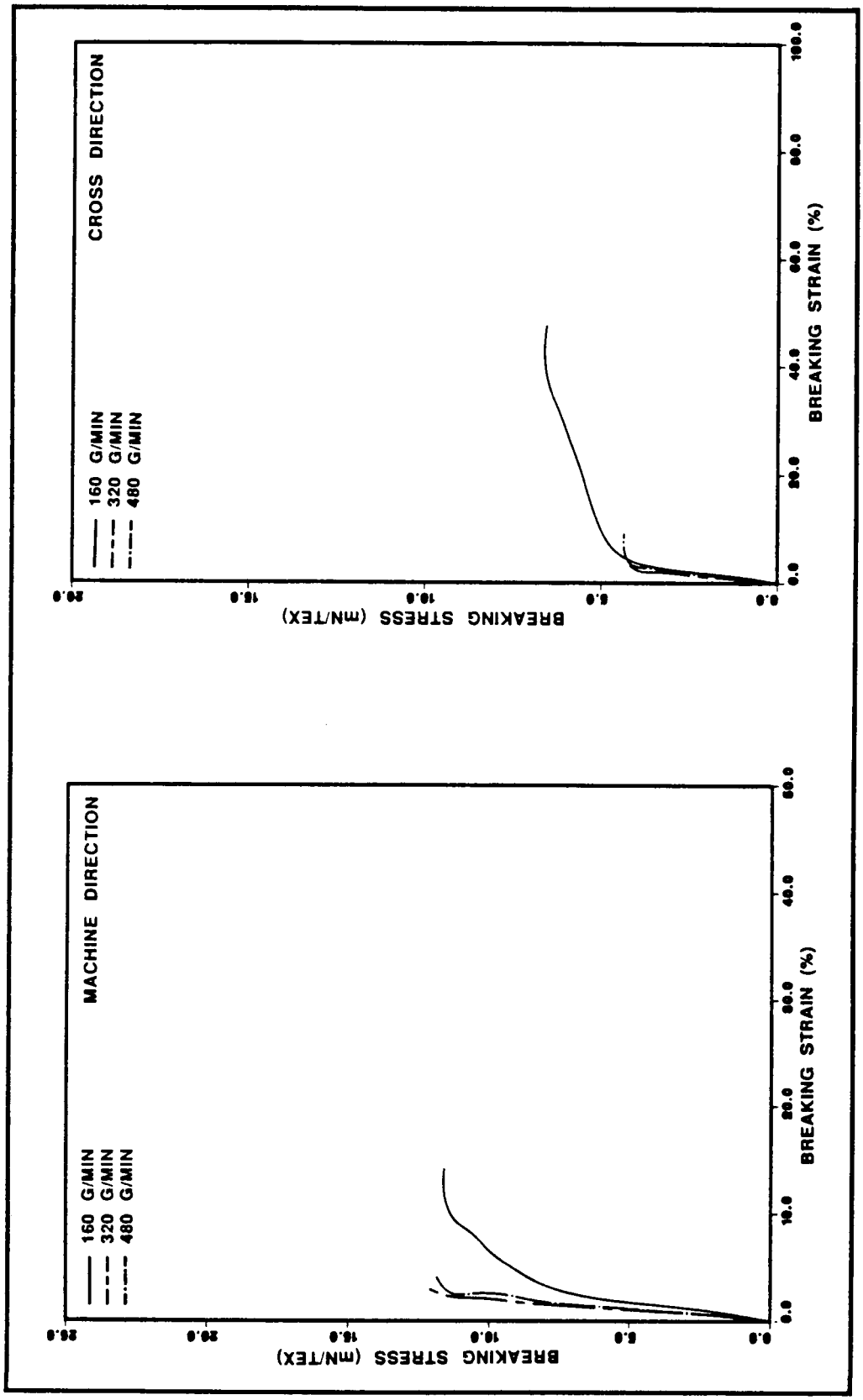

Figure E.19. Average MD and CD stress-strain curves of 1000 MFR webs processed at 75% air flow rate using standard orifice die.

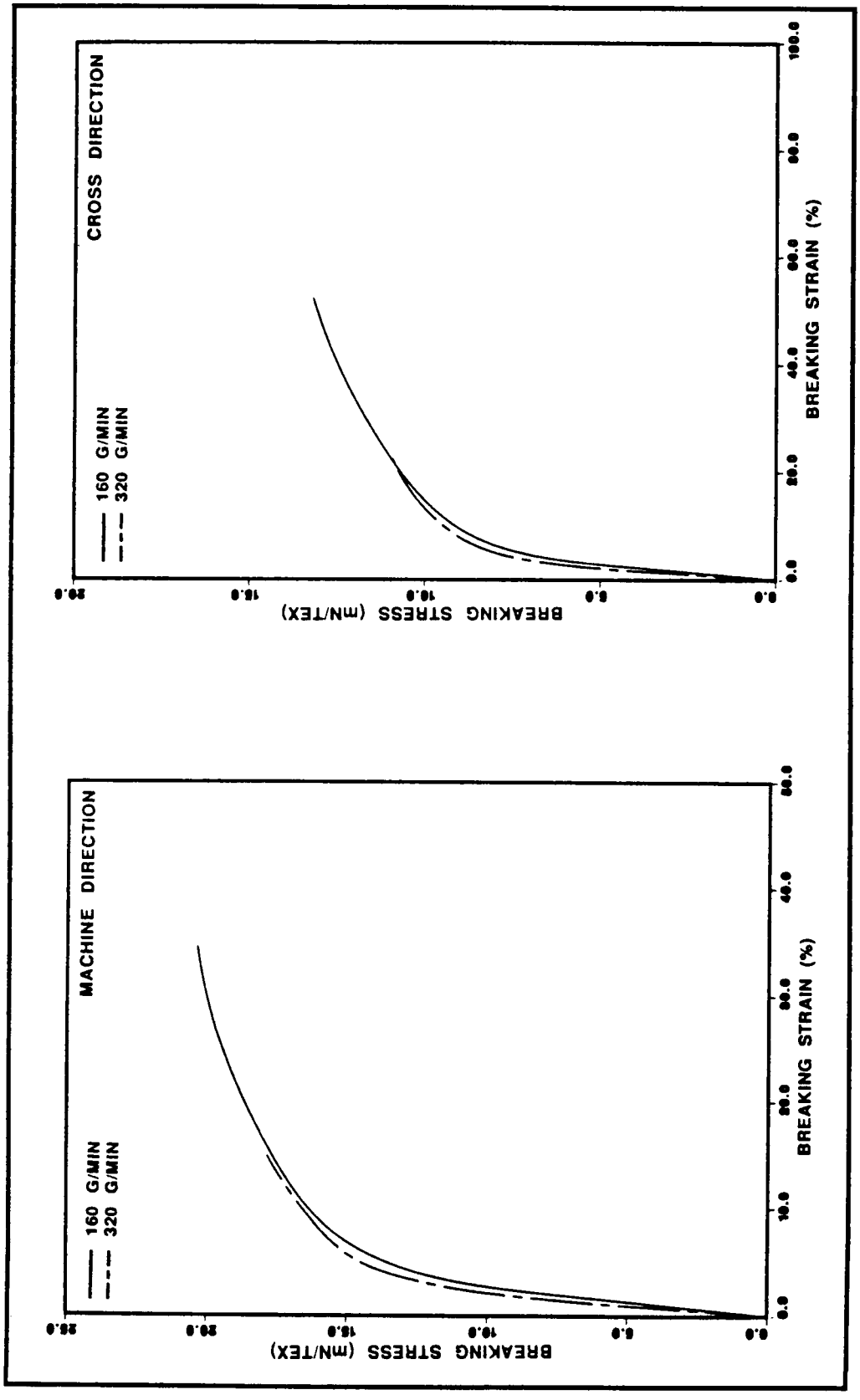

Figure E.20. Average MD and CD stress-strain curves of 35 MFR webs processed at 90% air flow rate using standard orifice die.

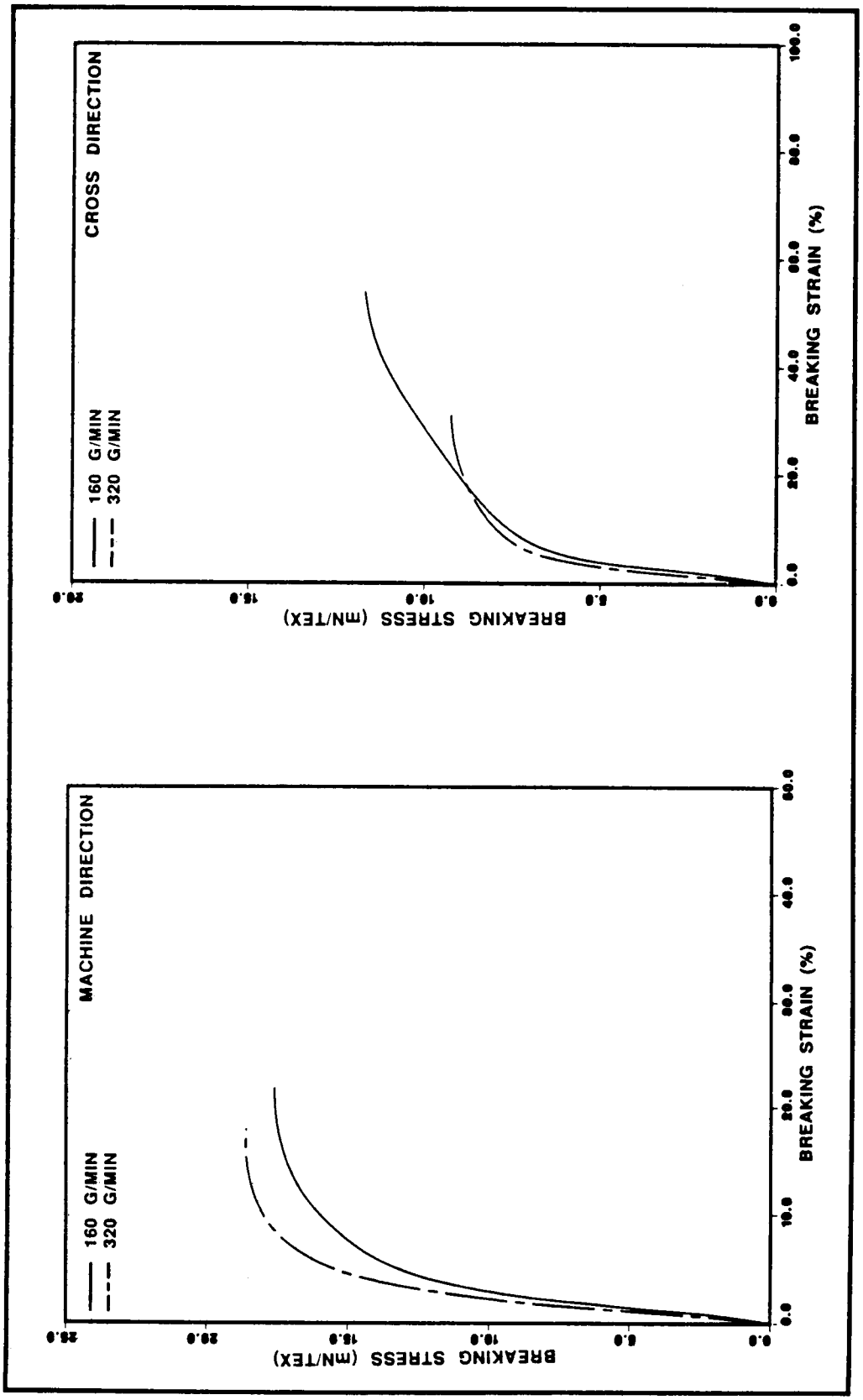

Figure E.21. Average MD and CD stress-strain curves of 300 MFR webs processed at 90% air flow rate using standard orifice die.

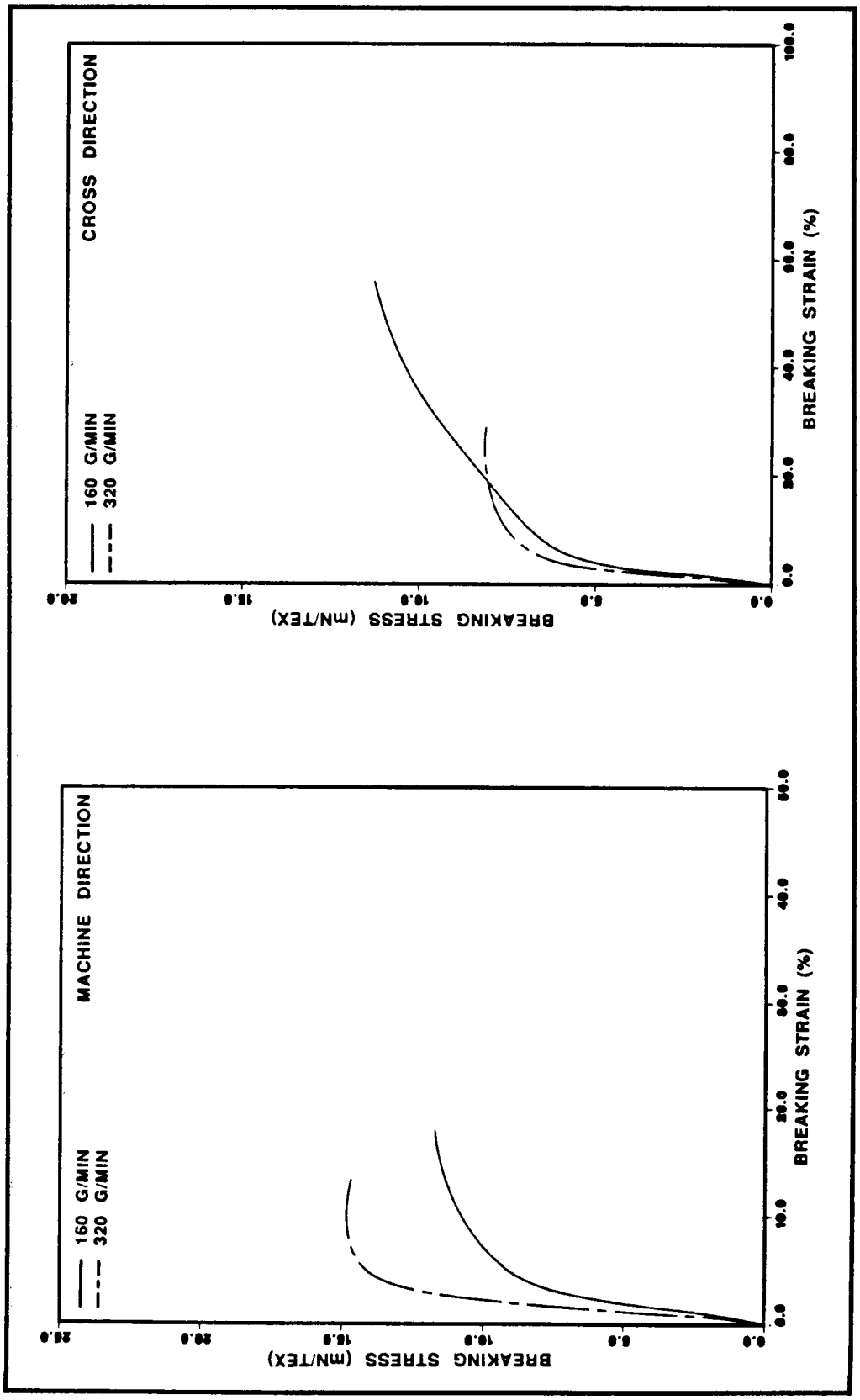

Figure E.22. Average MD and CD stress-strain curves of 600 MFR webs processed at 90% air flow rate using standard orifice die.

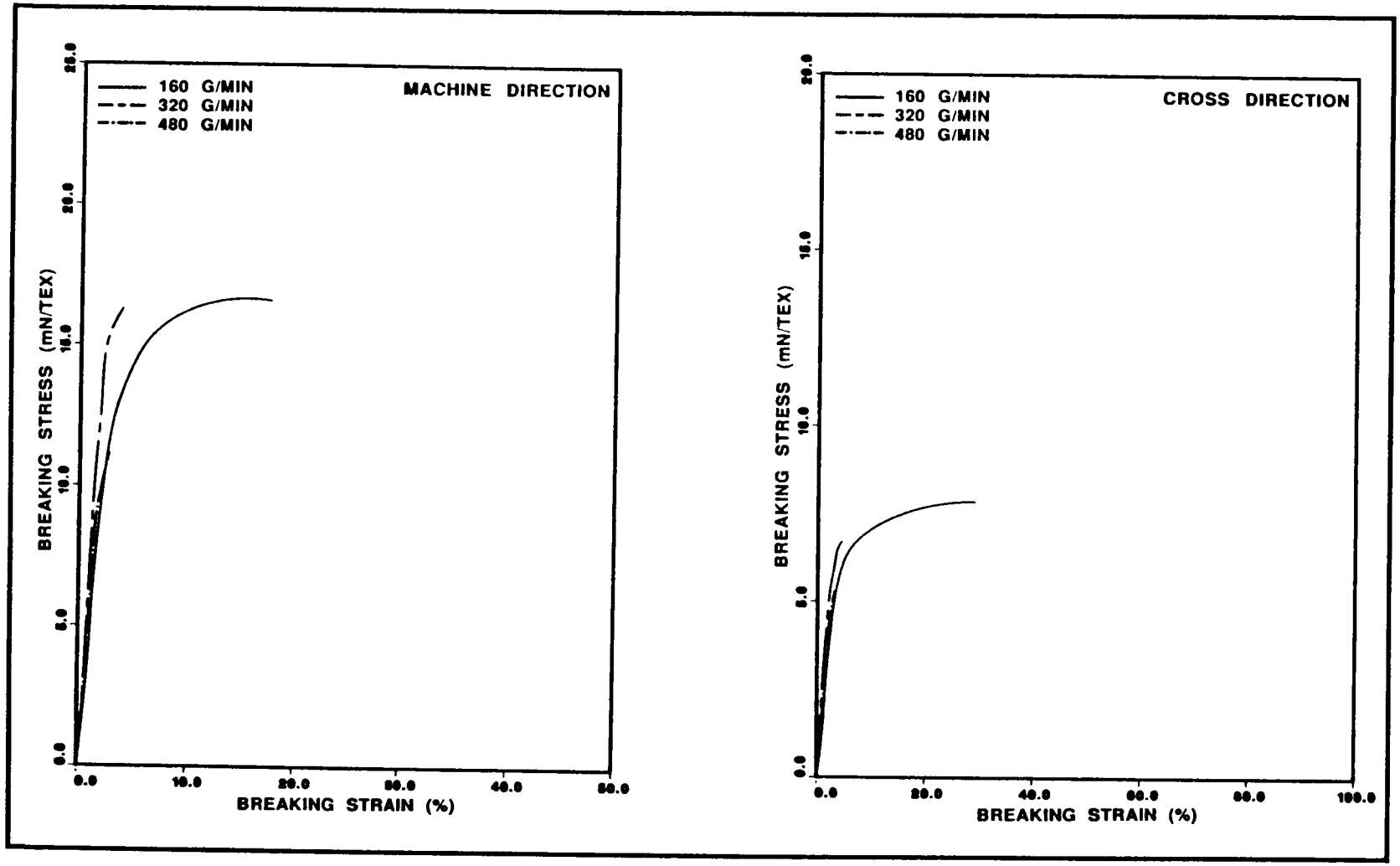

Figure E.23. Average MD and CD stress-strain curves of 300 MFR webs processed at 75% air flow rate using small orifice die.

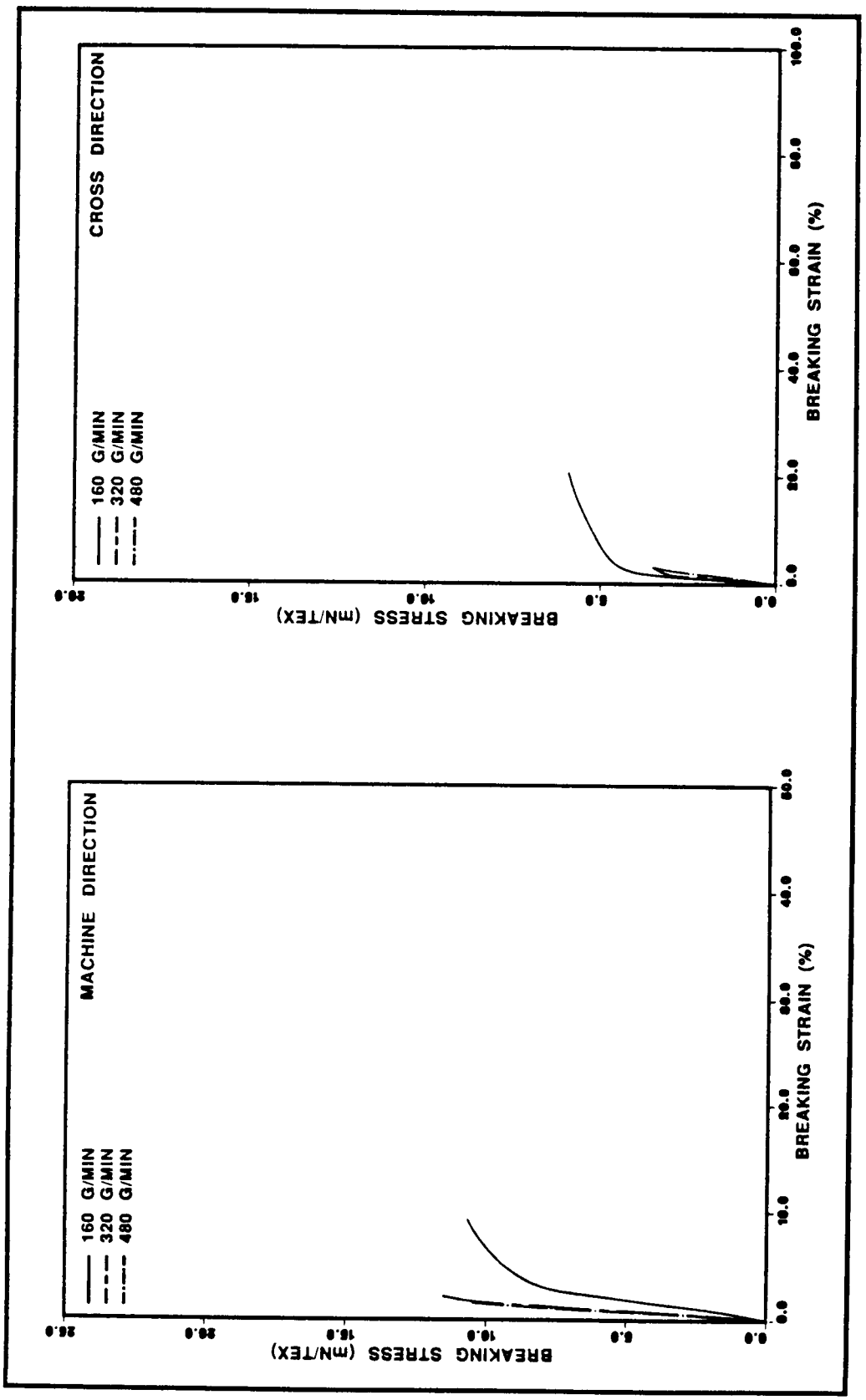

Figure E.24. Average MD and CD stress-strain curves of 1000 MFR webs processed at 75% air flow rate using small orifice die.

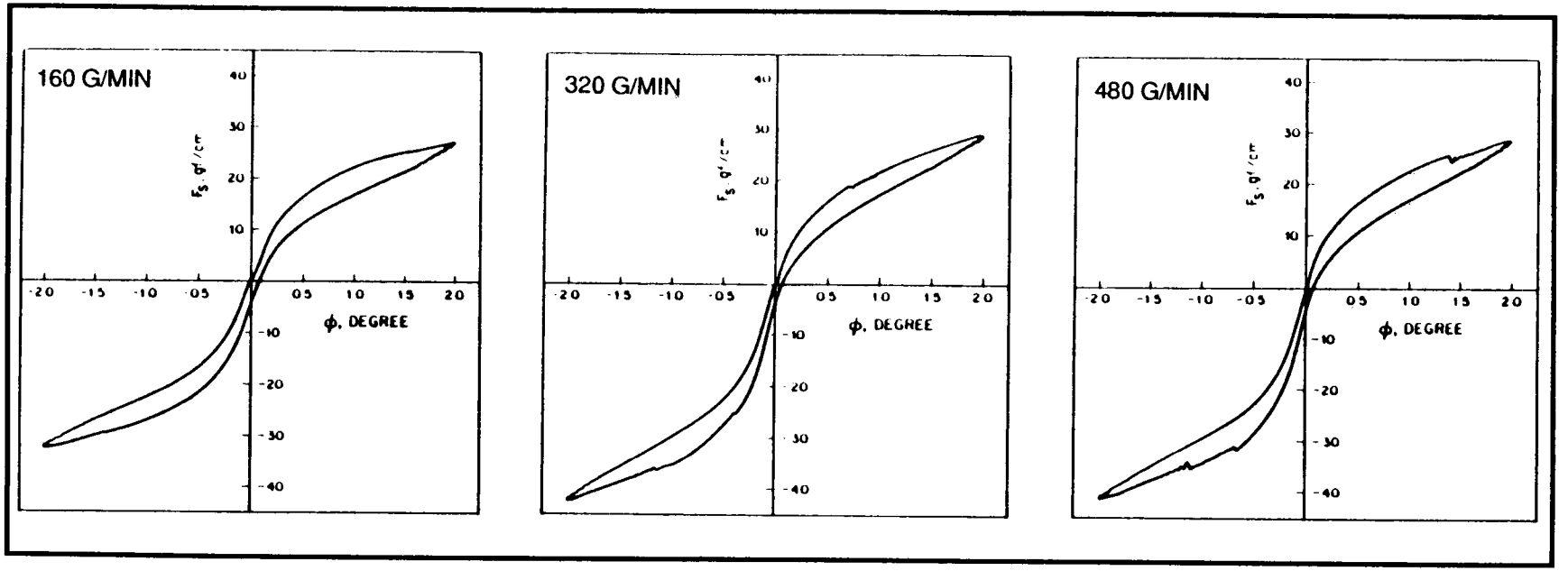

Figure E.25. Shear curves of 300 MFR webs processed at 75% air flow rate using standard orifice die.

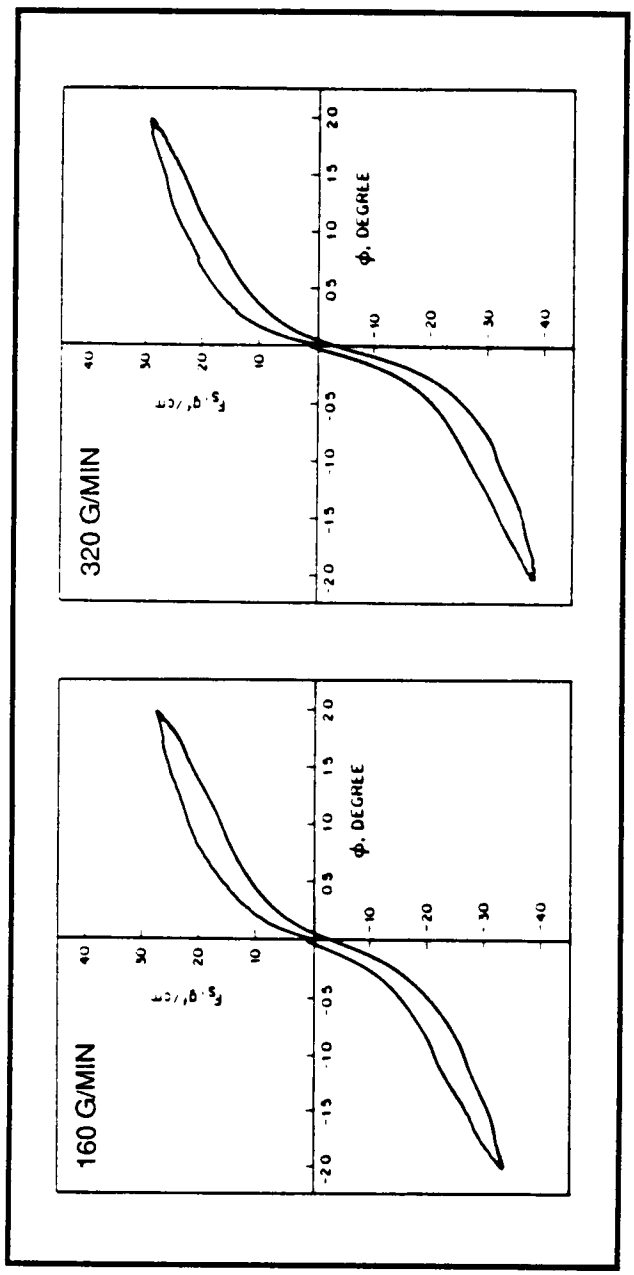

Figure E.26. Shear curves of 300 MFR webs processed at 90% air flow rate using standard orifice die.

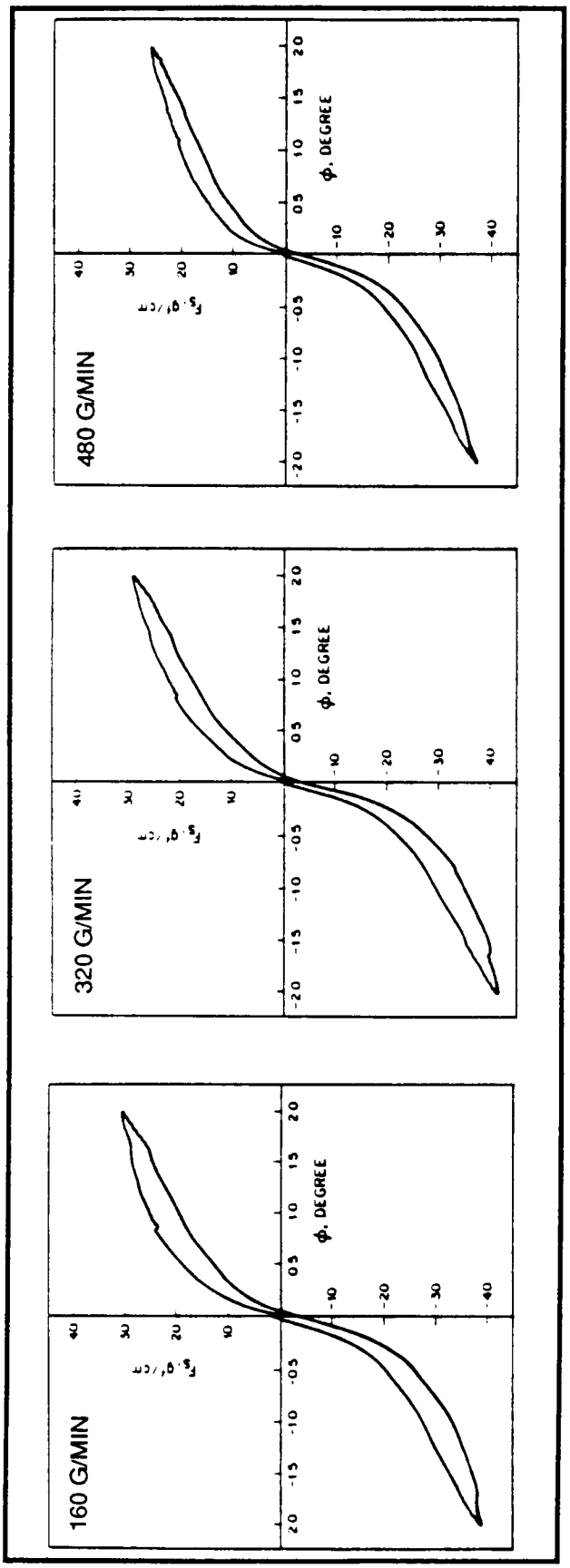

Figure E.27. Shear curves of 300 MFR webs processed at 75% air flow rate using small orifice die.

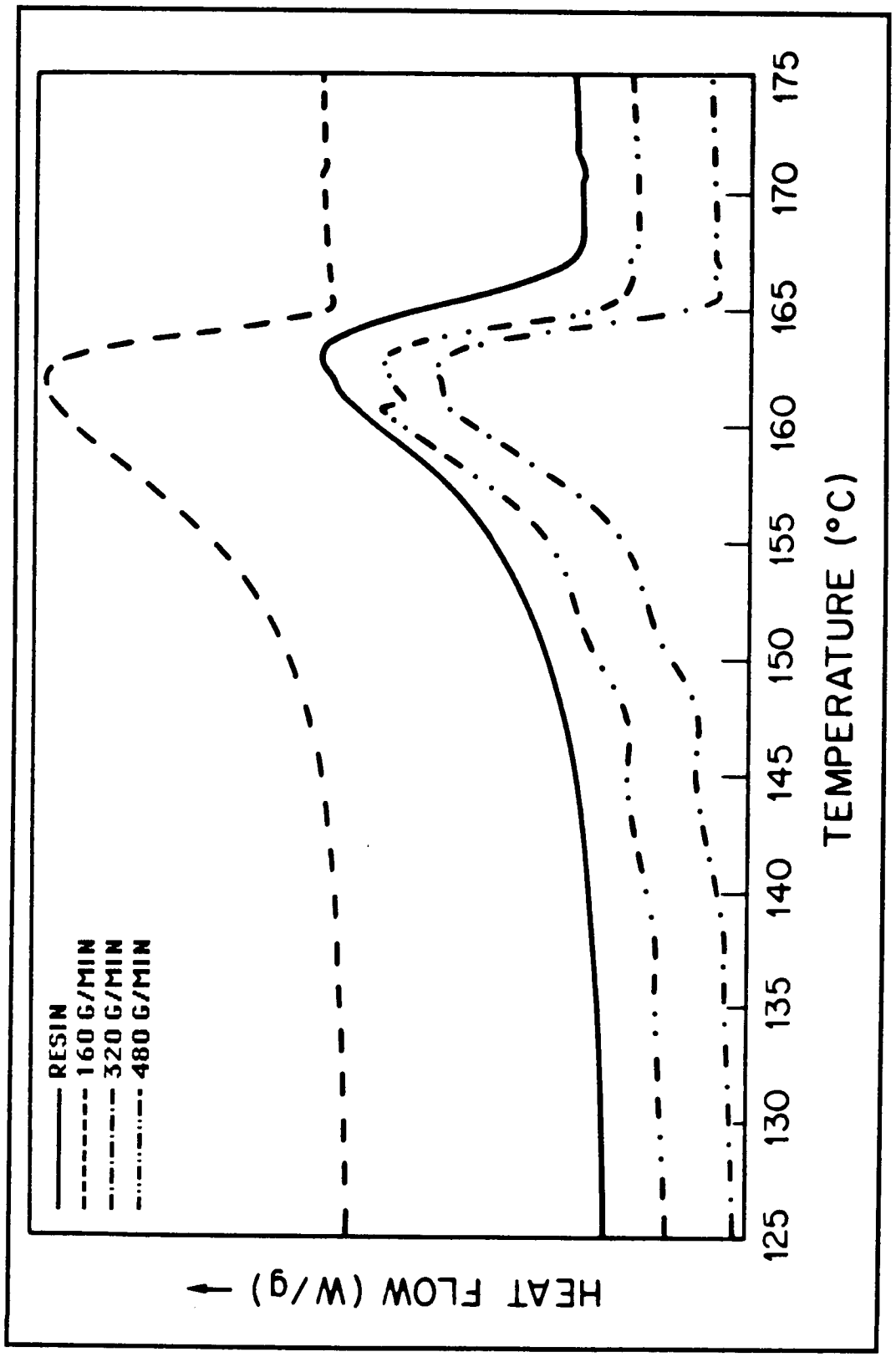

Figure E.28. DSC thermograms of 300 MFR resin and webs processed at 75% air flow rate using standard orifice die.

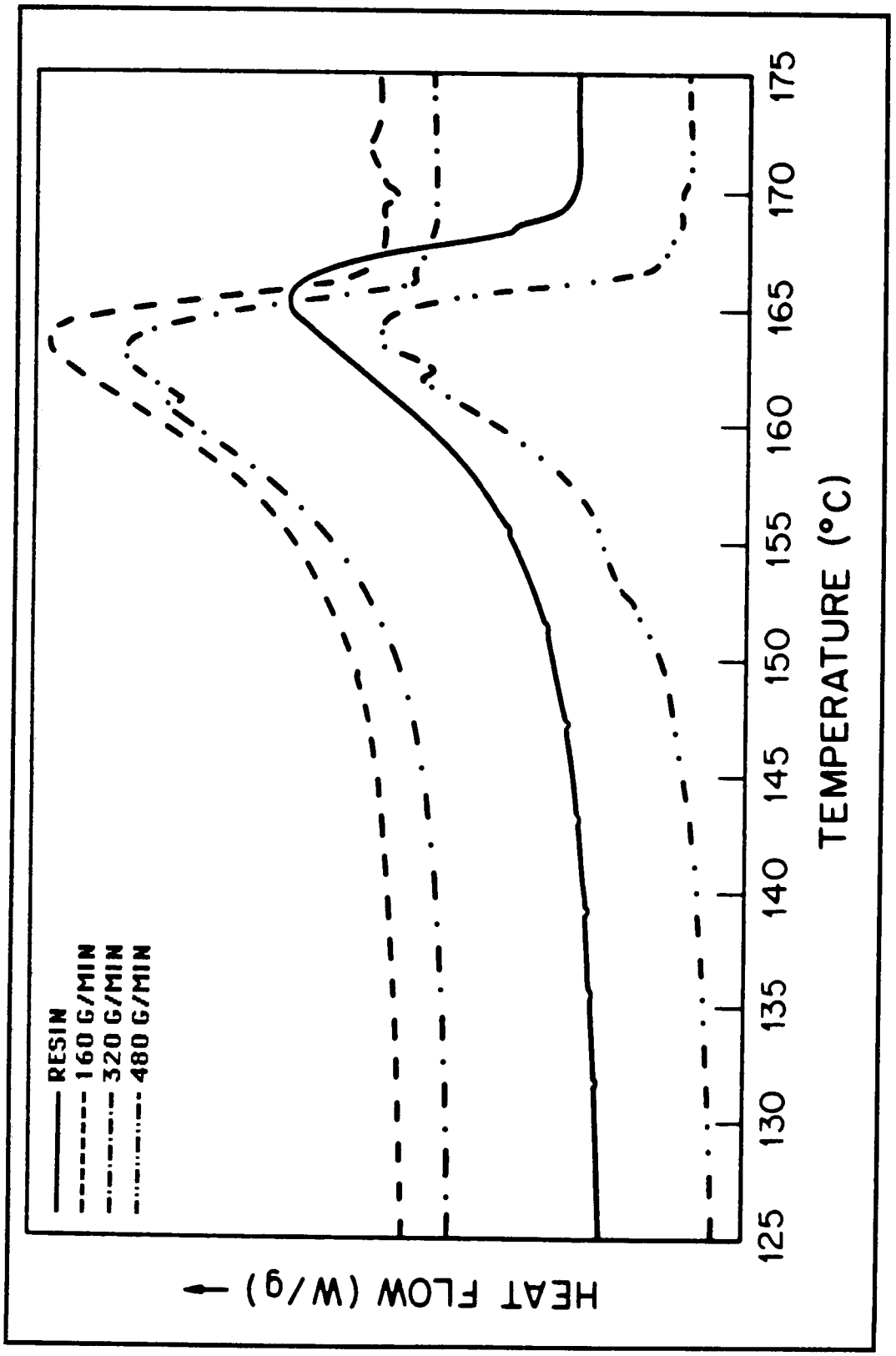

Figure E.29. DSC thermograms of 600 MFR resin and webs processed at 75% air flow rate using standard orifice die.

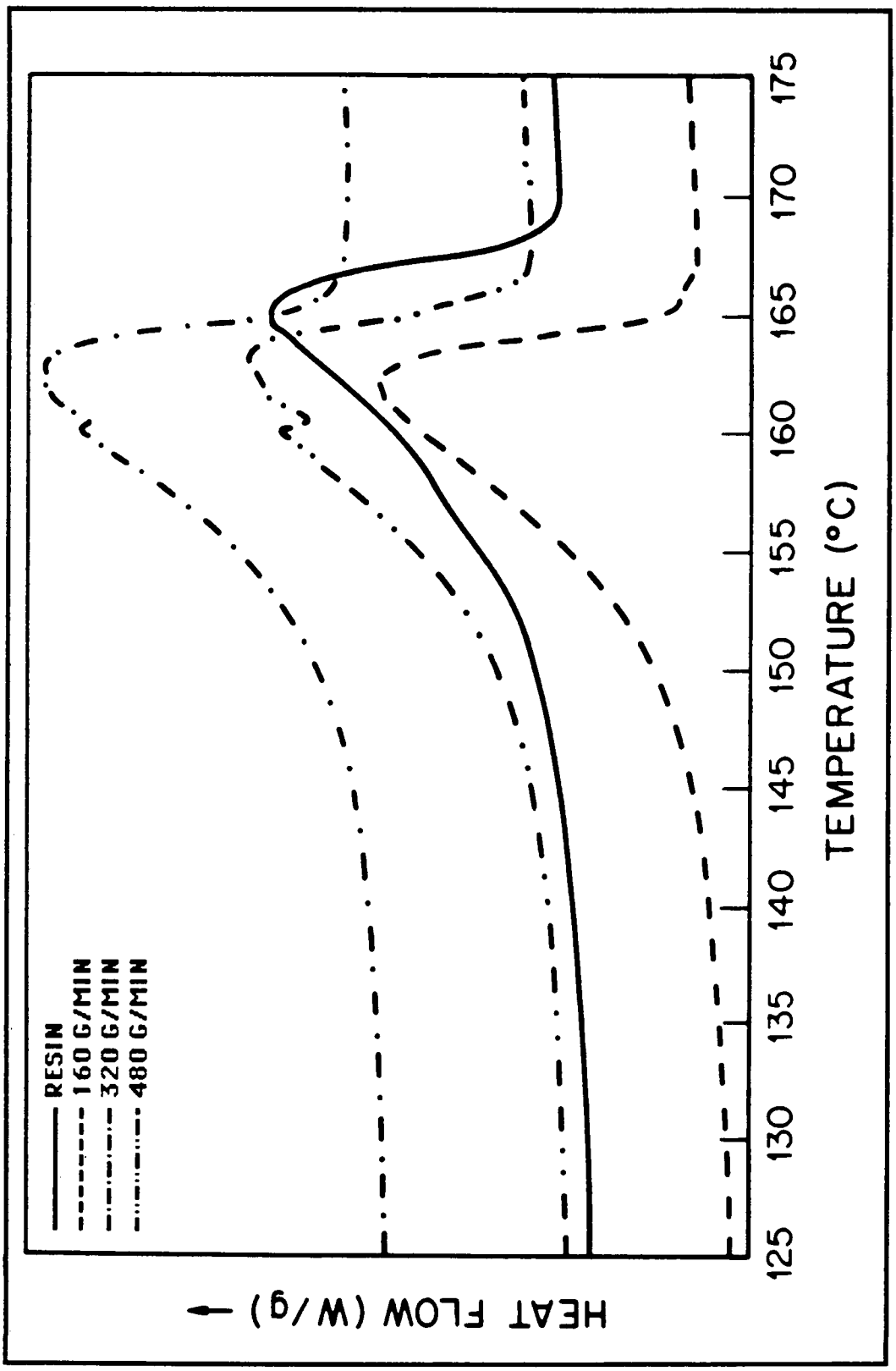

Figure E.30. DSC thermograms of 1000 MFR resin and webs processed at 75% air flow rate using standard orifice die.

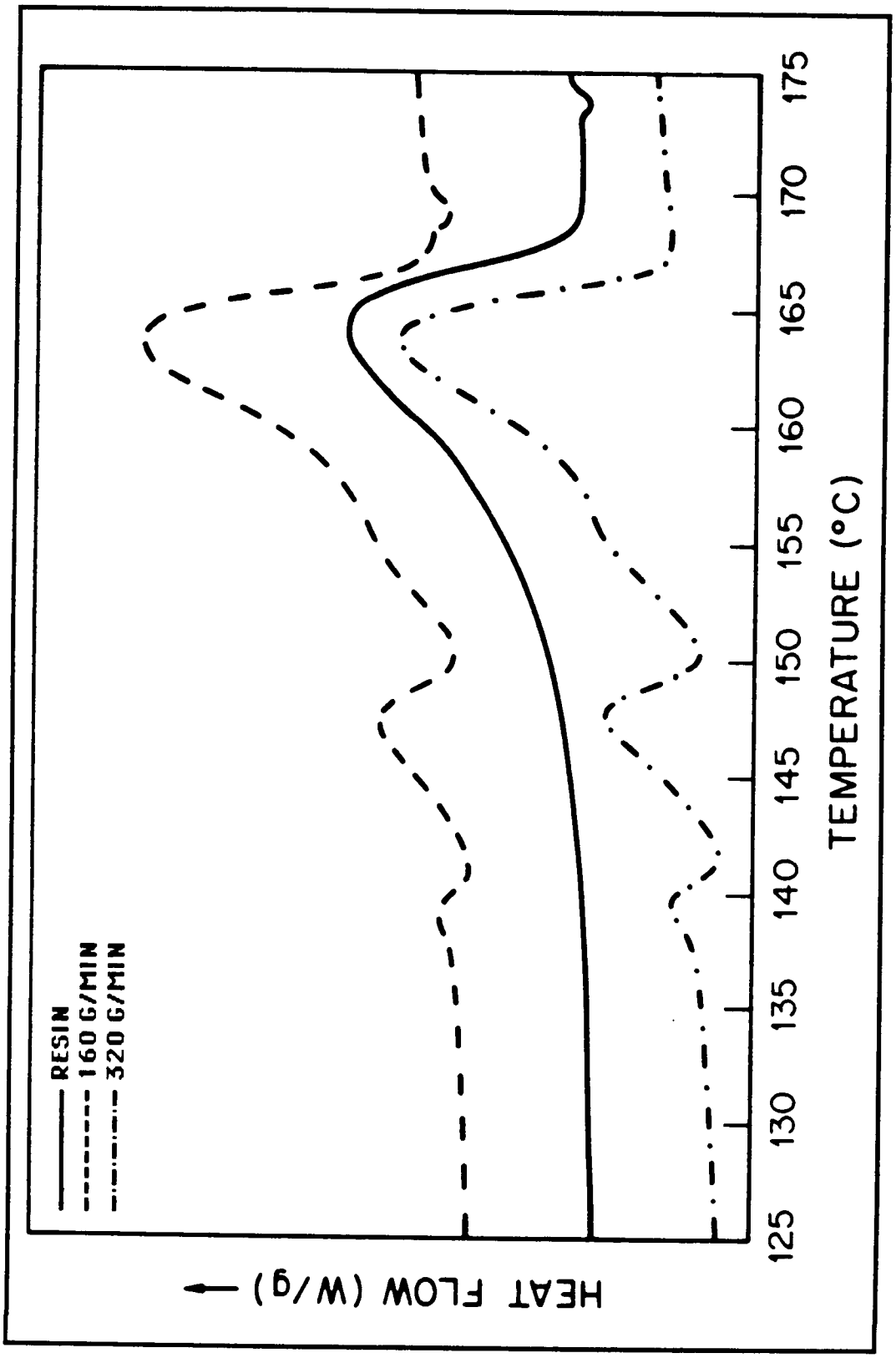

Figure E.31. DSC thermograms of 35 MFR resin and webs processed at 90% air flow rate using standard orifice die.

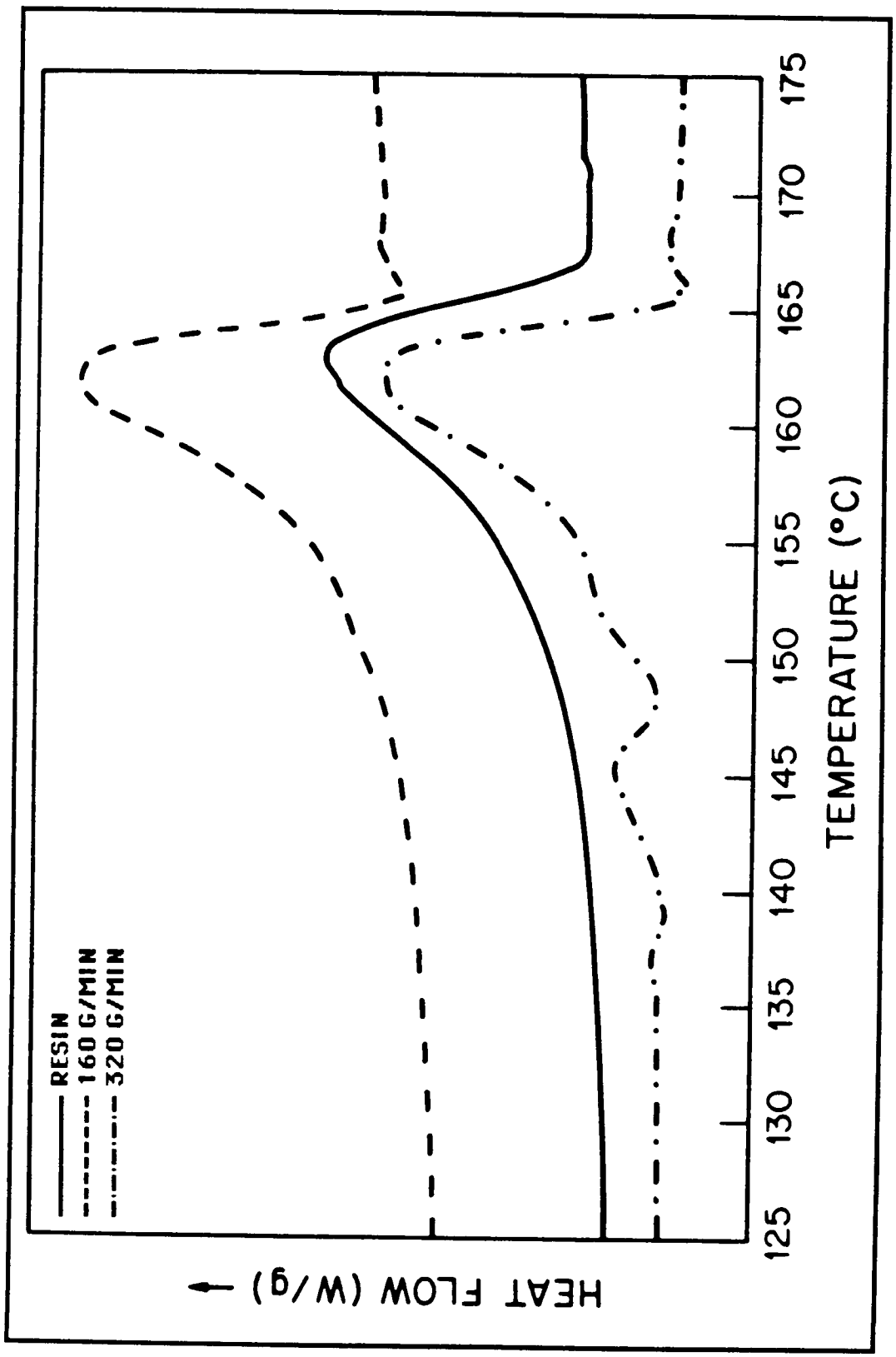

Figure E.32. DSC thermograms of 300 MFR resin and webs processed at 90% air flow rate using standard orifice die.

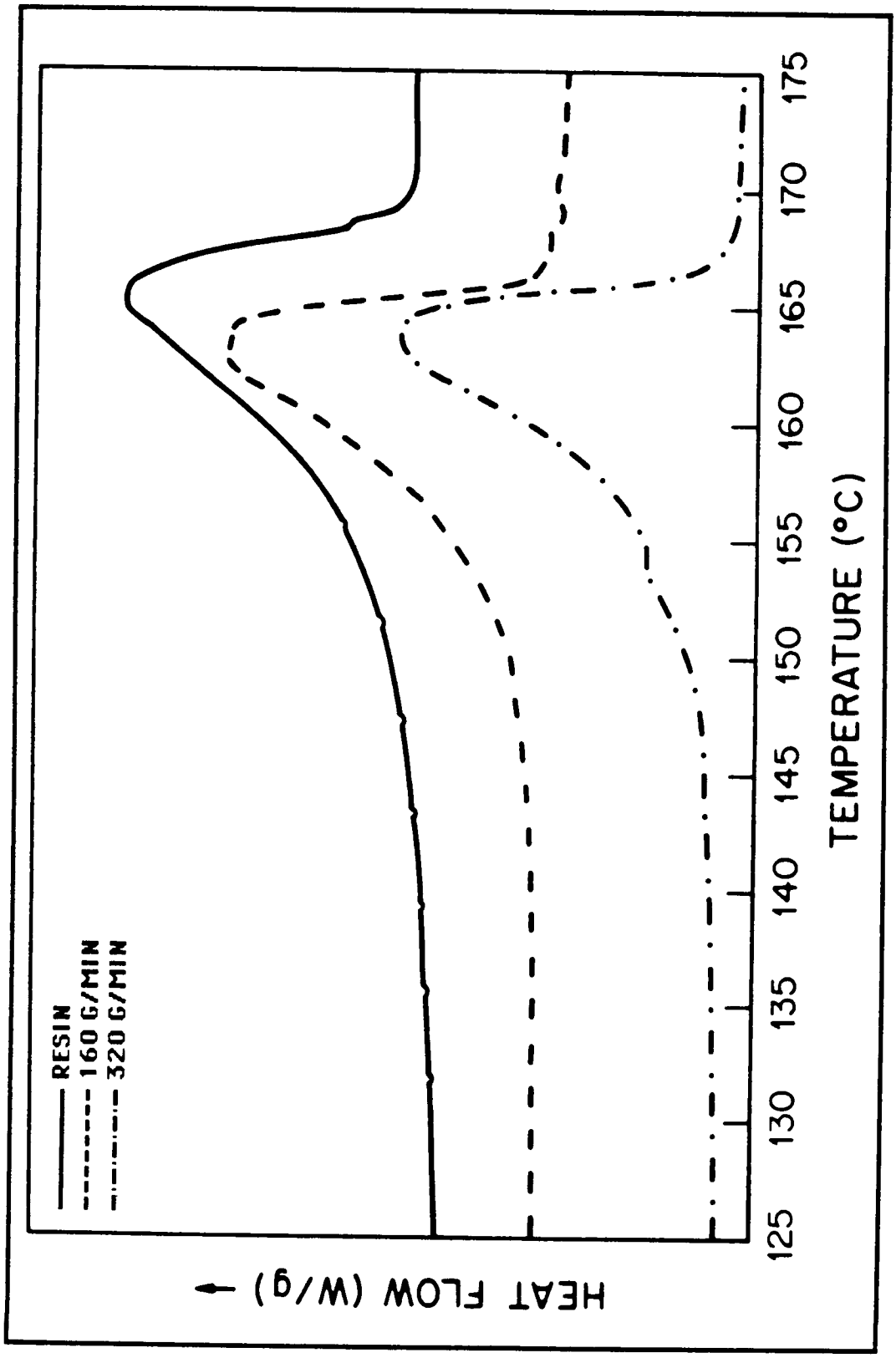

Figure E.33. DSC thermograms of 600 MFR resin and webs processed at 90% air flow rate using standard orifice die.

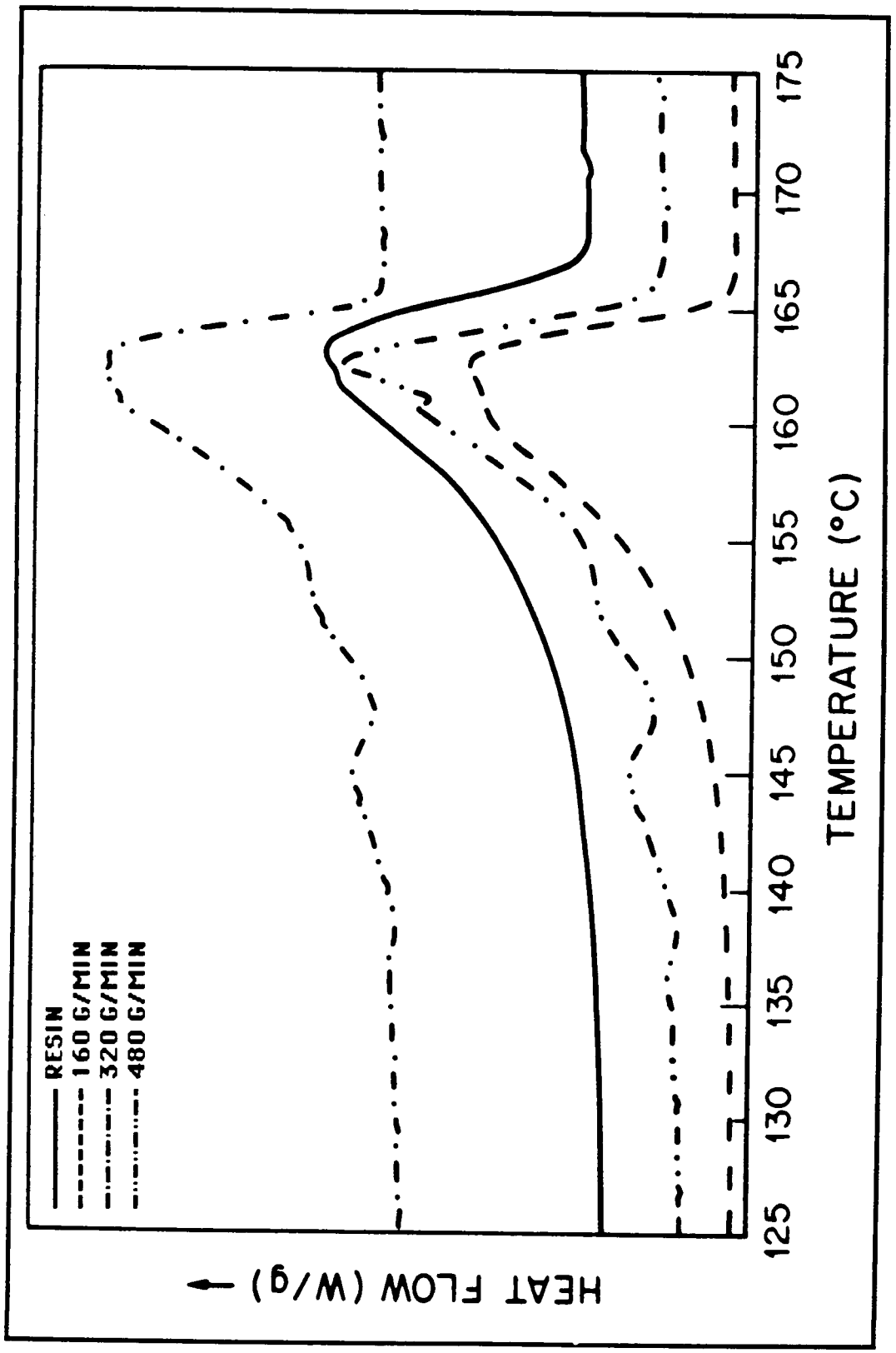

Figure E.34. DSC thermograms of 300 MFR resin and webs processed at 75% air flow rate using small orifice die.

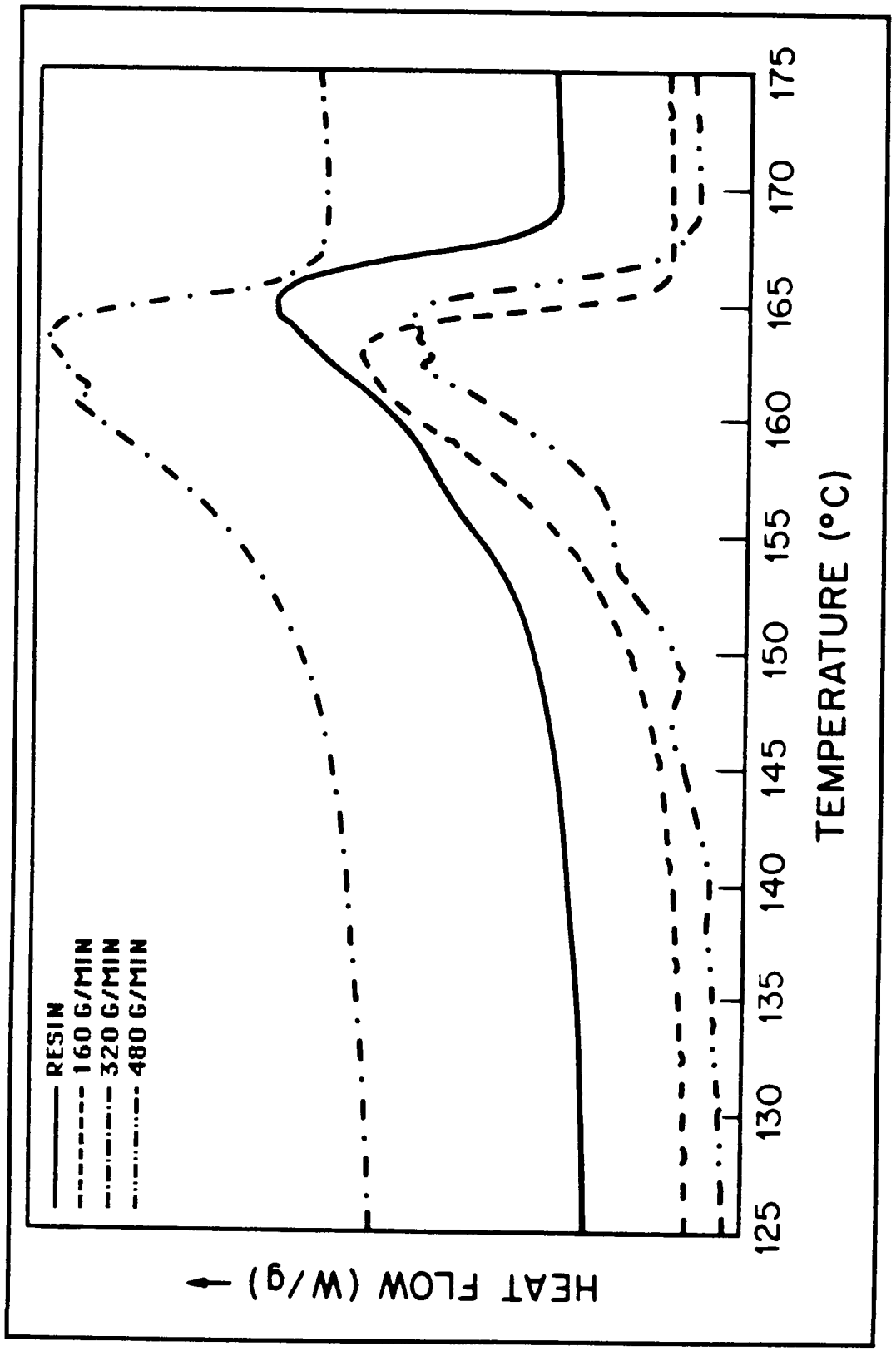

Figure E.35. DSC thermograms of 1000 MFR resin and webs processed at 75% air flow rate using small orifice die.

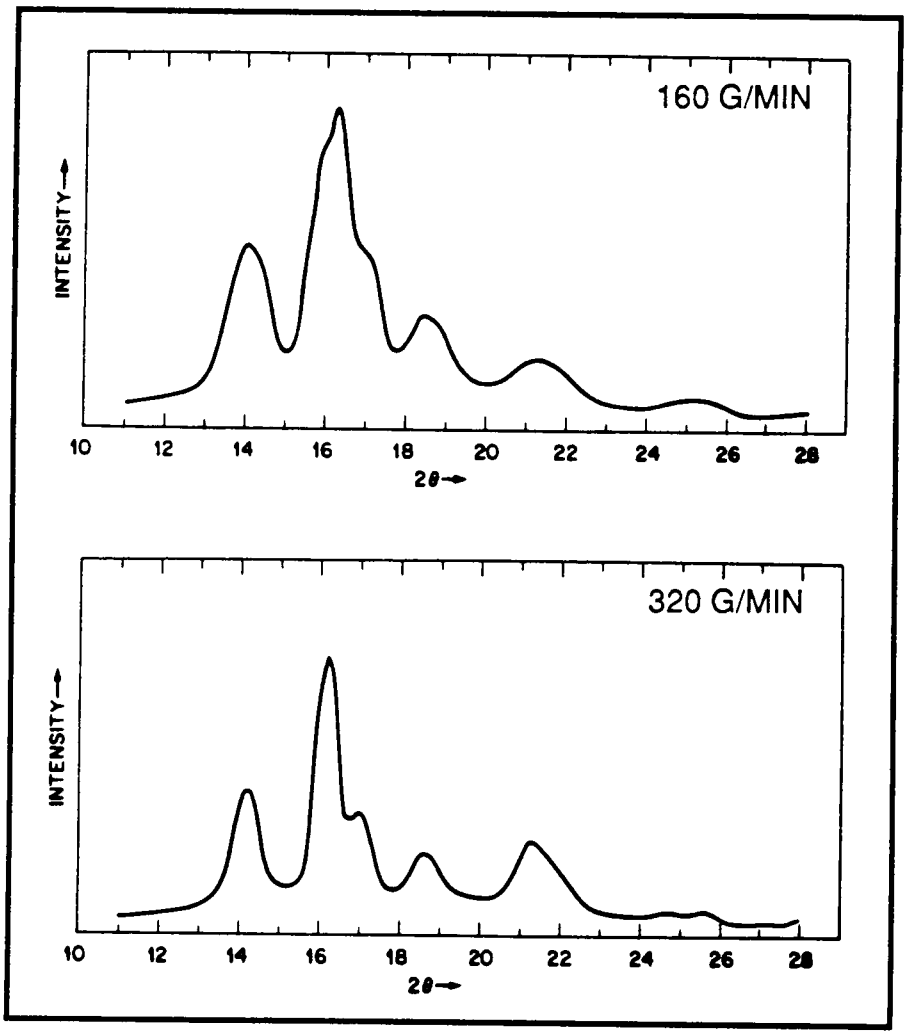

Figure E.36. X-ray diffractograms of 35 MFR webs processed at 75% air flow rate using standard orifice die.

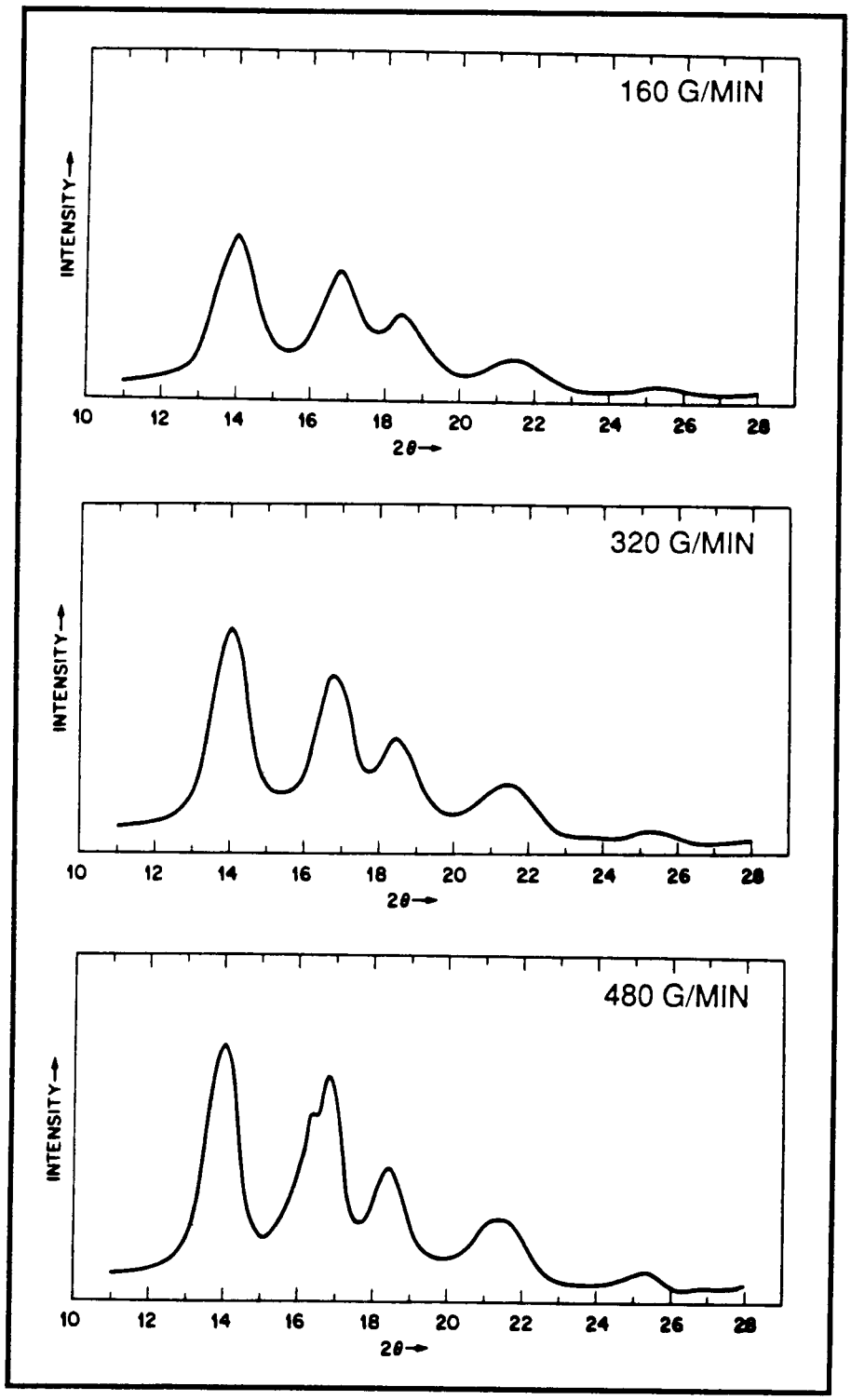

Figure E.37. X-ray diffractograms of 600 MFR webs processed at 75% air flow rate using standard orifice die.

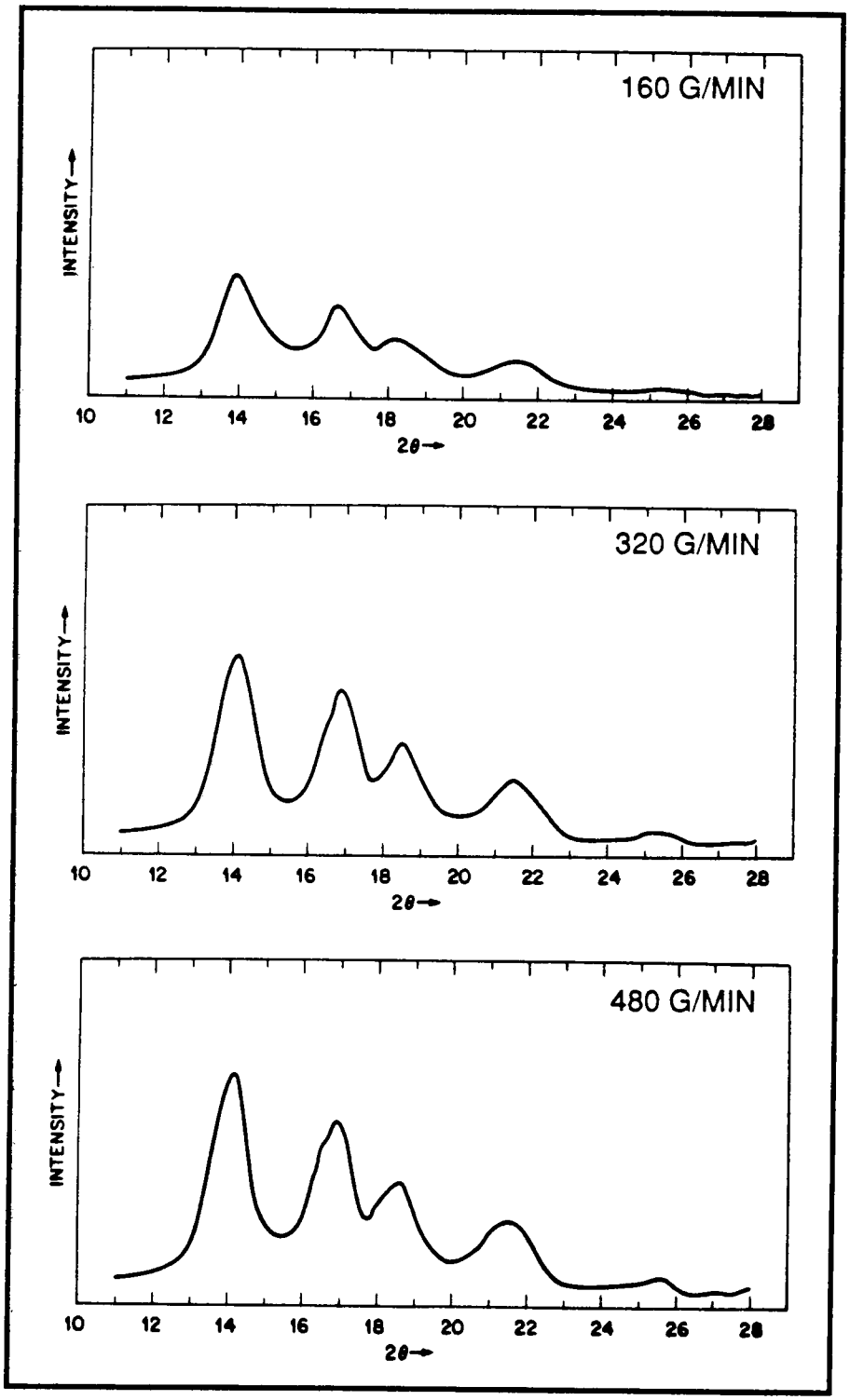

Figure E.38. X-ray diffractograms of 1000 MFR webs processed at 75% air flow rate using standard orifice die.

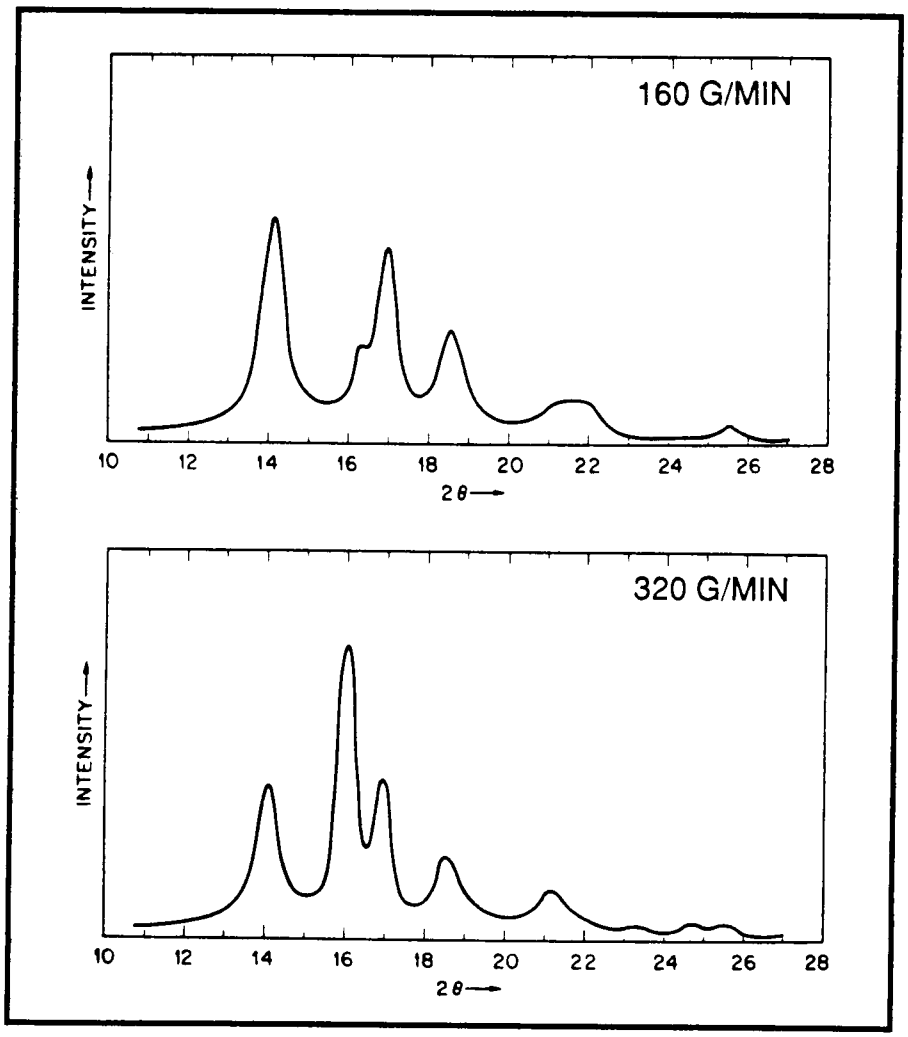

Figure E.39. X-ray diffractograms of 35 MFR webs processed at 90% air flow rate using standard orifice die.

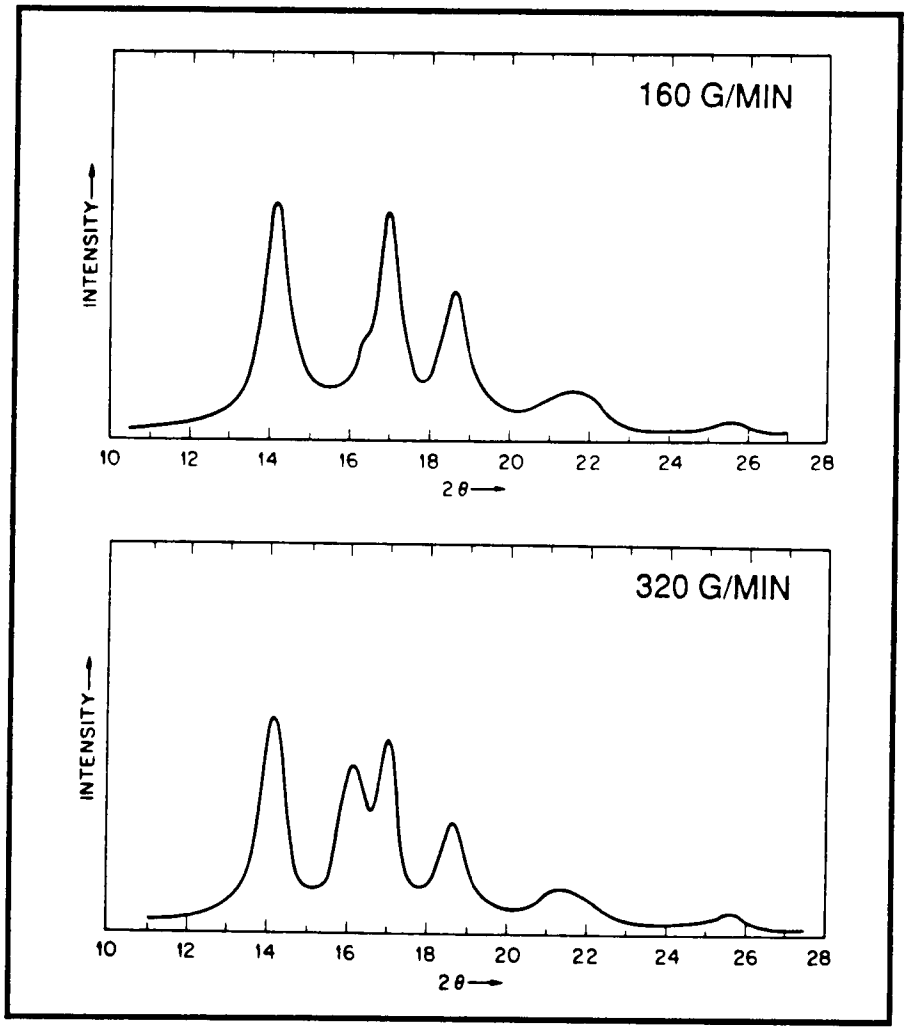

Figure E.40. X-ray diffractograms of 300 MFR webs processed at 90% air flow rate using standard orifice die.

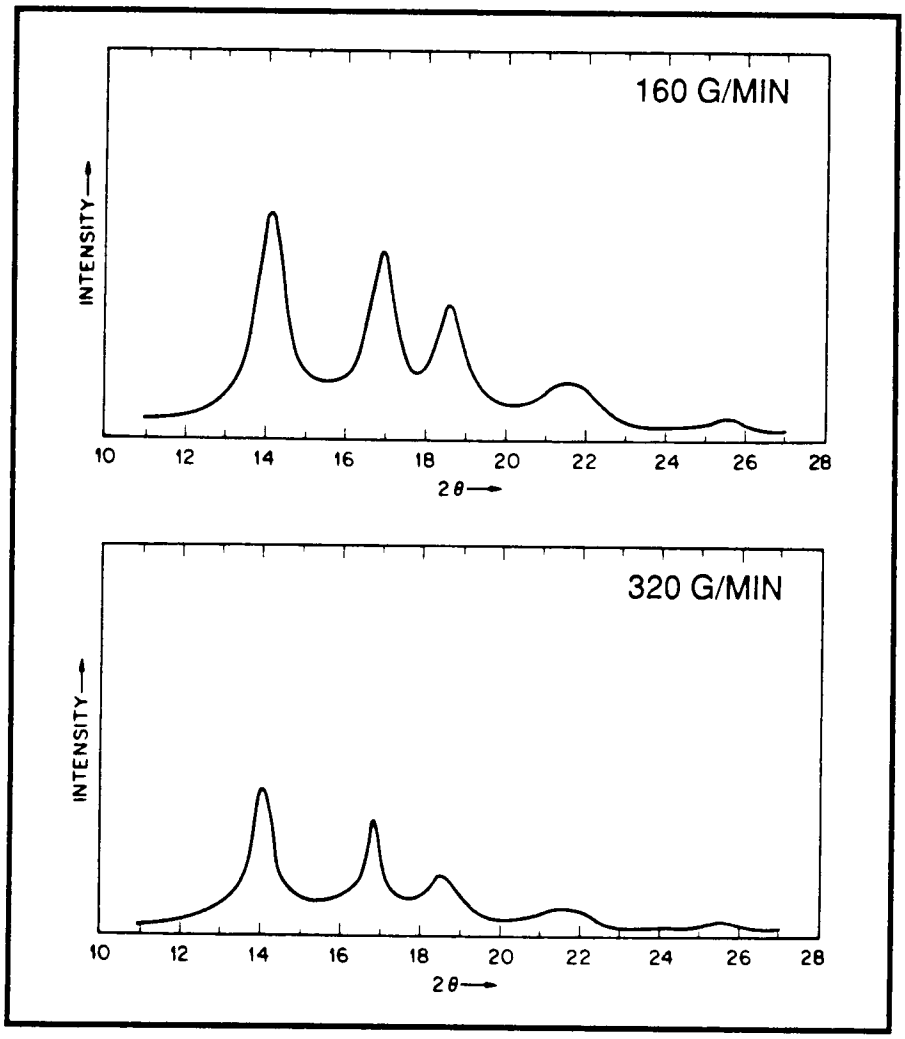

Figure E.41. X-ray diffractograms of 600 MFR webs processed at 90% air flow rate using standard orifice die.

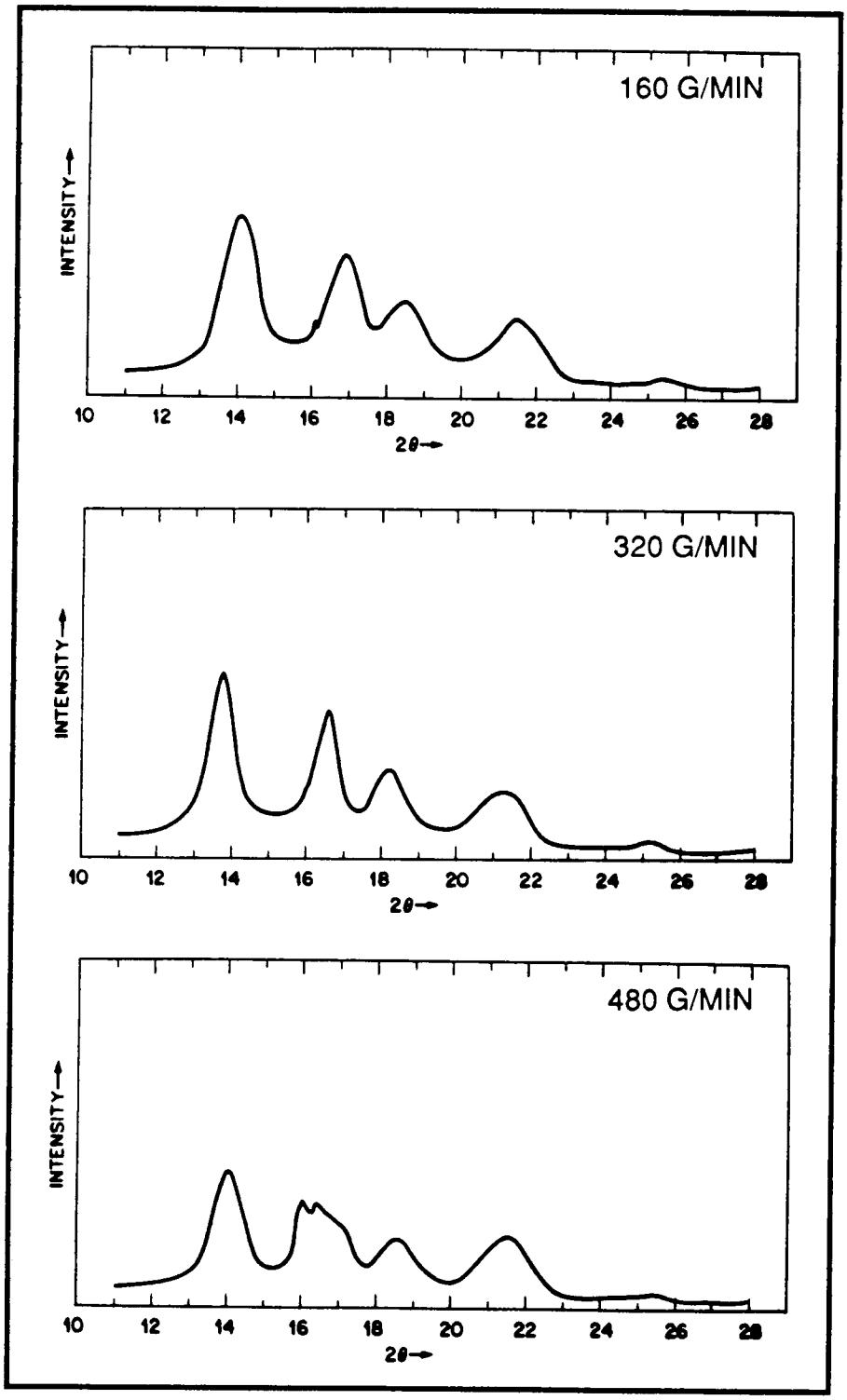

Figure E.42. X-ray diffractograms of 300 MFR webs processed at 75% air flow rate using small orifice die.

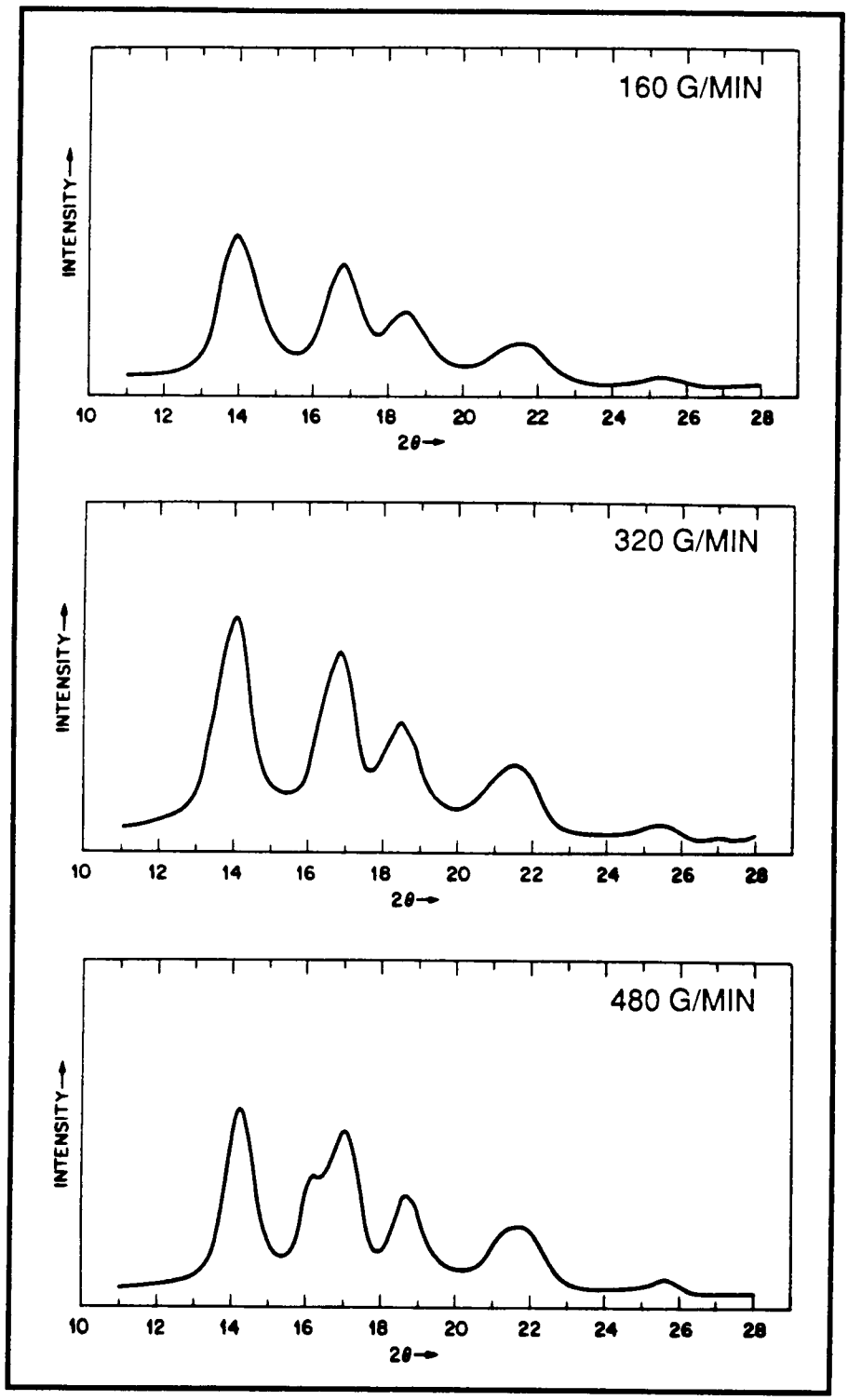

Figure E.43. X-ray diffractograms of 1000 MFR webs processed at 75% air flow rate using small orifice die.

APPENDIX F

CRYSTALLIZATION KINETICS STUDY OF POLYPROPYLENE RESINS

CRYSTALLIZATION KINETICS STUDY OF POLYPROPYLENE RESINS

The study of the crystallization kinetics of various melt blowable isotactic polypropylene resins using differential scanning calorimertry (DSC) technique is reported here. The DSC method allows investigation of crystallization under two conditions: isothermal and non-isothermal. The method is sensitive and fast enough for qualitative and quantitative measurements and presents the advantage that only a microsample is required.

Experimental. The polymers used in this study were commercial Exxon **35, 300, 600**, and **1000 MFR** homopolypropylene whose characteristics are given in Table 3.1. A model DSC-7 Perkin Elmer differential calorimerter was used to measure the crystallization kinetics under isothermal and non-isothermal conditions. Indium was selected as the standard to calibrate the instument. The exact weight of the sample (ranging from 3.5 to 4 mg) was determined with an accuracy of 0.001 mg in an aluminium pan. The rate of crystallization under isothermal conditions was studied at temperatures: **133 °C, 131 °C, 129 °C**, and **127 °C**; and, the rate of non-isothermal crystallization was studied at five cooling rates: **40, 20, 10, 5, 2 °C/min**. The rate of crystallization (rate of heat evolution) was very slow above T_c = 135 °C for the DSC technique to detect the rate of heat evolution accurately; and, the crystallization was very fast below T_c = 125 °C for the thermal equilibrium to be reached when cooled rapidly from 200 °C to T_c. Each sample was kept melted for five minutes prior to crystallization at 200 °C. This ensured that in all cases

the crystallization proceded from the equilibrium melt. Since the DSC method requires a very small amount of sample (3 to 5 mg), it has the advantage of attaining thermal equilibrium very quickly, with the consequence of following a more rapid crystallization rate than is possible for techniques such as dilatometry.

In the study of isothermal crystallization, the samples were cooled rapidly to the desired crystallization temperature (T_c) and were allowed to crystallize. While in the study of non-isothermal crystallization, the samples were cooled at a given rate. The rate of heat evolution was recorded as a function of time/temperature until crystallization was completed or the heat evolved was small enough to be detected. The DSC curves were normalized and evaluated using TAS7 Perkin Elmer software. Each DSC curve was rescaled and digitized using a digitizer available through The University of Tennessee computing center. The digitized calorimertic isotherm data were analyzed to obtain relative crystallinity as a function of time using a program written on an IBM PC (Figure F.1) [114]. The following equation was used to calculate the relative crystallinity at a given time/temperature [138]:

$$X_t = \frac{\int_0^t (dH_t / dt)\, dt}{\int_0^\infty (dH_t / dt) dt}$$

Where X_t = Weight fraction of crystallized material at time t.
The numerator of the expression gives integral heat of crystallization at time t; and, the denominator of the expression gives the total measured heat of crystallization.

This program calculates relative crystallinity versus time from DSC data for isothermal crystallization. Required input parameters are coefficients A0 to A9 of polynomial fitting of DSC trace; to compute fractional area.

```
10 A0=-0.0455332
20 A1=-6.50493
30 A2=10.5349
40 A3=-10.4825
50 A4=6.68217
60 A5=-2.65897
70 A6=0.657843
80 A7=-0.0987065
90 A8=0.00824317
100 A9=-0.000294377
```

FX = Total time for crystallization to complete

```
110 FX=5.5
120 N=550
130 H=FX/N
135 INPUT AA$
137 AA$="B:"+AA$+".DAT"
150 OPEN AA$ FOR OUTPUT AS #1
160 DEF FNA(X)=A0+A1*X+A2*X*X+A3*X^3+A4*X^4+A5*X^5
              +A6*X^6+A7*X^7+A8*X^8+A9*X^9
170 S1=FNA(0) : S2=FNA(FX)
180 S=S1+S2
190 FOR I=1 TO N-1
200 IF 2*INT((I+1)/2)=I THEN CO=2 ELSE CO=4
210 X=X+H
220 S=S+CO*FNA(X)
230 NEXT I
240 TAREA=S*H/3
250 FOR I=1 TO 55
260 X=0
270 FX=I*0.1
280 N=I*16
290 H=FX/N
300 S2=FNA(FX)
310 S=S1+S2
320 FOR J=1 TO N-1
330 IF 2*INT((J+1)/2)=J THEN CO=2 ELSE CO=4
340 X=X+H
350 S=S+CO*FNA(X)
360 NEXT J
370 PRINT USING "##.##        #.#####";FX,S*H/3/TAREA
380 PRINT
390 WRITE #1,FX,S*H/3/TAREA  'time v/s rel. cryst.
                              data file
400 NEXT I
410 CLOSE #1
420 END
```

Figure F.1. Computer program for calculating relative crystallinity.

After each isothermal crystallization, the melting point was determined during heating cycle at 10 °C/min. The peak temperature was used as the melting point coresponding to a given crystallization temperature (T_c). A plot of melting point (T_m) versus crystallization temperature (T_c) was used to estimate the equilibrium melting temperature ($T_m°$) for each sample -- a parameter of fundamental importance in testing various crystallization and melting theories. Since the isothermal crystallization in case of polypropylene can only be studied at lower temperatures (at higher under cooling), the extrapolation of T_m versus T_c to get $T_m°$ would not be unequivocal.

Results. The above equation was used to obtain relative crystallinity as function of: (1) time for isothermal condition; and, (2) temperature for non-isothermal condition. The plots of relative crystallinity versus time for 35, 300, 600, and 1000 MFR at different crystallization temperatures are shown in Figure F.2. The relative crystallinity versus time data for different polymers at a given crystallization temperature are shown in Figure F.3. The non-isothermal kinetics data for different polymers at cooling rates of 40, 20, 10, 5, and 2 °C/min are shown in Figures F.4 and F.5.

The isothermal crystallization data was analyzed using Avrami analysis to obtain crystallization rates 'k' and Avrami index 'n'. The values of Avarami index 'n', rate constant 'k', $t_{1/2}$, $T_m°$ as determined from peak temperature are shown in Table F.1. The value of 'n' close to 2 indicates hetrogeneous crystallization giving 2-dimensional disks. Pratt and Hobbs [139] have reported values of 'n' in the range 2.8-3.0 from calorimetric as well as light depolarization microscopy studies for their polypropylenes. Godovsky et al [140] have

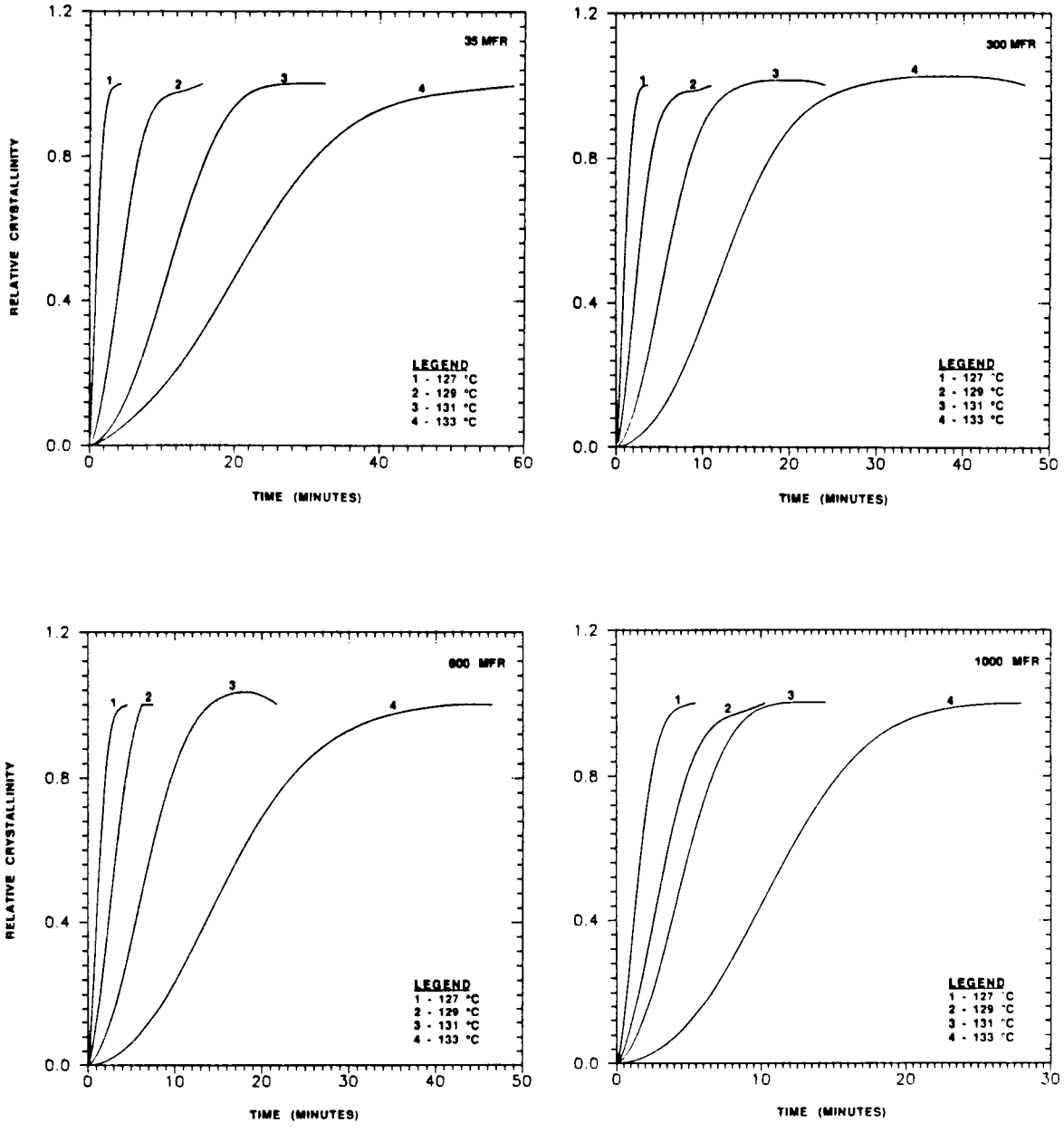

Figure F.2. Relative crystallinity versus time at different crystallization temperatures (T_c).

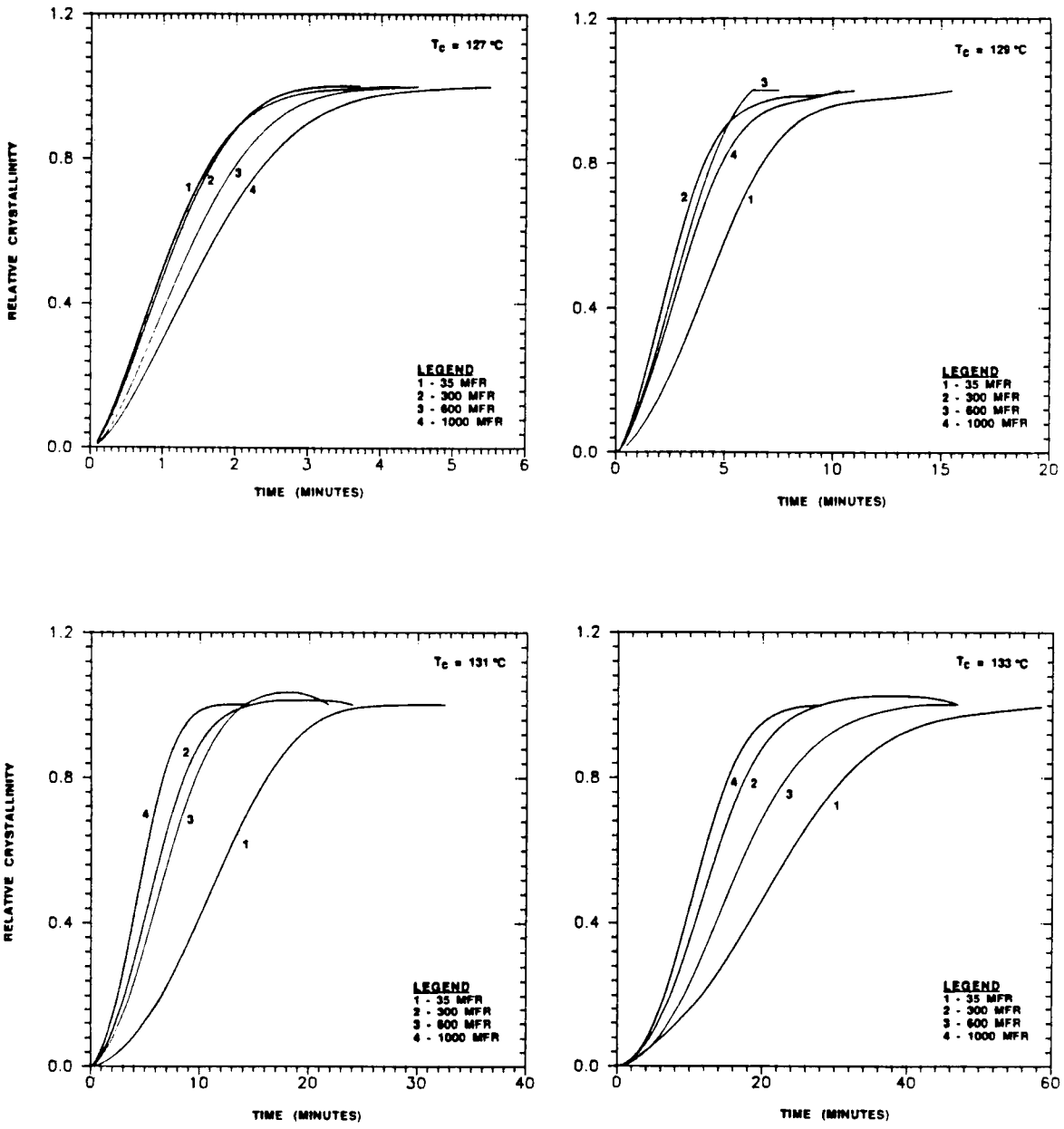

Figure F.3. Relative crystallinity versus time for different polymers at a given crystallization temperature (T_c).

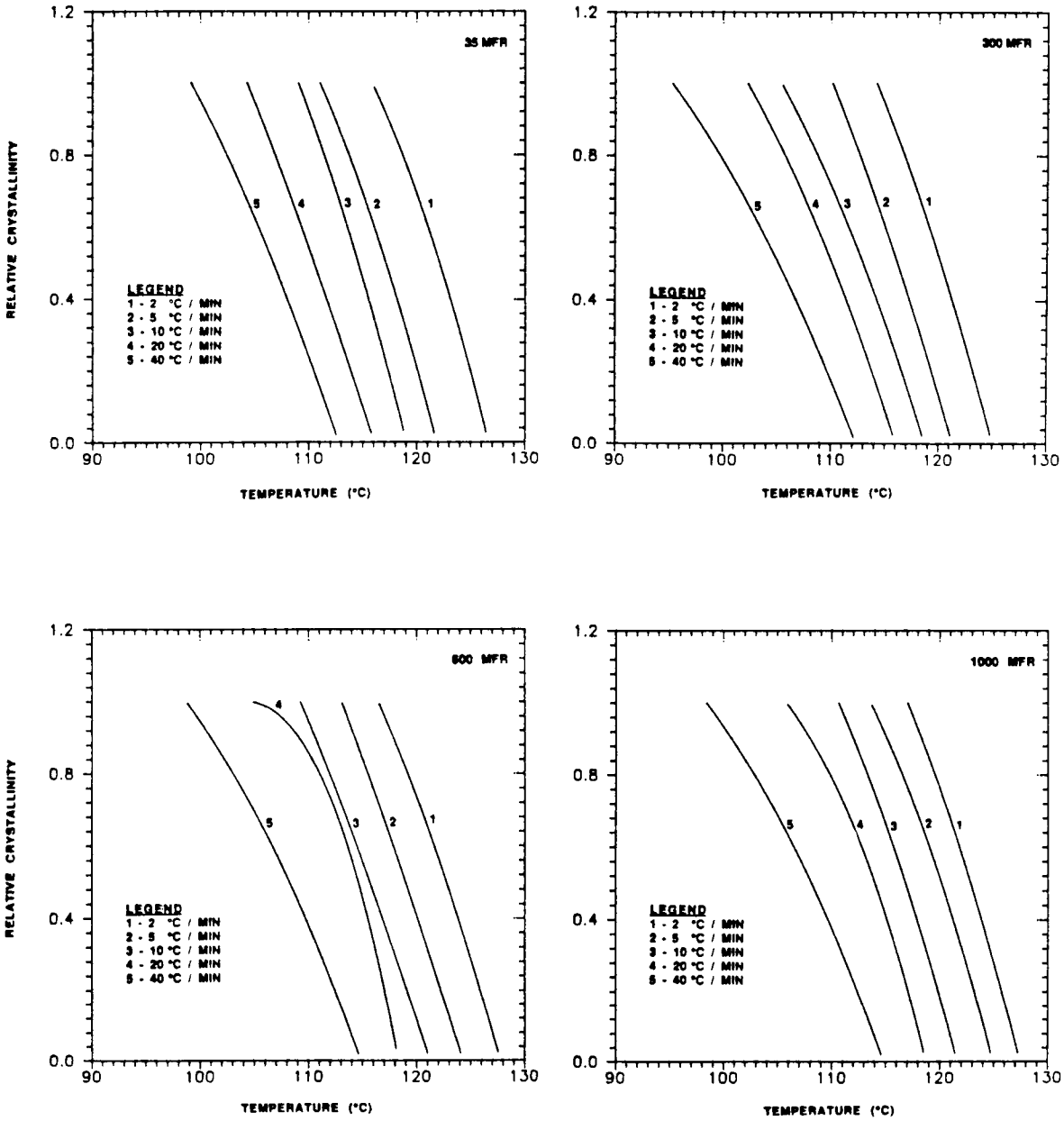

Figure F.4. Relative crystallinity versus temperature for different polymers.

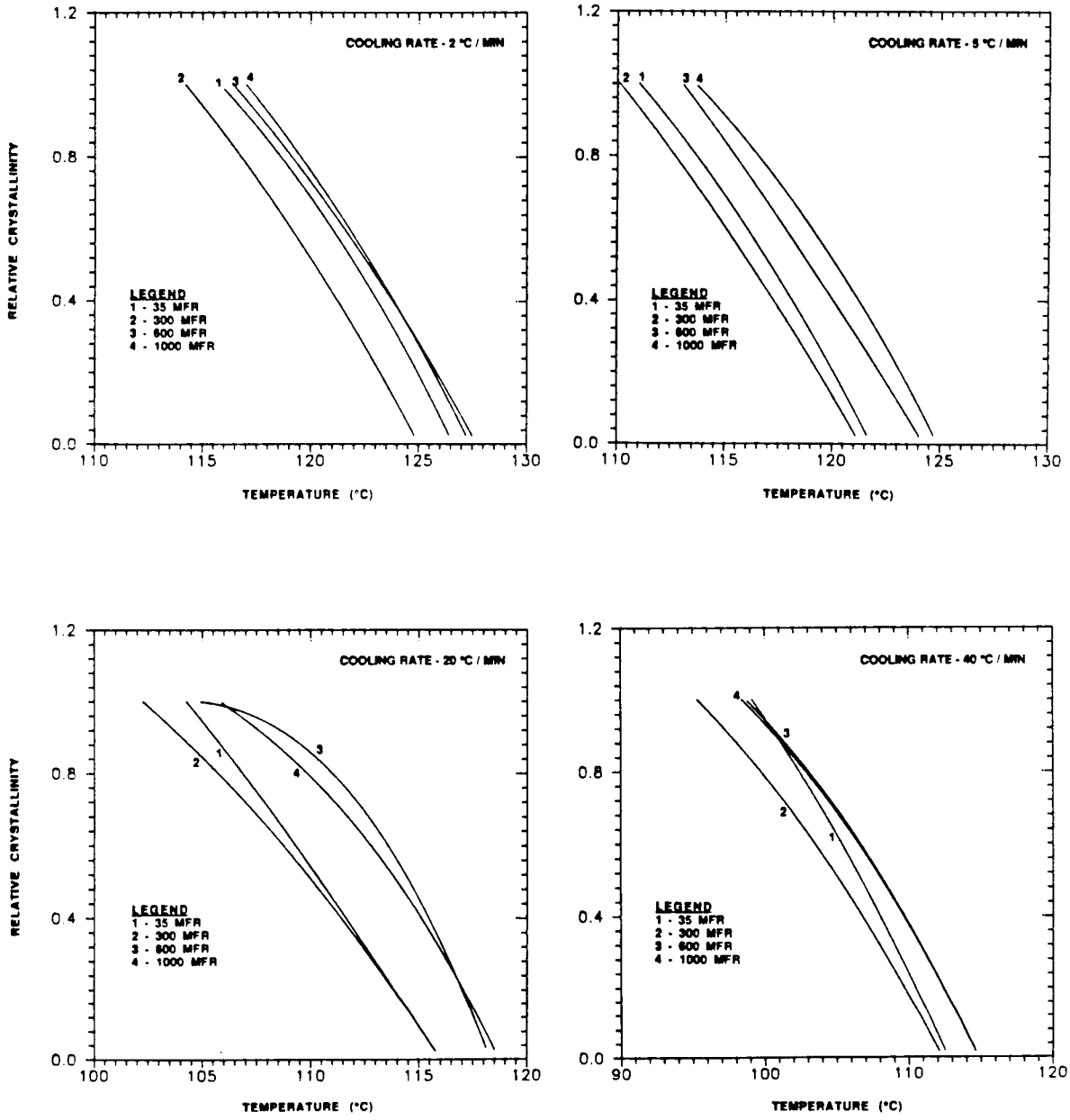

Figure F.5. Relative crystallinity versus temperature at different cooling rates.

Table F.1
Avarami Index, Rate Constant, Crystallization Half-Time ($t_{1/2}$), and Equilibrium Melting Point (T_m^o) for various PP Resins

Polymer MFR	T_c °C	n	k min^{-1}	$t_{1/2}$ min	T_m^o °C
PP-1400	133	2.35	2.64E-03	10.8	186.4
	131	2.11	2.97E-02	04.5	
	129	1.68	0.109	03.1	
	127	1.68	0.357	01.5	
PP-700	133	2.06	2.43E-03	15.7	193.1
	131	1.74	2.55E-02	06.5	
	129	1.63	0.124	02.9	
	127	1.66	0.481	01.3	
PP-300	133	2.02	4.24E-03	12.3	190.3
	131	1.84	2.89E-02	05.7	
	129	1.69	0.144	02.6	
	127	1.66	0.654	01.1	
PP-35	133	1.66	4.23E-03	21.0	200.3
	131	1.88	6.91E-03	11.2	
	129	1.74	0.053	04.5	
	127	1.60	0.697	01.03	

reported that their polypropylenes gave n=2 from calorimetric results and n=3 from dilatometric results.

As shown in Figure F.2 as well as in Table F.1, the rate of crystallization increased (or $t_{1/2}$ decreased) with a decrease in T_c (or at high undercoolings). This negative temperature coefficient of crystallization rate suggests a nucleation controlled crystallization. A marked effect of molecular weight on the crystallization rate is seen in Figure 2. At T_c = 133 °C, the rate of crystallization for 35 MFR (highest M_w) was slowest as one would expect. However, the rate of crystallization for 600 MFR was slower than that for 300 MFR at all crystallization temperatures (T_c) as seen in Figure F.3. Since all of the polymers studied were commercial polymers with broad molecular weight distributution, it would be difficult to draw any conclusions based on observed trends. The lower crystallization rate for 600 MFR may be due to the presence of a fraction of atactic polymer or more chain defects. The influence of molecular weight is not so strong at high undercoolings as can be observed in Figures F.4 and F.5.

VITA

The author, Sanjiv R. Malkan, was born in Bombay, India on August 27, 1961. His educational background is as follows:

Diploma in Man-Made Textile Chemistry, June 1981
SASMIRA'S INSTITUTE OF MAN-MADE TEXTILES, BOMBAY, INDIA
Thesis : "Finishing of Nonwoven Fabrics."
Graduated with 1st Class Honors

Bachelor of Science in Textile Engineering, May 1984
PHILADELPHIA COLLEGE OF TEXTILES AND SCIENCE, PHILA., PA
Major: Textile Structures

Master of Science in Materials Engineering, June 1986
DREXEL UNIVERSITY, PHILADELPHIA, PA
Major: Fibrous Composite Materials
Thesis : " Effect of Fiber Reinforcement Geometry On Single Shear and Fracture Behavior of Three Dimensionally Braided Glass/Epoxy Composite Pin."

Doctor of Philosophy in Textiles and Apparel, May 1990
THE UNIVERSITY OF TENNESSEE, KNOXVILLE, TN
Major: Textile Science / Minor: Polymer Engineering
Dissertation: "Process-Structure-Property Relationships in Different Molecular Weight Polypropylene Melt Blown Webs."